UNIVERSIDAD DE MÁLAGA

FACULTAD DE CIENCIAS

Programa de Doctorado: Química y Tecnologías Químicas, Materiales y Nanotecnología

TESIS DOCTORAL

Solid Acid Catalysts for the Dehydration of Hexoses to 5-Hydroxymethylfurfural.

Mercedes Moreno Recio

Directores:
Dr. Pedro Jesús Maireles Torres, Dr. Ignacio Jiménez Morales

2022

AUTOR: Mercedes Moreno Recio

https://orcid.org/0000-0003-3865-4571

EDITA: Publicaciones y Divulgación Científica. Universidad de Málaga

UNIVERSIDAD DE MÁLAGA

Departamento de Química Inorgánica, Cristalografía y Mineralogía

Solid Acid Catalysts for the Dehydration of Hexoses to 5-Hydroxymethylfurfural.

Memoria que presenta Dña. Mercedes Moreno Recio para optar al Grado de Doctor.

Málaga, 30 de Agosto de 2022

DIRECTORES

D. Pedro J. Maireles Torres

MAIRELES TORRES PEDRO JESUS - Firmado digitalmente por MAIRELES TORRES PEDRO JESUS Fecha: 2022.08.28 18:59:50 +02'00'

Catedrático de Universidad
Departamento de Química Inorgánica, Cristalografía y Mineralogía.
Universidad de Málaga

D. Ignacio Jiménez Morales

Jiménez Morales Ignacio- Firmado digiltamente por Jiménez Morales Ignacio- el día 28/08/2022

Ayudante Doctor

Departamento Química Inorgánica.
Universidad de Salamanca

DECLARACIÓN DE AUTORÍA Y ORIGINALIDAD DE LA TESIS PRESENTADA PARA OBTENER EL TÍTULO DE DOCTOR

Dña. Mercedes Moreno Recio, estudiante del programa de doctorado QUÍMICA Y TECNOLOGÍAS QUÍMICAS. MATERIALES Y NANOTECNOLOGÍA de la UNIVERSIDAD DE MÁLAGA, autora de la Tesis presentada para la obtención del título de Doctor por la Universidad de Málaga, titulada:

SOLID ACID CATALYSTS FOR THE DEHYDRATION OF HEXOSES TO 5-HYDROXYMETHYLFURFURAL

Realizada bajo la tutorización y dirección del Dr. D. Pedro Jesús Maireles Torres y la codirección del Dr. D. Ignacio Jiménez Morales,

DECLARO QUE:

La tesis presentada es una obra original que no infringe los derechos de propiedad intelectual ni los derechos de propiedad industrial u otros, conforme al ordenamiento jurídico vigente (Real Decreto Legislativo 1/1996, de 12 de abril, por el que se aprueba el texto refundido de la Ley de Propiedad Intelectual, regularizando, aclarando y armonizando las disposiciones legales vigentes sobre la materia), modificado por la Ley 2/2019, de 1 de marzo.

Igualmente asumo, ante a la Universidad de Málaga y ante cualquier otra instancia, la responsabilidad que pudiera derivarse en caso de plagio de contenidos en la Tesis presentada, conforme al ordenamiento jurídico vigente.

En Málaga, a 30 de agosto de 2022.

Fdo. Mercedes Moreno Recio Doctorando.	MORENO RECIO MERCEDES - Firmado digitalmente por MORENO RECIO MERCEDES Fecha: 2022.10.23 22:16:21 +02'00'
Fdo. Pedro Jesús Maireles Torres. Tutor y Director.	MAIRELES TORRES PEDRO JESUS - Firmado digitalmente por MAIRELES TORRES PEDRO JESUS - Fecha: 2022.10.23 20:06:54 +02'00'
Fdo. Ignacio Jiménez Morales. Director.	Jiménez Morales Ignacio- Firmado digiltamente por Jiménez Morales Ignacio- el día 23/10/2022 11:20:00

Success is not final, failure is not fatal:
it is the courage to continue that counts.

Winston Churchill

Aunque he dejado la parte de AGRADECIMIENTOS para el final, podría haberlos escrito al inicio, ya que a todos los que doy las gracias y a todos los que me acompañáis en mi vida en general, tengo que reconoceros el apoyo, el aliento y la paciencia para llegar hasta aquí y concluir una etapa importante de mi vida. El periodo que pasé trabajando sobre esta Tesis, no solo fue tiempo de aprendizaje y enriquecimiento, también de conocer gente maravillosa, tener dos hijos más y, sobre todo, fui muy FELIZ.

Agradezco a Pedro Maireles Torres su generosidad, apoyo y paciencia, su trabajo constante, su escucha activa, su capacidad de facilitarnos el trabajo a todos, su labor como director del Departamento, su minúsculo despacho para dejarnos una sala a los estudiantes. Su calidad como profesor es sólo superable por su calidad humana.

A Enrique Rodríguez Castellón, que me cogió de la mano, me animó no sólo a acabar la Carrera, no sólo a realizar un Máster, sino incluso a realizar la Tesis. Confió en mi desde que me dio clase allá por 1997, hace 25 años. Me apoyó académica y laboralmente, y, sobre todo, me trató como una hija. Gracias por ofrecer siempre una silla junto a la tuya en el despacho Gracias a Estrella y a Elena. Gracias, familia, porque así os siento.

A Antonio Jiménez-López y a Ignacio Jiménez Morales, Nacho, que comenzaron junto a mi este camino, aunque siguió en la distancia. A ti, Nacho, enhorabuena por lo que estás consiguiendo junto a esa familia maravillosa que has formado, como la formaron tus padres. Gracias y mucha suerte.

A José Santamaría por su gran ayuda en el trabajo de laboratorio, sus explicaciones, su simpatía y su sonrisa.

A Ramón Moreno por responder siempre paciente y amablemente mis dudas, y compartir charlas sobre Cabo de Gata.

A Antonia Infantes, Toñi, por su constante ayuda personal y académica, su compañerismo, su tenacidad, su escucha. Tu fortaleza es un ejemplo para mí.

A Carmen Ruíz, mi amiga Carmen, por estar siempre ahí. Te conocí en 1995, eras la mejor de la promoción, y no sólo por las notas, es que eras la mejor persona de todos, y lo sigues siendo. He tenido la suerte de sentir tu sonrisa sincera y tu buen corazón.

A Paco, Maroto, Carlos, Tomás, María Ángeles, Conchi y, en especial, a Nani y Ramiro, por ayudarme a reconciliarme con mi pasado, y abrirme las puertas del departamento.

A mis compañeros Lucía, Jose, Elena, Carmen Ana, Montse, Marta, María José, Cristina, Juan, Inma… y en especial a Rosario y Diana. Siempre me ayudasteis, me enseñasteis, compartisteis, me hicisteis reír, me hicisteis los regalos más originales a mí y a mis hijos, me tratasteis como una más, y… os sigo echando de menos. Suerte, mucha, a todos.

Y especialmente a mi marido Jesús que no sólo me apoya siempre, me escucha y me anima, no sólo tiramos de una familia de siete. Él me hace mejor persona. Y a mis hijos Martín, Rodrigo, Gonzalo y Catalina, que llenan cada día de mi vida. Con vosotros, La Vida es Bella.

GRACIAS

Table of Contents

Table of Contents

6. Results and Discussion

Abstract

1. Abstract

The increasing oil prices and the diminishing fossil fuel reserves, as well as the growing concern about environmental and specially about global warming, have made necessary the search of new sustainable sources of energy and products from renewable materials. Wind power, ocean and hydropower energies, solar energy, biofuels, biomethane and biomass are together needed. Biofuels are the alternative to fossil fuels for transportation. Biomethane is a renewable substitute of natural gas. Biomass, derived from organic material, from trees, plants, and agricultural and urban waste, is, as coal and oil, an available carbon source, constituting renewable alternative resources for energy, transport fuels, and chemicals. Biomass consists of, among others, carbohydrates, lignin, fatty acids and lipids. Its chemical composition is mainly cellulose, hemicellulose and lignin. Cellulose, a polysaccharide of glucose units is the most abundant. Lignocellulosic biorefineries breaks down biomass into different types of component carbohydrates, and the most important sugar platforms are mainly based on cellulose, starch, glucose and fructose. Firstly, biomass pretreatment is needed, modifying the physical and chemical properties of the plant cell wall, so that cellulose and hemicellulose can be converted into fermentable carbohydrates. After pretreatment, the polysaccharides are hydrolyzed to yield monomeric pentoses and hexoses, such as glucose, fructose and xylose. Finally, through fermentative or catalyzed chemical processes, monosaccharides are transformed into platform molecules.

Glucose is an important feedstock for the production of green platform chemicals. By glucose catalytic oxidation, many acids and

keto acids can be produced, as gluconic acid or formic acid. Through catalytic hydrogenation of biomass-derived sugars, many alcohols are yielded, mostly xylitol, sorbitol and mannitol. From sugar catalytic dehydration, hexoses produce 5-hydroxymethylfurfural (HMF), which can also be transformed into levulinic (LA) and formic (FA) acids. Similarly, pentoses dehydration leads to furfural through dehydration. With respect to biofuels, HMF is solid at room temperature and has poor fuel properties and, therefore, it is not useful as biofuel or a biofuel additive. However, furan derivatives are being studied for biofuel applications. As chemicals, HMF and LA have been identified as two of the top 12 bio-based platform chemicals by the United States Department of Energy. The reaction pathways for LA and HMF production are similar, because HMF is the intermediate for LA formation, as previously mentioned. HMF has numerous industrial applications, as it can be converted into 2,5-furandicarboxyl acid, 2,5-dihydroxymethylfuran or 2,5-bis(hydroxymethyl)tetrahydrofuran, among others. These molecules are considered as important building blocks to produce polyesters, and other chemicals by oxidation, hydrogenation, hydrogenolysis or aldol condensation.

The synthesis of HMF is based on the acid-catalyzed consecutive triple dehydration of glucose and fructose, although sucrose, cellobiose or inulin, as well as industrial wastes can be used after depolymerization. Not only HMF is produced from this acid-catalyzed dehydration, but also other products, such as levulinic and formic acids and degradation products because of side reactions, can be formed. Sugar dehydration chemistry is complex, and many aspects must be considered for acceptable yields. Thus, a specific pathway for the synthesis of HMF and derivatives has not yet been determined

from hexoses; on the contrary, two dehydration general pathways have been proposed: acyclic and cyclic mechanisms. Proposed acyclic and cyclic pathways require the isomerization of glucose to fructose before the dehydration, but other mechanisms not involving fructose have been suggested. HMF is soluble in water and in common organic solvents. Water is preferred as solvent for the production of HMF, but HMF yields are low compared to organic solvents. The use of biphasic water/organic solvent systems has become a strategy because the use of a single liquid phase system needs extracting the dehydration product and isolating it into a second liquid phase, increasing the operational and economic costs. The addition of organic solvents as a second phase leads the reaction towards higher yields, because the HMF rehydration, decomposition and/or condensation owing to side reactions are avoided. Solvents, such as toluene, 2-butanol, dimethylsulfoxide (DMSO), or tetrahydrofuran (THF), derived from petroleum, and 1-butanol or cyclopentyl methyl ether (CPME), which are "green solvents", have been employed for this reaction. Methyl isobutyl ketone (MIBK) has also been largely reported as efficient solvent for glucose dehydration. Not only the efficient HMF extraction (high partition coefficient) is a goal, but also the ease separation of HMF from the organic solvent before to be supplied to a subsequent processing.

The production of HMF from saccharides has been widely reported and many mineral acids have been used as homogeneous catalysts, achieving high HMF yields, but the use of these involves several important drawbacks, such as toxicity, corrosion, catalyst waste generation, large amount of catalyst and difficult separation operations. Therefore, their replacement by solid acids is preferred

from an environmental and economic point of view. Porous materials, with high surface areas, narrow pore size distributions and tunable pore diameter, are suitable for catalyst, adsorption or separation processed. They can be classified as macroporous, mesoporous and microporous, with pores wider than 50 nm, in the range 2-50 nm or narrowest than 2 nm, respectively. Macroporous materials are not as useful as catalysts as micro and mesoporous materials. Microporous catalysts are mainly zeolites, $AlPO_4$ (aluminophosphates), carbons, clays or metal organic frameworks (MOFs). Mesoporous solids as OMMs (ordered mesoporous materials) are very useful due to their homogenous mesoporosity, large pore size, high surface area, and mesoporous channels. Mesoporous material synthesis is mostly based on organic template molecules as structure-directing agents around which the precursor condenses. After condensation, the organic template is removed by extraction or calcination, resulting in the mesopore structure. The control of the local environment and morphology during the synthesis allows to obtain OMMs with different properties depending on the catalytic requirements. One of the interesting features of ordered mesoporous solids for catalysis is the large spectrum of possibilities to modify them. Since hydrothermal stability has been demonstrated as essential for applications of mesoporous materials in catalysis, several approaches have been developed to improve it, such as the addition of salts during the hydrothermal synthesis, the modification of the surface by silylation or post-synthesis grafting of inorganic compounds to increase the wall thickness and/or to chemically stabilize the wall surface of the mesoporous structures.

Many catalyzed reactions are acid-specific, as sucrose decomposition into glucose and fructose, others are base-specific, such as biodiesel from triglycerides and many others are catalyzed by both acids and bases under acid-base catalysis, as transformation of biomass-derived furanic compounds into chemicals. With respect to the active acid sites of catalysts, they are mainly classified into Brönsted and Lewis type. Regarding the glucose dehydration to HMF, it is assumed that catalysts acting as basic or Lewis acids facilitate glucose to fructose isomerization and ones acting as Brönsted acid promote glucose dehydration to HMF and side reactions. Bifunctional catalysts are therefore needed. Thus, several heterogeneous catalysts have been reported for HMF formation.

In general, HMF production from fructose, glucose or lignocellulosic biomass have been performed in lab scale. Thus, batch stirred reactors and continuous reactors have been used for HMF formation in mixed solvent systems. Nevertheless, HMF production starting from sugar cane or fructose have been performed in pilot scale. HMF production from sugars for biofuels is not profitable but producing directly from lignocellulosic biomass would be on the right path.

In this work, microporous and mesoporous solids were synthesized and/or modified to obtain porous materials with suitable textural and acid properties to enhance their activity in glucose dehydration to HMF: mesoporous tantalum oxide; mesoporous Al-doped MCM-41 and KIT-6 silica with different Si/Al ratios; ZSM-5, Y and Beta zeolite in protonated form and also as ion-exchanged with iron or copper cations; and phosphorus-containing activated carbons derived from olive stone (HA series) or lignin (L series). Mesoporous tantalum

oxide and silica-based materials were synthesized by different methods. Commercial zeolites (Zeolyst International) were post-synthesis modified to enhance their acidic properties. Porous carbons were provided by the group of Prof. T. Cordero (Dep. Chemical Engineering, University of Málaga). After catalyst preparation, their physico-chemical characterization was carried out through different techniques and analysis: X-ray diffraction (XRD), X-ray photoelectron spectroscopy (XPS), differential thermal analysis and thermogravimetry (DTA-TG), nitrogen sorption at -196 ºC, temperature-programmed desorption of ammonia (NH_3-TPD), pyridine adsorption coupled to FT-Infrared spectroscopy (Pyr-FTIR), solid-state nuclear magnetic resonance (MAS-NMR) and elemental analysis (CHNS/O). The characterization provided data of structural and morphological properties, chemical composition, total acidity and strength and types (Brönsted and Lewis) of acid sites, thermal, physical and chemical stabilities.

Once characterized, the solids were tested in the glucose dehydration to HMF. All the catalytic experiments were performed in 15 mL thick-walled glass reactors at temperatures in the range 155-195 ºC. Standard experiment consisted of 1.5 mL of an aqueous phase composed of hexose (glucose or fructose, 10 wt.%) combined with 3.5 mL of an extracting solvent, and 50 mg of catalyst. After reaction, mixture samples analyses were performed by means of high performance liquid chromatography (HPLC), providing reactant conversion, selectivity, and yield of products.

Mesoporous tantalum oxide was synthesized by acid hydrolysis of tantalum penta-ethoxide in the presence of a triblock co-polymer

Pluronic L-121, a non-ionic surfactant, at room temperature and subsequent calcination at 550 °C for 6 h. The XRD patterns of the mesoporous Ta_2O_5 revealed its amorphous structure, not being detected any crystalline phase of the tantalum oxide. A thermodiffraction study was undertaken between room temperature and 1000 ºC, although its catalytic performance was tested up to 200 ºC. Up to 500 ºC, diffractograms do not change, but above 600 ºC, narrow and well defined diffraction peaks, corresponding to an orthorhombic structure, are clearly visible. The use of templates with high molecular weight such us Pluronic® P-123 led to thicker pore walls with ordered mesostructures during the synthesis procedure. The catalyst exhibited a N_2 adsorption-desorption isotherm of Type IV(a), typical of mesoporous solids, in which hysteresis is associated to capillary condensation. (DFT) method was used to calculate the pore size distribution, which resulted to be extended from 2 to 6 nm. The solid exhibited a suitable specific surface area (79 $m^2\ g^{-1}$) and the surface composition determined from XPS data was close to the stoichiometric composition of Ta_2O_5. The core level regions of Ta *4f* and O *1s* confirmed the oxidation states expected of the tantalum oxide. Ammonia-TPD data (353 μmol $NH_3\ g^{-1}$) confirmed that the acidity of this catalyst was mainly originated by the presence of coordinated water molecules and coordinated OH groups to tantalum ions. The symmetry and oxidation state of the tantalum cation determined the acidic properties, and the catalyst exhibited both Brönsted and Lewis acid sites. The acidity was initially associated to water molecules and OH groups coordinated to tantalum ions, as Brönsted type acid sites, but Brönsted acid sites partially transformed into Lewis acid sites. This mesoporous Ta_2O_5 demonstrated to be

active as heterogenous catalyst in the dehydration of glucose to 5-hydroxymethylfurfural (HMF), in a biphasic system consisting of water/methyl-iso-butyl ketone (MIBK). By using a glucose/catalyst (S/C) weight ratio of 3:1, a glucose conversion of 69% and a HMF yield of 23% were achieved at 175 °C after 90 minutes. The catalytic process was selective towards HMF, which was preserved from ulterior hydration to levulinic acid, which was not detected. Fructose, from glucose isomerization, was also produced with a selectivity of 14%. The detection of fructose, mostly at lower temperatures, agreed with a two-stages process, with a first step in which glucose isomerized into fructose and a second step in which fructose was dehydrated to HMF. Nevertheless, a direct dehydration from glucose to HMF was also possible. The glucose to fructose isomerization was carried out on Lewis acid sites, whereas the dehydration occurred on Brönsted acid sites. After treatment with a KOH solution to reduce the acidity, the catalyst converted 15% less glucose and the HMF selectivity was 8% lower, showing the participation of Brönsted acid sites in the reaction. The catalyst was also tested by using HMF as reactant, under similar experimental conditions (biphasic water/MIBK system, 175 ºC, 90 minutes), and after reaction, levulinic or formic acid were not detected, and HMF was totally recovered, showing mesoporous Ta_2O_5 a low Lewis acidity to convert HMF. In addition, the surface acidity was modified by treatment with phosphoric acid, and after 120 minutes at 175 ºC, glucose conversion and HMF selectivity were improved, whereas fructose selectivity decreased. Mesoporous tantalum oxide was thermally and chemically stable, since no leaching of tantalum species to the liquid phase was detected. By increasing the amount of catalyst (lowering the substrate/catalyst

(S/C) weight ratio), glucose conversion and HMF yield did not increase linearly, due to diffusional limitations. The used catalyst, after a regeneration by thermal treatment at 550 ºC, showed similar activity than the fresh catalyst in a second reaction cycle, but without any treatment, glucose conversion drastically dropped. Thus, the lifetime of this catalyst with suitable catalytic activity, under the experimental conditions used in the present work, was only 1 cycle.

Mesoporous aluminum-doped MCM-41 silica catalysts with different Si/Al molar ratios (5 and 10) were prepared by a sol–gel method in two reaction steps (acid and alkaline hydrolysis) from joint hydrolysis of tetraethylortosilicate (TEOS) and aluminum triisoproxide, using n-dodecylammonium chloride as surfactant, at room temperature, and subsequent calcination at 550 °C. The XRD patterns confirmed the hexagonal structure and amorphous silica walls without crystalline phases. Nitrogen adsorption-desorption isotherms at -196ºC were Type IV(a), typical of mesoporous solids, and pointed out the existence of wide pores, which were confirmed by DFT analysis, resulting larger in 10Al-MCM-41 than in 5Al-MCM-41. BET surface areas increased with the amount of aluminum, from 587 to 734 $m^2 g^{-1}$ for 10Al-MCM-41 and 5Al-MCM-41, respectively. Ammonia-TPD and Pyr-FTIR spectra showed strong acidity with the presence of both Lewis and Brönsted acid sites, remaining even after pyridine evacuation at 300 ºC, mainly in 10Al-MCM-41. Brönsted acid sites, associated to silanol and isolated Si(OH)Al hydroxyl groups, were mainly responsible for the total acidity. XPS and ^{27}Al NMR data showed octahedral and tetrahedral aluminum species, because although both materials possessed aluminum well incorporated into the siliceous structure, some aluminum remained on the external

surface, as aluminum oxide, especially in 5Al-MCM-41, with higher aluminum content. By using a biphasic water/MIBK system and 10Al-MCM catalyst (30 wt.%), at 195 ºC, 87% of glucose conversion and 36% of HMF yield were achieved after 150 minutes. The reaction was quite selective towards HMF, not finding levulinic acid or furfural, and also fructose as byproduct. 5Al-MCM-41, under the same conditions, displayed a reduced effectiveness, perhaps due to its lower acidity, more extra-framework aluminum and a higher proportion of micropores which render difficult the accessibility of reactants to acid sites. The use of a sodium chloride aqueous solution (20 wt.%) instead of pure water, as aqueous phase, ameliorated the partition coefficient between the organic and the aqueous phases up to 1.9, leading to an enhancement of glucose conversion and HMF yield, attaining values of 98 and 63%, respectively, and shortening the reaction time to 30 minutes. The catalytic performance of 10Al-MCM-41 was well maintained after three catalytic cycles. The increasing fructose selectivity in subsequent reaction cycles corroborated that glucose isomerization to fructose is the limiting step.

Three similar methods of synthesis were followed for the preparation of KIT-6-type mesoporous silica materials (KIT6-A, KIT6-B and KIT6-C). For A and B types, Pluronic P-123, as template, and hydrochloric acid were employed, and n-butanol as solvent. A-type was stirred at 35 ºC for 24 hours after the addition of TEOS (tetraethyl orthosilicate), while B-type was longer stirred, 72 hours. After calcination at 550 ºC, KIT6-A and KIT6-B were obtained. KIT6-C used isopropanol instead of n-butanol as solvent, and, after TEOS addition, it was stirred for 36 hours. Concerning the XRD data and textural characterization, KIT6-C was chosen to be modified by

two different post-synthesis treatments to incorporate aluminum in order to enhance the acidity and consequently the catalytic activity. The first post-synthesis method used an aluminum chloride solution in dry ethanol, and, in the second one, tetramethylammonium hydroxide (TMAOH) instead of ethanol. Different synthesis conditions led to two aluminum-doped KIT6 solids: Al-KIT6-C1 and Al-KIT6-C2. These materials did not show structural changes after the heteroatom incorporation. XPS and XRF analysis found scarcity of Al in Al-KIT6-C1, whereas a Si/Al ratio close to that used in the synthesis step was found for Al-KIT6-C2. In this solid, as much tetrahedral framework aluminum (Al^{T}) as octahedral non-framework aluminum (Al^{O}) were confirmed with MAS-NMR data. Thus, only Al-KIT6-C2 evidenced a high degree of aluminum incorporation due to the most effective synthesis procedure, and only this solid was used for the catalytic study. In this Al-doped KIT6 catalysts, aluminum was located mostly on the surface, whereas it was mostly detected in the mesoporous structure of 10Al-MCM-41, giving rise to a more disorder structure than in KIT6-based materials. Thus, Al-KIT6-C2 was tested as catalyst under similar experimental conditions than 10Al-MCM-41, providing a high selective towards HMF but a low activity in glucose conversion, due mainly to its lower acidity. Considering both, strength and amount of acid sites, among the mesoporous catalysts employed in the present work, 10Al-MCM-41 could be considered the more acidic, followed by mesoporous tantalum oxide and 5Al-MCM-41, prior to Al-KIT6-C2. Moreover, at longer reaction times, the deactivation of the catalyst occurred due deposits of reaction byproducts, without any acid properties variation observed.

Three protonated zeolites (H-ZSM-5, H-Y and H-Beta) were prepared from commercial zeolites through calcination of their ammonium forms at 550 ºC. ZSM-5 is a MFI-type zeolite with an intersecting and three-dimensional channel system, with a high Si content. Thus, the precursor of H-ZSM5-15 possessed a Si/Al ratio of 15. Y zeolite, FAU zeolites type, possesses large internal cavities, named supercages, linked tetrahedrally through pore openings. Their Si/Al molar ratio are low and can be increased by dealumination. The precursor of H-Y-6 possessed a Si/Al ratio of 6. Beta zeolites, with a BEA structure, has a complex framework consisting of two intergrown structures, both containing a three-dimensional network of pores. It can be synthesized with high Si/Al molar ratios, in the range 10-100. The precursor of H-Beta-12.5 catalyst possessed a Si/Al ratio of 12.5. The zeolites exhibited Type I isotherms from nitrogen sorption at -196ºC, but whereas ZSM-5-type materials presented a H3 hysteresis loop due to aggregates of particles, which creates medium and wide sized cavities, Y-type materials showed a H4 hysteresis loop, typical of zeolites with micro and mesopores. ZSM-5 and Beta zeolites are considered shape selective due to their particular structures. H-Beta zeolite-based materials showed lower crystallinity then the other zeolite, associated with the presence of structural defects caused by the incorporation of aluminum species. The values of total acidity of protonated zeolites were much higher than those of mesoporous catalysts, although the surface density of adsorbed ammonia was similar and even the maxima desorption temperatures. H-ZSM5-15 acidity was originated by bridging hydroxyl groups, besides aluminum atoms. These protonated zeolites were tested in glucose dehydration to HMF under the same experimental conditions used for 10Al-MCM-

41, in order to assess the influence of textural and acid properties on the catalytic performance. Thus, dehydration process was carried out in a biphasic water/methyl-isobutyl ketone (MIBK) system, at 195 ºC. H-Beta-12.5 and H-Y-6 attained glucose conversion higher than that attained using 10Al-MCM-41, but lower fructose selectivity. However, the highest HMF selectivity of H-zeolites was lower than that of MCM-41-based catalyst, and it was achieved with H-Beta-12.5, due to its Lewis and Brönsted acid sites, a moderate-strong acidity, and overall, the important developed mesoporosity. These results pointed out the key role of textural properties in determining the catalytic performance of porous acid solids in glucose/fructose dehydration reactions. The addition of NaCl (20 wt.%) to the aqueous phase enhanced HMF selectivity and yield. Using the H-Beta zeolite in a NaCl aqueous solution/MIBK, at 195 °C, a high HMF yield, close to that obtained with 10Al-MCM-41, was achieved after only 30 minutes. Lower improvements were reached by using H-ZSM-5 and H-Y, demonstrating the positive effect of mesoporosity in the dehydration of glucose to HMF. The formation of undesirable products, which diminished the HMF, was observed in every reaction, even at lower reaction temperatures or shorter reaction times. Polymeric species from carbohydrates and HMF condensation are formed on Lewis acid sites, whereas degradation products of HMF are generated on Brönsted acid sites. Levulinic acid was not detected in any case. The influence of the organic phase was studied and its role in the HMF extraction, favoring the equilibrium towards the formation and also preventing from subsequent degradation reactions, was confirmed. In the absence of organic phase, a HMF yield lower than 4% was achieved due to rehydration of the formed HMF, which was

evidenced by the identification of levulinic acid in the reaction mixture. The role of others alkaline salts was also evaluated, confirming that the most positive effect was mainly due to sodium cations. Notably, NaCl in MFI-type zeolites, as ZSM-5, enhances the hydrolysis of Si–O–Al bridges, releasing Al^{3+} species which catalyze the conversion of glucose through a homogeneous catalytic process. The addition of $CaCl_2$ to the aqueous phase showed a different behavior. Even in the absence of catalyst, a high activity was observed, pointing out that this salt can be involved in glucose isomerization, which seemed to occur very fast, as well as in sugar dehydration. Different salts have promoted the glucose/fructose dehydration to HMF, but the cause and the effect were not only related to their respective ions, but also to the particular interactions with each catalyst and to the specific reaction conditions.

The introduction of heteroatoms in the zeolites modifies the nature and strength of the acidity, as a function of the number, coordination and framework position of these heteroatoms. Iron and copper were introduced by post-synthesis methods into the three zeolites, by ion-exchange treatment in order to modify their acidic properties. After iron and copper incorporation in ZSM-5 zeolite, followed by thermal treatment at 550 ºC, the structure stayed well preserved, as was deduced from XRD, with the cations preferently in extra-framework positions. Although the incorporation of iron into zeolites reduces the specific surface area and micropore volume due to the partial blockage of pores by iron species, in Beta zeolite, an increase was observed due to the presence of iron aggregates. The Si/Al ratio of Fe- and Cu-ZSM5-15 differed from that, H-ZSM5-15, but in opposite ways: while the aluminum content decreased on the surface of Fe-ZSM5-15, in

Cu-ZSM-15, it was enhanced, pointing out different preferential location of these cations after ion-exchange and calcination stages. MAS-NMR data of ZSM-5 zeolites revealed the presence of both tetrahedrally and octahedrally coordinated aluminum atoms, mostly tetrahedral, which corresponded to framework species. In H-Y-6, the framework Si/Al ratio was close to the synthesis ratio, and 73% of the aluminum was in the zeolitic framework. In Beta zeolites, the surface Si/Al atomic ratio resulted to be very similar to the synthesis ratio in the protonated form, although higher in the iron-exchanged zeolite and lower in the copper-exchanged one. Fe *2p* and Fe *3p* core level spectra (XPS data) of the iron-containing zeolites suggested a partial oxidation of Fe(II) to Fe(III) during the post-synthesis treatment. Si/Fe atomic ratios increased with the Si/Al ratio, as expected, thus the zeolite with the highest aluminum content, also possessed the highest iron content, Fe-Y-6, and Fe-ZSM5-15 had the lowest iron content. Regarding copper-based zeolites, Cu $2p_{3/2}$ (XPS) confirmed the presence of Cu(II), although Cu LMM Auger spectra also indicated the presence of Cu(I), which could be produced by photo-reduction during the X-ray exposure, but, in the case of Cu-ZSM5-15, could be caused by the interactions between Cu cations and the zeolite structure. There was a noticeable difference between copper- and iron-exchanged zeolites: the enrichment of aluminum on surface compared to the respective precursors, which were probably due to aluminum gradients from the inner to outer regions of zeolites. In cation-exchanged ZSM-5 zeolites, the acid sites kept constant, but diminished in Y and Beta zeolites. In ZSM-5 zeolites, the modifications of Brönsted acid sites stronger than Lewis ones, and, mostly, the Al atoms, were responsible for the acidity. Although ammonia-TPD

showed similar total acidity for H-, Fe- and Cu-ZSM5-15 catalysts, they possessed different acidity patterns. In cation-exchanged Beta zeolites, iron introduction lowered the total acidity and the strength, whereas copper notably increased the Lewis acidity, although diminished their strength. These data showed that it is feasible to modify the nature of acid sites of zeolites by thermal or ion-exchange treatments. The resulting acid zeolites demonstrated to be active in glucose dehydration. The influence of different experimental variables, such as reaction time and temperature, substrate: catalyst weight ratio, volume of the organic solvent and aqueous phase, as well as the density and nature of acid sites, on the catalytic behavior was investigated. Fe-and Cu-ZSM5-15 led to higher glucose conversion and HMF yields, lowering fructose selectivity, and thus, improving over the H-ZSM5-15 activity. Fe-Y-6 and Fe-Beta-12.5 enhanced the catalytic activity in comparison with the H-forms, although not as much as in ZSM-5 catalysts. H-ZSM5-15 was calcined for regeneration prior to reutilization, and a surface aluminum enrichment was produced due to the generation of extra-framework aluminum, modifying the active sites with respect to the fresh catalyst. These changes gave rise to higher glucose conversion, but lower HMF and higher fructose as reaction products, confirming the role of the acidity type in selectivity. The performance in a second catalytic cycle of H-Beta-12.5, which exhibited a similar activity than 10Al-MCM-41, was nevertheless far from the activity of 10Al-MCM-41, under similar experimental conditions. Regenerated Fe-Beta-12.5 lost much activity in a second catalytic cycle due to the decrease in acid sites because of iron removal. Also regenerated Cu-Beta-12.5 showed a different

behavior in a second catalytic cycle, due to partial dealumination, with detrimental consequences.

Two groups of acidic porous carbons, prepared from olive stones (HA-series) and from commercial lignin (L-series) were activated through a chemical treatment with phosphoric acid to obtain acidic catalysts: HA3500, 31500 and 31800, and L3500, 31500 and 31800. the labels 500 and 800 indicated the activation temperature. L31500 and HA31500, prepared by using similar impregnation method and ratio, resulted to be the most acidic samples, followed by HA3500 and L3500. The thermal treatment at 800 ºC during the synthesis did not improve the acidity and leading to lower acidity than samples activated at 500 ºC in their respective series (HA- or L-). Firstly, they were compared with 10Al-MCM-41 and zeolites, under similar experimental conditions, in glucose dehydration to HMF. No fructose and higher HMF selectivities than glucose conversion values were detected as a general trend. The highest activation temperature (HA31800 and L31800), the lowest activity. The -31500 carbons resulted the most selective to HMF, due to their largest surface area and wider micropores surface, with small micropores which limited the HMF degradation reactions, and a high porosity in combination to weak and medium acid sites. Glucose conversion was maximal by using L3500 and HA3500, associated to stronger Brönsted acid sites. As fructose were not detected, HA3500 was also studied for the HMF production directly from fructose. The results suggested a different mechanism for glucose conversion by using these carbon-based catalysts than by using the other reported catalysts. In this case, glucose would not isomerize to fructose previously to the dehydration of the sugar to HMF and be dehydrated through other intermediates. L3500 catalyst,

under identical reaction conditions, provided similar glucose conversion than H-ZSM5-15 catalyst and similar HMF selectivity than 10Al-MCM-41. Therefore, L3500 catalysts combine the advantage of the other two catalysts but from the economic and environmental point of view, as it has been obtained from biomass wastes, it would be preferred. These data highlight that the catalytic activity is determined by textural and acidic properties. The influence of the proportion of MIBK in the reaction medium was also studied in order to use as much lower amount as necessary, confirming an optimum ratio the one used in the other reactions, with 70 vol.% of MIBK in the reaction medium. As calcium chloride notably improved the activity in 10Al-MCM-41 and zeolites, it was introduced in the aqueous phase and tested with the acidic carbons as catalysts. Glucose conversions were doubled, although HMF selectivity was slightly increased. Cyclopentylmethyl ether (CPME), an eco-solvent, previously tested as MIBK substitute with 10Al-MCM-41, was also tested with HA31500, reaching higher glucose conversion after 90 minutes, but much lower HMF selectivity due to the lower partition coefficient. By using this solvent, furfural was detected as reaction product besides HMF. The presence of strong Brönsted acid sites together with Lewis acid sites, favored not only HMF but also furfural formation. A mechanism through 3-deoxyglucosone as key-intermediate, would be responsible, as it can be twice dehydrated to HMF, but it can also form furfural. CPME, with a lower partition coefficient, would be able to enable both reactions, although favoring HMF *versus* furfural. The formation of byproducts, such as, humins was also observed in the reaction medium when the acidic carbons were used as catalysts. In a second catalytic cycle, without any

treatment for regeneration, HMF selectivity decreased due to the deposition of byproducts, blocking active sites.

Resumen

2. Resumen

El aumento de los precios del petróleo y la disminución de las reservas de combustibles fósiles, así como la creciente preocupación por el medio ambiente y especialmente por el calentamiento global, han hecho necesaria la búsqueda de nuevas fuentes sostenibles de energía y productos a partir de materiales renovables. La energía eólica, las energías oceánicas e hidroeléctricas, la energía solar, los biocombustibles, el biometano y la biomasa son necesarios en conjunto. Los biocombustibles son la alternativa a los combustibles fósiles para el transporte. El biometano es un sustituto renovable del gas natural. La biomasa, derivada de la materia orgánica de árboles, plantas y residuos agrícolas y urbanos, es, como el carbón y el petróleo, una fuente de carbono y constituye un recurso alternativo renovables de energía, de combustibles y de productos químicos.

La biomasa se compone, entre otros, de hidratos de carbono, lignina, ácidos grasos y lípidos. Su composición química es principalmente celulosa, hemicelulosa y lignina. La celulosa, un polisacárido de unidades de glucosa, es el más abundante. Las biorrefinerías lignocelulósicas descomponen la biomasa en diferentes tipos de carbohidratos y las plataformas de azúcares más importantes de las biorrefinerías están basadas principalmente en celulosa, almidón, glucosa y fructosa. En primer lugar, es necesario un pretratamiento de la biomasa, modificando las propiedades físicas y químicas de la pared celular de la planta para que la celulosa y la hemicelulosa puedan ser fermentables. Después del pretratamiento, los polisacáridos se hidrolizan para producir pentosas y hexosas monoméricas, como glucosa, fructosa y xilosa. Finalmente, a través de vías químicas de

fermentación o catálisis, los monosacáridos se transforman en moléculas plataforma.

La glucosa es una materia prima muy importante para la producción de productos químicos. Así, mediante oxidación catalítica, se producen ácidos y cetoácidos como ácido glucónico o ácido fórmico. A través de la hidrogenación catalítica de azúcares derivados de la biomasa, se forman alcoholes, principalmente, xilitol, sorbitol y manitol. A partir de la deshidratación catalítica de los azúcares, las hexosas producen 5-hidroximetilfurfural (HMF), que también se puede transformar en ácido levulínico (LA) y ácido fórmico (FA). Del mismo modo, la deshidratación de pentosas conduce a furfural mediante deshidratación.

Con respecto a los biocombustibles, el HMF es sólido a temperatura ambiente y tiene propiedades de combustión deficientes y, por tanto, no es útil ni como biocombustible ni como aditivo. Sin embargo, los derivados furánicos se están investigando para su aplicación como biocombustibles. En cuanto a su utilización para obtener productos químicos, HMF y LA han sido identificados como dos de los 12 principales bioproductos químicos plataforma por el Departamento de Energía de los Estados Unidos. Las vías de producción de LA y HMF son similares porque el HMF es el intermediario para la formación de LA, como se mencionó anteriormente. El HMF tiene numerosas aplicaciones industriales, ya que se puede convertir en ácido 2,5-furandicarboxilo, 2,5-dihidroxi metil-furano o 2,5-bis(hidroximetil) tetrahidrofurano entre otros. Estas sustancias son importantes intermedios para producir poliésteres y otros productos químicos por oxidación, hidrogenación, hidrogenolisis o condensación de aldoles.

La síntesis de HMF se basa en la triple deshidratación consecutiva de glucosa y fructosa, aunque se puede utilizar sacarosa, celobiosa o inulina, así como desechos industriales, después de su despolimerización. No sólo se obtiene HMF en la deshidratación catalizada por ácidos, sino que también se obtienen otros productos de deshidratación como el ácido levulínico y el fórmico, así como otros productos de degradación, debido a la existencia de otras reacciones secundarias.

La química de deshidratación de los azúcares es compleja, y se deben tener en cuenta muchos aspectos para obtener rendimientos aceptables. Muestra de ello es el mecanismo de reacción. No se ha determinado una ruta específica para la obtención de HMF y derivados a partir de hexosas, sino que, por el contrario, se han propuesto dos vías generales de deshidratación, basadas en mecanismos acíclicos y cíclicos. Las vías acíclicas y cíclicas propuestas requieren la isomerización de la glucosa a fructosa antes de la deshidratación, pero también se han propuesto mecanismos que no involucran a la fructosa.

El HMF es soluble en agua y en disolventes orgánicos comunes. Aunque el agua sería el disolvente ideal por su bajo coste y no ocasionar contaminación, los rendimientos a HMF en reacciones con agua como único medio de reacción son bajos en comparación a los obtenidos en disolventes orgánicos. El uso de sistemas bifásicos se ha convertido en una estrategia adecuada porque el uso de una única fase líquida necesita extraer el producto de deshidratación y aislarlo en una segunda fase líquida, aumentando los costes operativos y económicos. Sin embargo, la adición de disolventes orgánicos como una segunda

fase conduce a mayores rendimientos a HMF porque evitan su rehidratación, su descomposición y/o su condensación en reacciones secundarias. Para esta reacción se han empleado disolventes como tolueno, 2-butanol, dimetilsulfóxido (DMSO) o tetrahidrofurano (THF), derivados del petróleo, y 1-butanol o ciclopentil metil éter (CPME), que son "disolventes verdes". La metilisobutil cetona (MIBK) también se ha utilizado como disolvente eficiente para la deshidratación de glucosa. La elección de la fase orgánica no debe basarse solo en la eficiencia en la extracción del HMF (alto coeficiente de partición), sino también en la facilidad de separación del HMF disuelto en la fase orgánica para su uso en un proceso posterior.

La producción de HMF a partir de sacáridos se ha evaluado ampliamente utilizando ácidos minerales como catalizadores homogéneos, logrando altos rendimientos de HMF, pero el uso de estas sustancias implica varios problemas como la toxicidad, la corrosión de equipos, el residuo que constituyen los catalizadores, las grandes cantidades necesarias, y las costosas operaciones de separación. Es por ello que se ha tendido a su sustitución por sólidos ácidos, mejores desde el punto de vista medioambiental y económico. Los materiales porosos, con elevadas áreas superficiales, estrecha distribución de tamaños de poro y diámetros de poro modulables, son muy adecuados para su uso como catalizadores, adsorbentes o para procesos de separación. Los sólidos porosos se pueden clasificar en macroporosos, mesoporosos y microporosos, con poros más anchos de 50 nm, en el rango 2-50 nm o menores de 2 nm respectivamente. Los materiales macroporosos no son tan útiles como catalizadores. Los catalizadores microporosos son principalmente zeolitas, $AlPO_4$ (aluminofosfatos), carbones, arcillas o compuestos metal-orgánicos

(MOFs). Los sólidos mesoporosos como los materiales ordenados mesoporosos (OMM) son muy útiles debido a su mesoporosidad homogénea, gran tamaño de poro, alta superficie y canales además de poros. La síntesis de estos materiales mesoporosos se basa principalmente en moléculas orgánicas que actúan como plantillas alrededor de las cuales se condensa el precursor. Después de la condensación, la plantilla orgánica se elimina por extracción o calcinación, quedando la estructura mesoporosa. El control del entorno local y de la morfología durante la síntesis permiten obtener OMMs con diferentes propiedades en función de los requerimientos catalíticos. Una de las características interesantes de los sólidos ordenados mesoporosos para catálisis es la multitud de posibilidades de modificación que ofrecen. Dado que la estabilidad hidrotermal es esencial para su uso como catalizadores, se han desarrollado modificaciones para mejorar esta estabilidad, como la adición de sales durante la síntesis hidrotermal, la modificación de la superficie por sililación o la inserción post-síntesis de compuestos inorgánicos para aumentar el grosor de las paredes y/o para estabilizar químicamente la superficie de las paredes de las estructuras mesoporosas.

Muchas reacciones catalíticas son ácido-específicas, como la descomposición de sacarosa en glucosa y fructosa. Otras son base-específicas, como la obtención de biodiésel a partir de triglicéridos. Y muchas otras son catalizadas por ácidos y bases conjuntamente, como la transformación de compuestos furánicos derivados de la biomasa en productos químicos. Con respecto a los sitios ácidos activos de los catalizadores, pueden ser de tipo Brönsted y de tipo Lewis. Con respecto a la deshidratación de glucosa a HMF, los catalizadores que actúan como ácidos de Lewis facilitan la isomerización de glucosa a

fructosa y los que actúan como ácido de Brönsted promueven la deshidratación de glucosa a HMF y las reacciones secundarias. No obstante, la reacción también se ha llevado a cabo empleando conjuntamente catalizadores básicos y ácidos, tanto homogéneos como heterogéneos, ya que también los sitios básicos promueven la isomerización de la glucosa y los ácidos favorecen las reacciones de deshidratación y condensación. Por lo tanto, se necesitan catalizadores bifuncionales. La deshidratación de hexosas a HMF se ha investigado utilizando una gran variedad de catalizadores heterogéneos.

La producción de HMF a partir de fructosa, glucosa o de biomasa lignocelulósica se ha realizado principalmente a escala de laboratorio, en reactores agitados tipo batch y en continuo, en sistemas de disolventes mixtos. También se ha llevado a cabo la producción de HMF a partir de caña de azúcar o directamente de fructosa a escala piloto. La producción de HMF a partir de azúcares directamente no es aún rentable, y se dirige a su obtención directamente a partir de biomasa lignocelulósica.

En este trabajo, se han sintetizado y/o modificado sólidos, tanto microporosos como mesoporosos, para obtener materiales porosos con propiedades texturales y ácidas adecuadas para potenciar la actividad de la reacción de deshidratación de glucosa a HMF: óxido de tántalo mesoporoso; materiales basados en sílices mesoporosas MCM-41 y KIT-6 con diferentes proporciones de Si/Al; zeolitas de tipo ZSM-5, Y y Beta, tanto en sus formas protonadas como con hierro o cobre, y carbones activados derivados del hueso de aceituna (serie HA) o lignina (serie L) con grupos funcionales de fósforo. El óxido de tántalo y los materiales a base de sílice se sintetizaron por diferentes

métodos. Las zeolitas comerciales (Zeolyst International) fueron modificadas mediante post-síntesis para mejorar sus propiedades ácidas. Los carbonos porosos fueron proporcionados por el grupo del profesor T. Cordero (Departamento de Ingeniería Química, Universidad de Málaga).

Tras la preparación de los catalizadores, se llevó a cabo su caracterización físico-química mediante diferentes técnicas y análisis: difracción de rayos X (XRD), espectroscopía fotoelectrónica de rayos X (XPS), análisis térmico diferencial y termogravimétrico (DTA-TG), adsorción-desorción de nitrógeno a -196 ºC, desorción a temperatura programada de amoníaco (NH_3-TPD), adsorción de piridina acoplada a la espectroscopía infrarroja por Transformada de Fourier (Pyr-FTIR), resonancia magnética nuclear en estado sólido (MAS-NMR) y análisis elemental (CHNS/O). Esta caracterización proporcionó datos de las propiedades estructurales y morfológicas, la composición química, la acidez total y su fortaleza y tipos (Brönsted y Lewis) de sitios ácidos, y las estabilidades térmica, física y química de los catalizadores.

Una vez caracterizados, se investigó la actividad de los catalizadores en la reacción de deshidratación de glucosa a HMF. Todos los experimentos catalíticos se realizaron en reactores de vidrio de paredes gruesas de 15 ml, y a temperaturas entre 155 y 195 ºC. El experimento estándar usaba 1,5 mL de fase acuosa compuesta de hexosa (glucosa o fructosa, 10 % en peso) combinada con 3,5 mL de un disolvente orgánico, así como 50 mg de catalizador. Después de la reacción, los análisis de las muestras de los productos de reacción se realizaron mediante cromatografía líquida de alta resolución (HPLC),

proporcionando los datos de conversión de reactivos, y de selectividad y rendimiento de los productos.

El óxido de tántalo mesoporoso se sintetizó mediante hidrólisis ácida de pentaetóxido de tántalo en presencia de Pluronic L-121, un surfactante no iónico, a temperatura ambiente, y posterior calcinación a 550 °C durante 6 h. Los patrones de difracción de rayos-X (XRD) confirmaron una estructura amorfa, no detectándose ninguna fase cristalina del óxido de tántalo. Se realizó un estudio de termodifracción desde temperatura ambiente hasta 1000 ºC, aunque la actividad catalítica no se estudió por encima de 200 ºC. Hasta 500 ºC, los difractogramas permanecieron invariables, pero, por encima de 600 ºC, aparecieron picos de difracción estrechos y bien definidos, correspondientes a una estructura ortorrómbica. El uso de plantillas con un elevado peso molecular como Pluronic® P-123 originó paredes de poros más gruesas con mesoestructuras ordenadas durante el procedimiento de síntesis. El catalizador presentaba una isoterma de adsorción-desorción de N_2 Tipo IV(a), típica de sólidos mesoporosos, con una histéresis asociada a la condensación capilar. Se utilizó el método (DFT) para calcular la distribución del tamaño de poros, siendo entre 2 y 6 nm. El catalizador poseía una superficie específica adecuada (79 $m^2\ g^{-1}$) y la composición de la superficie, determinada a partir de los datos de XPS, resultó ser cercana a la composición estequiométrica del óxido de tántalo. Los espectros de las regiones del Ta *4f* y O *1s* confirmaron los estados de oxidación esperados del óxido de tántalo. Los valores obtenidos mediante TPD de amoniaco confirmaron que la acidez de este catalizador residía principalmente en la presencia de moléculas de agua coordinadas y grupos OH coordinados a iones de tántalo. La simetría y el estado de oxidación

del tántalo también determinaron las propiedades ácidas. Aunque la acidez fue principalmente asociada a moléculas de agua coordinadas y grupos OH coordinados a los iones de tántalo, como sitios ácidos tipo Brönsted, los sitios ácidos de Brönsted se transformaron parcialmente en sitios ácidos de Lewis.

El Ta_2O_5 mesoporoso demostró ser activo como catalizador heterogéneo en la deshidratación de glucosa a 5-hidroximetilfurfural (HMF), en un sistema bifásico consistente en agua/metil-iso-butil cetona (MIBK). Con una relación másica glucosa/catalizador (S/C) de 3:1 se logró una conversión de glucosa del 69% y un rendimiento en HMF del 23%, a 175 °C después de 90 minutos. El proceso catalítico fue selectivo hacia el HMF, ya que no se detectó ácido levulínico procedente de una posterior hidratación del HMF. También se obtuvo fructosa, procedente de la isomerización de la glucosa, con una selectividad del 14%. La formación de fructosa se vio favorecida a temperaturas más bajas, y supone la existencia de un proceso en dos etapas, con una primera en la que la glucosa se isomeriza a fructosa y una segunda en la que la fructosa se deshidrata a HMF, aunque también cabe la posibilidad de deshidratación directa de glucosa a HMF. La isomerización de glucosa a fructosa se llevó a cabo sobre sitios activos ácidos de Lewis, mientras que la deshidratación se realiza sobre los sitios ácidos de Brönsted. Después del tratamiento con una solución de KOH para reducir la acidez del catalizador, éste convirtió un 15% menos de glucosa y la selectividad de HMF resultó ser un 8% inferior, mostrando la participación de los sitios ácidos de Brönsted en la reacción. El catalizador también se probó en una reacción partiendo de HMF, en las mismas condiciones de reacción (sistema bifásico agua/MIBK, 175 ºC, 90 minutos), y tras la reacción no se detectó

ácido levulínico ni fórmico, y se recuperó todo el HMF inicial, indicando que la acidez de Lewis era insuficiente para llevar a cabo reacciones desde HMF. También se llevó a cabo la modificación de la acidez superficial mediante el tratamiento del catalizador con ácido fosfórico, y tras 120 minutos de reacción a 175 ºC, se incrementaron tanto la conversión de glucosa como la selectividad a HMF, disminuyendo la selectividad a fructosa. El óxido de tántalo resultó ser térmica y químicamente estable, ya que no se encontró lixiviación de especies de tántalo en un análisis de la fase líquida. Al aumentar la cantidad de catalizador (reduciendo la relación sustrato/catalizador (S/C)), la conversión de glucosa y el rendimiento a HMF no aumentaron de forma lineal, debido a limitaciones difusionales. El catalizador usado, después de un tratamiento térmico de regeneración a 550 ºC, mostró una actividad similar a la del catalizador fresco, en un segundo ciclo de reacción, pero cuando no se sometió a tratamiento de regeneración, la conversión de glucosa disminuyó drásticamente. Por lo tanto, la vida útil de este catalizador para funcionar de forma adecuada en las condiciones de reacción empleadas fue de solo 1 ciclo.

Los catalizadores de sílice mesoporosa tipo MCM-41 dopados con aluminio en proporciones Si/Al 5 y 10 se prepararon mediante un método sol-gel en dos etapas (hidrólisis ácida y alcalina), a partir de la hidrólisis conjunta de tetraetilortosilicato (TEOS) y triisoproxido de aluminio, utilizando cloruro de n-dodecilamonio como surfactante, a temperatura ambiente, y realizando posteriormente su calcinación a 550 °C. Los patrones de DRX confirmaron una estructura hexagonal y paredes de sílice amorfas, sin fases cristalinas. Las isotermas de adsorción-desorción de nitrógeno que se obtuvieron fueron Tipo IV (a), típicas de sólidos mesoporosos, e indicaron la existencia de poros

anchos, que se confirmaron con el análisis DFT, resultando más anchos en 10Al-MCM-41 que en el catalizador 5Al-MCM-41. Las áreas superficiales BET aumentaron al hacerlo el contenido de aluminio, de 587 a 734 m^2 g^{-1} para 10Al-MCM-41 y 5Al-MCM-41, respectivamente. Los datos de TPD de amoniaco y los espectros FTIR de piridina adsorbida denotaron una fuerte acidez, con la presencia de sitios ácidos de Lewis y Brönsted, que permanecieron incluso después de la evacuación de piridina a 300 ºC, principalmente en 10Al-MCM-41. Los sitios ácidos de Brönsted, asociados a silanol y grupos hidroxilo Si(OH)Al aislados, fueron los principales responsables de la acidez total. Los datos de XPS y ^{27}Al RMN mostraron la presencia de aluminio coordinado en entornos octaédrico y tetraédrico, porque, aunque ambos materiales poseían aluminio bien incorporado a la estructura silícea, algo de aluminio se originó en la superficie externa en forma de óxido de aluminio, especialmente en el caso de 5Al-MCM-41 que tenía un mayor contenido de aluminio.

Mediante el empleo de un sistema bifásico agua/MIBK y con 10Al-MCM (S/ = 3:1) a 195 ºC, se alcanzó una conversión de glucosa del 87% y un rendimiento a HMF del 36%, después de 150 minutos. La reacción fue bastante selectiva hacia HMF, y no se detectaron ácido levulínico o furfural, tan sólo fructosa como subproducto. El catalizador 5Al-MCM-41, en las mismas condiciones de reacción, mostró una efectividad menor, que pudo deberse a su menor acidez, más aluminio fuera de la estructura mesoporosa y una mayor proporción de microporos que pudieron dificultar la accesibilidad de los reactivos a los sitios ácidos. El uso de una solución acuosa de cloruro de sodio (20 % en peso) en lugar de agua pura, como fase acuosa, mejoró el coeficiente de reparto entre las fases orgánica y

acuosa hasta un valor de 1.9, lo que elevó tanto la conversión de glucosa como el rendimiento a HMF, alcanzando valores de 98% y 63%, respectivamente, y acortando el tiempo de reacción a tan sólo 30 minutos. El rendimiento catalítico de 10Al-MCM-41 se mantuvo después de tres ciclos catalíticos. El aumento de la selectividad a fructosa en los ciclos de reacción posteriores al primero corroboró que la isomerización de la glucosa a la fructosa es la etapa limitante del proceso de deshidratación.

Para a la síntesis de materiales de sílices mesoporosas tipo KIT-6 (KIT6-A, KIT6-B y KIT6-C) se emplearon tres métodos similares. Para los tipos A y B, se emplearon Pluronic P-123 como agente estructurante y ácido clorhídrico, y se añadió n-butanol como disolvente. Para el tipo A se agitó a 35 ºC durante 24 horas después de la adición de TEOS (tetraetilortosilicato), mientras que el tipo B se agitó más tiempo, 72 horas. Tras la calcinación a 550 ºC, se obtuvieron los catalizadores KIT6-A y KIT6-B. Para el tercer material, KIT6-C, se utilizó isopropanol en lugar de n-butanol como disolvente, y después de la adición de TEOS se agitó durante 36 horas. Con los datos que aportó el estudio de los 3 sólidos, tanto de DRX como de su caracterización textural, se eligió KIT6-C para ser modificado por dos tratamientos post-síntesis diferentes para incorporar aluminio con el fin de mejorar la acidez y, en consecuencia, la actividad catalítica. El primer método post-síntesis utilizó una solución de cloruro de aluminio en etanol seco, y el segundo método, en hidróxido de tetrametilamonio (TMAOH) en lugar de etanol. Con las diferentes condiciones de síntesis se obtuvieron dos sólidos tipo KIT6 dopados con aluminio: Al-KIT6-C1 y Al-KIT6-C2. Estos materiales no mostraron cambios estructurales después de la incorporación del

heteroátomo. Los análisis por XPS y FRX indicaron escasez de Al en Al-KIT6-C1, mientras que mostraron una relación Si/Al cercana al valor prefijado en el caso de Al-KIT6-C2. En este segundo catalizador se confirmaron tanto la presencia de aluminio en coordinación tetraédrica (Al^{T}) como aluminio octaédrico (Al^{O}) a partir de los datos de MAS-NMR. Por lo tanto, sólo Al-KIT6-C2 contenía aluminio incorporado debido a un procedimiento de síntesis más adecuado, y sólo este sólido se probó en el estudio catalítico posterior. El aluminio se localizó principalmente sobre la superficie, mientras que en 10Al-MCM-41 se encontraba principalmente en la estructura mesoporosa, conformando una estructura más desordenada que en los materiales basados en KIT6.

Así, Al-KIT6-C2 se estudió como catalizador bajo las mismas condiciones de reacción que 10Al-MCM-41, resultando altamente selectivo hacia HMF, pero poco activo en la conversión de glucosa, debido principalmente a una menor acidez. Teniendo en cuenta tanto la fortaleza como la cantidad de sitios ácidos de los catalizadores mesoporosos empleados, 10Al-MCM-41 podría considerarse el catalizador más ácido, seguido del óxido de tántalo mesoporoso y del 5Al-MCM-41, siendo Al-KIT6-C2 el menor. Además, en estudios a mayores tiempos de reacción se observó la desactivación del catalizador debido a la presencia de subproductos de reacción, sin que se observara ninguna variación de sus propiedades ácidas.

En cuanto a las zeolitas, se prepararon tres zeolitas protonadas (H-ZSM-5, H-Y y H-Beta) a partir de zeolitas comerciales mediante calcinación de sus formas amónicas a 550 ºC. ZSM-5 es una zeolita con un sistema de canales interseccional y tridimensional, con alto

contenido en silicio. El material comercial precursor de H-ZSM5-15 poseía una relación molar Si/Al de 15. La zeolita Y, de tipo faujasita, posee grandes cavidades internas llamadas supercavidades, unidas tetraédricamente a través de poros abiertos. La relación Si/Al de zeolitas Y es baja y puede aumentarse mediante la dealuminación. El material comercial precursor de H-Y-6 poseía una relación Si/Al de 6. La zeolita Beta tiene una estructura tipo BEA, siendo una estructura compleja que consiste a su vez en dos estructuras intercrecidas, conteniendo ambas una red tridimensional de poros. Se pueden sintetizar con altas relaciones molares Si/Al, entre 10 y 100. El precursor comercial del catalizador H-Beta-12.5 poseía una relación Si/Al de 12.5. Las zeolitas mostraron isotermas de adsorción-desorción de nitrógeno de Tipo I, pero mientras que los materiales de tipo ZSM-5 mostraron histéresis tipo H3 debido a agregados de partículas que originaron cavidades medianas y anchas, los materiales de tipo Y mostraron un tipo de histéresis H4, típico de zeolitas con micro y mesoporos. Las zeolitas ZSM-5 y Beta, se consideran selectivas de forma debido a sus particulares estructuras. Los materiales basados en zeolita H-Beta mostraron una cristalinidad menor que los otros tipos de zeolita, que se asocia a la presencia de defectos estructurales debido a la incorporación de especies de aluminio. Los valores de acidez total de las zeolitas protonadas fueron muy superiores a los de los catalizadores mesoporosos, aunque la densidad superficial del amoníaco adsorbido fue similar e incluso lo fueron las temperaturas máximas de desorción. La acidez H-ZSM5-15 se debió tanto a los grupos hidroxilo como a los átomos de aluminio.

Estas zeolitas protonadas se probaron en la deshidratación catalítica de glucosa a HMF bajo las mismas condiciones de reacción del

catalizador 10Al-MCM-41 con el fin de evaluar la influencia de las propiedades texturales y ácidas en el rendimiento catalítico. Así, el proceso de deshidratación se llevó a cabo en un sistema bifásico de agua/metil-isobutil cetona (MIBK), a 195 ºC. Los catalizadores H-Beta-12.5 y H-Y-6 alcanzaron una conversión de glucosa superior a la lograda utilizando 10Al-MCM-41, pero menores selectividades de fructosa. Sin embargo, la mayor selectividad a HMF de las zeolitas protonadas fue inferior a la conseguida con el catalizador MCM-41, y se logró empleando H-Beta-12.5. Esto se debió a los sitios ácidos de Lewis y Brönsted, a su acidez moderada-fuerte y, en general, a la importante mesoporosidad desarrollada en la zeolita. Estos resultados confirman el papel esencial que desempeñan las propiedades texturales de los catalizadores en el rendimiento catalítico de la reacción de deshidratación de glucosa y fructosa a HMF. La adición de NaCl a la fase acuosa, como en el caso de 10Al-MCM-41, mejoró tanto la selectividad como el rendimiento a HMF. Así, con la zeolita H-Beta-12.5 en una solución acuosa de NaCl/MIBK, a 195 °C, se logró un alto rendimiento a HMF, cercano al obtenido con 10Al-MCM-41, después de tan sólo 30 minutos de reacción. La mejora obtenida con H-ZSM-5 y H-Y no fue tan importante, lo que demuestra el efecto positivo de la mesoporosidad en la deshidratación de glucosa a HMF. En todas las reacciones se observó la formación de productos no deseados, que disminuyeron la cantidad de HMF, incluso a temperaturas de reacción más bajas o en tiempos de reacción más cortos. Las especies poliméricas obtenidas a partir de los carbohidratos y del HMF se forman en los sitios ácidos de Lewis, mientras que los productos de degradación de HMF tienen lugar en los sitios ácidos de Brönsted. El ácido levulínico, procedente de la rehidratación de HMF,

no se detectó en ningún experimento. También se estudió la influencia de la fase orgánica en el rendimiento y se confirmó su papel en la extracción del HMF formado, desplazando el equilibrio hacia su formación y evitando también reacciones de degradación posteriores. En ausencia de fase orgánica, se logró un rendimiento de HMF inferior al 4% debido a la rehidratación del HMF formado, lo que se evidenció mediante la identificación de ácido levulínico en los productos de reacción. También se evaluó el papel de otras sales alcalinas además de NaCl en la fase acuosa, confirmando que el efecto más positivo se debe principalmente a los cationes de sodio. En particular, el NaCl en zeolitas de tipo MFI, como ZSM-5, mejora la hidrólisis de los puentes Si-O-Al, liberando especies de Al^{3+} que catalizan la conversión de glucosa a través de procesos catalíticos homogéneos. La adición de $CaCl_2$ como fase acuosa en lugar de agua, mostró, sin embargo, un comportamiento diferente. Incluso en ausencia de catalizador, se observó una alta actividad, señalando que esta sal está involucrada tanto en la isomerización de la glucosa, que parece ser muy rápida, como en la deshidratación de la hexosa. Diferentes sales promueven la deshidratación de glucosa/fructosa a HMF, pero la causa y el efecto de sus iones respectivos, se deben, además a los tipos de iones, a las interacciones particulares de éstos con cada catalizador y a las condiciones de reacción específicas.

La introducción de heteroátomos en las zeolitas modifica la naturaleza y la fortaleza de la acidez de las mismas, en función del número, la coordinación y la posición de estos heteroátomos en la zeolita. El hierro y el cobre fueron introducidos en las zeolitas comerciales de partida por métodos post-síntesis, en concreto mediante intercambio iónico, para modificar las propiedades ácidas de los catalizadores

basados en zeolitas. Después de la incorporación de hierro y cobre y de calcinación a 550 ºC, en las zeolitas tipo ZSM-5, las estructuras se mantuvieron intactas según los patrones de DRX, con los cationes preferentemente en posiciones extra-red. Aunque la incorporación de hierro en las zeolitas reduce el área superficial específica y el volumen de microporos debido al bloqueo parcial de los poros por las especies de hierro, en la zeolita Fe-Beta-12.5, ambos se incrementaron debido a la presencia de agregados de hierro. La relación Si/Al de Fe- y Cu-ZSM5-15 difirió de la de la zeolita H-ZSM5-15 de manera opuesta. Mientras que en la superficie de Fe-ZSM5-15 disminuyó el contenido de aluminio, en Cu-ZSM-15 aumentó el aluminio en superficie, indicando una ubicación preferencial diferente de estos cationes después de las etapas de intercambio iónico y calcinación. Los datos de MAS-NMR de las zeolitas tipo ZSM-5 revelaron la presencia de átomos de aluminio coordinados tetraédrica y octaédricamente, siendo en su mayoría tetraédricos, correspondientes a especies intra-red. En H-Y-6, la relación Si/Al fue muy parecida a la relación del precursor, con el 73% del aluminio dentro de la red zeolítica. En las zeolitas Beta, la relación atómica Si/Al en la superficie resultó ser muy similar a la relación Si/Al de la forma protonada, aunque mayor en la zeolita intercambiada con hierro y menor en la intercambiada por cobre. Los espectros en las regiones Fe *2p* y Fe *3p* (datos XPS) del hierro de las zeolitas mostraron una oxidación parcial de Fe (II) a Fe(III) durante la post-síntesis. Las relaciones atómicas Si/Fe aumentaron con la relación Si/Al, como se esperaba, por lo tanto, la zeolita con el mayor contenido de aluminio tenía también la mayor proporción de hierro, Fe-Y-6, mientras que Fe-ZSM5-15 tuvo el menor contenido en hierro de los tres catalizadores. Con respecto a las zeolitas con cobre, el

espectro Cu 2p*3/2* (XPS) confirmó la presencia de Cu(II), aunque el Cu LMM Auger también indicó la existencia de Cu(I), que pudo producirse por foto-reducción durante la exposición a los rayos X, pero en el caso de Cu-ZSM5-15, también pudo ser causada por las interacciones entre los cationes de cobre y la estructura de la zeolita, que mantienen el cobre(I) incluso a elevadas temperaturas. Se observó una diferencia notable entre las zeolitas intercambiadas con cobre y las intercambiadas con hierro en cuanto al enriquecimiento de aluminio en superficie en comparación con sus precursores respectivos, lo que probablemente se debió a la existencia de gradientes de aluminio desde las regiones internas a las externas de las zeolitas. En las zeolitas ZSM-5 intercambiadas con cationes, los sitios ácidos se mantuvieron constantes tras el intercambio, pero en las zeolitas tipo Y y Beta, éstos disminuyeron. En las zeolitas ZSM-5, las fuertes modificaciones en los sitios ácidos de Brönsted, principalmente, y en los sitios ácidos de Lewis y, sobre todo, el aluminio, conformaban la acidez. Aunque en la TPD de amoniaco se obtuvo una acidez total similar para los catalizadores H-, Fe- y Cu-ZSM5-15, su acidez era de diferente tipo. En las zeolitas intercambiadas tipo Beta, la introducción de hierro disminuyó la acidez total y su fortaleza, mientras la introducción de cobre aumentó notablemente los sitios ácidos de Lewis, aunque disminuyó su fortaleza. Estos datos muestran que es factible modificar la naturaleza de los sitios ácidos de las zeolitas mediante tratamientos térmicos o de intercambio iónico.

Las zeolitas ácidas resultantes demostraron ser también activas en la deshidratación de glucosa. Se investigó la influencia de diferentes variables experimentales, como el tiempo de reacción y la temperatura, la relación molar sustrato: catalizador, el volumen de disolvente

orgánico y de fase acuosa, así como la densidad y la naturaleza de los sitios ácidos, en el comportamiento catalítico. Fe-y Cu-ZSM5-15 condujeron a una mayor conversión de glucosa y rendimientos a HMF, reduciendo la selectividad a fructosa y, por lo tanto, mejorando la actividad respecto a la de H-ZSM5-15. Fe-Y-6 y Fe-Beta-12.5 mejoraron la actividad catalítica en comparación con las formas protonadas, aunque no tanto como en los catalizadores tipo ZSM-5. El catalizador H-ZSM5-15 se calcinó para ser regenerado previamente a su reutilización. Este tratamiento produjo un enriquecimiento de aluminio en la superficie debido a la generación de aluminio extra-red, modificando los sitios activos con respecto al catalizador fresco inicial. Estos cambios condujeron a una mayor conversión de glucosa, pero a una menor producción de HMF y mayor de fructosa como productos de reacción, confirmando la relación que existe entre el tipo de acidez y las selectividades. El rendimiento catalítico en un segundo ciclo del catalizador H-Beta-12.5, que resultó inicialmente casi tan activo como 10Al-MCM-41, fue sin embargo muy diferente a la actividad del catalizador 10Al-MCM-41 en un segundo ciclo en condiciones experimentales similares. El catalizador Fe-Beta-12.5 regenerado también redujo mucho su actividad en un segundo ciclo catalítico debido a la disminución de los sitios ácidos, lo que se debió a la pérdida de hierro. El catalizador Cu-Beta-12.5 regenerado mostró también un comportamiento distinto del primer al segundo ciclo, pero debido a otros motivos, como la dealuminación parcial.

Una vez estudiados los materiales mesoporosos y las zeolitas, dos grupos de carbones ácidos porosos, preparados a partir de huesos de aceituna (serie HA) y de lignina comercial (serie L) se activaron mediante un tratamiento químico con ácido fosfórico para obtener

catalizadores ácidos: HA3500, 31500 y 31800, y L3500, 31500 y 31800. Las etiquetas 500 y 800 indican las temperaturas de activación. L31500 y HA31500, que se prepararon utilizando un método y una proporción de impregnación similares, dieron como resultado carbonos más ácidos, seguidos de HA3500 y L3500. El tratamiento térmico a 800 ºC durante la síntesis originó materiales con menor acidez que los activados a 500 ºC en sus respectivas series (HA- o L-).

En primer lugar, se compararon con 10Al-MCM-41 y las zeolitas en las mismas condiciones de reacción, en la deshidratación de glucosa a HMF. En general, no se detectó fructosa en ningún experimento, y se obtuvieron selectividades a HMF más altas que los valores de conversión de glucosa, como tendencia general. A mayor temperatura de activación, menor actividad catalítica (HA31800 y L31800). Los carbones tipo -31500 resultaron más selectivos a HMF debido a su mayor área superficial y su mayor superficie de microporos, con microporos pequeños que limitan las reacciones de degradación de HMF, y a su alta porosidad combinada con sitios ácidos de fortaleza media y débiles adecuados también para la conversión de glucosa. Los carbones L3500 y HA3500, resultaron los de máxima conversión de glucosa, asociada a sitios ácidos de Brönsted más fuertes. Como no se detectó fructosa en ningún caso, HA31500 se probó para la obtención de HMF directamente desde fructosa. Los resultados sugirieron un mecanismo diferente para la conversión de glucosa sobre estos carbones catalizadores que para los otros catalizadores estudiados. En este caso, la glucosa no se isomerizaría a fructosa previamente a su deshidratación a HMF, sino que se deshidrataría a través de otros intermedios. Con el catalizador L3500, en idénticas condiciones de reacción, se alcanzó una conversión de glucosa similar a la obtenida

con el catalizador H-ZSM5-15 y una selectividad a HMF similar a la de 10Al-MCM-41. Por lo tanto, los catalizadores L3500 aunaron las ventajas de los otros dos catalizadores, pero, desde el punto de vista económico y ambiental, como estos materiales se obtuvieron a partir de residuos biomásicos, serían preferibles. También se estudió la influencia de la proporción de MIBK, la fase orgánica, con el fin de utilizar la menor cantidad necesaria posible. Los resultados confirmaron que la proporción óptima es justamente la utilizada en las otras reacciones, con un 70 vol.% de MIBK en el medio de reacción. Como el cloruro de calcio mejoró notablemente la actividad en el caso de 10Al-MCM-41 y de las zeolitas, también se evaluó la adición de cloruro de calcio al medio acuoso y la reacción se realizó con los carbonos ácidos como catalizadores. En este caso, la conversión de glucosa se duplicó, aunque la selectividad a HMF sólo aumentó ligeramente, y los datos indicaron una participación diferente de los iones de la sal a la indicada en las reacciones con los otros catalizadores. El ciclopentilmetil éter (CPME), un eco-disolvente, que previamente se probó como alternativa al MIBK como fase orgánica con 10Al-MCM-41, también se probó con HA31500 como catalizador, alcanzando en este caso una mayor conversión de glucosa después de 90 minutos, pero una selectividad a HMF mucho menor, debido al coeficiente de partición, más pequeño en CPME que en MIBK. Mediante el uso de este disolvente, se detectó furfural como producto de reacción, además de HMF. La presencia de sitios ácidos de Brönsted fuertes, además de sitios ácidos de Lewis, favoreció no sólo el HMF sino también el furfural. Esto se debería a un mecanismo de reacción no a través de fructosa sino a través de 3-desoxiglucosona como intermedio de reacción, ya que ésta puede sufrir una doble

deshidratación para dar HMF, pero también puede formar furfural vía otro intermediario inestable. El CPME, con un coeficiente de reparto menor, posibilitaría ambas reacciones, aunque favoreciendo el HMF sobre el furfural. La formación de subproductos como las huminas también se observó con el empleo de los carbones ácidos como catalizadores. En un segundo ciclo catalítico, sin ningún tratamiento para regenerar los catalizadores, la selectividad de HMF disminuyó debido al depósito de subproductos en los mismos, bloqueando los sitios activos.

Introduction

3. Introduction

3.1. Current world energy situation

The world has become increasingly dependent on fossil-based resources, mainly oil and natural gas, for the production of fuels and chemicals. North America and Europe since the beginning, and China and India growing strongly, demand a large amount of oil and natural gas, while diminishing reserves. In 2019, European Union consumed 10.2% world energy, being China and Asia the largest consumers (21 and 25.6%, respectively). Renewable energies only account for 16.4% as is shown in Figure 1,[1].

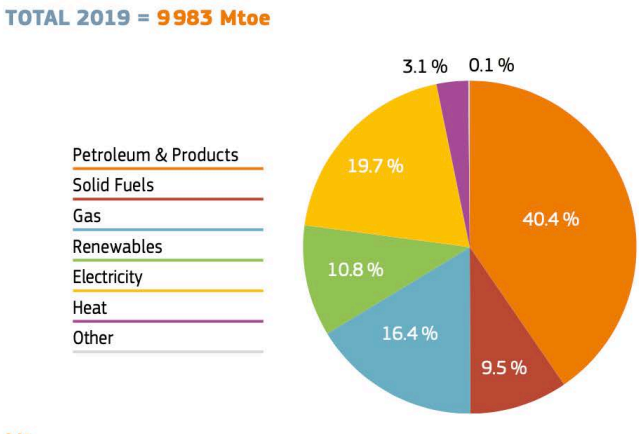

Figure 1. World total final consumption by fuel (2019) [2].

The Renewable Energy Directive sets a series of greenhouse gases emission and sustainability criteria that EU countries must comply to reach a 32% renewable target by 2030, in order to ensure a sustainable growth [3]. These are also necessary to achieve the EU's objective of

climate neutrality by 2050. On 18 May 2022, the UE Commission published the REPowerEU plan, including measures to reduce de dependence on Russian fossil fuels and accelerate the green energy transition [4]. This REPowerEU means saving energy, producing green energy and diversifying the energy supplies. This recent plan also proposes to increase the renewable target to 45%, which would bring the total renewable energy generation capacity to 1236 GW instead of 1067 GW proposed in 2021. A modeling analysis has been recently taken out on the energy mix in 2030 by the European Commission [5]. Different scenarios have been compared: Fit-for-55 "Ff55", achieving the 2030 targets adopted, with 40% for the renewable energy; "Ff55 high prices" with high fossil fuel prices; REPowerEU "RPE" context achieving 45% renewable energy, 13% energy efficiency and phased out Russian gas by 2027; "RPE50" including RPE context and 50% renewable energy and "RPE56" increasing renewable energy target to 56% (Figure 2, [6]).

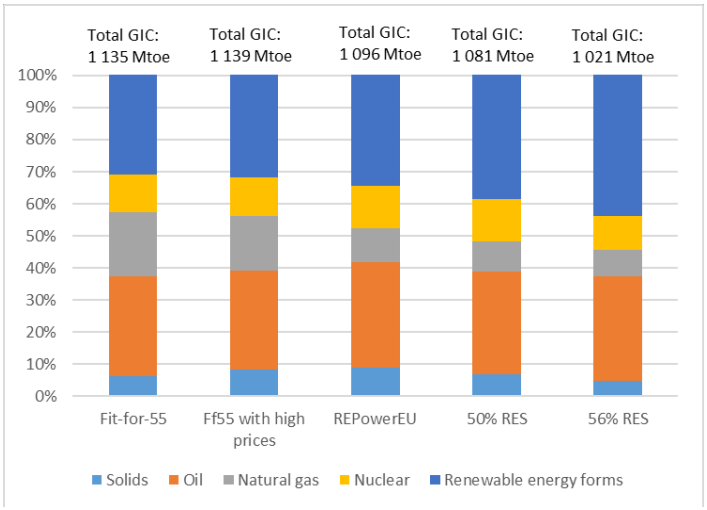

Figure 2. Energy mix in 2030 (% by fuels, total GIC in Mtoe) [6].

In the current context of a globalized and polluted world, highly dependent on fossil fuels, it has been necessary the development of sustainable resources for both energy and bulk chemicals. To achieve the renewable target, wind power, ocean and hydropower energies, solar energy, biofuels, biomethane and biomass are together needed. Biofuels are the alternative to fossil fuels for transports, whereas biomethane is a renewable substitute of natural gas. Biomass, derived from organic material, from trees, plants, and agricultural and urban wastes, are the main source of renewable energy in the EU (60%). Biomass is, as coal and oil, an available carbon source, constituting renewable alternative resources for energy, transport fuels, and chemicals [7].

3.2. Biomass

Biomass consists of, among others, carbohydrates, lignin, fatty acids and lipids, although the most important components are cellulose, hemicellulose and lignin, which form the lignocellulose (75%), and also includes volatiles, water and ash (Figure 3). Cellulose, which is a polysaccharide consisting of a linear chain of several hundred to many thousands of β (1→4) linked D-glucose units, is the most abundant. Hemicellulose (polyose) is a heterogeneous polymer which is composed of many C5 and C6 sugars such as xylose, arabinose, mannose or galactose. Lignin, the encrusting material in which the cellulose microfibrils are embedded, is a macromolecule composed by aromatic polymers [8].

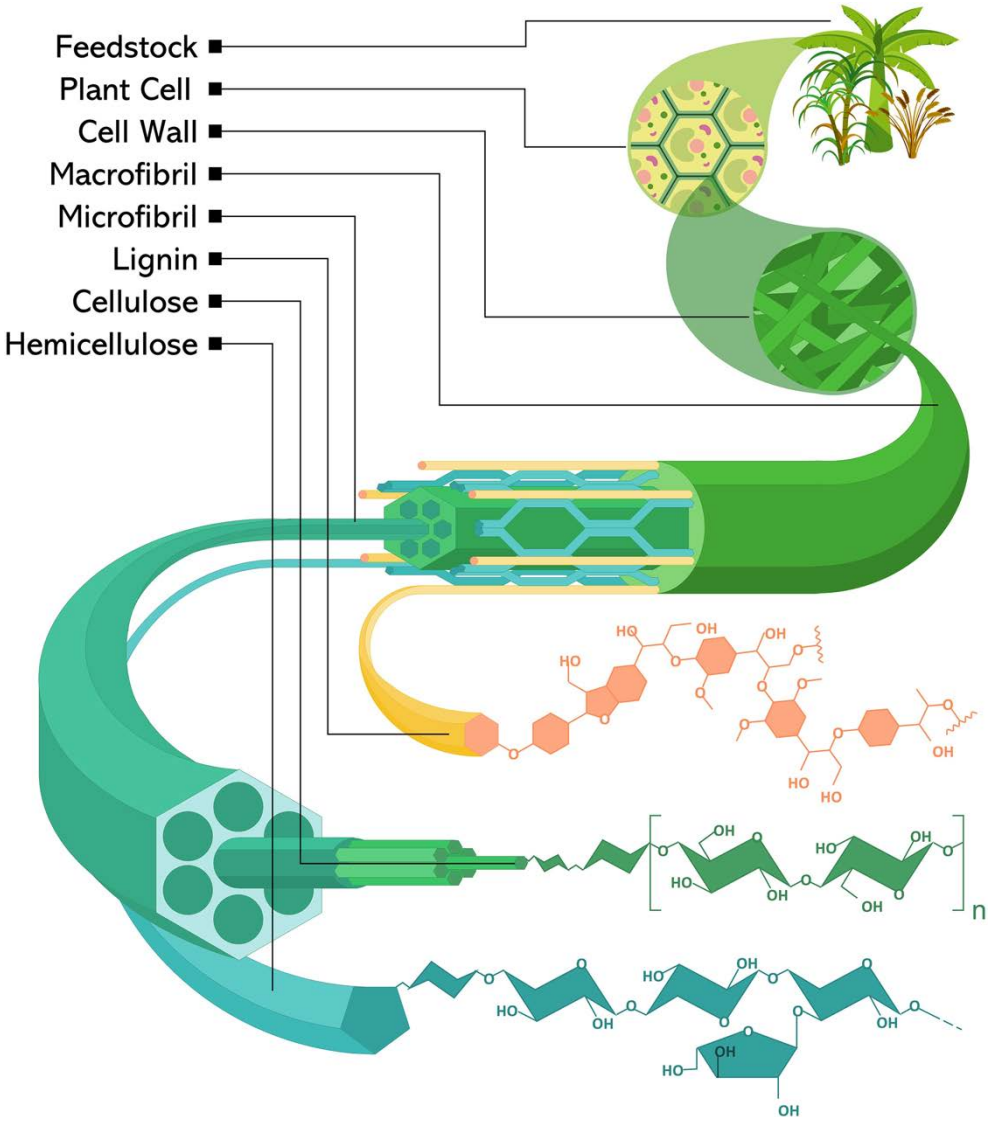

Figure 3. Lignocellulosic biomass composition [9].

3.2.1. Biomass to energy:

Biomass can provide direct energy for electricity generation, heat and steam, and most biomass power plants in European countries have accomplished cogeneration. Production and operation of biomass power plants are similar to thermal power production, but the fuel system of biomass power plants is more complicated. Biomass materials are not purely carbon, oxygen and hydrogen, but also nitrogen, potassium, phosphorous, sulphur and chlorine elements are contained, involving continuous challenges to combustion engineering technology due to deposition, fouling, slagging and corrosion of equipment. Depending on the quality of the combustion process and the produced emissions, the use of biomass can be cleaner or even dirtier than coal (Figure 4).

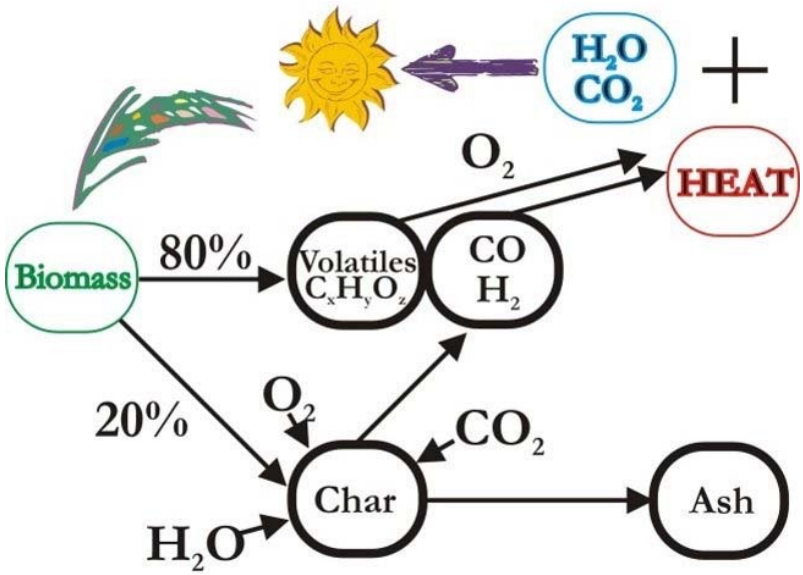

Figure 4. Biomass combustion diagram [10].

The combustion process, called pyrolysis, converts the biomass into gases, volatile liquids and char, a carbon rich solid. An illustrative and exampling of this use of the biomass is the European Project LIFE03 ENV/SK/00057 in Slovakia, which produced wood pellets for the heating installations at schools ([11]).

3.2.2. Biomass to fuels:

Besides providing renewable electricity and thermal energy, biomass can be used to produce biofuels, especially for the transportation sector. Main strategies using biomass instead of fossil fuels are aimed to reduce the oxygen content in order to improve energy density [12] and to increase the molecular weight of the hydrocarbons by creating new C-C bonds. Depending on the biomass feedstock, different biofuel generations can be produced.

- First generation fuels are directly produced from edible feedstocks, mostly sugarcane and corn, though others as barley, potato wastes or sugar beets:

  - Bioethanol is produced through fermentation and subsequent alcohol distillation of sugars present in sucrose and starch. Sugarcane is common in Brazil, leader country for this use, whereas, in USA, corn is mostly used. Firstly, carbohydrates are isolated, through biomass pretreatment and hydrolysis, to obtain an aqueous solution of carbohydrates. These steps involve higher costs, but the solutions can be selectivity processed into other processes. Obtained bioethanol is blended

with gasoline at low percentages, because percentages around 85% would need to modify the engines [13].

- Biodiesel is obtained mainly from vegetable oils, coming from seeds of sunflower, soybean, palm, among others, which account of around 75% process cost. Any other animal fats or vegetable oils could be used. While bioethanol is produced through the sugar platform, oleochemical platform is used for biodiesel production by transesterification. This is a catalyzed chemical reaction between triglycerides and an alcohol, giving rise to fatty acid alkyl esters (i.e., biodiesel) and glycerol as by-product [14,15].

•The main drawback of first-generation biofuels is the use of edible feedstock, which rises food price. Thus, second generation biofuels are manufactured from agricultural lignocellulosic wastes. With respect to first generation biofuels, there are many advantages, such as no additional fertilizer, water, or land are required to grow this feedstock, and non-edible and cheaper feedstock is used. However, expensive processes are needed.

- Second generation bioethanol is also obtained through hydrolysis and fermentation of carbohydrates (sugar platform).
- Fischer–Tropsch bio-diesel, bio-DME (dimethyl eter) and bio-SNG (synthetic natural gas) are obtained through thermochemical conversion processes, which include direct combustion, gasification, liquefaction, and pyrolysis gasification (thermochemical platform)[16].

•Third generation biofuels are mostly related to algae as feedstock. Also low lignin trees should produce better biofuels [17]. Microalgae´s advantages as biofuel feedstock are the rapid growth rate, CO_2 fixation ability, high production of lipids, non-arable lands requirement and not competitive with food or feed crops. They can be used to produce liquid transportation and heating fuels, such as biodiesel and bioethanol. Algae cultivation can be developed through different ways: open ponds, close-loop systems or photobioreactors. Nevertheless, large-scale implementation to produce biofuels still need large investment into research and investment. One such fuel-based biorefinery is called CAP (combined algal processing), designed by the NREL [18].

•Fourth generation biofuels are being researched and various methods have already been proposed for a more efficient and sustainable biofuel production. Biomass feedstock consists of genomically prepared microorganisms and genetically engineered feedstock. Bioengineering implementation would allow to modify algae metabolism and properties to enhance the oil content in the cells and to CO_2 mitigation [19].

3.2.3. Biomass to chemicals and materials:

Lignocellulosic biomass can provide very important chemical building blocks for the manufacture of fuel additives, resins, solvents, nylon, etc, similarly to petrochemical derived products (Figure 5, [20,21]).

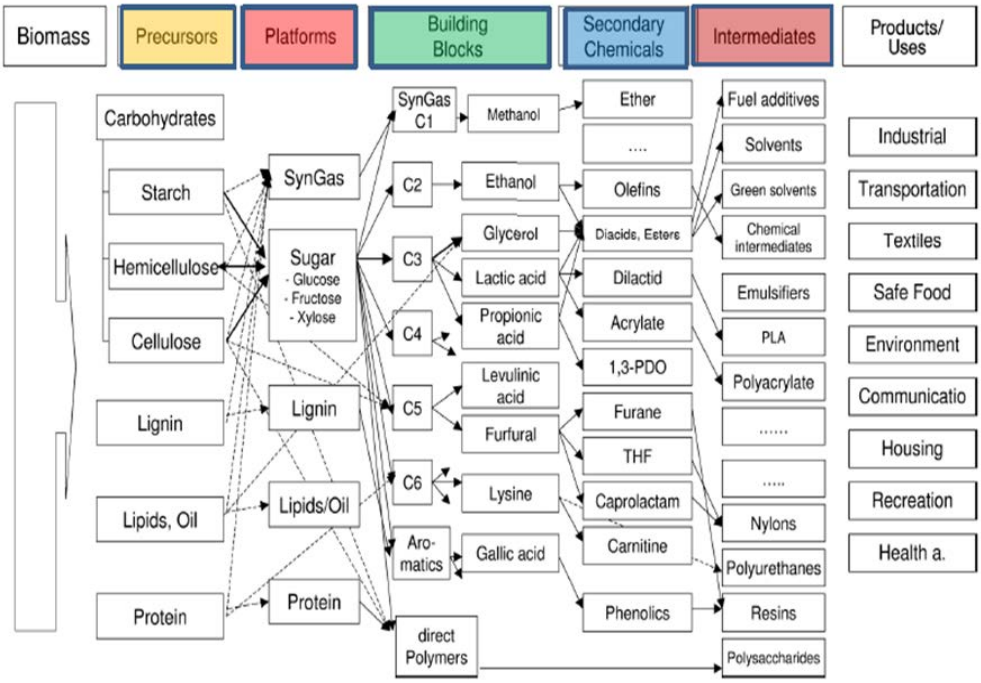

Figure 5. Lignocellulosic biomass for chemicals and products [20].

Thus, specially twelve building blocks derived from biomass has been proposed by DOE/NREL (Top Twelve Building Blocks from Biomass) [20]. Most potential products in the next years would be:

•Oxygenated bulk chemicals, such as ethylene and propylene glycols, iso-propanol, acetone, butylene and methyl ethyl ketone.

•Bio-based production of acrylic acid and N-containing bulk chemicals, such as acrylonitrile, acrylamide and ε-caprolactam.

•Bio-based production of ethylene and vinylchloride.

•Aromatic building blocks, mostly related to functionalized aromatics (e.g., phenols, styrene).

3.3. Biomass-based refineries: biorefineries

Depleting fossil reserves and raising environmental concerns require to develop alternative and sustainable processes for the production of fuels and chemicals. Since 19th century, biomass has been widely used to obtain cellulose from wood, sugars from wood saccharification, viscose rayon from cellulose nitration, fibers from soluble cellulose and polymers from furfural. Several technologies were firstly used for sugars refining, starch production, protein separation and chlorophyll extraction in food industries and ethanol, acetic acid, lactic and citric acids bioproduction:

•Sugar refining: in 1747, a German scientific, A.S. Marggraf discovered beet sugar, leading to the development of the modern sugar industry. In 1801, his student F. C. Achard devised a process to produce sugar from sugar beets, opening the first sugar beet refinery at Gut Kunern near Steinau, Prussia.

•Starch hydrolysis: in 1835, the Swedish chemist J.J. Berzelius developed the enzymatic hydrolysis of starch to sugar and proposed the term *catalysis*: "the property of exerting on other bodies an action which is very different from chemical affinity" [22].

•Wood saccharification: acid hydrolysis of wood to glucose can be achieved at low temperature and high acid concentrations, or at high temperature and low acid concentrations. The first commercial process was developed in 1901 by H. Classen using sulfuric acid [23], though the economically viable processes were developed in the inter-war period. One important product from wood sugars fermentation is

ethanol, which can be used as fuel by itself, or blended with hydrocarbons, and it is also an important platform molecule [24].

•Furfural production: the industrial technology for furfural production from biomass pentoses was started by Quaker Oats Company in 1922 using agricultural by-products, such as sugarcane bagasse and corn cobs [25]. Furfural has been the most economical aldehyde and was used by Du Pont for nylon 6-6 manufacture until 1960, when it was replaced by petrochemicals.

•Cellulose: in 1839, the French chemist A. Payen discovered that, treating wood with nitric acid and sodium hydroxide, a residue, which he called cellulose, was produced. In 1900, there were about 5200 cellulose production plants around the world, mainly in USA, Germany and France.

•Levulinic acid: in 1840, levulinic acid was first prepared by Dutch chemist G.J. Mulder by heating fructose with hydrochloric acid [26]. During the 1940s, the production of levulinic acid from hexoses was studied. In the next decade, it was considered as an important platform molecule.

•Lipids*:* they were firstly considered as raw materials for soaps production, but also the textile industry development required them. In 1902, the German chemist W. Normann produced stearic acid by catalytic hydrogenation of liquid fatty acids (fats and oils hardening), becoming an increasing popular process for the preparation of stable oils and fats, such as margarines [27].

•Vanillin: in 1874, the German chemists W. Haarmann y F. Tiemann first synthesized vanillin from sap conifers. The first chemical

precursor was coniferin, a glucoside of coniferyl alcohol, being isolated from lignin and oxidized to glucovanillin and hydrolyzed to glucose and vanillin. This led to the first vanillin industrial production and the first use of lignin in the chemical industry. Vanillin production is currently based on lignosulfonic acid from wood pulp [28].

- Lactic acid: in 1895, Boehringer pharma industry developed the industrial fermentation of lactic acid. In 1932, W.H. Carothers, inventor of polyamide-6,6, prepared the poly(lactic acid) PLA, which was marketed by NatureWorks company LLC [29].

- Integrated biorefineries: in 1940, the German chemist P. von Walden estimated in 13 million tonnes the cellulose production in Germany, discarding about 6 million tonnes of lignin, and he wondered whether it was economically reasonable. One integral use of the resources was furfural production from oat unprofitable products by Quaker Oats in 1922 [30].

Biorefineries are based on the utilization of the optimum energy potential of organic wastes, helping to solve the problems of waste management and emissions. In the biomass derived biorefineries, biomass wastes are converted, through appropriate enzymatic/chemical treatments, into fuels or bulk chemicals.

From a biorefinery perspective, depending on the feedstocks, they can be classified into three main generations:

- first generation biorefineries, which use crops, edible or non edible, also needing land and water. They are poorly flexible with regards to feedstocks and products. One example is ethanol production from corn stover, producing ethanol, byproducts and carbon dioxide [31].

•second generation ones, which use agro-industrial residues, such as sugarcane bagasse, cereal straws, bananas or oil-palm biomass. They are more flexible tan first ones. Thus, ethanol production from straw can also produce starch, high content fructose syrup, corn oil and corn gluten [32]. These plants are more flexible considering the resulting products [30]. Thus, for instance, a production plant of ethanol from straw (wet biomass) can generate starch, corn syrup with high fructose content, ethanol, corn oil and corn gluten.

•third generation, which start from a variety of raw materials, especially considering algae, because they have a rapid growth rate, fix CO_2, possess high production capacity of lipids, do not compete with food and do not need arable land. Biofuels, including bioethanol, can be produced from the same microalgae feedstock [33–36].

Feedstocks need pre-treatment processes, such as thermochemical or chemicals, being then processed through different platforms, generating biorefining products like solvents, fuel enhancers, undigested sugars, etc, which are not traditionally untapped. The more variety of biomass resources can be used as feedstock, ant the more integral use of byproducts and energy, the more sustainable biorefineries. This concept of sustainable biorefinery is still in early stages at most places in the world. Research and technological processes are being improved to make biorefineries profitable and sustainable in economic and environmental terms. A general scheme of biorefinery and its different types is shown in Figure 6.

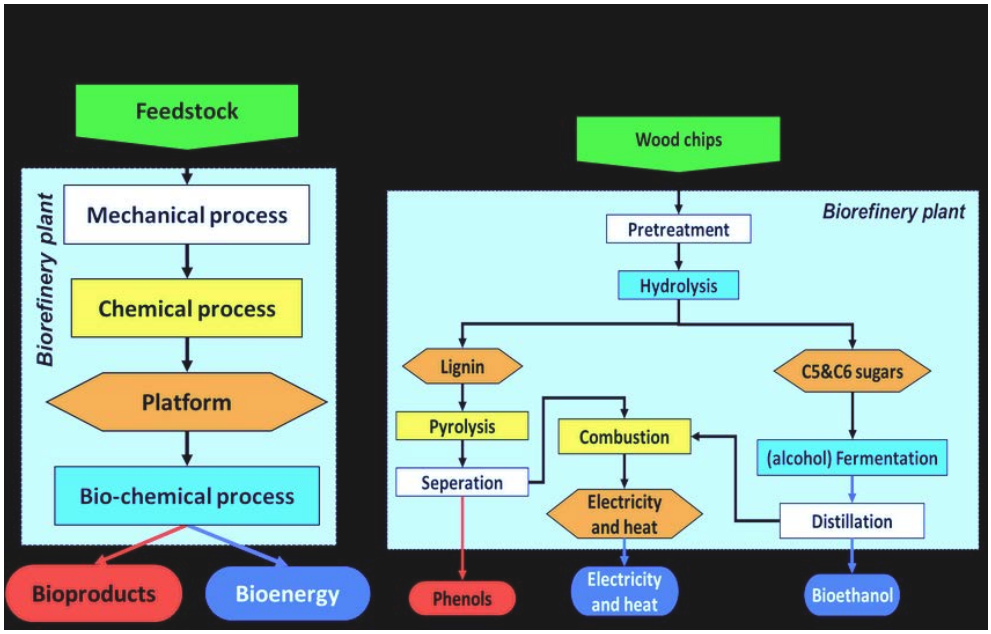

Figure 6. Example of a wood biorefinery scheme [37].

3.3.1. Biorefinery platforms

Depending on the intermediates which link feedstocks and final marketable products, there are several biorefinery platforms, similarly to the concept used in the petrochemical industry, being the thermochemical and carbohydrates ones the most important:

- Thermochemical platform: also known as Syngas platform, produces gas from biomass (Syngas) for biofuels production [38].

- Oleochemical platform: uses renewable fatty acids, fatty esters, and glycerol from oil crops as raw materials. They are about 5% content of the green biomass and are used to produce biosurfactants, biodiesel and lubricants [39].

•Biogas platform: biogas is produced through anaerobic digestion of organic compounds from a broad range of feedstocks, such as bio-wastes. It is composed of methane (50-70%), carbon dioxide (30-40%), hydrogen sulfide, hydrogen and other gases. The methane content can be upgraded to 97-99% purity to be used as a substitute of natural gas. This is a very versatile platform to be integrated in advanced biorefineries for waste valorization.

•Carbohydrates platform (Section 3.4).

3.4. Carbohydrate platform

Lignocellulosic biorefineries breaks down biomass into different types of carbohydrates for biofuels and chemicals. The most important sugar platforms are mainly based on cellulose, starch, glucose and fructose. Carbohydrates, the major renewable carbon source for chemicals, coming from cellulose and hemicellulose, provides polysaccharides. Firstly, pretreatment is needed, modifying the physical and chemical properties of the plant cell walls, so that cellulose and hemicellulose can be converted into fermentable sugars. Furthermore, another aim would be to facilitate the recovery of lignin. After pretreatment, the polysaccharides are hydrolyzed to yield monomeric pentoses and hexoses, such as glucose, fructose and xylose. After, through fermentative or catalyzed chemical processes, these monosaccharides are transformed into platform molecules such as HMF or levulinic acid ([40]).

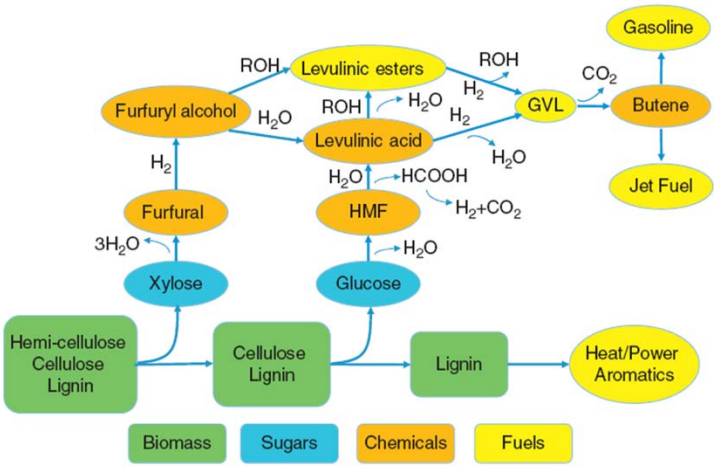

Figure 7. Lignocellulosic biomass (green) to biofuels (yellow) and chemicals (orange) through intermediates (furfural, levulinic acid and HMF) from C5 and C6 sugars (blue) [40].

From sucrose, starch and lignocellulose, a variety of building blocks molecules can be obtained, such as [41–45]:

- C2 for ethanol.
- C3 for glycerol, lactic acid, malonic acid and propionic acid
- C4 for succinic acid, fumaric acid, maleic acid, aspartic acid
- C5 for itaconic acid, furfural, levulinic acid, glutamic acid, xylitol
- C6 for 5-hydroxymethylfurfural (HMF), citric acid, gluconic acid, glucaric acid, sorbitol.
- C2-C4 alcohol production from biomass and other feedstocks are shown in (Figure 8 [46]).

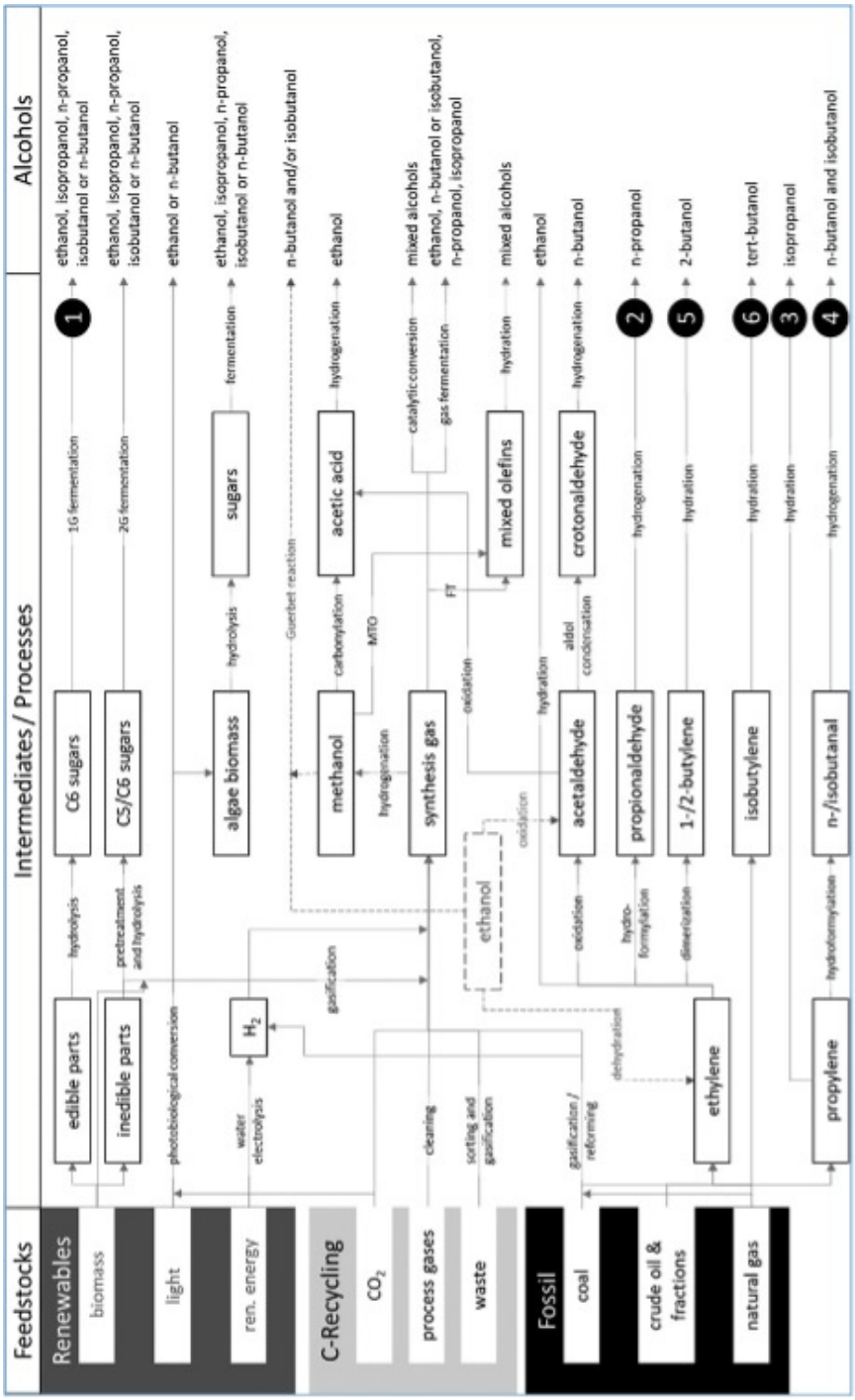

Figure 8. Overview production pathways to C2-C4 alcohols including biomass as feedstock [46].

3.4.1. Biomass pretreatment

Biomass pretreatment is an essential step to release sugars and is one of the more expensive stages in a lignocellulosic biomass refinery. Goals are to access to each component of the lignocellulose (cellulose, hemicellulose and lignin), reducing the particle size, weakening lignin, solving or hydrolyzing hemicellulose, lowering cellulose crystalline material, using low cost reagents, etc [47,48]. Many pretreatment types have been carried out, highlighting:

•Steam explosion (SE). Lignocellulosic material is exposed to a high-pressure saturated steam at a temperature of 160–260ºC and a pressure of 5–50 atm for a few minutes. The pressure is gradually released, and the steam expands within the lignocellulosic matrix. This treatment causes individual fibers to separate and the cell wall structure of the lignocellulose to be disrupted. Acid catalysis can also be carried out. More extensive lignin depolymerization can be achieved with 1% acid treatment [49].

•Ammonia fiber expansion (AFEX). Another thermochemical pretreatment that uses volatile ammonia as the main reactant. Its advantage is that it does not produce any black liquor stream after pretreatment, which may provoke loss of sugars in the waste liquors. Excess volatile ammonia is recovered, resulting in reduced waste generation and processing costs [50].

•Organosolv process. An organic solvent, such as methanol or ethanol, facilitates lignin solubilization, obtaining pure lignin as by-product. External catalysts (acid) promote the efficiency and improve

lignin and hemicellulose degradation, solvation and solubilization under less severe conditions [49,51].

- Acid treatment with diluted solutions (concentrated acids are corrosive and should be recovered, increasing the costs) of sulfuric acid, hydrochloric acid, phosphoric acid or maleic acid. They produce the hydrolysis of hemicellulose to its monomeric units. Alkali is needed to neutralize the hydrolysate [52].

3.4.2. Hydrolysis

Hydrolysis is a process for lignocellulosic biomass saccharification, leading to glucose and fructose. It is carried out through acids or enzymes, followed by a fermentation process by a bacteria or yeast. This step can be influenced by the porosity of the biomass feedstock, content of hemicellulose and lignin, crystallinity of cellulose, etc. To improve the extent of the hydrolysis process, previous pretreatments, previously explained, should be carried out. The hydrolysis of cellulose, or starch from corn, wheat or barley produces glucose. From hemicellulose, D-galactose, D-glucose, D-manose (hexoses), D-xylose and D-arabinose (pentoses) are obtained. Also saccharification and fermentation can be simultaneously carried out, reducing operation costs [53,54].

3.4.3. Bio-based platform molecules

In petroleum refineries, catalytic cracking and distillation lead to naphta, gasoline, kerosene, diesel and also residues. Depending on the pro-

cesses, conditions and petrol composition, different amounts of each fraction can be formed. Naphta is processed for the synthesis of platform molecules, which are used for the manufacture of solvents, polymers, etc. These platform molecules are mainly ethylene, propylene, C4 olefines and BTX (benzene, toluene and xylene) [55,56]. Similarly, in the carbohydrate platform of biorefineries, through fermentative or catalytic ways, the production of other platform molecules is feasible. These are after used in cosmetics, food, pharmaceutical, dyes, plastics, adhesives or lubricants industries, among others. Bio-based platform molecules can be, among others (Figure 9 [57,58]):

- 1,4 diacids (succinic, fumaric and malic acids)
- 2, 5-furandicarboxylic acid (2,5-FDCA)
- 3 hydroxipropionic acid
- 3-hydroxi-γ-butyrolactone
- 5-hydroxymethylfurfural (HMF)
- Aspartic acid
- Citric acid
- Furfural
- Glucaric acid
- Gluconic acid
- Glutamic acid
- Glycerol
- Itaconic acid

- Lactic acid
- Levulinic acid
- Malonic acid
- Propionic acid
- Sorbitol
- Xylitol

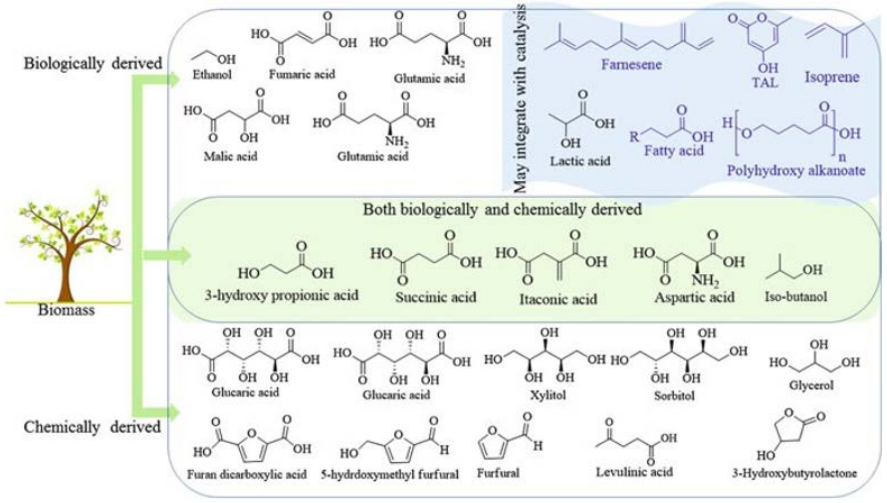

Figure 9. Top chemicals produced from biomass [58].

Main C6 (glucose and fructose) and C5 (xylose) sugars are transformed into bio-based molecules and fuels through oxidation, reduction and dehydration [59,60]. These processes diminish the oxygen content of carbohydrates, which is the main drawback of biomass as feedstock.

3.4.4. Catalytic oxidation of biomass-derived carbohydrates:

D-glucose is the most abundant natural monosaccharide, whose catalytic oxidation can provide many acids and keto acids (Figure 10).

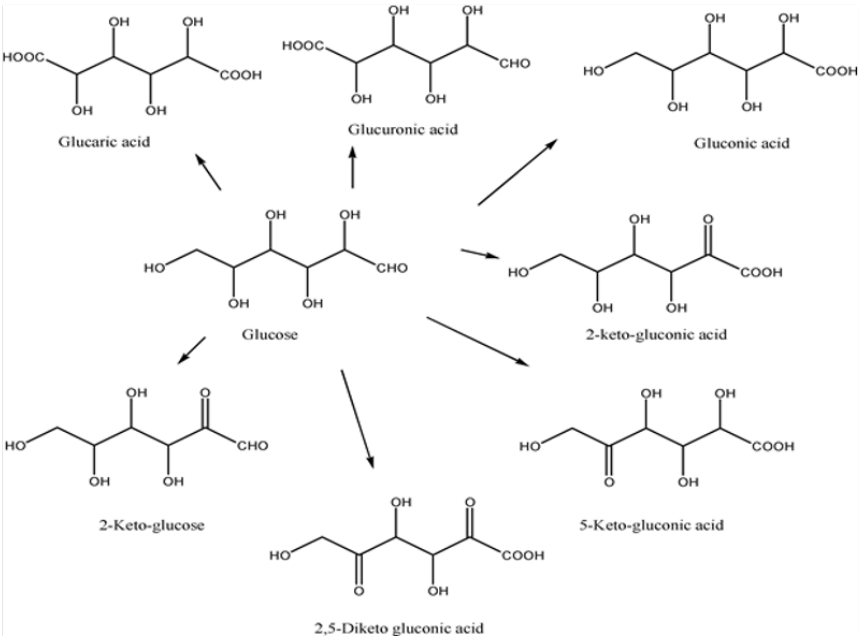

Figure 10. Glucose oxidation products [61].

There has been a great deal of scientific research on catalytic glucose oxidation into gluconic acid, formic acid, etc [62–65]. For instance, gluconic acid is produced from glucose through a dehydrogenation reaction catalyzed by glucose oxidase. It is very soluble in water and has a mild and refreshing taste. Gluconic acid is used in beverage, food and pharmaceutical industries. Gluconic acid is used in the food, beverage, and pharmaceutical industries. It is non-corrosive and non-toxic. Sodium gluconate is a good chelator at high pH, better than

commonly used chelators like EDTA. In addition, it is easily biodegradable (98% at 48 hours) [63].

3.4.5. Catalytic hydrogenation of biomass-derived sugars:

The hydrogenation of mono, di or polysaccharides gives rise to sugar alcohols, such as erythritol, xylitol, sorbitol, mannitol, lactitol, isomalt or maltitol. They are very important for food and pharmaceutical industries owing to their lower caloric value, prebiotic effect or bulking agent capacity. Xylitol, sorbitol and mannitol are the most produced. The direct catalytic hydrogenation of hemicellulose can lead to sorbitol, as shown in Figure 11[61,66].

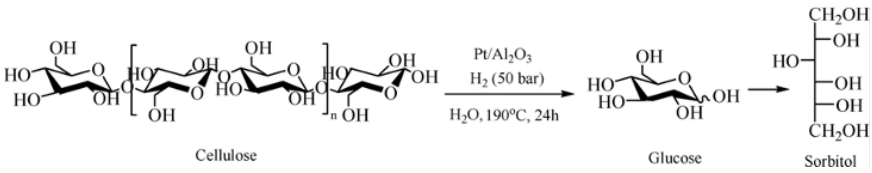

Figure 11. Catalytic hydrogenation of cellulose over Pt/Al_2O_3 [61].

3.4.6. Catalytic dehydration of derived-biomass hexoses and pentoses

The third option for oxygen content lowering is removing water, leading the dehydration reactions to very interesting compounds, especially furans and levulinic acid. Sucrose, starch, cellulose, hemicellulose and inuline contain hexoses and pentoses. Hexoses dehydrates to 5-hydroxymethylfurfural (HMF), which is transformed into levulinic

acid (LA) and formic acid (FA) by rehydration. Similarly, pentoses lead to furfural through dehydration (Figure 12).

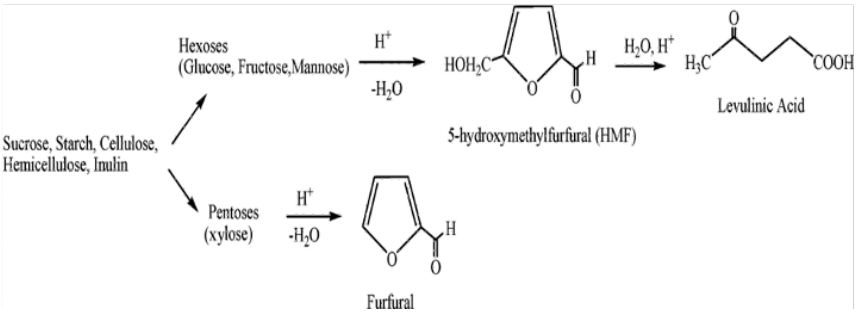

Figure 12. Catalytic dehydration of hexoses and pentoses to HMF, LA and furfural [61].

The first sugar dehydration under acidic conditions reported formic acid production, which later was found to be LA [67]. Sugar dehydration to furfural was discovered by Döbereiner, catalyzed by manganese oxide and sulfuric acid, and reported by Newth [68]. First HMF synthesis publications date from 1895 [69,70]. The importance of furans to produce important bulk chemicals and fuels has generated growing interest and research on their synthesis.

Furfural, derived from acid hydrolysis of sugar cane bagasse, maize cob, rice husk or any material containing C5 carbohydrates to xylose and subsequent dehydration, is useful in the synthesis of a range of specialized chemical products. Moreover, chemical modification of its aldehyde functional group into nitro, imine and chalcone groups, provides different reactivity to furfural. For instance, an efficient xylose and xylene conversion process with 72% furfural yield, using maleic

acid as catalyst, in water at 200 ºC, has been reported [71]. Furfural is a versatile platform chemical for the production of liquid hydrocarbons and gasoline additives, such as 2-methyltetrahydrofuran (2-MTHF). Furan hydrogenation is the most versatile way to upgrade furan-based molecules to fuels, leading to biofuels for gasoline blends, such as 2-methylfuran (2-MF), 2,5-dimethylfuran (DMF) and 2-methyltetrahydrofuran (2-MTHF) [30,72,73].

Levulinic acid can be upgraded to levulinate esters, which serve as a transportation fuel and fuel additives. Moreover, hydrogenation of LA to γ-valerolactone and further to liquid alkanes with eight or more carbon atoms, are well known. Levulinic acid is also useful for the manufacture of resins, solvents, polymers, fungicides or pesticides, among other applications [74–76]. Formic acid, produced in the biomass hydrolysis process, can be used as a hydrogen donor for LA hydrogenation to produce fuel additive, such as γ-valerolactone [77].

HMF and LA have been identified as two of the top 12 bio-based platform chemicals by the United States Department of Energy. The reaction pathways for LA and HMF production are similar because HMF is the intermediate for LA formation through rehydration.

The synthesis of HMF is based on the acid-catalyzed consecutive triple dehydration of glucose and fructose, although sucrose, cellobiose or inulin, as well as industrial wastes, can be used after depolymerization. Not only HMF is produced from the acid catalyzed dehydration, but also other products such as LA, formic acid and insoluble and soluble polymers, because of side reactions, are obtained. Sugar dehydration chemistry is complex, and many aspects must be taken into account for attaining acceptable yields.

3.4.7. HMF as platform chemical

HMF is solid at room temperature (melting point 303-307 K), but its poor fuel properties limit its use as fuel or fuel additive. However, its furan derivatives are being studied for biofuel applications. Thus, Avantium has produced derived C5 and C6 biofuels. The results have shown that smoke and sulfur content decrease with increasing furanic concentration in diesel-biofuel blends, and no difference in the diesel engine operation has been observed [78]. Dumesic research group has also researched on HMF upgrading to liquid fuels. Thus, hydrogenolysis of HMF can produce 2,5-dimethylfuran, which can be used as blender in fuels, being obtained with yields near 80% over a Cu-Ru/C catalyst [73].

HMF, as building block, is very important due to a wide range of possible reactions. Besides, LA from HMF rehydration (Figure 13), other furan derivatives (such as 2,5-dimethylfuran or 2,5-furandicarboxilic acid, FDCA) and also non-furanic ones (caprolactam, 1,6-hexanediol), can be produced from HMF, although it is true that many difficulties are found to achieve high yields and selectivities, resulting in high production costs [79]. Avantium has produced PEF polyester (polyethylene furanoate) from both biobased FDCA and ethylene glycol in a pilot-scale plant and will start a flagship plant in Delfzijl (Netherlands) in 2021. The objective is PEF replacing PET bottles.

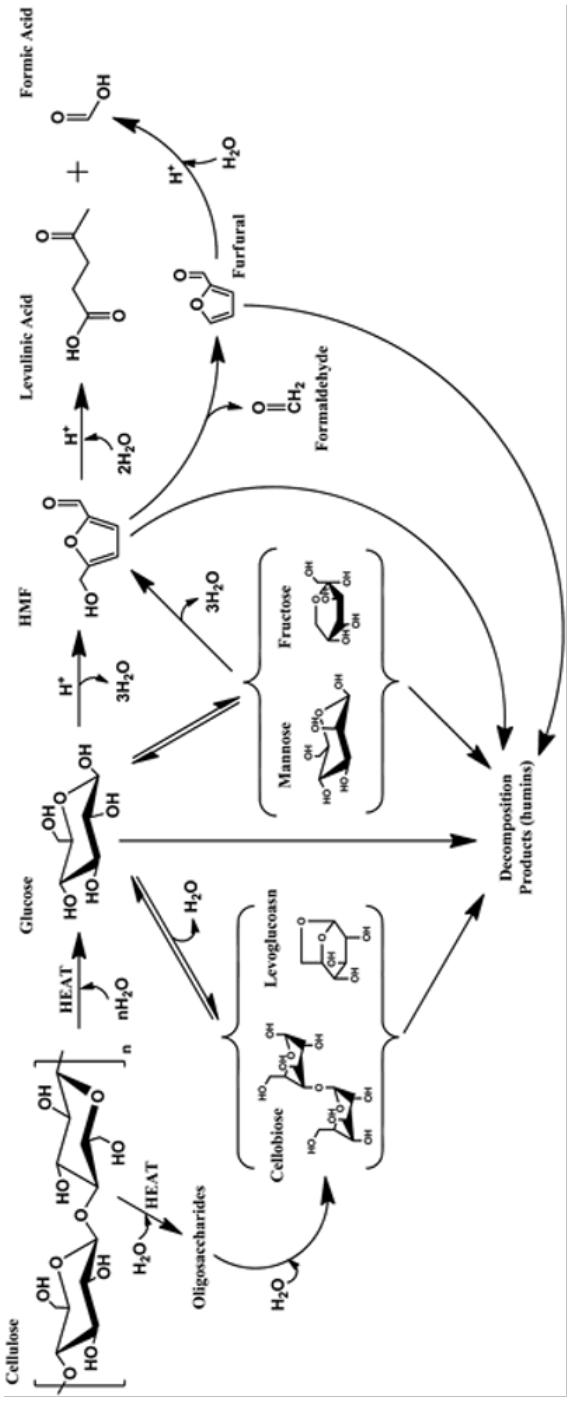

Figure 13. From cellulose to LA (HMF) [80].

In addition to FDCA monomers, HMF can produce 2,5-bis(hydroxymethyl)furan by hydrogenation (US3083236A Patent) [81].

From HMF, via oxidation, 2,5-diformylfuran (DFF), an interesting building block for polypinacols and polyvinyls, can be synthesized [82]. HMF and methylated derivatives are also very useful for the manufacture of polymers with good thermal stability [83].

HMF can also provide agrochemicals (5-amino-levulinic acid) and flavors (alapyridaine), among other products [84,85]. HMF as platform chemical is schemed in Figure 14.

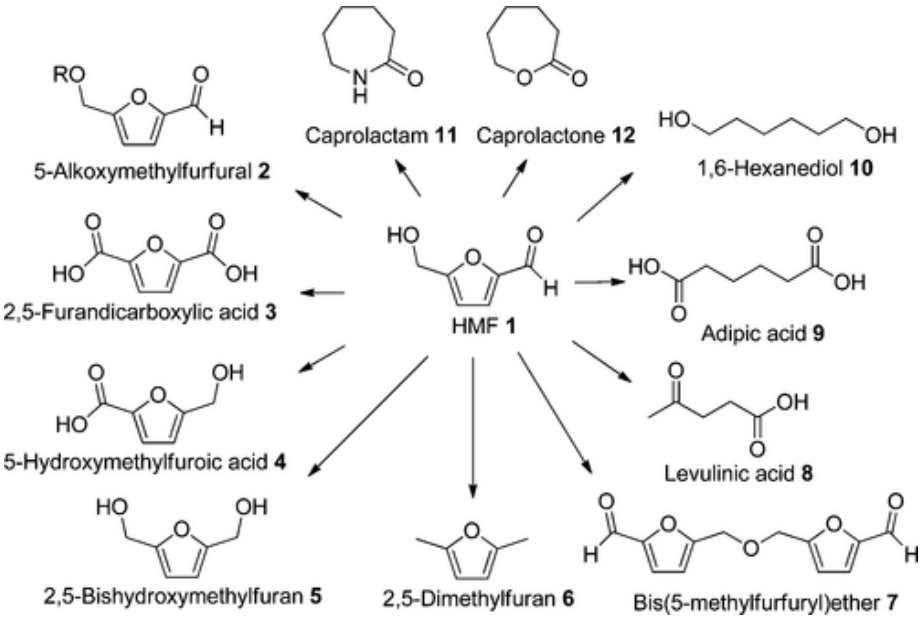

Figure 14. HMF as platform chemical [86].

3.5. C6 sugars dehydration to HMF

Through hexoses dehydration, furan-type platform molecules can be obtained, being HMF, with six carbon atoms, especially important as chemical platform (previous Section). However, besides HMF, furfural, levulinic acid and byproducts, like humins, can be obtained. Due to the occurrence of these side processes, experimental conditions, reaction mechanism, separation and isolation methods and type of acid catalysis must be specially considered, without neglecting techno-economic aspects.

3.5.1. Mechanism reaction

There has been not determined one specific route for HMF synthesis from hexoses through dehydration; on the contrary, two general dehydration pathways have been proposed: acyclic and cyclic mechanisms. The acyclic pathway for hexose dehydration to HMF was put forward by Anet *et al.* and Moreau *et al.*, being based on the glucose isomerization to fructose through a 1,2-enediol, which was assumed to be the rate-limiting step (Figure 15 [87,88]). In addition, other cyclic pathways have been proposed by Antal *et al.* and Newth [68,89], all of them starting form cyclic ketofuranose, followed by three consecutive dehydrations (Figure 16). This cyclic mechanism also requires glucose isomerization to fructose. The dehydration of fructose to HMF is more favorable than glucose, which Kuster attributed to the stability of its ring structure [90].

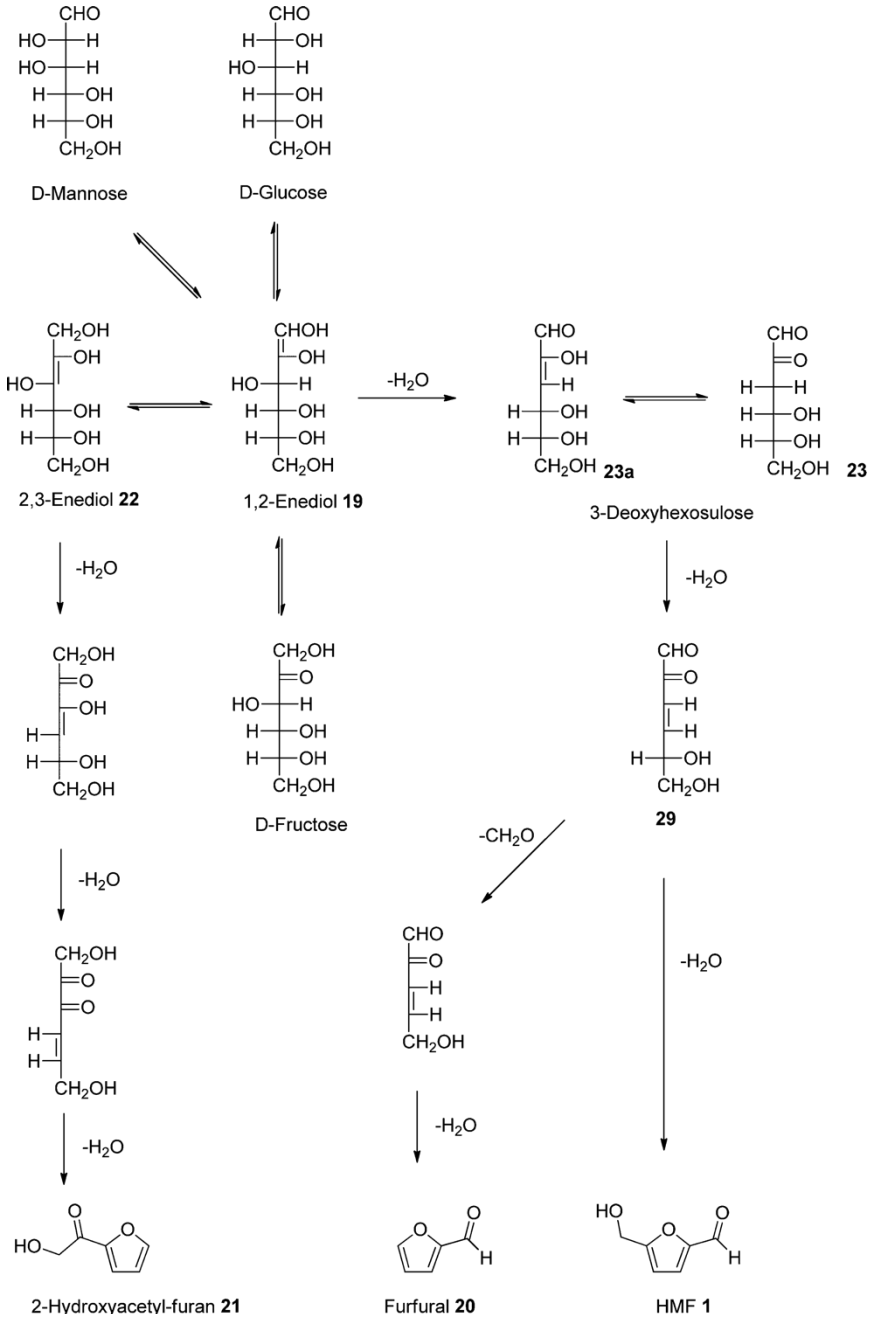

Figure 15. Formation of HMF from fructose: acyclic pathway [86].

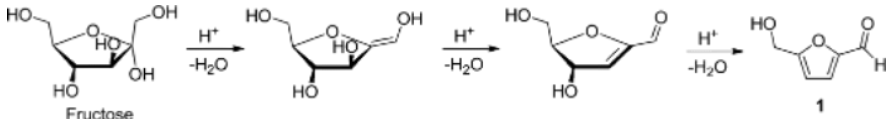

Figure 16. Cyclic pathway in HMF formation from fructose [86].

These factors are either related to temperature and reaction medium. Thus, in aqueous phase and at room temperature, glucose is mostly as pyranose (glucopyranose), while fructose is as both pyranose and furanose (fructopyranose and fructofuranose, respectively) forms. In other solvents as DMSO, fructofuranose is more abundant, being a cyclic mechanism more consistent with the experimental results [91]. Despite fructose is more reactive than glucose, this latter is most abundant and cheaper in lignocellulosic biomass, and therefore, understanding reaction mechanism from glucose is necessary. Several studies have found that glucose to fructose isomerization coexisting with small amounts of glucose. At high temperature in aqueous systems, fructose has been widely detected compared to glucose [89]. In addition, in non-aqueous phase, as in DMSO, glucose isomerization to fructose has been suggested [92]. In this reported work, catalysts were also demonstrated to influence on the reaction mechanism. Without catalyst, fructose dehydrated to HMF but did not glucose, and with a bifunctional heterogeneous catalyst, fructose formation was in correlation to the base sites on the catalyst, acting as an isomerization catalyst more than a dehydration one. It could be concluded that glucose isomerization to fructose is needed, and its efficiency would determine the HMF selectivity. A catalyst with active sites that favor isomerization is desirable.

3.5.2. Reaction medium

HMF is soluble in water and in common organic solvents (methanol, ethanol, acetone, ethyl acetate, dimethylformamide, ether, benzene, chloroform, DMSO, DFM). Water is natural, cheap and environmental benign, but HMF yields are low compared to organic solvents.

Aqueous solutions

In pioneering studies, hexose dehydration was mainly carried out in water, with sulfuric and hydrochloric acids as homogeneous acid catalysts.

From fructose, high HMF yields (50%) and fructose conversion (95%) were reported in aqueous system at high temperature (250 ºC) and pressure (340 bar), under homogeneous acid catalysis (2 M H_2SO_4) by Antal *et al.* [89]. Carlini *et al.* attained high HMF selectivities (85-100%) in aqueous phase at 100 ºC, using heterogeneous acid phosphate catalysts (niobium, zirconium and titanium). However, fructose conversion was very low, but it was improved extracting the formed HMF with MIBK [93,94].

From glucose, it is important to study thermal decomposition in water, without catalyst, because HMF can be also obtained, although yields were low [95,96]. Therefore, the use of catalysts is needed. Li *et al.* reached a 49% HMF yield from glucose (MW irradiation, 400 W, 1 min) using sulfuric acid (10 wt %) as catalyst, while by thermal decomposition only 1% HMF yield was obtained. Many heterogeneous catalysts have also been employed for glucose dehydration to HMF in aqueous phase. Thus, Watanabe *et al.* reported 19 % HMF yield and 64 % glucose conversion using TiO_2 as catalyst (MW, 5 min) [97]. A

TiO_2-ZrO_2 catalyst showed better results than in homogenous catalysis, because ZrO_2 also possesses basic sites, improving glucose to fructose isomerization, and TiO_2 catalyzes dehydration to HMF, achieving 29% HMF yield and 44% glucose conversion [98]. Also, this bifunctional catalyst was tested for lignocellulose dehydration to HMF.

Cellulose and lignocellulose lead to low yields, but after a previous hydrolysis pre-treatment, HMF yield can be improved.

Organic solvents

Regarding the HMF yield, the use of homogeneous or heterogeneous acid catalysts is not decisive, but the addition of organic solvents provided higher yields because HMF rehydration was avoided, as well as decomposition and/or condensation associated to side reactions. In this sense, DMSO has been widely used. Nakamura and Morikawa reported 90% HMF yield from fructose, using an ion-exchange resin [99]. Studies in DMSO with acid and basic catalysts have been carried out, showing acid catalysts promote HMF formation whereas basic ones inhibit. While DMSO leads to high yields, its separation from HMF is difficult, and other organic solvents have been evaluated.

Another advantage over aqueous conditions are milder operation conditions.

Moreover, DMSO has been employed as solvent when starting from glucose. Ebitani *et al.* used hydrotalcite as catalyst, obtaining fructose, and, using hydrotalcite and Amberlyst 15 for both isomerization and dehydration reactions, respectively, no fructose was observed, and 42% MHF yield was reached, revealing important aspects of the glucose dehydration to HMF [100].

Biphasic reaction medium

As already indicated, hexose dehydration to HMF may result in LA because of HMF rehydration. HMF can also react with sugars or intermediates leading to condensation or decomposition compounds, such as humins (Figure 17).

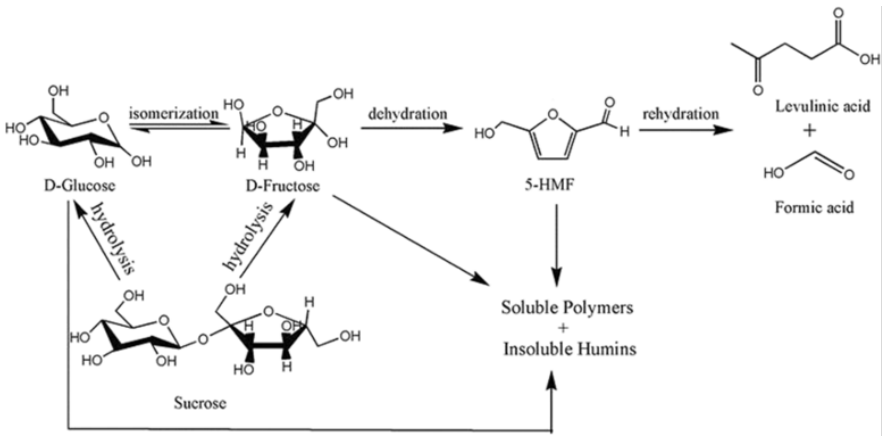

Figure 17. HMF from glucose and fructose [101].

Kuster and Van der Steen studied fructose dehydration to HMF in a MIBK/water biphasic system, using phosphoric acid as acid catalyst, demonstrating that both high temperature and acid concentration increased the reaction rate, longer residence times yielded more HMF and higher MIBK/water ratio increased selectivity and yield [102].

Also, heterogeneous catalysis has been employed for fructose dehydration in biphasic systems. With regard to MIBK/water systems, Moreau *et al.* studied sugar dehydration using zeolites with different Si/Al molar ratio, finding that the most active catalyst provided high conversion, but low selectivity to HMF, and, when zeolites were dealuminated, a higher selectivity at lower conversion was found, which pointed

out, as expected, the influence of aluminum on the acid-base properties of these zeolites. The best result was 69% HMF yield and 76% fructose conversion in the presence of a H-mordenite (Si/Al= 11), after 60 min at 165 ºC in MIBK/water (volume ratio of 5) [103,104]. Ordomsky *et al.* tested also H-mordenite (Si/Al= 11.7) for fructose dehydration in MIBK, water and water/MIBK, and observed that, after zeolite deactivation, higher conversion and selectivity were achieved in water. It was explained as due to deactivation reduced oligomerization processes and other fructose reactions. MIBK improved selectivity only for high fructose conversion, and this was because this solvent suppressed the activity of some acid sites which favored fructose side reactions [105]. They also studied glucose dehydration in biphasic medium, resulting in lower HMF yields. Thus, glucose dehydration to HMF in MIBK/2-butanol using HCl as catalyst, at 170 ºC for 17 min, led only to a 24% HMF yield at 50% glucose conversion [106].

With regard to the use of heterogeneous catalysts in biphasic systems, a 35 % HMF yield and 50% glucose conversion were achieved using water/DMSO (volume ratio of 2:8) and extracting with MIBK/2-BuOH (volume ratio of 7:3), at 150 ºC in 3 h, using $CrCl_2$ as catalyst in a thin immobilized ionic liquid layer [107], TiO_2 has also been evaluated as catalyst in water/MIBK (1:10 v:v), at 180 ºC in 2 min by Fedie *et al.* [108].

Despite biphasic systems lead to better results than aqueous systems, HMF yields are low when starting from glucose.

On the other hand, dehydration of di- and polysaccharides, such as cellulose, sucrose or starch, has been carried out in biphasic systems,

without catalyst, with homogeneous catalysts, such as HCl, and with heterogeneous ones, such as H-zeolites or TiO_2 [104,108,109].

Ionic liquids

Ionic liquids have also been widely employed as reaction medium for sugar dehydration to HMF, because they possess organic and inorganic ions, which play key roles in these reactions, low melting points (bellow 100 ºC), low vapor pressure (barely volatile) and low viscosity.

Moreau *et al.* performed fructose dehydration to HMF using 1-butyl 3-methyl imidazolium tetrafluoroborate (BMIM+$BF4^-$) and 1-butyl 3-methyl imidazolium hexafluorophosphate (BMIM+$PF6^-$), reporting faster reaction rates than with DMSO, with HMF yields around 80% in 24 h [110]. Later, they also published a work using acidic methylimidazolium chloride (Brönsted acidic) for fructose dehydration, reaching 92% HMF yield at 98% fructose conversion, at 90 ºC after 45 min. This ionic liquid acted as both solvent and catalyst [111]. Heterogeneous catalysts combined with ionic liquids as solvents have been studied for hexose dehydration to HMF. Thus, conversion of fructose and glucose into HMF with lignin-derived carbonaceous catalysts, under microwave irradiation, in dimethyl sulfoxide–ionic liquid mixtures, were studied by Zhou *et al.*, reporting 99% glucose conversion and 68% HMF yield (160 °C for 50 min) and the catalyst could be used for several catalytic cycles [112].

Several publications about glucose dehydration using ionic liquids have shown that chromium is important for attaining high HMF yield. Besides, studies using $CrCl_2$ and $SnCl_4$ indicated that these catalysts

were mainly isomerization catalysts, and chloride ions could be responsible for dehydration by generation of hydrochloric acid [86].

3.5.3. Operation conditions and reactors

Operation conditions and reactors design must be defined in such a way that higher HMF yields and lower environmental and economic costs can be achieved. High HMF yield is hindered by instability of HMF and side reactions, which should be avoided. Moreover, produced humins can block up and deactivate solid catalysts. In addition, humins can be deposited on the reactor walls, reducing heat transfer, adversely affecting maintenance and operation conditions. When cellulose or lignocellulose are used as feedstock, design and operation conditions must be adapted for solids.

HMF production from fructose, glucose or lignocellulosic biomass have been performed in lab scale. Thus, batch stirred and continuous reactors have been evaluated for HMF production in mixed solvent systems. McNeff *et al.* have worked on continuous production of HMF from cellulose, starch, glucose and fructose in water/MIBK, in a fixed bed reactor with zirconia and titania as solid catalysts [108].

Pilot scale HMF productions have been also reported. Teunissen used 1 kg sugar cane, in the presence of an acid catalysis in water, to obtain 40-50 g of HMF [113]. Suedzucker patented the pilot scale production from 11 kg of fructose in water, obtaining a filtrate with 55% fructose conversion and 33 % HMF yield. After chromatographic separation, salts, unreacted fructose, HMF and other fractions were obtained. The

HMF fraction was concentrated and crystallized to give rise 99% pure HMF. This process is shown in Figure 18 .

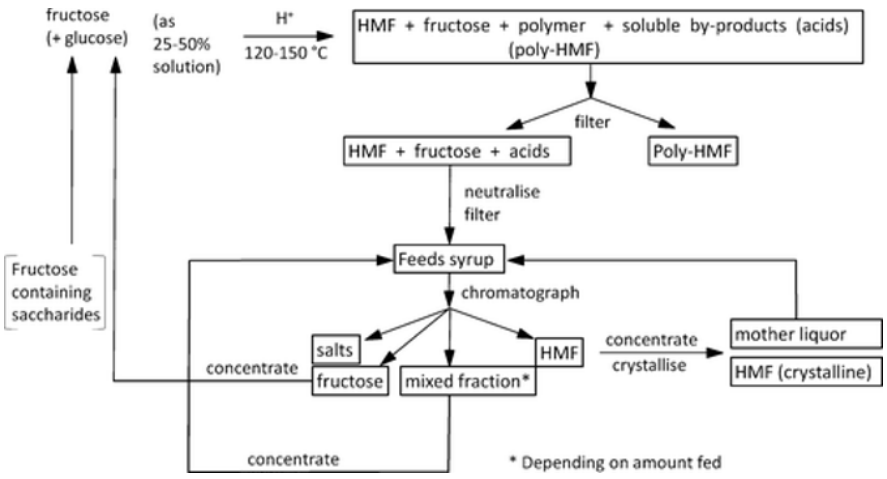

Figure 18. HMF pilot scale production [86].

Other pilot scale plants have been reported using organic solvents, or biphasic reaction medium. Furchim patented a pilot scale batch process for HMF production from fructose in DMSO, Cope produced HMF from sucrose using MIBK as extracting solvent, and Roquette Frères performed HMF production from fructose in a water/MIBK system [114–116].

Figure 19 shows a continuous flow system for HMF production in biphasic systems by using MIBK as organic phase.

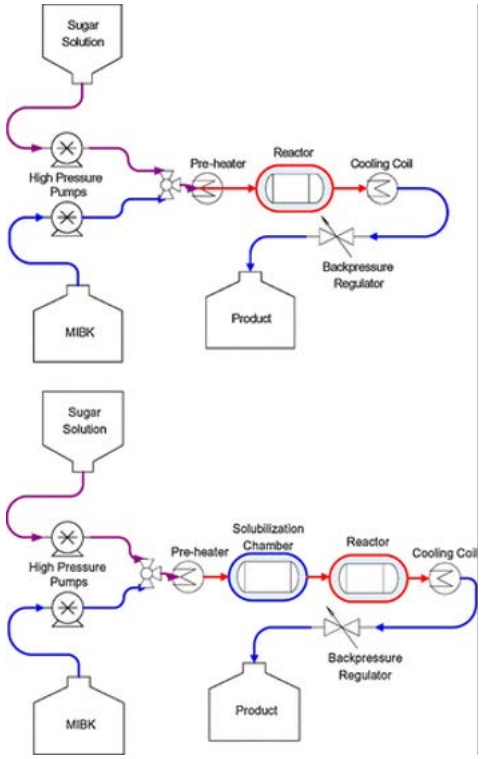

Figure 19. Continuous flow systems for HMF production in biphasic systems [86,108].

3.5.4. HMF separation and isolation

HMF produced can be solved in water, an organic solvent, an ionic liquid or in a biphasic system. In biphasic water-organic phases, MIBK has been suitable as in situ extraction solvent. Partition coefficient, defined as HMF concentration in the organic phase divided by HMF concentration in the aqueous phase, R, was determined and a relation between R and HMF selectivity tried to be established by Dumesic *et al.* in saturated NaCl aqueous systems for fructose dehydration, using different organic solvents (alcohols, ketones and ethers) not finding a clear relation (Figure 20 [117]).

HMF extraction with organic solvents must be studied considering thermodynamic costs, which will determine operation conditions.

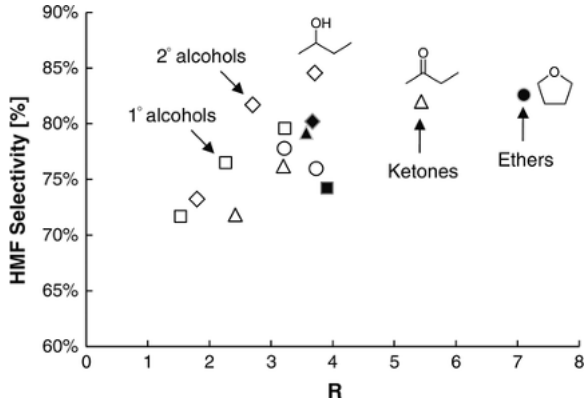

Figure 20. Correlation of partition coefficient (R) and HMF selectivity in saturated NaCl aqueous systems for fructose dehydration [86,117].

On the other hand, HMF separation and purification can be carried out by filtration, separating insoluble products from HMF. Filtration with a pressure filter was reported by Rapp [118], who also proposed a chromatographic process after removing solids and liquid neutralization, by using a calcium loaded ion-exchange column to separate HMF from sugars and other byproducts.

More recent methods are based on HMF adsorption, for instance, on nonfunctional polymeric resins, activated carbon or activated biochars [119–121].

Distillation under reduced pressure has been used to obtain HMF, but the boiling point of solvents has an important impact on separation, and besides thermal degradation of HMF can occur during the distilla-

tion. Several patents about procedures to prevent HMF degradation have been published [122,123].

3.5.5. Techno-economic aspects

In addition to separation and purification costs, other aspects must be considered and evaluated from an economic point of view.

The use of acid homogeneous catalysts, such as liquid mineral acids, for HMF production is cheap, but a neutralization step is needed with bases, producing salts as waste. Moreover, these acids are corrosive, deriving in maintenance and equipment replacement. Thus, heterogeneous catalysts are more desirable; however, they are more expensive and their activity decreases owing to the formation of by-products, like humins, which can deactivate the solid catalyst.

Several techno-economic studies have dealt with HMF production in biphasic systems. Thus, Blecker *et al.* evaluated HMF production from fructose with MIBK and 2-butanol as extraction solvents. They found the fructose price as the main determining factor in production costs, and also considered relevant the use with solvents with higher partitioning coefficient (R) [124].

An interesting plant was designed by *et al.* for 2,5-dimethylfuran and HMF from fructose in a biphasic NaCl saturated water/1-butanol system. The most important evaluated costs for HMF production were ordered as follows [125]:

- Feedstock price (fructose)

- HMF yield
- Byproduct price (2,5-dimethylfuran)
- Catalyst
- Equipment

HMF desirable cost must be similar to other fossil fuel-based platform chemicals.

The most favorable properties of HMF derived bulk products, the most favorable HMF production. As reported in Section 3.4.7, Avantium will pretend to open a FDCA production plant from HMF and biobased ethylene glycol to produce PET bottles substitutes.

In any case, HMF production from sugars for biofuels is not profitable, but producing directly from lignocellulosic biomass would be on the right path.

3.6. Solid acid catalysts for dehydration of hexoses

3.6.1. Homogeneous and heterogeneous catalysts

By using catalysts, chemical processes can occur faster through different mechanisms and selectivity is managed. Catalysts are not consumed or altered in the process.

Catalysts are classified into two groups:

- homogeneous; catalyst is in solution and in the same state as reactants, thus leading to homogeneous catalysis. Main types of homogeneous catalysts are:

- Gas-phase catalysts, i.e. catalytic ozone decomposition [126]
- Acid-base catalysts for cracking, alkylation… [127]
- Transition metal catalysts, i.e. for autooxidation reactions [128]

•Heterogeneous: catalysts are in a different phase than the reaction components. There are many types:

- Dispersed metal catalysts, where the active metal component is supported on high surface area carriers, i.e. Pt/Al_2O_3 [129]
- Bulk metal oxides, mixed or dispersed. metal oxide catalysts. Useful in acid-base reactions, selective partial oxidation reactions, total oxidation reactions, depollution, biomass conversion, photocatalysis, among others. Thus, Ni/Al_2O_3 has been employed for partial oxidation of methane to syngas [130]; mesoporous Nb_2O_5 has been reported as solid acid catalyst for dehydration of D-xylose into furfural by García-Sancho *et al.* [131]
- Sulfides as transition metal sulfides (TMS), reported by Infantes-Molina *et al.* for petroleum upgrading–hydrodesulfurization reactions [132]
- Heterogeneous acid catalysts zeolites, metal oxides, clays and zeolites. Dehydration of xylose to furfural have been carried out with MCM-41-Supported Niobium-Oxide Catalysts by García-Sancho *et al.* [133].
- Heterogeneous basic catalysts, such as alkali metal oxides, alkali ion-exchanged zeolites, clays, supported metal alkali ion, etc.

Albuquerque *et al.* reported CaO supported on mesoporous silicas as basic catalysts for transesterification reactions [133].

Main properties of homogeneous and heterogeneous catalysts are compared in Table 1.

Table 1. Homogeneous and heterogeneous catalysts comparison.

	HOMOGENEOUS	**HETEROGENEOUS**
Activity	high	variable
Selectivity	high	variable
Reaction conditions	mild	severe
Catalyst lifetime	variable	long
Catalyst deactivation	low sensitive	sensitive
Diffusion problems	no	yes
Catalyst reuse	difficult	easy

Homogenous catalysis has been widely used because of easy use and lower prices, but has disadvantages with respect to heterogeneous catalysis, such as difficult catalyst recovery and reuse and corrosion of the equipment. Thus, heterogeneous catalysts are preferred from environmental and economical point of views.

Energy sector is particularly dependent on heterogeneous catalysis and future hydrogen-based energy technologies and other sectors will require future new heterogeneous catalysts and catalytic processes.

Solid surface working as catalyst plays three coupled functions: i), adsorbing the reactants and cleaving specific bonds; ii), bringing reactants close and in the required positions; and iii), desorbing the products. To make more efficient catalysts, determining factors in surface behavior must be elucidated. Mechanistic insights and computational methods can be used to reduce the number of possible catalysts for specific reactions. Besides manipulating the performance of heterogeneous catalysts by modification of their composition and tuning the structure of active sites, future research will likely go beyond the catalyst itself, promoting the activity of the reagents, enabling catalyst-adsorbate interactions and even enabling spatially and temporally variable modifications of catalyst surfaces [134].

3.6.2. Acid-base catalysts

Many reactions are acid-specific, such as sucrose hydrolysis into glucose and fructose in acid solutions [135], whereas others are base-specific, such as biodiesel formation from triglycerides [136], and many others are catalyzed by both acid and basic sites present on acid-base catalysts, as Rojas-Buzo *et al.* reported for the transformation of biomass-derived furanic compounds into chemicals using Hf-based metal–organic frameworks as acid–base catalysts [137].

Acid sites can be classified as:

- Brönsted type. There is an initial transfer of protons from the catalyst to the reactant (proton donors)

•Lewis type. An electron pair from the reactants is accepted by the catalyst (electron pair acceptor)

Catalytic activity does not only depend on the strength of acid-base sites, but also their acidity types. Thus, Connell and Dumesic studied the generation of Brönsted and Lewis acid sites on the surface of silica by addition of doping cations, such as B(III), Fe(III), Al(III), Mg(II), as oxides, finding different Brönsted and Lewis acid sites proportions [138]. These authors determined acidity by pyridine adsorption coupled to FTIR spectroscopy, observing a correlation between the cation electronegativity and the IR absorption frequency of adsorbed pyridine on the Lewis acid sites. The cations responsible of Brönsted acid sites were those tetrahedrally coordinated inside the silica structure, not on its surface. They also found "anionic" Brönsted acid sites induced by high electronegative cations.

Concerning glucose to HMF dehydration, both homogeneous and heterogeneous catalysts have been employed, especially with mineral and solid acids.

In this sense, Watanabe *et al.* studied glucose dehydration through basic (NaOH) and acid (H_2SO_4) homogeneous catalysts, and also through acid and basic heterogeneous catalysts (ZrO_2 y TiO_2) in water (200ºC), concluding that bases promoted glucose isomerization and acids are required for dehydration and condensation reactions [139,140]. ZrO_2 produced similar effects to NaOH, acting as a basic heterogeneous catalyst, and TiO_2 acted as basic for glucose isomerization and as acid for glucose dehydration (bifunctional), leading to the best results (24% HMF yield at 85% glucose conversion).

On the other hand, Ohara *et al.* reported glucose conversion to HMF in the presence of basic, acid and mixed basic and acid solids. Aldose–ketose isomerization of glucose to fructose occurred preferentially with base catalysis, and, in coexistence with a solid acid, led to the subsequent dehydration of fructose to 5-hydroxymethylfurfural. A combination of Amberlyst-15 and hydrotalcite, an anionic layered clay, afforded high HMF selectivity under moderate reaction temperature in one-pot processes, as the formation of anhydroglucose was prevented [141]. In addition, Choudhary *et al.* investigated HMF and LA production from glucose in cascade reactions using a Lewis acid catalyst ($CrCl_3$) together with a Brönsted acid one (HCl) in aqueous media. Lewis acid catalyst was active in glucose isomerization to fructose, and the combined Lewis and Brönsted acid catalysts performed isomerization and dehydration/rehydration processes. The hydrolyzed Cr(III) complex $[Cr(H_2O)_5OH]^{2+}$ was the most active Cr species in glucose isomerization and was probably acting as a Lewis acid–Brönsted base bifunctional site. Moreover, complex interactions between the two catalysts were revealed: Brönsted acidity retarded aldose-to-ketose isomerization and Lewis acidity increased the overall rate of consumption of fructose and HMF compared to Brönsted acid catalysis, by promoting side reactions. This effect was produced because even in the absence of HCl, hydrolysis of Cr(III) decreased the pH solution, and this Brönsted acidity conducted dehydration and rehydration reactions [142].

These are some examples of many focusing on glucose dehydration, Therefore, it can be assumed that catalysts acting as basic or Lewis acid facilitate glucose to fructose isomerization and ones acting as

Brönsted acid promote glucose dehydration to HMF and side reactions, and, in consequence, bifunctional catalysts are needed.

3.6.3. Synthesis of heterogeneous catalysts

There is such a variety of chemicals for catalyst preparation that there is a large plethora of methods for synthesizing solid catalysts. Nevertheless, there are some common steps to be followed based on the knowledge of the chemical and physical laws and/or empirical evidence. Many industries manufacture catalysts, but the methodologies followed are mostly confidential. A general scheme for catalyst synthesis, adapted from [143], is shown in Figure 21.

The catalyst synthesis must achieve three targets: texture, attrition resistance and shape for a specific reaction. Texture means pore structure, surface area and bulk density characteristics.

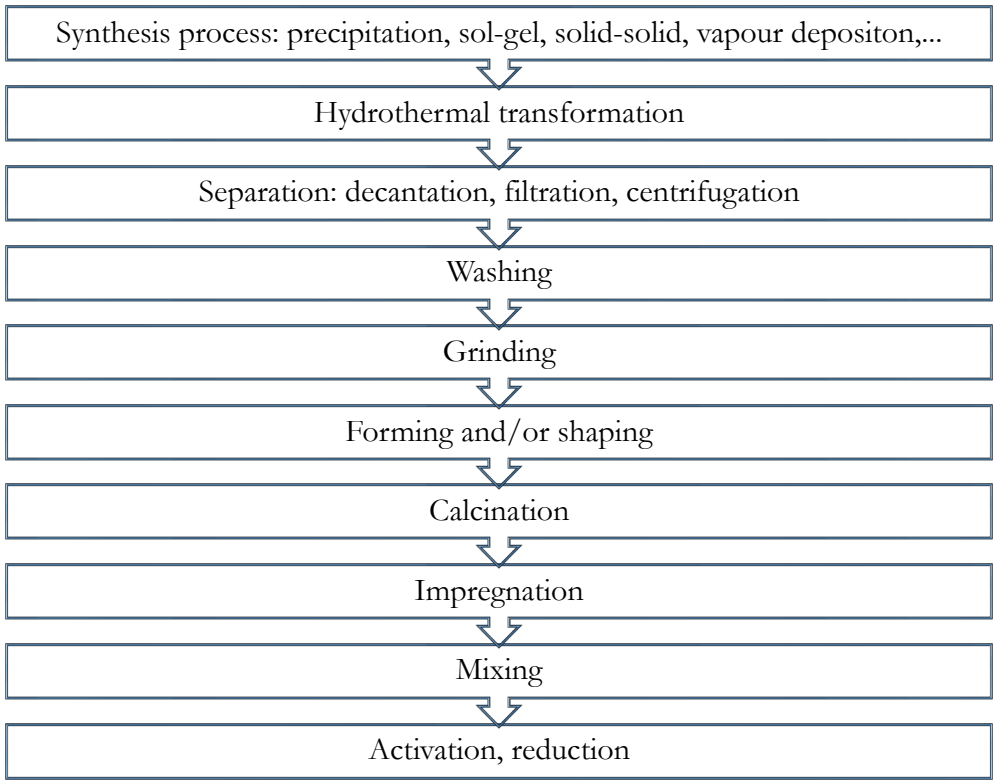

Figure 21. Industrial process for manufacturing catalysts [143].

Three groups of catalysts can be distinguished: bulk catalysts and the supports, impregnated catalysts and mixed or agglomerated catalysts. Bulk catalysts are used as prepared or with an inert binder, i.e. shaped Beta and Y zeolites with binders has been synthesized for cyclization of citronellal by Vajglová *et al.* [144]. Supported catalysts are needed because of expensive substances, obtaining bifunctional catalysts, high dispersion of the active phase, better mechanical resistance, among other properties.

Bulk catalysts can be prepared by different methods: precipitation or co-precipitation, sol-gel methods, hydrothermal synthesis, flame hydrolysis, vapor deposition, grafting, etc.

Precipitation methods

Precipitation methods are usually performed from a first solution by adding a second selected solution to reach the required precipitation pH. Later, separation is needed. Some acid catalyst prepared by precipitation are SiO_2-Al_2O_3 and $AlPO_4$ [143].

Sol-gel methods

These methods can employ monometallic alkoxides which are hydrolyzed to form polymeric oxide gels. Water/alkoxide ratios, nature of alkyl groups, size and oxidation state of the cation, pH, ageing and temperature are determinant parameters. Gao *et al.* synthesized a hierarchically porous niobium phosphate monolith by a sol–gel method for fructose dehydration to HMF [145].

Hydrothermal synthesis

It can consist of solid-solid reaction at high temperature under hydrothermal conditions, being used, in particular, for zeolites and other molecular sieves. Typical syntheses are those of MFI (ZSM-5) by using tetrapropyl ammonium hydroxide as templating agent [146], and mesoporous materials of controlled pore size and narrow size distribution such as MCM-41, in the presence of bulky surfactant molecules [147].

3.6.4. Micro and mesoporous materials

Porous materials, with high surface area, narrow pore size distribution and tunable pore diameter, are suitable for catalysis, adsorption or separation processes. The development of a large variety of porous materials with different morphologies, structures and functionalities, has largely contributed to the advance of material science. Novel porous catalysts require the formation of relevant porous structures (micro-, meso- or hierarchical), and the structural incorporation of a particular heteroatom for specific purposes.

A complete description and classification of porous materials was reported by Rouquerol *et al.* [148]. According to the accessibility to an external fluid or molecules, they were classified into two groups: closed and open pores. First ones influence on bulk density or mechanical strength, but are inactive for adsorption and catalysis, thus catalysis mainly focuses on open pores (Figure 22, [148]).

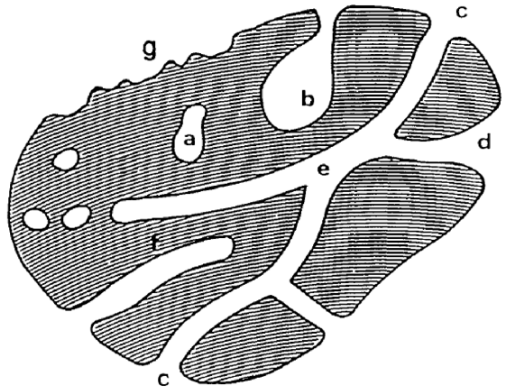

Figure 22. Schematic pore classification according to their availability: a - closed pores, b, f - open pores only at one end, c, d, g - open pores, e - open at two ends (through) pores [148].

According to their width (diameter in cylindrical pores, smallest dimension in cracks and distance between two sides in slide-shape pores), they can be classified into:

•Macroporous: width > 50 nm. For instance, macroporous Al_2O_3 catalyst have been used for residue oil hydrodemetallization [149].

•Mesoporous: width in the range 2-50 nm. Mesoporous tantalum phosphate were used as catalyst for glucose to HMF dehydration by Jiménez-Morales *et al.* [150].

•Microporous: smaller than 2 nm. If they are in the range 0.7-2 nm, are called "supermicropores", and if they are smaller than 0.7 nm, they are "narrow" or "ultra" micropores. Bifunctional crystalline microporous organic polymers have been reported as catalysts for HMF synthesis from different hexoses by Bhanja *et al.* [151].

For active carbons, pores are usually classified as follows:

•Transport pores: radius > 25nm

•Adsorbing pores: mesopores (radius 1-25 nm), micropores (0.2-1 nm) and submicropores (smaller than 0.2 nm) [152].

• Concerning micropores, it may be desirable to subdivide them into micropores smaller than about 0.7 nm as narrow micropores, or ultramicropores, and those micropores in the range of 0.7 to 2.0 nm, which are called supermicropores. .

Macroporous materials possess both specific surface area and total pore volume and greater average pore size, not being as useful as micro and mesoporous materials in catalysis. Examples of microporous materials are zeolites, $AlPO_4$ (aluminophosphates), carbons, clays or

metal organic frameworks (MOFs). OMMs (ordered mesoporous materials), which are very useful when large surface areas and easy diffusion are needed, such as in catalysis, because of their homogeneous mesoporosity, large pore size, high surface area, and mesoporous channels.

3.6.5. Synthesis of mesoporous materials

Mesoporous material synthesis is mostly based on organic template molecules as structure-directing agents around which precursor condense. After condensation, the organic template is removed by extraction or calcination, resulting in the mesoporous structure. Depending on the nature of templates, different mesopores sizes can be obtained. The most common templates are cationic, amphiphilic or anionic surfactants, but also emulsions, or others, can be used. These are called soft-templating methods. Another method, hard-templating method, use a hard template (i.e., mesoporous silica) for other mesoporous material preparations. This method is applied in mesoporous carbon synthesis. Both methods are schematized in Figure 23.

Control of local environment and morphology during the synthesis allows to obtain catalysts with different properties depending on the catalytic requirements.

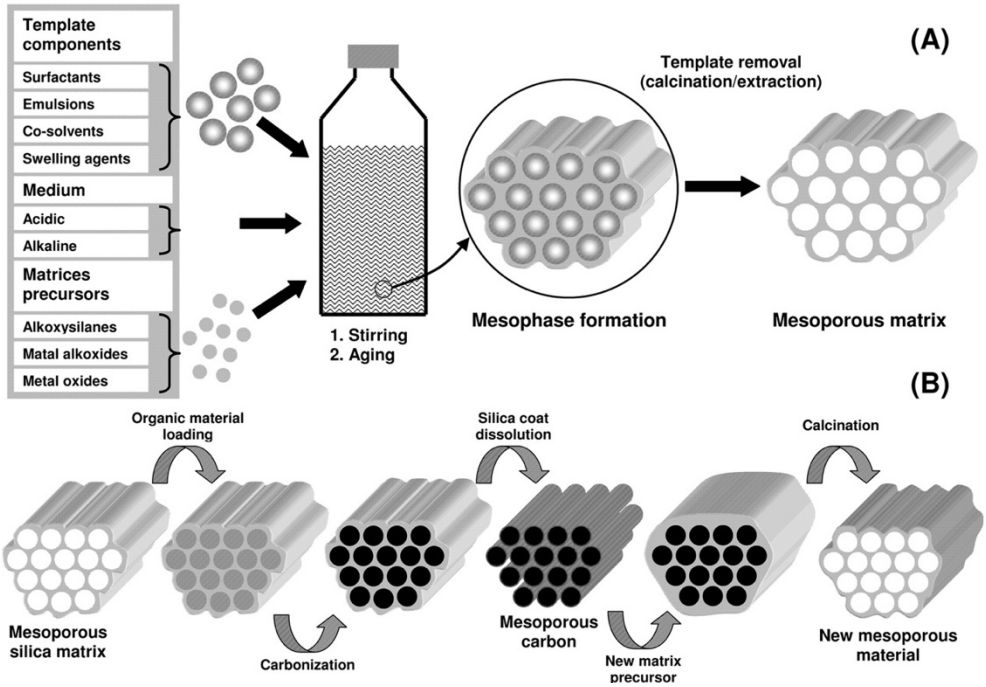

Figure 23. Soft-template (A) and hard-template (B) methods for mesoporous materials synthesis [153].

One of the interesting features of ordered mesoporous solids for catalysis is the multitude of possibilities to modify them. Since hydrothermal stability has been demonstrated as an essential aspect for applications of mesoporous materials in catalysis, several approaches have been developed to improve it, such as the addition of salts during the hydrothermal synthesis, the modification of the surface by silylation or post-synthesis grafting of inorganic compounds to increase the wall thickness and/or to chemically stabilize the wall surface of the mesoporous structure [154].

In 1992, researchers from Mobil Oil Corporation patented the synthesis of a family of nanostructured mesoporous materials known as

M41S, being the hexagonal MCM-41 phase the most studied. For its synthesis, TEOS (tetraethyl orthosilicate) was used as silica precursor, the structure directing agent was cetyltrimethylammonium hydroxide and the synthesis was carried out in an alkaline medium. Another known mesoporous silica, SBA-15, uses also TEOS as precursor, Pluronic P123 as structure directing agent and is synthesized in acid medium [155,156].

OMMs started with ordered mesoporous silica (M41S, SBA-15, KIT-6), but also organosilicas, metal oxides, carbons, metal–organic frameworks and zeolites has been synthesized as ordered mesoporous solids. Well-developed porosity and crystallinity in these materials are still a great challenge in their synthesis.

3.6.6. Mesoporous tantalum oxide

Tantalum pentoxide is one of the most important transition metal oxide because of its physical and chemical properties, used in many applications such as photovoltaic devices or antireflective materials.It is semiconducting and has been employed as photocatalyst.

Tantalum-based catalysts also show high stability in water-containing systems.

Nanosized Ta_2O_5 can be obtained from tantalum pentabutoxide or tantalum oxide gel, both expensive methods.

Mesoporous tantalum pentoxide is commonly prepared by a ligand-assisted templating method with surfactant molecules, followed by

precipitation or gelation. It can also be synthesized by sol-gel methods [157].

Thus, Stodolny *et al.* synthesized Ta_2O_5, TiO_2 and both mixed photocatalysts by a sol-gel technique, obtaining a mesoporous tantalum pentoxide with a relatively high surface area (100–130 $m^2\ g^{-1}$) [158]. Tantalum oxide supported on Al_2O_3, TiO_2, ZrO_2, and SiO_2 supports were prepared by the incipient wetness impregnation method for methanol oxidation reaction, finding a relation between the acidic sites of tantalum oxide and the specific oxide support due to the formation of bridging Ta−O−bonds [159].

Ushikubo and Wada prepared hydrated tantalum and niobium oxides, demonstrating that hydrated tantalum oxide also showed strong acid properties, even at higher temperatures [160].

Yue *et al.* [161] synthesized a mesoporous tantalum oxide according to the method of Antonelli and Ying [162], as catalyst for nitrogen activation and ammonia synthesis. The synthesized catalyst possessed a large BET surface area (541 $m^2\ g^{-1}$) and an HK (Horvath Kowazoe) pore size of 2.3 nm. X-ray diffraction confirmed its mesoporous structure.

Yang *et al.* reported in 2011 the synthesis of an hydrated tantalum oxide ("tantalum hydroxide")-based catalyst for saccharide dehydration into HMF in a water/2-butanol biphasic system, achieving a high catalytic activity, and they also used this catalyst for HMF production from Jerusalem artichoke juice[163].

Mesoporous tantalum phosphate was also synthesized by Jiménez-Morales *et al.* as catalyst for glucose dehydration to HMF in a water/MIBK biphasic system. The catalyst exhibited a high specific sur-

face area (256 m^2 g^{-1}) and strong acidity, with both Lewis and Brönsted acid sites [164].

3.6.7. Mesoporous Al-MCM-41

The mesoporous aluminosilicate MCM-41 is the most well-known and studied nanostructured mesoporous material of the M41S family, synthesized by researchers from Mobil, as explained in Section 3.6.5. M41S family refers to different structures: MCM-41 hexagonal, MCM-48 cubic and MCM-50 lamellar (Figure 24).

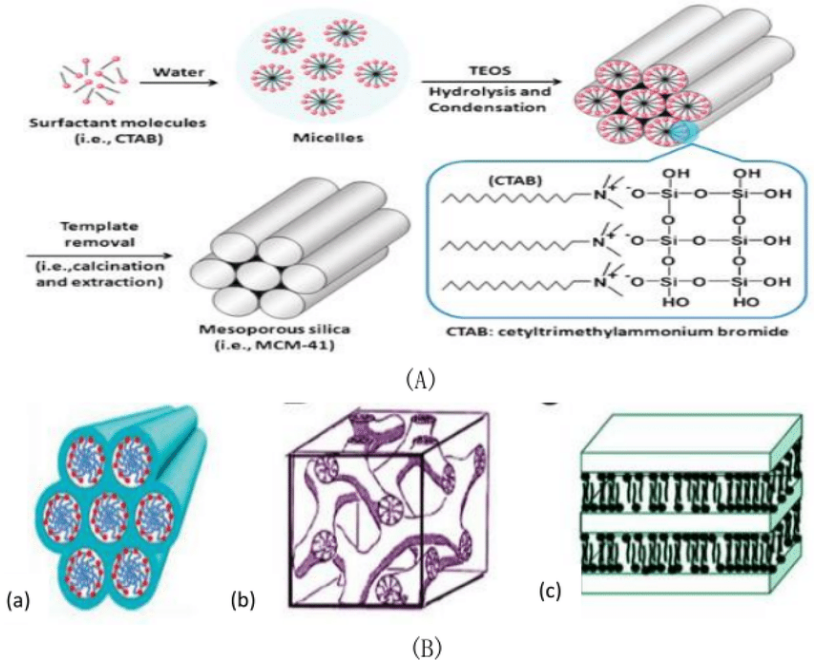

Figure 24. Formation mechanism of MCM-41 (A) and structure arrangements of M41S materials (a, MCM-41 hexagonal; b, MCM-48 cubic and c, MCM-50 layered)[165].

MCM-41 possesses a hexagonal structure with ordered arrangement of cylindrical mesopores, whose diameters are in the range 2 to 6.5 nm, forming an one-dimensional pore system with well-defined pore distribution, large surface area and high pore volume. Since it was produced at first, more outstanding syntheses has been later reported. Thus, MCM-41 nanoparticles with control of particle size and specific structural properties have been reported by Castillo *et al.* [166].

The introduction of heteroatoms, such as Ti or Sn, and specially Al, in the siliceous framework is very important for catalytic purposes, because substitution of Si by a heteroatom allows tuning the acidity or obtaining redox catalysts. The incorporation of heteroatoms can be carried out through direct methods, or through post-treatment of a mesoporous silica. The first ones produce more homogenous composition, while the second ones concentrate the heteroatoms on the surface of the mesoporous silica. Shen *et al.* synthesized Al-MCM-41 by hydrothermal synthesis and studied the effect of Al substitution on the hydrothermal stability under different treatment conditions, focused on the effect on both geometrical and chemical properties of MCM-41 [167]. Mokaya and Jones introduced aluminum into MCM-41 by a post-synthesis method with aluminum chlorohydrate (ACH). They found that the amount of incorporated Al into de MCM-41 framework was dependent on the Al concentration in the ACH solution and that a large proportion of the incorporated Al was into tetrahedral positions. The obtained aluminosilicate was useful as acid catalyst [168].

Aluminum incorporation into MCM-41 results in a broader pore size distribution, in Brönsted acid sites and also ion-exchange sites, and

thus, in different catalytic properties. The strength of acid sites and the proportion of Brönsted and Lewis acid sites depend on the Si/Al ratio. Chen *et al.* compared post-synthesis alumination and sol-gel synthesis of MCM-41 with high framework aluminum content. They found decreasing surface area, pore diameter, crystallinity and thermal stability of Al-MCM-41 with increasing Al content. The post-synthesized Al-MCM-41 showed better thermal stability and lower acidity than the directly synthesized. They also reported that the total concentration of acid sites increased linearly with the aluminum loaded, but, at high aluminum loading levels, it became independent due to the agglomeration of aluminum species [154,169].

Many catalytic reactions have been carried out by using MCM-41 derived materials as acid, acid-base or redox catalysts. Koh *et al.* prepared a catalyst based on Pd supported on MCM-41, which was very active for 1-hexene hydrogenation at 25 ºC, although it was not active for benzene hydrogenation [170]. With regard to biomass valorization, many MCM-41-based catalysts have been reported for biomass pyrolysis and gasification. Adam *et al.* synthesized Al-MCM-41 and Cu-Al-MCM-41 mesoporous catalysts for pyrolysis of vapors of spruce wood [171].

On the other hand, De la Iglesia *et al.* prepared a mesoporous Sn-In-MCM-41 catalysts for the selective sugar conversion to methyl lactate, reaching a 69.4% methyl lactate yield from glucose and 73.9% in the case of sucrose [172].

One-pot catalytic conversion of cellobiose into sorbitol has been reported using nickel phosphide supported on MCM-41- and Al-MCM-41 [172].

Xu *et al.* evaluated a Sn-MCM-41 heterogeneous catalyst as bifunctional catalyst in glucose dehydration to HMF in ionic liquid, reaching 70% HMF yield at 110 ºC after 4 h. The catalyst was more active in fructose dehydration, reaching a 80% HMF yield [173].

3.6.8. Mesoporous Al-KIT-6

Mesoporous MCM-41, SBA-15 and KIT-6 silicas have been widely studied and employed as mesoporous silica-based catalysts or adsorbents. The mesoporous system of SBA-15 is composed of a hexagonal arrangement of cylindrical pores surrounded by amorphous silica walls. These walls are thicker than MCM-41´s ones, demonstrating to be more thermally stable. The mesoporous system of cubic Ia3d in KIT-6 material possesses an interpenetrating cylindrical pore system with channels separated by an amorphous silica wall. This structure is similar to that of MCM-48, but KIT-6 has larger pore sizes and thicker walls. All of them are characterized by very well-developed specific surface areas and large pore volumes. Hydrothermal stability is better in SBA-15 owing to its thicker walls. The 3D network affords a highly opened space with easy and direct access to active sites for reactants, which can diffuse through the pore channels, being suitable as catalyst and adsorbent. Direct imaging of surface topology and pore System of MCM-41, SBA-15, and KIT-6 silicas have been obtained by Tüysüz *et al.*, confirming the proposed arrangements [174].

This KIT-6 material was first synthesized by Kleitz *et al.* and replicated to platinum nanowires, carbon nanorods and carbon nanotubes [175]. Pore size, wall-thickness and particle size can be tunable for specific

purposes [176]. Thus, increasing aging temperature in the KIT-6 synthesis, the interconnectivity between the two channel systems is increased.

As in based MCM-41 catalysts, the introduction of heteroatoms allows tuning the acidity. Thus, Mu *et al.* have incorporated Zr and Mo species through a one-pot method to improve the amount of acid sites in mesoporous KIT-6 silica. DFT calculation have been applied to explore the formation mechanism of Brönsted acid sites, showing an association between the experimental acidity and the structure in the tested catalysts [177].

As other mesoporous silicas, KIT-6 materials have been used as catalysts and/or catalyst supports for biomass valorization. The group of Maireles-Torres [178] synthesized and tested different zirconium-doped mesoporous silicas (Zr-KIT-6, Zr-SBA-15, Zr-MCM-41 and Zr-HMS) with a Si/Al molar ratio of 5 for glucose dehydration to HMF. They found that the presence of a high amount of Zr affected to the textural properties of mesoporous silica. Moreover, specially Zr-KIT catalysts possessed a high total acidity, which enhanced with increasing incorporated Zr into the framework. Lewis acidity was detected by pyridine adsorption coupled to FTIR spectroscopy, but they did not detected Brönsted acid sites, although they no discarded the formation of Brönsted acid sites from Lewis acid sites in water at high temperature. Accordingly, Omata *et al.* have proposed a mechanism for explaining Lewis acid sites transformation into Brönsted ones by adsorbed water molecules [179].

Varkolu *et al.* prepared and tested catalysts based on Ni supported over 3D architecture silicas with KIT-6 and SBA-15 typologies for

hydrogenation of biomass-derived levulinic acid to 2-methyltetrahydrofuran [180].

3.6.9. ZSM-5, Y and Beta zeolites

Zeolites are also aluminosilicates with a three-dimensional framework, but unlike KIT-6 3D materials, they are crystalline with uniformly sized pores of molecular dimensions. These pores act as sieves on a molecular scale, thus zeolites are molecular sieves (pores of the size of molecular dimensions, 0.3–2.0 nm diameter). The substitution of Si^{4+} by Al^{3+} creates a negatively charged framework and other cations within cavities contribute to electroneutrality. Some of these cations can be exchanged, providing many properties for industrial uses, such as catalysis or environment purifications. The framework is formed by corner-sharing TO_4 tetrahedra, where T is any tetrahedrally coordinated cation, and this framework is relatively open, with channels and cavities.

The main aspects to be investigated for zeolite applications are the framework type, the geometry and composition of the framework, the location and nature of extra-framework species, and the number and type of defects. Also, post-synthesis modifications are very important. The presence of large cations can block or reduce the effective size of pores, while small cations might distort the pore opening. Thus, ZSM-5 zeolite with adsorbed neopentane has a 0.62 nm near-circular pores, whereas after the adsorption of substituted aromatics, the pore assumes an elliptical shape, 0.45 to 0.70 nm in diameter [181]. Moreover, selectivity depends on many factors. Thus, the position of an Al atom

and the neighboring framework O atoms influence on the transition-state-restricted selectivity. But also, the specific spatial geometry of the mutual approach of the reactants at the specific T site enables creation of the most favorable transition state complex, explaining the selective in trans-alkylation of isopropyl benzene or isopropyl toluene to n-propyl benzene or n-propyl toluene to be possible in the intersecting narrow 10-MR channels of ZSM-5 zeolites, but not in the wide channels of BEA or FAU zeolites [182].

The *Atlas of Zeolite Framework Types* (Structure Commission of the International Zeolite Association, iza-structure.org) assigns a three-letter code to be used for a known framework topology, such as BEA (Beta), FAU (Faujasite), MFI (ZSM-5 structure) or MOR (Mordenite).

With regard to the framework Si/Al ratio, if it is in the range 1-1.5, they are "low" silica zeolites; in the range 2-5, they are "intermediate" and in the range 10-100, they are "high" silica zeolites. Only silicon-containing zeolites are silica molecular sieves. Thermal stability increases from 700 ºC in low silica zeolites to 1300 ºC in silica molecular sieves. Surface is highly hydrophilic in low silica zeolites and hydrophobic in high silica zeolites and silica molecular sieves. In addition, acidity tends to be stronger with increasing Si/Al ratio, which also produces decreasing cation concentration and, consequently, ion-exchange capacity (proportional to aluminum content) [181].

For acid-base and redox catalysis in the presence of high (or rich) silica zeolites, Al species plays a key role. This involves Al location (T sites occupied by Al atoms) and Al distribution (relation of neighboring Al atoms in the framework which can cooperate forming active sites). Both Al location and distribution depend on the hydrothermal synthe-

sis conditions [182]. Variability of the location and distribution of Al atoms in the framework represents a general feature of Si-rich zeolites, resulting in zeolites of the same chemical Si/Al composition, but significantly different properties.

The framework negative charge can be balanced by protons, resulting in the formation of structural bridging Si-OH-Al groups. A substantial difference in the acid strength is found between Si- and Al- rich zeolites, which is attributed to the interaction between Si-OH-Al groups. Calculated deprotonation energies of OH groups in faujasite, ZSM-5, mordenite and ferrierite, showed similar values, and the acid strength of the Al-rich zeolites decreased after zeolites dealumination.

Brönsted acid sites are constituted by bridging OH groups linking Si to Al and depend on the Si/Al ratio as mentioned above, and on the structure, the channels and the cage geometry. Brönsted acid sites are influenced by synthesis conditions, but they can also be created by different post-synthesis methods. Thus, by direct proton-exchange methods, which can be performed in water, i.e. with inorganic acids solutions, sodium cations of zeolites X and A can be replaced by hydrated hydrogen ions [183].

Another method, but under anhydrous conditions, consists of hydrogen reduction of a silver-exchanged NaA zeolite to metallic silver and proton-exchanged zeolite, reported by Wolf and Frtig [184], or by treatment of a NaA zeolite with p-toluenesulphonic acid in dioxane solution [185].

The most common method is through ammonium-exchange, followed by calcination which decomposes the ammonium and originate protons on the zeolite surface [186].

Another way is through metal cation exchange, which could be reduced to lower oxidation states, generating protons on the surface of the zeolite [187]. This Brönsted acidity is responsible for many petrochemical reactions using zeolites as catalysts.

Lewis acid sites are produced by extra-framework aluminum species, or by intra-framework species substituting Al or Si cations, as can been observed in Figure 25.

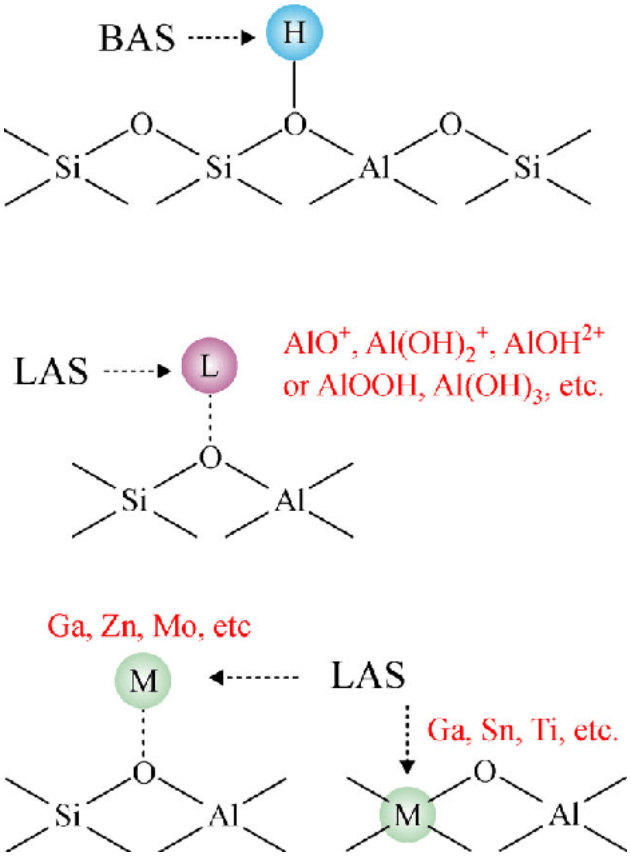

Figure 25. Brönsted (BAS) and Lewis (LAS) acid sites in zeolites, downloaded from [188].

These Lewis acid sites can also be produced from dehydroxilation of Brönsted acid sites at high temperature, originating Si and Al with lower coordination number, and thus, Brönsted are converted into Lewis acid sites. Moreover, at high temperature, the framework dealumination often occurs, generating octahedral aluminum species, associated to Lewis acidity. The concentration, type and strength of acid sites are determined by synthesis conditions, by they can be tuned.

Batool *et al.* have introduced Lewis acid sites into zeolite Y (Si/Al = 30) by ion-exchange with aluminum cations followed by calcination, increasing the total extra-framework aluminum, and preserving the Brönsted acid sites [189].

Wu and Weitz prepared metal cation-functionalized Mn^{+}-ZSM-5 (Mn^{+} = Al^{3+}, Ca^{2+}, and Ba^{2+}) and H^{+}-ZSM-5 zeolites by a standard ion-exchange procedure using aqueous solutions of metal nitrate salts or nitric acid [190].

Other method is SSI (solid-state incorporation), consisting of introducing heteroatoms into the vacancies of the tetrahedral framework by a both, a combination of chemical and thermal treatments [191].

In addition to the importance of zeolites in petrochemical processes, these materials can also catalyze biomass conversion. Zeolites possess the required Brönsted and Lewis acidity, but one challenge is related to its microporosity, with too small pores to allow the diffusion of large biopolymers. Thus, mesopores must be generated in zeolites. In this sense, hierarchical (mesoporous) zeolites have emerging by generating a secondary level of porosity to the intrinsic zeolitic micropores [192].

Another challenge is to control the synthesis to obtain stable materials under hydrothermal, acidic or basic, at ambient or more drastic conditions [193].

On the other hand, H-Y zeolite has been employed by Lourvanij and Rorrer [194] for glucose transformation in aqueous solutions, achieving a full glucose conversion at 160 ºC after 8 hours, identifying several catalytic processes, such as glucose to fructose isomerization, dehydration to HMF, HMF rehydration to formic and levulinic acids.

Roman-Leshkov and Davis prepared a tin-containing zeolite with large pores (Sn-Beta), which was able to isomerize glucose into fructose in aqueous media, showing high activity and selectivity [194].

ZSM-5 zeolites

ZSM-5 (Zeolite Socony Mobil – five) is a high siliceous zeolite with an intersecting and three-dimensional channel system. Its chemical formula is, $Na_nAl_nSi_{96-n}O_{192}$. $16H_2O$ (n >27), whose framework is MFI type, and thus, unit cell is orthorhombic. Channels are formed by a 10-membered rings (10-MR) pore structure. The ZSM-5 framework contains two sets of 10-MR perpendicular channels (Figure 26).

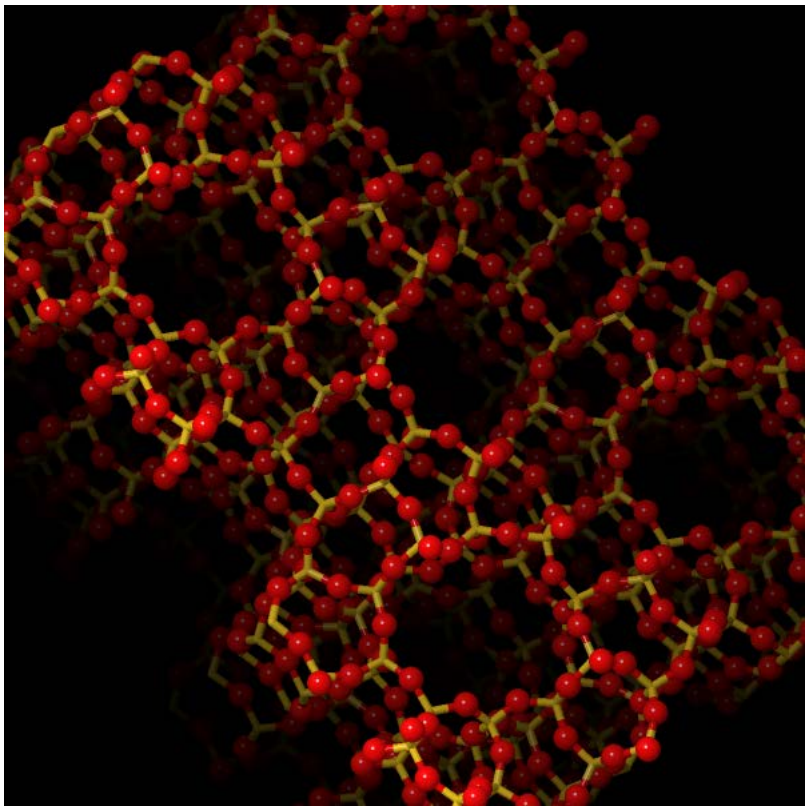

Figure 26. ZSM-5 channels, from IZA-structure.org.

This structure is especially useful in shape selectivity applications, which can be associated to reactant, restricted transition state and product selectivity. In addition, this zeolite is highly resistant to coke formation. Because of its strong acidity and well separated sites owing to a high Si/Al molar ratio, it is very useful for a broad spectrum of catalytic processes, such as hydrocarbon cracking or olefin oligomerization [195,196].

Moreover, some cation-promoted ZSM-5 zeolites, (Ga-ZSM-5 and Zn-ZSM-5) are used in aromatization reactions for both gasification and pyrolysis [197].

Hierarchical nano-ZSM-5 zeolites with different particle sizes were synthesized varying the hydrothermal conditions. These zeolites were more coke resistant and exhibited higher activity and selectivity in methanol to aromatics (BTA) reactions [198].

Ma *et al.* prepared Y-ZSM-5 zeolite for catalytic production of methyl lactate from fructose-based carbohydrates, reporting 61.3 % of methyl lactate yield from fructose, 39.6 % from sucrose and 45.6 % from inulin [199].

Y zeolites

Y zeolites belong to FAU type with a structure based on a cubic unit cell. It is characterized by large internal cavities named supercages, tetrahedrally linked through pore openings of about 0.8 nm. Rings are formed by twelve oxygen atoms (Figure 27). FAU-type zeolites with different Si/Al molar ratio can be synthesized from conventional Na_2O–SiO_2–Al_2O_3–H_2O systems, but with Si/Al molar ratio limited to 3. For catalytic purposes, higher Si/Al molar ratios must be obtained by dealumination, usually by steam treatment, to prevent the collapse of its framework.

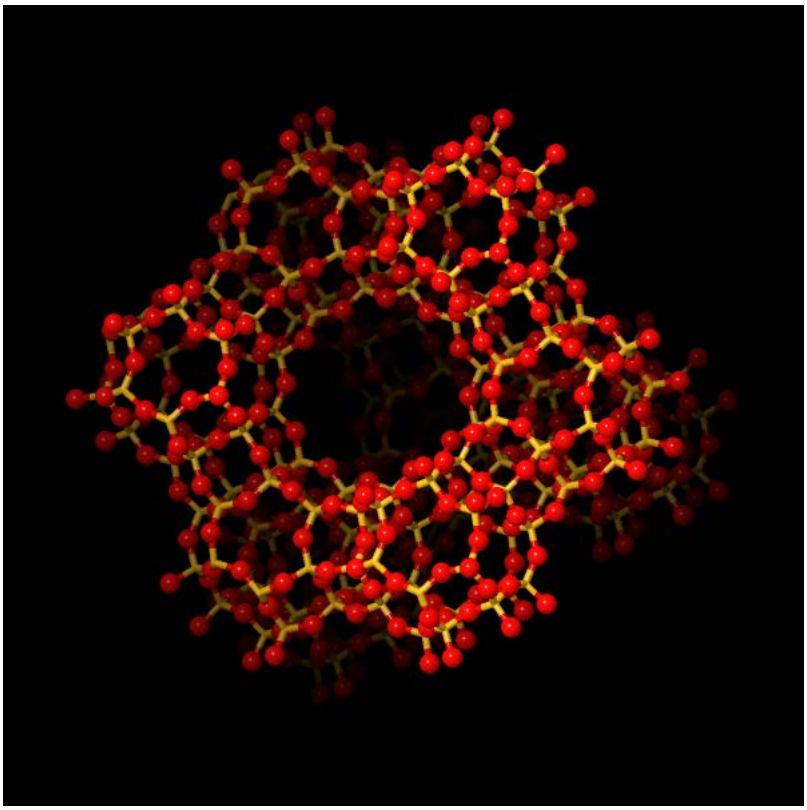

Figure 27. FAU structure, from IZA-structure.org.

Although Y zeolite is excellent for cracking processes [200], long-chain hydrocarbons require larger pores. In general, the generation of, mesopores in zeolites can be carried out by different methods. In particular, in Y zeolites, desilication and dealumination can introduce mesopores. Thus, dealumination processes influence not only the intra-framework Si/Al molar ratio, but also extra-framework Si and Al and the porosity [201].

The acidity in Y zeolites can be generated through post synthesis methods. Afgaei *et al.* have modified NaY zeolite by a sequential

steam-alkali-acid treatment, using NaOH, Na_2CO_3 and $CaCO_3$ at different concentrations, obtaining better acid properties after alkali treatment, and improving the heavy oil conversion and gasoline selectivity [202].

Sohn *et al.* prepared dealuminated Y zeolites by treatment with $SiCl_4$ and reaction with steam, over a range of Si/Al molar ratio from 4.7 to 255, increasing the cracking catalytic activity. The results were accorded to a model in which strong Brönsted acid sites are related to structural Al atoms that have no next-nearest Al neighbors [203].

Batool *et al.* have introduced Lewis acidity into Y zeolite (Si/Al= 30) by ion-exchange of aluminum cations, increasing total extra-framework aluminum. FTIR spectroscopy of adsorbed pyridine showed a pronounced increase in the number of Lewis acid sites, whereas no significant change in the number of Brönsted acid sites was observed. This acidity increased the catalytic activity in the reduction of 4-ter-butyl cyclohexanone [189].

Y zeolites have been also employed in biomass valorization. West *et al.* have used H-USY (Si/Al= 6) for lactic acid production, which is an interesting platform chemical for the production of biodegradable plastics or environmentally friendly solvents, among other products. They carried out the liquid-phase conversion of the triose-sugars, glyceraldehyde and dihydroxyacetone directly to methyl lactate and lactic acid with good catalytic activity. Under aqueous conditions, H-USY zeolite was easily deactivated because of coke deposition and irreversible framework damages, but using methanol instead of water, catalyst deactivation was suppressed [204].

Beta zeolites

Beta zeolite was the first high-silica zeolite synthesized with organic additives [205]. Its structure is BEA type, with a tetragonal unit cell. Beta zeolite has a complex structure consisting of two intergrown structures, A and B polymorphs, both containing a three-dimensional network of 12-ring pores (Figure 28).

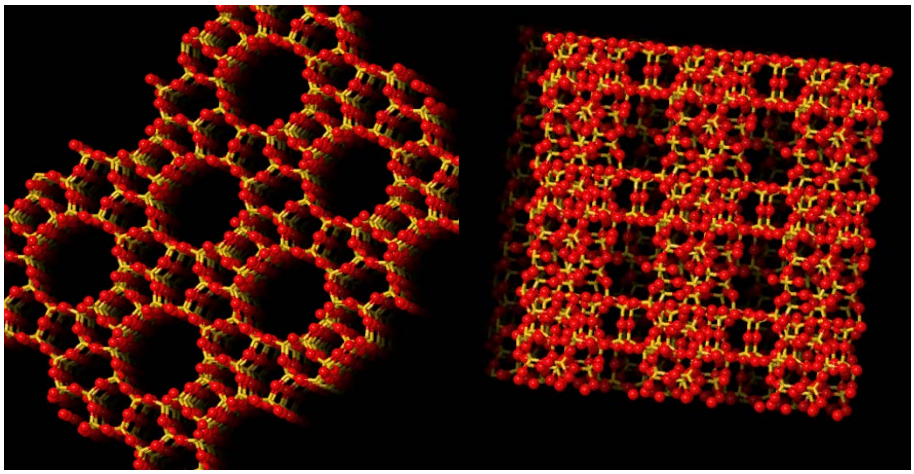

Figure 28. BEA structure, from IZA-structure.org.

Beta zeolite is, as ZSM-5, shape selective and its acidity can be tuned. High Si/Al molar ratios, from 10 to 100, can be reached through different methods. Thus, it is very useful as catalyst in many industrial applications. Nevertheless, micropores are not wide enough for large molecules, and lead soon to deactivation. As in other zeolites, the development of mesopores is needed. They can be introduced directly in the synthesis (bottom-up methods) or post-synthesis (top-down

methods). Similar to that was stated for Y zeolite, post-synthesis methods are preferred, and involve dealumination and desilication.

As previously mentioned, acid strength and type are influenced by the Si/Al molar ratio, synthesis and post-synthesis treatments. Kiricsi *et al.* studied the effect of all these parameters on H-Beta type zeolites with different Si/Al molar ratios, synthesized by hydrothermal method and dealuminated with diluted HCl. They found both Lewis and Brönsted acid sites. With regard to the OH- groups, different types and distributions were detected depending on the zeolite treatment [206].

Guisnet *et al.* also studied the effect of dealumination on the acidity of Beta zeolites. The parent H-Beta (Si/Al= 10) zeolite and the dealuminated (Si/Al from 20 to 90) ones possessed fewer Brönsted acid sites than those expected considering the Al loading, because extra-framework Al species, such as Al-OH and Lewis acid sites were detected. Dealuminated zeolites exhibited a lower amount of extraframework aluminum species and, consequently, fewer Lewis acid sites [207].

For the conversion of renewable feedstock, MFI and BEA zeolites have been preferred, although other modified structures can be useful as well. Moliner *et al.* prepared and compared Sn or Ti incorporated to Beta zeolite, with large pores, TS-1 zeolite (MFI type, medium pores) and MCM-41 (OMM). Sn-Beta and Ti-Beta showed the highest glucose to fructose isomerization activity, while TS-1 was barely active and Sn-MCM41 and Ti-MCM41 were moderately active. In addition, the incorporation of metals into the mesoporous silica is relevant, being better into Beta zeolite than into MCM-41 structures [208]. Bermejo *et al.* also studied glucose to fructose isomerization over Sn-Beta

zeolites and their data provided evidence that Lewis acidity associated to Sn species, with proximal silanol groups, were active sites for the isomerization reaction [209]. Rai *et al.* had previously reported DFT calculations suggesting that the silanol group adjacent to the active Sn hydroxyl (Sn(OH) sites in Sn-Beta, synergistically, promoted the hydride transfer in glucose isomerization to fructose [210].

Taarning *et al.* [212] also tested Sn-Beta in the conversion of triose sugars to lactic acid, in water at 125 ºC, reaching a 90% lactic acid yield, as well as in methanol, forming methyl lactate at 80 ºC in quantitative yields [211]. The isomerization-esterification to methyl lactate have also been studied by Holm *et al.* using Sn-Beta zeolites, from glucose, fructose and sucrose in methanol at 160 ºC. The zeolite could be easily recovered by filtration and reused during several catalytic cycles after calcination, without any substantial change in the product selectivity

Another Sn-Beta application for biomass valorization reported by the research group of Vlachos was a one-step process for the production of diesel fuel from biomass-derived 5-hydroxymethylfurfural (HMF), which is converted into 2,5-bis(alkoxymethyl)furan over Lewis acid zeolites, Sn-Beta and Zr-Beta. With Sn-Beta, 80% product yield was achieved [213].

Lewis acid Sn-βeta type zeolites with different amounts of Brönsted acid Al in the framework were synthesized by partial dealumination of Beta zeolite in acid, followed by grafting with $SnCl_4 \cdot 5H_2O$ in dry isopropanol by Dijkmans *et al.* [214]. Characterization data demonstrated the existence of framework Brönsted acid (Al^{III}) and tetrahedral Lewis acid (Sn^{IV}) sites. The zeolite was tested in the catalytic conversion of

1,3-dihydroxyacetone (DHA) into ethyl lactate (ELA), proceeding via pyruvic aldehyde, showing high activity. It was demonstrated the co-operative effect of Lewis Sn^{IV} and Brönsted Al^{III} acid sites by comparison with physical mixtures of partially dealuminated Beta zeolite and Al-free Sn-Beta.

Choudhary *et al.* carried out a non-enzymatic xylose isomerization in water over Sn-Beta zeolite, reporting 27% xylulose, 11% lyxose with 60% xylose conversion at 100 ºC [215].

Relating to glucose to HMF conversion, both Brönsted and Lewis acid sites in Beta zeolites were produced after dealumination by steam and calcination [216]. ^{27}Al MAS NMR measurement and FTIR spectroscopy showed that part of Si–O–Al bonds in the framework were cleaved to form extra-framework Al species, which acted as Lewis acid sites. Dealuminated Beta zeolite and calcined at 750 °C showed 55% HMF selectivity at 78% glucose conversion. The role of Lewis and Brönsted acidity and their relationship with glucose to fructose isomerization was studied by an isotopic analysis starting from deuterated glucose. The experiment revealed that glucose was isomerized to fructose through a hybrid intermediate, and this fructose was immediately dehydrated to HMF over Brönsted acid sites.

3.6.10. Activated porous carbon materials

Porous carbons possess huge surface areas and hierarchical porosity, including macro, meso and micropores. These characteristics make these carbons suitable as adsorbents and catalysts in many industrial applications. Not only textural properties determine their activity, but

also the surface chemistry. These parameters can be tailored by synthesis or post synthesis methods. As catalysts, porous carbons also possess two additional advantages: inertness, facilitating the interaction between active phases or between active phases and promoters, and they are able to block undesirable reactions i.e., coking, which are responsible of catalyst deactivation [217].

Porous carbon materials can be present as activated carbons, carbon molecular sieves, high-surface-area graphite, activated carbon fiber, among others, being the most important as catalysts or catalyst supports the high-surface-area activated carbons.

Activated carbon is mainly carbon constituting an amorphous solid with large internal surface and pore volume. Besides carbon, it contains heteroatoms, mainly oxygen, and hydrogen, nitrogen and sulfur, either from de raw material or added. These atoms form complexes or functional groups (carboxyl, phenol, carbonyl) on the surface and are mainly acidic. Type and concentration of these groups determine the application of the carbon as acid catalyst, as many of them will be active sites.

Over another supports as silica or alumina, these carbons have many advantages: surface resistant to acid and basic medium, structural stability at high temperatures, preparation under different physical forms (fibers, pellets,..), active phase can be easily recovered by burning away the support and lower costs than silica or alumina [218].

The design and control of the mesoporosity is needed for many applications. It can be developed by several methods, such as catalytic activation, carbonization of mesoporous gel, carbonization of polymer blends and porous carbons prepared by template carbonization [219].

Activation can be physical or chemical, both strongly affecting the surface depending on the specific method.

Physical activation is a two-step process: firstly, raw material is pyrolyzed and, secondly, it is activated with oxidant gases (steam, CO_2). Carrot *et al.* prepared activated carbons by physical activation of cork wood, virgin cork and adult cork in carbon dioxide. Activated cork wood gave good results, similar to other lignocellulosic materials. Virgin cork, after activation, retained the characteristic honeycomb structure and had low C/O ratios. Activation of the adult cork was 10-times faster than the others [220].

Chemical activation consists of impregnation of the precursor carbon with a chemical agent (dehydrating or oxidant) followed by heating under inert atmosphere at temperatures in the range 400-800 ºC. Both physical and chemical activation can be performed simultaneously [221]. Activation is mainly for cellulosic material degradation. The main role of the activating agent is the degradation of the cellulosic material and is achieved upon thermal treatment. Dehydrating compounds in chemical activation inhibit the formation of tar and other products, achieving higher carbon yields than by thermal treatment. The higher the degree of impregnation, the larger the pore sizes.

Rosas *et al.* carried out chemical activation of different lignocellulosic materials with phosphoric acid, which had higher oxidation resistance than free chars obtained from the same biomass at similar conditions. They also possessed more developed porous structure because of the presence of thermally stable phosphorus complexes on the carbon surface, which seemed to stabilize the active carbon sites. Multiple scanning micrographs were taken to study the modification of the

particle size distribution of the carbons after partial gasification, showing that the activated carbon suffered an important reduction of the particle size, as is shown in Figure 29, indicating surface chemistry modifications [222].

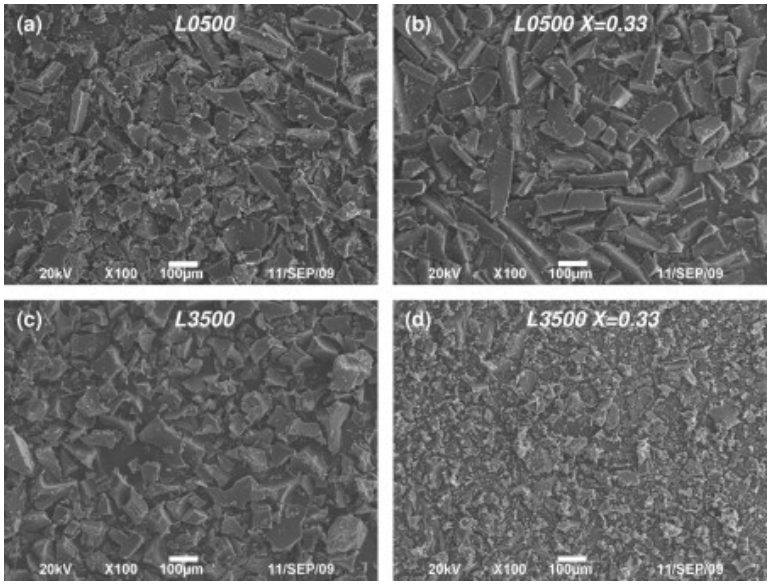

Figure 29. SEM micrographs of char (a, b) and activated carbon (c, d) before and after partial oxidation (X = 0.33) from [222].

Activated carbon fibers (ACF) are also porous carbons, with micropores, a narrow pore size distribution and high surface areas. This is a fibrous material, light, easily moldable into a variety of physical forms as required by the specific application, and also can be adapted into the reactors. They are prepared by controlled carbonization of high carbon content fibrous materials (coal tar, petroleum pitch, rayon, polyacrylonitrile) and then, they are activated thorough several

treatment to develop porosity (mesoporosity). They are very useful as adsorbents (as fibers or clothes), but also as catalysts.

Adapa *et al.* studied the catalytic oxidation of NO with various ACFs prepared from different precursors: viscose rayon, phenolic resin-based samples and pitch-based ACF samples. The characterization results of the activated carbon fibers showed that BET surface area, total and micropore volumes, increased with the activation time independent on the type of activation agent (steam or CO_2), up to a limit time, at which area and pore volume decreased. They observed that the conversion depended on the reaction temperature, on the reactants concentration, and on the ACF catalyst (types and treatments) [223].

García-Mateos *et al.* prepared porous carbon fibers catalysts by electrospinning of Alcell lignin. They were chemically activated with H_3PO_4 at several mass ratios and carbonized at different temperatures, providing acid carbon fibers which showed high catalytic activities and selectivities in different alcohol decomposition reactions (isopropanol, ethanol and methanol) [224].

Other interesting porous carbons for catalysis (catalyst or catalyst support) are carbon molecular sieves (CMS), which contain micropores able to select molecules depending on their size and shape. Besides, their narrow micropore size distribution can be modified to be adapted for specific applications. They are produced by different combination of methods such as: pyrolysis or carbonization of polymers or coals, activation (with CO_2, by oxidation…), impregnation and thermal treatments, providing sieving capacity for adsorption or catalysis.

Holbrook *et al.* [225] synthesized molecular sieving carbon catalysts for liquid phase hydrogenation reactions by pyrolysis of platinum nanoparticles in polyfurfuryl alcohol (PFA) resulting in platinum embedded in PFA-carbon nanocomposites. Through several liquid phase alkene dehydrogenation reactions, they studied steric and conformational restriction effects on size and shape of the catalysts, showing these catalyst are enable to be adapted to specific reactions.

In terms of biomass valorization, porous carbon materials, mainly activated carbons, can be obtained from biomass wastes, reducing the cost of raw materials. Wet or dry biomass is converted by a thermochemical process "hydrothermal carbonization" to carbonaceous precursors. After activation (physical, chemical), highly porous activated carbons with tunable porosity are obtained, being useful as adsorbents, separation or catalysts, among other applications. Sevilla *et al.* produced functionalized carbonaceous materials by hydrothermal carbonization of cellulose (220–250 °C) [226]. Tsoncheva *et al.* have prepared catalyst supports of activated carbon from waste biomass for catalytic methanol decomposition with copper and cobalt as active phase [227].

Beyond biomass as raw material for activated porous carbons preparation, carbon-based catalysts can be used for biomass valorization reactions. Thus, Cattaneo *et al.* synthesized and studied Ru supported on activated or mesoporous carbons for hydrogenation of biomass-derived molecules: hydrogenation of levulinic acid and glycerol hydrogenolysis [228].

3.7. List of Figures

3.8. List of Tables

3.9. References

[1] E. Commission, D.-G. for Energy, EU energy in figures : statistical pocketbook 2021, Publications Office of the European Union, 2021. https://doi.org/doi/10.2833/511498.

[2] International Energy Agency, (2019).

[3] European Parlament, Directive (EU) 2018/2001 of the European Parliament and of the Council of 11 December 2018 on the promotion of the use of energy from renewable sources, 2018.

[4] European Comission, Communication From The Commission To The European Parliament, The European Council, The Council, The European Economic And Social Committee And The Committee Of The Regions Repowereu Plan, 2022.

[5] European Comission, Delivering the European Green Deal, 2021.

[6] European Parlament, Fir for 55 package, 2021.

[7] D.-G. for E.E.C. Energy, No Title, (n.d.).

[8] J. Pérez, J. Muñoz-Dorado, T. de la Rubia, J. Martínez, Biodegradation and biological treatments of cellulose, hemicellulose and lignin: an overview., Int. Microbiol. Off. J. Spanish Soc. Microbiol. 5 (2002) 53–63. https://doi.org/10.1007/s10123-002-0062-3.

[9] A.I. Magalhães, J.C. de Carvalho, G.V.M. Pereira, S.G. Karp, M.C. Câmara, J.D.C. Medina, C.R. Soccol, Lignocellulosic biomass from agro-industrial residues in South America: current developments and perspectives, Biofuels. 13 (2019).

[10] R. Overend, Thermochemical conversion of biomass, Combustion. (1999).

[11] Ex-Post Evaluation of Projects and Activities Financed under the LIFE Programme, 2009.

[12] H. Chen, 4 - Lignocellulose biorefinery conversion engineering, in: H.B.T.-L.B.E. Chen (Ed.), Woodhead Publishing, 2015: pp. 87–124. https://doi.org/https://doi.org/10.1016/B978-0-08-100135-6.00004-1.

[13] Y. Sun, J. Cheng, Hydrolysis of lignocellulosic materials for ethanol production: a review, Bioresour. Technol. 83 (2002) 1–11. https://doi.org/https://doi.org/10.1016/S0960-8524(01)00212-7.

[14] T. Dragos, I. Dumitru, L. Racila, O. Otat, L. Matei, I. Geonea, Characterization of Sunflower Oil Biodiesel as Alternative for Diesel Fuel, in: 2019: pp. 172–180. https://doi.org/10.1007/978-3-319-94409-8_21.

[15] I. Malpartida Garcia, P. Maireles-Torres, C. Vereda, J. Rodríguez-Maroto, S. Halloumi, V. Lair, J. Thiel, F. Lacoste, Semi-continuous mechanochemical process for biodiesel production under heterogeneous catalysis using calcium diglyceroxide, Renew. Energy. 159 (2020) 117-126. https://doi.org/10.1016/j.renene.2020.05.020.

[16] S.N. Naik, V. V Goud, P.K. Rout, A.K. Dalai, Production of first and second generation biofuels: A comprehensive review, Renew. Sustain. Energy Rev. 14 (2010) 578–597. https://doi.org/https://doi.org/10.1016/j.rser.2009.10.003.

[17] R. van Noorden, Transgenic trees make easy-chew wood for biofuelstle, Nature. (2014).

[18] G. Schiano di Visconte, A. Spicer, C.J. Chuck, M.J. Allen, The Microalgae Biorefinery: A Perspective on the Current Status and Future Opportunities Using Genetic Modification, Appl. Sci. 9 (2019). https://doi.org/10.3390/app9224793.

[19] R. Kumar, R. Dhurandhar, S. Chakrabortty, A.K. Ghosh, Chapter 12 - Downstream process: toward cost/energy effectiveness, in: S.B.T.-H. of B. Sahay (Ed.), Academic Press, 2022: pp. 249–260. https://doi.org/https://doi.org/10.1016/B978-0-12-822810-4.00012-9.

[20] T. Werpy, G. Petersen, Top Value Added Chemicals from Biomass, 2004. http://www.nrel.gov/docs/fy04osti/35523.pdf.

[21] J. Haveren, E. Scott, J. Sanders, Bulk Chemicals From Biomass, Biofuels, Bioprod. Biorefining. 2 (2008) 41–57. https://doi.org/10.1002/bbb.43.

[22] J. Wisniak, The History of Catalysis. From the Beginning to Nobel Prizes, Educ. Química. 21 (2010) 60–69. https://doi.org/https://doi.org/10.1016/S0187-893X(18)30074-0.

[23] C.F. Cross, Recent Research In Cellulose Industry. Lecture I, J. R. Soc. Arts. 68 (1920) 707–712. http://www.jstor.org/stable/41355272.

[24] J.M. Gallo, J.M.C. Bueno, U. Schuchardt, Catalytic Transformations of Ethanol for Biorefineries, J. Braz. Chem. Soc. 25 (2014) 2229. https://doi.org/10.5935/0103-5053.20140272.

[25] M. Dashtban, Production of furfural: overview and challenges, j-for-journal Sci. Technol. For. Prod. Process. 2 (2012) 44–53.

[26] G.J. Mulder, Untersuchungen über die Humussubstanzen, J. Für Prakt. Chemie. 21 (1840) 203–240. https://doi.org/https://doi.org/10.1002/prac.18400210121.

[27] W. Normann, Die Schmelzausdehnung der Fette, Chem. Umschau Auf Dem Gebiet Der Fette, Oele, Wachse Und Harze. 38 (1931). https://doi.org/10.1002/lipi.19310380202.

[28] F. Tiemann, W. Haarmann, Ueber eine Methode zur quantitativen Bestimmung des Vanillins in der Vanille, Zeitschrift Für Anal. Chemie. 15 (1876). https://doi.org/10.1007/BF01344681.

[29] C. Zhang, Chapter 1. Biodegradable Polyesters: Synthesis, Properties, Applications in Book "Biodegradable Polyesters" Stoyko Fakirov (Editor) ISBN: 978-3-527-33086-7, in: 2015: pp. 1–19.

[30] K.J.B.T.-S.S. Zeitsch, ed., 10. Furfural processes, in: Chem.

Technol. Furfural Its Many by-Products, Elsevier, 2000: pp. 36–74. https://doi.org/https://doi.org/10.1016/S0167-7675(00)80010-X.

[31] R.J. Bothast, M.A. Schlicher, Biotechnological processes for conversion of corn into ethanol, Appl. Microbiol. Biotechnol. 67 (2005) 19–25. https://doi.org/10.1007/s00253-004-1819-8.

[32] F. Adom, J. Fan, J. Davis, P. Dunn, D. Shonnard, Compositional Analysis of Defatted Syrup from a Corn Ethanol Dry-Grind Process as a Feedstock for Biobased Products, ACS Sustain. Chem. Eng. 2 (2014) 1139–1146. https://doi.org/10.1021/sc400508p.

[33] K. Kadam, F. Forrest, J. Jacobson, Rice straw as a lignocellulosic resource: Collection, processing, transportation, and environmental aspects, Biomass and Bioenergy. 18 (2000) 369–389. https://doi.org/10.1016/S0961-9534(00)00005-2.

[34] F. Cherubini, The biorefinery concept: Using biomass instead of oil for producing energy and chemicals, Energy Convers. Manag. 51 (2010) 1412–1421. https://doi.org/https://doi.org/10.1016/j.enconman.2010.01.015.

[35] R. Harun, M. Singh, G.M. Forde, M.K. Danquah, Bioprocess engineering of microalgae to produce a variety of consumer products, Renew. Sustain. Energy Rev. 14 (2010) 1037–1047. https://doi.org/10.1016/j.rser.2009.11.004.

[36] G. Dragone, B.D. Fernandes, A.A. Vicente, J.A.C. Teixeira, Third generation biofuels from microalgae, in: 2010.

[37] D. Bacovsky, N. Ludwiczek, M. Ognissanto, M. Wörgetter, Status of advanced biofuels demonstration facilities in 2012, A Rep. to IEA Bioenergy Task 39. 39 (2013) 1–209.

[38] T. Salan, A Brief Review of the Thermochemical Platform as a Promising Way to Produce Sustainable Liquid Biofuels in Biorefinery Concept, Pet. Petrochemical Eng. J. 1 (2017) 123. https://doi.org/10.23880/PPEJ-16000123.

[39] A. Yaguchi, M. Spagnuolo, M. Blenner, Engineering yeast for

utilization of alternative feedstocks, Curr. Opin. Biotechnol. 53 (2018) 122–129. https://doi.org/10.1016/j.copbio.2017.12.003.

[40] L. da Costa Sousa, S.P.S. Chundawat, V. Balan, B.E. Dale, 'Cradle-to-grave' assessment of existing lignocellulose pretreatment technologies, Curr. Opin. Biotechnol. 20 (2009) 339–347. https://doi.org/https://doi.org/10.1016/j.copbio.2009.05.003.

[41] L. Yang, J. Su, S. Carl, J. Lynam, X. Yang, H. Lin, Catalytic conversion of hemicellulosic biomass to lactic acid in pH neutral aqueous phase media, Appl. Catal. B Environ. 162 (2015) 149–157. https://doi.org/10.1016/j.apcatb.2014.06.025.

[42] A.A. Koutinas, A. Vlysidis, D. Pleissner, N. Kopsahelis, I. Lopez Garcia, I.K. Kookos, S. Papanikolaou, T.H. Kwan, C.S.K. Lin, Valorization of industrial waste and by-product streams via fermentation for the production of chemicals and biopolymers, Chem. Soc. Rev. 43 (2014). https://doi.org/10.1039/c3cs60293a.

[43] L. Hu, G. Zhao, W. Hao, X. Tang, Y. Sun, L. Lin, S. Liu, Catalytic conversion of biomass-derived carbohydrates into fuels and chemicals via furanic aldehydes, RSC Adv. 2 (2012) 11184–11206. https://doi.org/10.1039/C2RA21811A.

[44] Y. Zhang, J. Wang, J. Ren, X. Liu, X. Li, Y. Xia, G. Lu, Y. Wang, Mesoporous niobium phosphate: an excellent solid acid for the dehydration of fructose to 5-hydroxymethylfurfural in water, Catal. Sci. Technol. 2 (2012) 2485–2491. https://doi.org/10.1039/C2CY20204B.

[45] F. Menegazzo, E. Ghedini, M. Signoretto, 5-Hydroxymethylfurfural (HMF) Production from Real Biomasses., Molecules. 23 (2018). https://doi.org/10.3390/molecules23092201.

[46] S. Gehrmann, N. Tenhumberg, Production and Use of Sustainable C2-C4 Alcohols – An Industrial Perspective, Chemie Ing. Tech. 92 (2020). https://doi.org/10.1002/cite.202000077.

[47] H. Wang, M. Tucker, Y. Ji, Recent Development in Chemical Depolymerization of Lignin: A Review, J. Appl. Chem. 2013 (2013) 9. https://doi.org/10.1155/2013/838645.

[48] S.I. Mussatto, G.M. Dragone, Chapter 1 - Biomass Pretreatment, Biorefineries, and Potential Products for a Bioeconomy Development, in: S.I.B.T.-B.F.T. for a L.F.B.B. Mussatto (Ed.), Elsevier, Amsterdam, 2016: pp. 1–22. https://doi.org/https://doi.org/10.1016/B978-0-12-802323-5.00001-3.

[49] F.R. Amin, H. Khalid, H. Zhang, S.U. Rahman, R. Zhang, G. Liu, C. Chen, Pretreatment methods of lignocellulosic biomass for anaerobic digestion., AMB Express. 7 (2017) 72. https://doi.org/10.1186/s13568-017-0375-4.

[50] S.P.S. AU - Chundawat, R.K. AU - Pal, C. AU - Zhao, T. AU - Campbell, F. AU - Teymouri, J. AU - Videto, C. AU - Nielson, B. AU - Wieferich, L. AU - Sousa, B.E. AU - Dale, V. AU - Balan, S. AU - Chipkar, J. AU - Aguado, E. AU - Burke, R.G. AU - Ong, Ammonia Fiber Expansion (AFEX) Pretreatment of Lignocellulosic Biomass, JoVE. (2020) e57488. https://doi.org/doi:10.3791/57488.

[51] J. Zhang, H. Zhou, D. Liu, X. Zhao, Chapter 2 - Pretreatment of lignocellulosic biomass for efficient enzymatic saccharification of cellulose, in: A. Yousuf, D. Pirozzi, F.B.T.-L.B. to L.B. Sannino (Eds.), Academic Press, 2020: pp. 17–65. https://doi.org/https://doi.org/10.1016/B978-0-12-815936-1.00002-2.

[52] A.A. Shah, T.H. Seehar, K. Sharma, S.S. Toor, Chapter 7 - Biomass pretreatment technologies, in: S.K. Maity, K. Gayen, T.K.B.T.-H.B. Bhowmick (Eds.), Elsevier, 2022: pp. 203–228. https://doi.org/https://doi.org/10.1016/B978-0-12-823306-1.00014-5.

[53] V.A. Marulanda, C.D.B. Gutierrez, C.A.C. Alzate, Chapter 4 - Thermochemical, Biological, Biochemical, and Hybrid Conversion Methods of Bio-derived Molecules into Renewable Fuels, in: M.B.T.-A.B. for A.F. Hosseini Biobased Chemicals, and Bioproducts (Ed.), Woodhead Publ. Ser. Energy,

Woodhead Publishing, 2019: pp. 59–81. https://doi.org/https://doi.org/10.1016/B978-0-12-817941-3.00004-8.

[54] S. Alrumman, Enzymatic saccharification and fermentation of cellulosic date palm wastes to glucose and lactic acid, Brazilian J. Microbiol. 47 (2016) 110–119. https://doi.org/10.1016/j.bjm.2015.11.015.

[55] V.P. Haribal, Y. Chen, L. Neal, F. Li, Intensification of Ethylene Production from Naphtha via a Redox Oxy-Cracking Scheme: Process Simulations and Analysis, Engineering. 4 (2018) 714–721. https://doi.org/https://doi.org/10.1016/j.eng.2018.08.001.

[56] M. Ellouh, Z. Qureshi, Muhammad, M. Akhtar, Y. Jin, O. Koseoglu, H. Alasiri, Catalysis Light Paraffinic Naphtha to BTX Aromatics over Metal- Modified Pt/ZSM-5, 2020. https://doi.org/10.1002/slct.202003492.

[57] T. Farmer, M. Mascal, Platform Molecules, in: Introd. to Chem. from Biomass Second Ed., 2014: pp. 89–155. https://doi.org/10.1002/9781118714478.ch4.

[58] M.I. Alam, A. Ali, S. Gupta, A. Haider, Biological Routes for the Synthesis of Platform Chemicals from Biomass Feedstocks, in: Microb. Appl., 2017: pp. 153–166. https://doi.org/10.1007/978-3-319-52669-0_8.

[59] I. Agirrezabal-Telleria, I. Gandarias, P.L. Arias, Production of furfural from pentosan-rich biomass: Analysis of process parameters during simultaneous furfural stripping, Bioresour. Technol. 143 (2013) 258–264.https://doi.org/https://doi.org/10.1016/j.biortech.2013.05.082.

[60] M.G.A. Felipe, M. Vitolo, I.M. Mancilha, S.S. Silva, Fermentation of sugar cane bagasse hemicellulosic hydrolysate for xylitol production: Effect of pH, Biomass and Bioenergy. 13 (1997) 11–14. https://doi.org/https://doi.org/10.1016/S0961-9534(97)00032-9.

[61] M.J. Climent, A. Corma, S. Iborra, Converting carbohydrates to bulk chemicals and fine chemicals over heterogeneous catalysts, Green Chem. 13 (2011) 520. https://doi.org/10.1039/c0gc00639d.

[62] J.S. Brindle, P.S. Nelson, R.P. Charde, S.A. Sufyan, M.M. Nigra, Catalytic cooperativity between glucose oxidase and gold nanoparticles in the sequential oxidation of glucose to saccharic acid, Green Chem. 24 (2022) 5162–5170. https://doi.org/10.1039/D1GC03453G.

[63] A. Liu, Z. Huang, X. Wang, Efficient Oxidation of Glucose into Gluconic Acid Catalyzed by Oxygen-Rich Carbon Supported Pd Under Room Temperature and Atmospheric Pressure, Catal. Letters. 148 (2018) 2019+. https://link.gale.com/apps/doc/A543934418/AONE?u=anon~baf7886b&sid=googleScholar&xid=6c7331d7.

[64] J. Li, D.-J. Ding, L. Deng, Q.-X. Guo, Y. Fu, Catalytic air oxidation of biomass-derived carbohydrates to formic acid., ChemSusChem. 5 (2012) 1313–1318. https://doi.org/10.1002/cssc.201100466.

[65] L. Yang, J. Su, X. Yang, H. Lin, Catalytic Oxidation Pathways for the Production of Carboxylic Acids from Biomass, in: 2016: pp. 171–202. https://doi.org/10.1007/978-981-287-688-1_7.

[66] G. Araujo Barahona, K. Eränen, J. Oña, D. Murzin, J. García-Serna, T. Salmi, Solid Foam Ru/C Catalysts for Sugar Hydrogenation to Sugar Alcohols─Preparation, Characterization, Activity, and Selectivity, Ind. Eng. Chem. Res. (2022). https://doi.org/10.1021/acs.iecr.1c04501.

[67] G.J. Mulder, No Title, J. Prakt. Chem. (1840) 203–204.

[68] F.H. Newth, The Formation of Furan Compounds from Hexoses, in: C.S. Hudso, S.M.B.T.-A. in C.C. Canto (Eds.), Academic Press, 1951: pp. 83–106. https://doi.org/https://doi.org/10.1016/S0096-5332(08)60064-8.

[69] J. Kiermayer, A derivative of furfuraldehyde from laevulosa,

Chem. Ztg. 19 (1895) 1003–1006.

[70] G. Dull, No Title, Chem. Ztg. 19 (1895) 166–216. https://www.scopus.com/inward/record.uri?eid=2-s2.0-84909786991&partnerID=40&md5=5481110b5f6a2900e8ee9daab692dc9b.

[71] T. vom Stein, P.M. Grande, H. Kayser, F. Sibilla, W. Leitner, P. de María, From biomass to feedstock: one-step fractionation of lignocellulose components by the selective organic acid-catalyzed depolymerization of hemicellulose in a biphasic system, Green Chem. 13 (2011) 1772–1777. https://doi.org/10.1039/C1GC00002K.

[72] M. Przydacz, M. Jędrzejczyk, J. Rogowski, M. Szynkowska-Józwik, A.M. Ruppert, Highly efficient production of DMF from biomass-derived HMF on recyclable Ni-Fe/TiO2 catalysts, Energies. 13 (2020). https://doi.org/10.3390/en13184660.

[73] Y. Román-Leshkov, C.J. Barrett, Z.Y. Liu, J.A. Dumesic, Production of dimethylfuran for liquid fuels from biomass-derived carbohydrates., Nature. 447 (2007) 982–985. https://doi.org/10.1038/nature05923.

[74] Y.W. Tiong, C.L. Yap, S. Gan, W.S.P. Yap, Conversion of Biomass and Its Derivatives to Levulinic Acid and Levulinate Esters via Ionic Liquids, Ind. Eng. Chem. Res. 57 (2018) 4749–4766. https://doi.org/10.1021/acs.iecr.8b00273.

[75] J.-P. Lange, R. Price, P.M. Ayoub, J. Louis, L. Petrus, L. Clarke, H. Gosselink, Valeric biofuels: A platform of cellulosic transportation fuels, Angew. Chemie - Int. Ed. 49 (2010) 4479–4483. https://doi.org/10.1002/anie.201000655.

[76] J.Q. Bond, D.M. Alonso, D. Wang, R.M. West, J.A. Dumesic, Integrated catalytic conversion of γ-valerolactone to liquid alkenes for transportation fuels, Science (80-.). 327 (2010) 1110–1114. https://doi.org/10.1126/science.1184362.

[77] H. Heeres, R. Handana, D. Chunai, C. Borromeus Rasrendra, B. Girisuta, H. Jan Heeres, Combined dehydration/(transfer)-

hydrogenation of C6-sugars (D-glucose and D-fructose) to [gamma]-valerolactone using ruthenium catalysts, Green Chem. 11 (2009) 1247–1255. https://doi.org/10.1039/B904693C.

[78] E. de Jong, G.-J. Gruter, Furanics: A Novel Diesel Fuel with Superior Characteristics, SAE Tech. Pap. (2009). https://doi.org/10.4271/2009-01-2767.

[79] P. Bhaumik, P. Dhepe, Solid Acid Catalyzed Synthesis of Furans from Carbohydrates, Catal. Rev. 58 (2016) 36–112. https://doi.org/10.1080/01614940.2015.1099894.

[80] S. Kang, J. Fu, G. Zhang, From lignocellulosic biomass to levulinic acid: A review on acid-catalyzed hydrolysis, Renew. Sustain. Energy Rev. 94 (2018) 340–362. https://doi.org/https://doi.org/10.1016/j.rser.2018.06.016.

[81] J.M. Timko, D.J. Cram, Furanyl unit in host compounds, J. Am. Chem. Soc. 96 (1974) 7159–7160. https://doi.org/10.1021/ja00829a085.

[82] H.-J. Yoon, J.-W. Choi, H.-S. Jang, J. Cho, J.-W. Byun, W.-J. Chung, S.-M. Lee, Y.-S. Lee, Selective Oxidation of 5-Hydroxymethylfurfural to 2,5-Diformylfuran by Polymer-Supported IBX Amide, Synlett. 2011 (2010) 165–168. https://doi.org/10.1055/s-0030-1259284.

[83] N. Yoshida, N. Kasuya, N. Haga, K. Fukuda, Brand-new Biomass-based Vinyl Polymers from 5-Hydroxymethylfurfural, Polym. J. 40 (2008) 1164–1169. https://doi.org/10.1295/polymj.PJ2008170.

[84] M. Mascal, S. Dutta, Synthesis of the natural herbicide δ-aminolevulinic acid from cellulose-derived 5-(chloromethyl)furfural, Green Chem. 13 (2011) 40–41. https://doi.org/10.1039/C0GC00548G.

[85] R. Villard, F. Robert, I. Blank, G. Bernardinelli, T. Soldo, T. Hofmann, Racemic and enantiopure synthesis and physicochemical characterization of the novel taste enhancer N-(1-carboxyethyl)-6-(hydroxymethyl)pyridinium-3-ol inner salt., J. Agric. Food Chem. 51 (2003) 4040–4045.

https://doi.org/10.1021/jf034246+.

[86] R.-J. van Putten, J.C. van der Waal, E. de Jong, C.B. Rasrendra, H.J. Heeres, J.G. de Vries, Hydroxymethylfurfural, A Versatile Platform Chemical Made from Renewable Resources, Chem. Rev. 113 (2013) 1499–1597. https://doi.org/10.1021/cr300182k.

[87] E.F. ANET, 3-DEOXYGLYCOSULOSES (3-DEOXYGLYCOSONES) AND THE DEGRADATION OF CARBOHYDRATES., Adv. Carbohydr. Chem. 19 (1964) 181–218. https://doi.org/10.1016/s0096-5332(08)60282-9.

[88] C. Moreau, R. Durand, S. Razigade, J. Duhamet, P. Faugeras, P. Rivalier, P. Ros, G. Avignon, Dehydration of fructose to 5-hydroxymethylfurfural over H-mordenites, Appl. Catal. A Gen. 145 (1996) 211–224. https://doi.org/https://doi.org/10.1016/0926-860X(96)00136-6.

[89] M.J. Antal, W.S.L. Mok, G.N. Richards, Mechanism of formation of 5-(hydroxymethyl)-2-furaldehyde from d-fructose and sucrose, Carbohydr. Res. 199 (1990) 91–109. https://doi.org/10.1016/0008-6215(90)84096-D.

[90] B.F.M. Kuster, 5-Hydroxymethylfurfural (HMF). A Review Focussing on its Manufacture, Starch - Stärke. 42 (1990) 314–321. https://doi.org/10.1002/star.19900420808.

[91] A.S. Amarasekara, L.D. Williams, C.C. Ebede, Mechanism of the dehydration of D-fructose to 5-hydroxymethylfurfural in dimethyl sulfoxide at 150 degrees C: an NMR study., Carbohydr. Res. 343 (2008) 3021–3024. https://doi.org/10.1016/j.carres.2008.09.008.

[92] H. Yan, Y. Yang, D. Tong, X. Xiang, C. Hu, Catalytic conversion of glucose to 5-hydroxymethylfurfural over SO42−/ZrO2 and SO42−/ZrO2–Al2O3 solid acid catalysts, 2009. https://doi.org/10.1016/j.catcom.2009.04.020.

[93] C. Carlini, M. Giuttari, A. Maria Raspolli Galletti, G. Sbrana, T. Armaroli, G. Busca, Selective saccharides dehydration to 5-

hydroxymethyl-2-furaldehyde by heterogeneous niobium catalysts, Appl. Catal. A Gen. 183 (1999) 295–302. https://doi.org/http://dx.doi.org/10.1016/S0926-860X(99)00064-2.

[94] F. Benvenuti, C. Carlini, P. Patrono, A.M. Raspolli Galletti, G. Sbrana, M.A. Massucci, P. Galli, Heterogeneous zirconium and titanium catalysts for the selective synthesis of 5-hydroxymethyl-2-furaldehyde from carbohydrates, Appl. Catal. A Gen. 193 (2000) 147–153. https://doi.org/https://doi.org/10.1016/S0926-860X(99)00424-X.

[95] Q. Jing, X. Lü, Kinetics of Non-catalyzed Decomposition of Glucose in High-temperature Liquid Water, Chinese J. Chem. Eng. 16 (2008) 890–894. https://doi.org/https://doi.org/10.1016/S1004-9541(09)60012-4.

[96] T.M. Aida, Y. Sato, M. Watanabe, K. Tajima, T. Nonaka, H. Hattori, K. Arai, Dehydration of d-glucose in high temperature water at pressures up to 80MPa, J. Supercrit. Fluids. 40 (2007) 381–388. https://doi.org/https://doi.org/10.1016/j.supflu.2006.07.027.

[97] X. Qi, M. Watanabe, T.M. Aida, R.L. Smith Jr, Catalytical conversion of fructose and glucose into 5-hydroxymethylfurfural in hot compressed water by microwave heating, Catal. Commun. 9 (2008) 2244–2249. https://doi.org/http://dx.doi.org/10.1016/j.catcom.2008.04.025.

[98] A. Chareonlimkun, V. Champreda, A. Shotipruk, N. Laosiripojana, Catalytic conversion of sugarcane bagasse, rice husk and corncob in the presence of TiO_2, ZrO_2 and mixed-oxide TiO_2–ZrO_2 under hot compressed water (HCW) condition, Bioresour. Technol. 101 (2010) 4179–4186. https://doi.org/https://doi.org/10.1016/j.biortech.2010.01.037.

[99] Y. Nakamura, S. Morikawa, The Dehydration of D-Fructose to 5-Hydroxymethyl-2-furaldehyde, Bull. Chem. Soc. Jpn. 53

(1980) 3705–3706. https://doi.org/10.1246/bcsj.53.3705.

[100] M. Ohara, A. Takagaki, S. Nishimura, K. Ebitani, Syntheses of 5-hydroxymethylfurfural and levoglucosan by selective dehydration of glucose using solid acid and base catalysts, Appl. Catal. A Gen. 383 (2010) 149–155. https://doi.org/http://dx.doi.org/10.1016/j.apcata.2010.05.040.

[101] X. Tian, B. Qi, S. Zhang, J. Luo, W. Yinhua, Catalytic production of 5-hydroxymethylfurfural from sucrose and molasses by aluminum chloride in green aqueous γ-valerolactone system, Biomass Convers. Biorefinery. 11 (2021). https://doi.org/10.1007/s13399-020-00603-6.

[102] B. Kuster, H. Steen, Preparation of 5-Hydroxymethylfurfural Part I. Dehydration of Fructose in a Continuous Stirred Tank Reactor, Starch - Stärke. 29 (2006) 99–103. https://doi.org/10.1002/star.19770290306.

[103] C. Moreau, R. Durand, S. Razigade, J. Duhamet, P. Faugeras, P. Rivalier, P. Ros, G. Avignon, Dehydration of fructose to 5-hydroxymethylfurfural over H-mordenites, Appl. Catal. A Gen. 145 (1996) 211–224. https://doi.org/10.1016/0926-860X(96)00136-6.

[104] C. Moreau, R. Durand, C. Pourcheron, S. Razigade, Preparation of 5-hydroxymethylfurfural from fructose and precursors over H-form zeolites, Ind. Crops Prod. 3 (1994) 85–90. https://doi.org/http://dx.doi.org/10.1016/0926-6690(94)90080-9.

[105] V. V Ordomsky, J. van der Schaaf, J.C. Schouten, T.A. Nijhuis, The effect of solvent addition on fructose dehydration to 5-hydroxymethylfurfural in biphasic system over zeolites, J. Catal. 287 (2012) 68–75. https://doi.org/http://dx.doi.org/10.1016/j.jcat.2011.12.002.

[106] J.N. (Wisconsin A.R.F. Dumesic, J. A.; Román-Leshkov, Y.; Chheda, Int. Patent WO 2007/146636, 2007.

[107] H.E. Degirmenci V, Pidko EA, Magusin PCMM, Towards a

Selective Heterogeneous Catalyst for Glucose Dehydration to 5-Hydroxymethylfurfural in Water: CrCl2 Catalysis in a Thin Immobilized Ionic Liquid Layer, ChemCatChem. 3 (2011) 969–972.

[108] C. V McNeff, D.T. Nowlan, L.C. McNeff, B. Yan, R.L. Fedie, Continuous production of 5-hydroxymethylfurfural from simple and complex carbohydrates, Appl. Catal. A Gen. 384 (2010) 65–69. https://doi.org/https://doi.org/10.1016/j.apcata.2010.06.008.

[109] J.N. Chheda, Y. Roman-Leshkov, J.A. Dumesic, Production of 5-hydroxymethylfurfural and furfural by dehydration of biomass-derived mono- and poly-saccharides, Green Chem. 9 (2007) 342–350. https://doi.org/10.1039/B611568C.

[110] C. Lansalot-Matras, C. Moreau, Dehydration of fructose into 5-hydroxymethylfurfural in the presence of ionic liquids, Catal. Commun. 4 (2003) 517–520. https://doi.org/https://doi.org/10.1016/S1566-7367(03)00133-X.

[111] C. Moreau, A. Finiels, L. Vanoye, Dehydration of fructose and sucrose into 5-hydroxymethylfurfural in the presence of 1-H-3-methyl imidazolium chloride acting both as solvent and catalyst, J. Mol. Catal. A Chem. 253 (2006) 165–169. https://doi.org/https://doi.org/10.1016/j.molcata.2006.03.046.

[112] F. Guo, Z. Fang, T.-J. Zhou, Conversion of fructose and glucose into 5-hydroxymethylfurfural with lignin-derived carbonaceous catalyst under microwave irradiation in dimethyl sulfoxide–ionic liquid mixtures, Bioresour. Technol. 112 (2012) 313–318. https://doi.org/http://dx.doi.org/10.1016/j.biortech.2012.02.108.

[113] H.P. Teunissen, Velocity measurements on the opening of the furane ring in hydroxy-methylfurfuraldehyde, Recl. Des Trav. Chim. Des Pays-Bas. 49 (1930) 784–826. https://doi.org/10.1002/recl.19300490902.

[114] A. (Furchim S. M'Bazoa, C.; Raymond, F.; Rigal, L.; Gaset, Fr. Patent FR 2669635, 1990.

[115] A.C. Cope, US 2917520, 1959.

[116] P. (Roquette F. Fleche, G.; Gaset, A.; Gorrichon, J.-P.; Truchot, E.; Sicard, U.S. Patent 4339387, 1982.

[117] Y. Roman-Leshkov, J. A. Dumesic, Solvent Effects on Fructose Dehydration to 5-Hydroxymethylfurfural in Biphasic Systems Saturated with Inorganic Salts, 2009. https://doi.org/10.1007/s11244-008-9166-0.

[118] K.M. (Süddeutsche Z.-A. Rapp, U.S. Patent 4740605, 1987, n.d.

[119] P. Vinke, H. Van Bekkum, The Dehydration of Fructose Towards 5-Hydroxymethylfurfural Using Activated Carbon as Adsorbent, Starch-Starke. 44 (1992) 90–96.

[120] L.L. Klasson, K. T.; Uchimiya, M.; Lima, I. M.; Boihem, Feasibility of removing furfurals from sugar solutions using activated biochars made from agricultural residues, Jr. Bioresour. 5 (2011) 32–42.

[121] J.G. (Archer D.M.C. Geier, D. F.; Soper, WO2008157617, n.d.

[122] I.. Jones, R. E.; Lange, H. B. (Merch & Co, U.S. Patent 2994645, 1961.

[123] I.. Hunter, R. H. (Atlas Chemical Industries, U.S. Patent 3201331, 1965.

[124] C. Blecker, C. Fougnies, J.-C. Van Herck, J.-P. Chevalier, M. Paquot, Kinetic Study of the Acid Hydrolysis of Various Oligofructose Samples, J. Agric. Food Chem. 50 (2002) 1602–1607. https://doi.org/10.1021/jf010905b.

[125] F.K. Kazi, A.D. Patel, J.C. Serrano-Ruiz, J.A. Dumesic, R.P. Anex, Techno-economic analysis of dimethylfuran (DMF) and hydroxymethylfurfural (HMF) production from pure fructose in catalytic processes, Chem. Eng. J. 169 (2011) 329–338. https://doi.org/https://doi.org/10.1016/j.cej.2011.03.018.

[126] X. Li, J. Ma, H. He, Recent advances in catalytic decomposition of ozone, J. Environ. Sci. 94 (2020) 14–31. https://doi.org/https://doi.org/10.1016/j.jes.2020.03.058.

[127] K. Tanabe, W.F. Hölderich, Industrial application of solid acid–base catalysts, Appl. Catal. A Gen. 181 (1999) 399–434. https://doi.org/https://doi.org/10.1016/S0926-860X(98)00397-4.

[128] D.M. Miller, G.R. Buettner, S.D. Aust, Transition metals as catalysts of "autoxidation" reactions, Free Radic. Biol. Med. 8 (1990) 95–108. https://doi.org/https://doi.org/10.1016/0891-5849(90)90148-C.

[129] K. Foger, Dispersed Metal Catalysts BT - Catalysis: Science and Technology Volume 6, in: J.R. Anderson, M. Boudart (Eds.), Springer Berlin Heidelberg, Berlin, Heidelberg, 1984: pp. 227–305. https://doi.org/10.1007/978-3-642-93250-2_4.

[130] C. Ding, W. Liu, J. Wang, P. Liu, K. Zhang, X. Gao, G. Ding, S. Liu, Y. Han, X. Ma, One step synthesis of mesoporous NiO–Al2O3 catalyst for partial oxidation of methane to syngas: The role of calcination temperature, Fuel. 162 (2015) 148–154. https://doi.org/https://doi.org/10.1016/j.fuel.2015.09.002.

[131] C. García Sancho, J. Rubio, J.M. Mérida-Robles, R. Moreno-Tost, J. Santamaría gonzalez, P. Maireles-Torres, Mesoporous Nb2O5 as solid acid catalyst for dehydration of D-xylose into furfural, Catal. Today. 234 (2014) 119–124. https://doi.org/10.1016/j.cattod.2014.02.012.

[132] A. Infantes-Molina, Transition Metal Sulfide Catalysts for Petroleum Upgrading – Hydrodesulfurization Reactions, in: A. Romero-Pérez (Ed.), IntechOpen, Rijeka, 2012: p. Ch. 9. https://doi.org/10.5772/45629.

[133] C. García Sancho, I. Sadaba, R. Moreno-Tost, J. Mérida-Robles, J. Santamaría gonzalez, M. López-Granados, P. Maireles-Torres, Dehydration of Xylose to Furfural over MCM-41-Supported Niobium-Oxide Catalysts, ChemSusChem. 6 (2013). https://doi.org/10.1002/cssc.201200881.

[134] M.J. Hülsey, C.W. Lim, N. Yan, Promoting heterogeneous catalysis beyond catalyst design, Chem. Sci. 11 (2020) 1456–1468. https://doi.org/10.1039/C9SC05947D.

[135] J.G. Dawber, D.R. Brown, R.A. Reed, Acid-catalyzed hydrolysis of sucrose: A student study of a reaction mechanism, J. Chem. Educ. 43 (1966) 34. https://doi.org/10.1021/ed043p34.

[136] L. Faba, E. Díaz, S. Ordóñez, Base-Catalyzed Reactions in Biomass Conversion: Reaction Mechanisms and Catalyst Deactivation, in: 2016: pp. 87–122. https://doi.org/10.1007/978-981-287-688-1_5.

[137] S. Rojas-Buzo, P. García-García, A. Corma, Hf-based metal–organic frameworks as acid–base catalysts for the transformation of biomass-derived furanic compounds into chemicals, Green Chem. 20 (2018) 3081–3091. https://doi.org/10.1039/C8GC00806J.

[138] G. Connell, J.A. Dumesic, The generation of Brønsted and Lewis acid sites on the surface of silica by addition of dopant cations, J. Catal. 105 (1987) 285–298. https://doi.org/https://doi.org/10.1016/0021-9517(87)90059-5.

[139] M. Watanabe, Y. Aizawa, T. Iida, T.M. Aida, C. Levy, K. Sue, H. Inomata, Glucose reactions with acid and base catalysts in hot compressed water at 473 K, Carbohydr. Res. 340 (2005) 1925–1930. https://doi.org/http://dx.doi.org/10.1016/j.carres.2005.06.017.

[140] M. Watanabe, Y. Aizawa, T. Iida, R. Nishimura, H. Inomata, Catalytic glucose and fructose conversions with TiO2 and ZrO2 in water at 473K: Relationship between reactivity and acid–base property determined by TPD measurement, Appl. Catal. A Gen. 295 (2005) 150–156. https://doi.org/10.1016/j.apcata.2005.08.007.

[141] M. Ohara, A. Takagaki, S. Nishimura, K. Ebitani, Syntheses of 5-hydroxymethylfurfural and levoglucosan by selective

dehydration of glucose using solid acid and base catalysts, Appl. Catal. A Gen. 383 (2010) 149–155. https://doi.org/10.1016/j.apcata.2010.05.040.

[142] V. Choudhary, S.H. Mushrif, C. Ho, A. Anderko, V. Nikolakis, N.S. Marinkovic, A.I. Frenkel, S.I. Sandler, D.G. Vlachos, Insights into the Interplay of Lewis and Brønsted Acid Catalysts in Glucose and Fructose Conversion to 5-(Hydroxymethyl)furfural and Levulinic Acid in Aqueous Media, J. Am. Chem. Soc. 135 (2013) 3997–4006. https://doi.org/10.1021/ja3122763.

[143] G. Hutchings, J. Védrine, Heterogeneous Catalyst Preparation, in: Springer Ser. Chem. Phys., 2004: pp. 215–258. https://doi.org/10.1007/978-3-662-05981-4_6.

[144] Z. Vajglová, N. Kumar, P. Mäki-Arvela, K. Eränen, M. Peurla, L. Hupa, M. Nurmi, M. Toivakka, D.Y. Murzin, Synthesis and Physicochemical Characterization of Shaped Catalysts of β and Y Zeolites for Cyclization of Citronellal, Ind. Eng. Chem. Res. 58 (2019) 18084–18096. https://doi.org/10.1021/acs.iecr.9b02829.

[145] D.-M. Gao, B. Zhao, H. Liu, K. Morisato, K. Kanamori, Z. He, M. Zeng, H. Wu, J. Chen, K. Nakanishi, Synthesis of a hierarchically porous niobium phosphate monolith by a sol–gel method for fructose dehydration to 5-hydroxymethylfurfural, Catal. Sci. Technol. 8 (2018) 3675–3685. https://doi.org/10.1039/C8CY00803E.

[146] R.J. Argauer, G.R. Landolt, Crystalline zeolite ZSM-5 and method of preparing the same, U.S. Pat. 3 (1972).

[147] C.T. Kresge, M.E. Leonowicz, W.J. Roth, J.C. Vartuli, J.S. Beck, Ordered mesoporous molecular sieves synthesized by a liquid-crystal template mechanism, Nature. 359 (1992) 710–712. https://doi.org/10.1038/359710a0.

[148] K.S.W.S. and K.K.U. J. Rouquerol, D. Avnir, C. W. Fairbridge, D. H. Everett, J. M. Haynes, N. Pernicone, J. D. F. Ramsay, Recommendations for the characterization of porous solids, Pure App.Chem. 8 (1996) 1739–1758.

[149] B. Sui, G. Wang, S. Yuan, W. Yang, F. Ling, S. Wang, H. He, Macroporous Al_2O_3 with three-dimensionally interconnected structure: Catalytic performance of hydrodemetallization for residue oil, J. Fuel Chem. Technol. 49 (2021) 1201–1207. https://doi.org/https://doi.org/10.1016/S1872-5813(21)60096-8.

[150] I. Jiménez-Morales, A. Teckchandani-Ortiz, J. Santamaría-González, P. Maireles-Torres, A. Jiménez-López, Selective dehydration of glucose to 5-hydroxymethylfurfural on acidic mesoporous tantalum phosphate, Appl. Catal. B Environ. 144 (2014) 22–28. https://doi.org/http://dx.doi.org/10.1016/j.apcatb.2013.07.002.

[151] P. Bhanja, S.K. Sharma, S. Chongdar, B. Paul, A. Bhaumik, Bifunctional crystalline microporous organic polymers: Efficient heterogeneous catalysts for the synthesis of 5-hydroxymethylfurfural, Mol. Catal. 515 (2021) 111877. https://doi.org/https://doi.org/10.1016/j.mcat.2021.111877.

[152] B. Zdravkov, J. Čermák, M. Šefara, J. Janků, Pore classification in the characterization of porous materials: A perspective, Open Chem. 5 (2007) 385–395. https://doi.org/doi:10.2478/s11532-007-0017-9.

[153] M. Moritz, M. Geszke-Moritz, Mesoporous materials as multifunctional tools in biosciences: Principles and applications, Mater. Sci. Eng. C. 49 (2015) 114–151. https://doi.org/https://doi.org/10.1016/j.msec.2014.12.079.

[154] A. Taguchi, F. Schüth, Ordered mesoporous materials in catalysis, Microporous Mesoporous Mater. 77 (2005) 1–45. https://doi.org/http://dx.doi.org/10.1016/j.micromeso.2004.06.030.

[155] J.S. Beck, J.C. Vartuli, K.D. Schmitt, D.H. Olson, E.W. Sheppard, S. Mccullen, J. Higgins, J. Schlenker, W.J. Roth, M.E. Leonowicz, C.T. Kresge, C.T.W. Chu, A New Family of Macro-Porous Molecular Sieves Prepared With Liquid Crystal Template, J. Am. Chem. Soc. - J Am Chem Soc. 114 (1992) 10834–10843. https://doi.org/10.1021/ja00053a020.

[156] D. Zhao, Q. Huo, J. Feng, B.F. Chmelka, G.D. Stucky, Nonionic Triblock and Star Diblock Copolymer and Oligomeric Surfactant Syntheses of Highly Ordered, Hydrothermally Stable, Mesoporous Silica Structures, J. Am. Chem. Soc. 120 (1998) 6024–6036. https://doi.org/10.1021/ja974025i.

[157] E. Grabowska, M. Marchelek, M. Paszkiewicz-Gawron, A. Zaleska-Medynska, 3 - Metal oxide photocatalysts, in: A.B.T.-M.O.-B.P. Zaleska-Medynska (Ed.), Met. Oxides, Elsevier, 2018: pp. 51–209. https://doi.org/https://doi.org/10.1016/B978-0-12-811634-0.00003-2.

[158] M. Stodolny, M. Laniecki, Synthesis and characterization of mesoporous Ta2O5–TiO2 photocatalysts for water splitting, Catal. Today. 142 (2009) 314–319. https://doi.org/https://doi.org/10.1016/j.cattod.2008.07.034.

[159] Y. Chen, J.L.G. Fierro, T. Tanaka, I.E. Wachs, Supported Tantalum Oxide Catalysts: Synthesis, Physical Characterization, and Methanol Oxidation Chemical Probe Reaction, J. Phys. Chem. B. 107 (2003) 5243–5250. https://doi.org/10.1021/jp0276451.

[160] T. Ushikubo, K. Wada, Catalytic properties of hydrated tantalum oxide, Appl. Catal. 67 (1990) 25–38. https://doi.org/https://doi.org/10.1016/S0166-9834(00)84429-2.

[161] C. Yue, M. Trudeau, D. Antonelli, Electroactive mesoporous tantalum oxide catalysts for nitrogen activation and ammonia synthesis, Chem. Commun. (2006) 1918–1920. https://doi.org/10.1039/B517415E.

[162] D.M. Antonelli, J.Y. Ying, Synthesis of a Stable Hexagonally Packed Mesoporous Niobium Oxide Molecular Sieve Through a Novel Ligand-Assisted Templating Mechanism, Angew. Chemie Int. Ed. English. 35 (1996) 426–430. https://doi.org/https://doi.org/10.1002/anie.199604261.

[163] F. Yang, Q. Liu, M. Yue, X. Bai, Y. Du, Tantalum compounds

as heterogeneous catalysts for saccharide dehydration to 5-hydroxymethylfurfural, Chem. Commun. 47 (2011) 4469–4471. https://doi.org/10.1039/C0CC05138A.

[164] I. Jiménez-Morales, A. Teckchandani-Ortiz, J. Santamaría-González, P. Maireles-Torres, A. Jiménez-López, Selective dehydration of glucose to 5-hydroxymethylfurfural on acidic mesoporous tantalum phosphate, Appl. Catal. B Environ. 144 (2014) 22–28. https://doi.org/10.1016/j.apcatb.2013.07.002.

[165] X. Tong, L. Ga, J. ai, Y. Wang, Progress in cancer drug delivery based on AS1411 oriented nanomaterials, J. Nanobiotechnology. 20 (2022). https://doi.org/10.1186/s12951-022-01240-z.

[166] R.R. Castillo, L. de la Torre, F. García-Ochoa, M. Ladero, M. Vallet-Regí, Production of MCM-41 Nanoparticles with Control of Particle Size and Structural Properties: Optimizing Operational Conditions during Scale-Up, Int. J. Mol. Sci. . 21 (2020). https://doi.org/10.3390/ijms21217899.

[167] S.-C. Shen, S. Kawi, Understanding of the Effect of Al Substitution on the Hydrothermal Stability of MCM-41, J. Phys. Chem. B. 103 (1999) 8870–8876. https://doi.org/10.1021/jp991831y.

[168] R. Mokaya, W. Jones, Efficient post-synthesis alumination of MCM-41 using aluminium chlorohydrate containing Al polycations, J. Mater. Chem. 9 (1999) 555–561. https://doi.org/10.1039/A807312K.

[169] L.Y. Chen, Z. Ping, G.K. Chuah, S. Jaenicke, G. Simon, A comparison of post-synthesis alumination and sol-gel synthesis of MCM-41 with high framework aluminum content, Microporous Mesoporous Mater. 27 (1999) 231–242. https://doi.org/https://doi.org/10.1016/S1387-1811(98)00257-1.

[170] C.A. Koh, R. Nooney, S. Tahir, Characterisation and catalytic properties of MCM-41 and Pd/MCM-41 materials, Catal. Letters. 47 (1997) 199–203. https://doi.org/10.1023/A:1019025609426.

[171] J. Adam, M. Blazsó, E. Mészáros, M. Stöcker, M.H. Nilsen, A. Bouzga, J.E. Hustad, M. Grønli, G. Øye, Pyrolysis of biomass in the presence of Al-MCM-41 type catalysts, Fuel. 84 (2005) 1494–1502. https://doi.org/https://doi.org/10.1016/j.fuel.2005.02.006.

[172] Ó. de la Iglesia, M. Sarango, M. Munárriz, M. Malankowska, A. Navajas, L.M. Gandía, J. Coronas, C. Téllez, Mesoporous Sn-In-MCM-41 Catalysts for the Selective Sugar Conversion to Methyl Lactate and Comparative Life Cycle Assessment with the Biochemical Process, ACS Sustain. Chem. Eng. 10 (2022) 2868–2880. https://doi.org/10.1021/acssuschemeng.1c04655.

[173] Q. Xu, Z. Zhu, Y. Tian, J. Deng, J. Shi, Y. Fu, Sn-MCM-41 as Efficient Catalyst for the Conversion of Glucose into 5-Hydroxymethylfurfural in Ionic Liquids, BioResources. 9 (2013). https://doi.org/10.15376/biores.9.1.303-315.

[174] H. Tüysüz, C.W. Lehmann, H. Bongard, B. Tesche, R. Schmidt, F. Schüth, Direct Imaging of Surface Topology and Pore System of Ordered Mesoporous Silica (MCM-41, SBA-15, and KIT-6) and Nanocast Metal Oxides by High Resolution Scanning Electron Microscopy, J. Am. Chem. Soc. 130 (2008) 11510–11517. https://doi.org/10.1021/ja803362s.

[175] F. Kleitz, S. Hei Choi, R. Ryoo, Cubic Ia3d large mesoporous silica: synthesis and replication to platinum nanowires, carbon nanorods and carbon nanotubes, Chem. Commun. (2003) 2136–2137. https://doi.org/10.1039/B306504A.

[176] W. Wang, R. Qi, W. Shan, X. Wang, Q. Jia, J. Zhao, C. Zhang, H. Ru, Synthesis of KIT-6 type mesoporous silicas with tunable pore sizes, wall thickness and particle sizes via the partitioned cooperative self-assembly process, Microporous Mesoporous Mater. 194 (2013). https://doi.org/10.1016/j.micromeso.2013.10.028.

[177] J. Mu, M. Liang, H. Huang, J. Meng, L. Xu, Z. Song, M. Wu, Z. Miao, S. Zhuo, J. Zhou, Experimental and theoretical study of ZrMo-KIT-6 solid acid catalyst with abundant Brønsted acid sites, RSC Adv. 12 (2022) 9310–9322. https://doi.org/10.1039/D2RA00586G.

[178] C. García-Sancho, J.M. Rubio-Caballero, J.M. Mérida-Robles, R. Moreno-Tost, J. Santamaría-González, P. Maireles-Torres, Mesoporous Nb2O5 as solid acid catalyst for dehydration of d-xylose into furfural, Catal. Today. 234 (2014) 119–124. https://doi.org/https://doi.org/10.1016/j.cattod.2014.02.012.

[179] K. Omata, T. Nambu, Catalysis of water molecules acting as Brönsted acids at Lewis acid sites on niobium oxide, Appl. Catal. A Gen. 607 (2020) 117812. https://doi.org/https://doi.org/10.1016/j.apcata.2020.117812.

[180] S.R. Varkolu, M.; Velpula, V.; Ganji, S.; Burri, D.R.; Rao Kamaraju, Ni nanoparticles supported on mesoporous silica (2D, 3D) architectures: highly efficient catalysts for the hydrocyclization of biomass-derived levulinic acid, RSC Adv. (2015) 2046–2069.

[181] E.M. Flanigen, Chapter 2 Zeolites and molecular sieves: An historical perspective, in: H. van Bekkum, E.M. Flanigen, P.A. Jacobs, J.C.B.T.-S. in S.S. and C. Jansen (Eds.), Introd. to Zeolite Sci. Pract., Elsevier, 2001: pp. 11–35. https://doi.org/https://doi.org/10.1016/S0167-2991(01)80243-3.

[182] J. Dědeček, Z. Sobalík, B. Wichterlová, Siting and Distribution of Framework Aluminium Atoms in Silicon-Rich Zeolites and Impact on Catalysis, Catal. Rev. 54 (2012) 135–223. https://doi.org/10.1080/01614940.2012.632662.

[183] M.J. Stephenson, M.P. Attfield, S.M. Holmes, R.A.W. Dryfe, Electrochemically controlled ion exchange: proton ion exchange with sodium zeolite X and A, J. Solid State Electrochem. 19 (2015) 1985–1992. https://doi.org/10.1007/s10008-015-2851-6.

[184] F.H. Wolf F, Molecular sieves, London, 1968.

[185] D.P. Roelofsen, E.R.J. Wils, H. Van Bekkum, Proton-exchanged type a molecular sieves, J. Inorg. Nucl. Chem. 34 (1972) 1437–1448. https://doi.org/https://doi.org/10.1016/0022-1902(72)80344-0.

[186] M. Dyballa, U. Obenaus, S. Lang, B. Gehring, Y. Traa, H. Koller, M. Hunger, Brønsted sites and structural stabilization effect of acidic low-silica zeolite A prepared by partial ammonium exchange, Microporous Mesoporous Mater. 212 (2015) 110–116. https://doi.org/https://doi.org/10.1016/j.micromeso.2015.03.030.

[187] J.R. Di Iorio, S.A. Bates, A.A. Verma, W.N. Delgass, F.H. Ribeiro, J.T. Miller, R. Gounder, The Dynamic Nature of Brønsted Acid Sites in Cu–Zeolites During NOx Selective Catalytic Reduction: Quantification by Gas-Phase Ammonia Titration, Top. Catal. 58 (2015) 424–434. https://doi.org/10.1007/s11244-015-0387-8.

[188] X. Zhao, J. Xu, F. Deng, Solid-state NMR for metal-containing zeolites: From active sites to reaction mechanism, Front. Chem. Sci. Eng. 14 (2020). https://doi.org/10.1007/s11705-019-1885-1.

[189] S.R. Batool, V.L. Sushkevich, J.A. van Bokhoven, Correlating Lewis acid activity to extra-framework aluminum species in zeolite Y introduced by Ion-exchange, J. Catal. 408 (2022) 24–35. https://doi.org/https://doi.org/10.1016/j.jcat.2022.02.010.

[190] W. Wu, E. Weitz, Modification of acid sites in ZSM-5 by ion-exchange: An in-situ FTIR study, Appl. Surf. Sci. 316 (2014) 405–415. https://doi.org/https://doi.org/10.1016/j.apsusc.2014.07.194.

[191] A. V Kucherov, A.A. Slinkin, Solid-state reaction as a way to transition metal cation introduction into high-silica zeolites, J. Mol. Catal. 90 (1994) 323–354. https://doi.org/https://doi.org/10.1016/0304-5102(93)E0320-G.

[192] D. Verboekend, J. Pérez-Ramírez, Design of hierarchical zeolite catalysts by desilication, Catal. Sci. Technol. 1 (2011) 879–890. https://doi.org/10.1039/C1CY00150G.

[193] T. Ennaert, J. Van Aelst, J. Dijkmans, R. De Clercq, W. Schutyser, M. Dusselier, D. Verboekend, B.F. Sels, Potential

and challenges of zeolite chemistry in the catalytic conversion of biomass, Chem. Soc. Rev. 45 (2016) 584–611. https://doi.org/10.1039/C5CS00859J.

[194] K. Lourvanij, G.L. Rorrer, Reactions of aqueous glucose solutions over solid-acid Y-zeolite catalyst at 110-160 .degree.C, Ind. Eng. Chem. Res. 32 (1993) 11–19. https://doi.org/10.1021/ie00013a002.

[195] N. Rahimi, R. Karimzadeh, Catalytic cracking of hydrocarbons over modified ZSM-5 zeolites to produce light olefins: A review, Appl. Catal. A Gen. 398 (2011) 1–17. https://doi.org/https://doi.org/10.1016/j.apcata.2011.03.009.

[196] S. Moon, H.-J. Chae, M.B. Park, Oligomerization of light olefins over ZSM-5 and beta zeolite catalysts by modifying textural properties, Appl. Catal. A Gen. 553 (2018) 15–23. https://doi.org/https://doi.org/10.1016/j.apcata.2018.01.015.

[197] C.M. Lok, J. Van Doorn, G. Aranda Almansa, Promoted ZSM-5 catalysts for the production of bio-aromatics, a review, Renew. Sustain. Energy Rev. 113 (2019) 109248. https://doi.org/https://doi.org/10.1016/j.rser.2019.109248.

[198] Y. Jia, Q. Shi, J. Wang, C. Ding, K. Zhang, Synthesis, characterization, and catalytic application of hierarchical nano-ZSM-5 zeolite, RSC Adv. 10 (2020) 29618–29626. https://doi.org/10.1039/D0RA06040B.

[199] H. Ma, Y. Wen, C. Yu, Y. Qiao, J. Teng, H. Ji, Catalytic Production of Methyl Lactate from Fructose-Based Carbohydrates Using Yttrium Modified ZSM-5 Zeolite, ChemistrySelect. 6 (2021) 10674–10681. https://doi.org/10.1002/slct.202102418.

[200] E.T.C. Vogt, B.M. Weckhuysen, Fluid catalytic cracking: recent developments on the grand old lady of zeolite catalysis, Chem. Soc. Rev. 44 (2015) 7342–7370. https://doi.org/10.1039/C5CS00376H.

[201] W. Lutz, Zeolite Y: Synthesis, Modification, and Properties—A Case Revisited, Adv. Mater. Sci. Eng. 2014 (2014) 1–20.

https://doi.org/10.1155/2014/724248.

[202] E. Aghaei, R. Karimzadeh, H.R. Godini, A. Gurlo, O. Gorke, Improving the physicochemical properties of Y zeolite for catalytic cracking of heavy oil via sequential steam-alkali-acid treatments, Microporous Mesoporous Mater. 294 (2020) 109854. https://doi.org/https://doi.org/10.1016/j.micromeso.2019.109854.

[203] J.R. Sohn, S.J. DeCanio, P.O. Fritz, J.H. Lunsford, Acid catalysis by dealuminated zeolite Y. 2. The roles of aluminum, J. Phys. Chem. 90 (1986) 4847–4851. https://doi.org/10.1021/j100411a026.

[204] R. West, M. Holm, S. Shunmugavel, J. Xiong, Z. Beversdorf, E. Taarning, C. Christensen, Zeolite H-USY for the Production of Lactic Acid and Methyl Lactate from C-3-Sugars, J. Catal. - J CATAL. 269 (2010) 122–130. https://doi.org/10.1016/j.jcat.2009.10.023.

[205] B.M. Lok, T.R. Cannan, C.A. Messina, The role of organic molecules in molecular sieve synthesis, Zeolites. 3 (1983) 282–291. https://doi.org/https://doi.org/10.1016/0144-2449(83)90169-0.

[206] I. Kiricsi, C. Flego, G. Pazzuconi, W.O.J. Parker, R. Millini, C. Perego, G. Bellussi, Progress toward Understanding Zeolite .beta. Acidity: An IR and 27Al NMR Spectroscopic Study, J. Phys. Chem. 98 (1994) 4627–4634. https://doi.org/10.1021/j100068a024.

[207] M. Guisnet, P. Ayrault, C. Coutanceau, M. Fernanda Alvarez, J. Datka, Acid properties of dealuminated beta zeolites studied by IR spectroscopy, J. Chem. Soc. Faraday Trans. 93 (1997) 1661–1665. https://doi.org/10.1039/A607609B.

[208] M. Moliner, Y. Román-Leshkov, M.E. Davis, Tin-containing zeolites are highly active catalysts for the isomerization of glucose in water, Proc. Natl. Acad. Sci. 107 (2010) 6164–6168. https://doi.org/10.1073/pnas.1002358107.

[209] R. Bermejo-Deval, M. Orazov, R. Gounder, S.-J. Hwang, M.E. Davis, Active Sites in Sn-Beta for Glucose Isomerization to Fructose and Epimerization to Mannose, ACS Catal. 4 (2014) 2288–2297. https://doi.org/10.1021/cs500466j.

[210] N. Rai, S. Caratzoulas, D.G. Vlachos, Role of Silanol Group in Sn-Beta Zeolite for Glucose Isomerization and Epimerization Reactions, ACS Catal. 3 (2013) 2294–2298. https://doi.org/10.1021/cs400476n.

[211] E. Taarning, S. Saravanamurugan, M. Spangsberg Holm, J. Xiong, R.M. West, C.H. Christensen, Zeolite-Catalyzed Isomerization of Triose Sugars, ChemSusChem. 2 (2009) 625–627. https://doi.org/https://doi.org/10.1002/cssc.200900099.

[212] M.S. Holm, S. Saravanamurugan, E. Taarning, Conversion of Sugars to Lactic Acid Derivatives Using Heterogeneous Zeotype Catalysts, Science (80-.). 328 (2010) 602–605. https://doi.org/10.1126/science.1183990.

[213] J. Jae, E. Mahmoud, R.F. Lobo, D.G. Vlachos, Cascade of Liquid-Phase Catalytic Transfer Hydrogenation and Etherification of 5-Hydroxymethylfurfural to Potential Biodiesel Components over Lewis Acid Zeolites, ChemCatChem. 6 (2014) 508–513. https://doi.org/https://doi.org/10.1002/cctc.201300978.

[214] J. Dijkmans, M. Dusselier, D. Gabriëls, K. Houthoofd, P.C.M.M. Magusin, S. Huang, Y. Pontikes, M. Trekels, A. Vantomme, L. Giebeler, S. Oswald, B.F. Sels, Cooperative Catalysis for Multistep Biomass Conversion with Sn/Al Beta Zeolite, ACS Catal. 5 (2015) 928–940. https://doi.org/10.1021/cs501388e.

[215] V. Choudhary, A.B. Pinar, S.I. Sandler, D.G. Vlachos, R.F. Lobo, Xylose Isomerization to Xylulose and its Dehydration to Furfural in Aqueous Media, ACS Catal. 1 (2011) 1724–1728. https://doi.org/10.1021/cs200461t.

[216] R. Otomo, T. Yokoi, J.N. Kondo, T. Tatsumi, Dealuminated Beta zeolite as effective bifunctional catalyst for direct transformation of glucose to 5-hydroxymethylfurfural, Appl.

Catal. A Gen. 470 (2014) 318–326. https://doi.org/https://doi.org/10.1016/j.apcata.2013.11.012.

[217] F. Rodríguez-Reinoso, A. Sepúlveda-Escribano, Chapter 9 - Porous Carbons In Adsorption And Catalysis, in: H.S.B.T.-H. of S. and I. of M. Nalwa (Ed.), Academic Press, Burlington, 2001: pp. 309–355. https://doi.org/https://doi.org/10.1016/B978-012513910-6/50066-9.

[218] J.W. Patrick, Porosity in carbons : characterization and applications, Edward Arnold, London, 1995.

[219] T. Kyotani, Chapter 7 - Porous Carbon, in: E. Yasuda, M. Inagaki, K. Kaneko, M. Endo, A. Oya, Y.B.T.-C.A. Tanabe (Eds.), Elsevier Science, Oxford, 2003: pp. 109–127. https://doi.org/https://doi.org/10.1016/B978-008044163-4/50007-3.

[220] P. Carrott, M. Ribeiro Carrott, P. Mourão, R. Lima, Preparation of Activated Carbons from Cork by Physical Activation in Carbon Dioxide, Adsorpt. Sci. Technol. - Adsorpt Sci Technol. 21 (2003) 669–681. https://doi.org/10.1260/026361703772776457.

[221] I. Matos, M. Bernardo, I. Fonseca, Porous carbon: A versatile material for catalysis, Catal. Today. 285 (2017) 194–203. https://doi.org/https://doi.org/10.1016/j.cattod.2017.01.039.

[222] J.M. Rosas, R. Ruiz-Rosas, J. Rodríguez-Mirasol, T. Cordero, Kinetic study of the oxidation resistance of phosphorus-containing activated carbons, Carbon N. Y. 50 (2012) 1523–1537. https://doi.org/10.1016/j.carbon.2011.11.030.

[223] S. Adapa, V. Gaur, N. Verma, Catalytic oxidation of NO by activated carbon fiber (ACF), Chem. Eng. J. 116 (2006) 25–37. https://doi.org/https://doi.org/10.1016/j.cej.2005.10.007.

[224] F.J. García-Mateos, R. Ruiz-Rosas, J.M. Rosas, J. Rodríguez-Mirasol, T. Cordero, Phosphorus containing carbon (submicron)fibers as efficient acid catalysts, Catal. Today. 383 (2022) 308–319.

https://doi.org/https://doi.org/10.1016/j.cattod.2020.10.025.

[225] B.P.M. Holbrook, R. Rajagopalan, K. Dronvajjala, Y.K. Choudhary, H.C. Foley, Molecular sieving carbon catalysts for liquid phase reactions: Study of alkene hydrogenation using platinum embedded nanoporous carbon, J. Mol. Catal. A Chem. 367 (2013) 61–68. https://doi.org/https://doi.org/10.1016/j.molcata.2012.10.026.

[226] M. Sevilla, A.B. Fuertes, The production of carbon materials by hydrothermal carbonization of cellulose, Carbon N. Y. 47 (2009) 2281–2289. https://doi.org/https://doi.org/10.1016/j.carbon.2009.04.026.

[227] T. Tsoncheva, I. Genova, I. Stoycheva, I. Spassova, R. Ivanova, B. Tsyntsarski, G. Issa, D. Kovacheva, N. Petrov, Activated carbon from waste biomass as catalyst support: formation of active phase in copper and cobalt catalysts for methanol decomposition, J. Porous Mater. 22 (2015). https://doi.org/10.1007/s10934-015-9988-7.

[228] S. Cattaneo, M. Stucchi, G.M. Veith, L. Prati, D. Wang, W. Wang, A. Villa, Ru supported on micro and mesoporous carbons as catalysts for biomass-derived molecules hydrogenation, Catal. Today. 357 (2020) 143–151. https://doi.org/https://doi.org/10.1016/j.cattod.2019.05.009.

Research Aims and Objectives

4. Research Aims and Objectives

4.1. Research Aims

5-hydroxymethylfurfural is a very versatile platform molecule for the synthesis of chemicals and biofuels which can be produced from biomass derived hexoses by heterogeneous acid-catalyzed processes. Research aims of this thesis are the evaluation of different solid acid catalysts (synthesized or commercial) for the production of HMF from glucose and/or fructose dehydration, as well as the establishment of the optimal experimental conditions for each type of heterogeneous catalyst.

4.2. Research Objectives

•Synthesis of mesoporous tantalum oxide as catalyst for the glucose to HMF dehydration reaction and optimization of the reaction conditions.

•Synthesis of mesoporous silica-based catalysts, such as MCM-41 type, for HMF production from glucose, optimizing the reaction conditions.

•Modification of different H-zeolites to be used as catalysts in the production of HMF from glucose, optimizing the reaction conditions in each case.

•Tuning Brönsted-Lewis acidity of zeolites by introducing iron and copper ions into these solids in order to achieve better HMF yields in the glucose dehydration to HMF.

•Study and comparison of the catalytic behavior of different commercial zeolites in the production of HMF from glucose and fructose, optimizing the reaction conditions.

•Research on the catalytic behavior of acid carbons in the glucose/fructose dehydration to HMF.

•Physico-chemical characterization of all the studied catalysts by techniques such as X-ray diffraction (XRD), X-ray photoelectron spectroscopy (XPS), nitrogen sorption at -196ºC, differential thermal analysis and thermogravimetric (DTA, TG), solid-state nuclear magnetic resonance (ss-NMR), among others

•Study of acidity (concentration, strength and type) by temperature-programmed desorption of ammonia (NH_3-TPD) and pyridine adsorption coupled to Fourier-transform infrared (FT-IR) spectroscopy.

•Elucidation of structure-acidity-activity relations in order to optimize catalysts and experimental conditions.

•Evaluation of the catalyst reusability, since this is a key advantage of the heterogeneous catalysts compared to homogeneous ones.

Experimental Procedure

5. Experimental Procedure

5.1. Catalysts

Tantalum oxide and silica-based materials were synthesized to obtain mesoporous acid catalysts. Commercial zeolites (Zeolyst International) were modified to modify their acidic properties. Porous carbons were provided by the group of Prof. Cordero (Department of Chemical Engineering at University of Málaga). Phosphoric acid was used as homogeneous catalyst.

5.1.1. Mesoporous tantalum oxide

Chemicals

- Hydrochloric acid (VWR Chemicals, 37%)
- Tantalum(V) ethoxide (Sigma-Aldrich, 99.98%)
- Ethanol (VWR Chemicals, 96%)
- Poly(ethylene glycol)-block-poly(propylene glycol)-block-poly(ethylene glycol) average MW~4400, Pluronic® L-121 (Sigma-Aldrich)
- Phosphoric acid (Sigma-Aldrich, 85 wt.%)
- Potassium hydroxide (Prolabo, 86.1%)

Synthesis procedure

The synthesis method was based on the work published by Xu *et al.* [1], consisting of the successive addition of 8 mL of 2 M hydrochloric acid and 4.6 mmol of tantalum (V) ethoxide to a Pluronic® L-121

ethanolic solution (1 g in 40 mL) . After stirring for 30 minutes, the obtained sol was 24 hours aged (40º C) and the resulting solid was washed, filtered off and finally dried in vacuum at 60 ºC. The white solid was calcined at 550 ºC for 6 h (heating rate of 1 ºC min^{-1}) to remove the surfactant and create the mesoporous framework. Synthesis steps are shown in Image 1.

Image 1. Mesoporous tantalum oxide synthesis procedure.

A post-synthesis treatment was carried out in order to incorporate phosphoric groups onto the surface of the mesoporous tantalum (V) oxide. Thus, 300 mg of mesoporous tantalum oxide was treated, under vigorous stirring, with 20 mL of 1 M phosphoric acid aqueous solution for 24 hours [2]. Then, the solid was washed with deionized water, dried and calcined at 300 ºC for 2 hours. Another similar post-synthesis treatment was performed, but omitting the calcination step. A third post-synthesis catalyst modification was made by stirring 100 mg of mesoporous tantalum(V) oxide with 25 mL of potassium hydroxide (aqueous solution, 0.35 mmol per g catalyst) for 24 h, and then washing with deionized water and drying the resulting solid.

5.1.2. Al-MCM-41

Two aluminum-doped MCM-41 type silica materials with Si/Al molar ratios of 5 and 10 were synthesized.

Chemicals

- Tetraethyl orthosilicate (Sigma-Aldrich, 98%)
- Aluminum isopropoxide (Sigma-Aldrich, 98%)
- Ethanol (VWR Chemicals, 96%)
- Dodecylamine (Sigma-Aldrich, 98%)
- Nitric acid (VWR Chemicals, 68%)
- Hydrochloric acid (VWR Chemicals, 37%)
- Ammonia (VWR Chemicals, 28%)

Synthesis procedure

The synthesis method, based on the paper published by Aguado *et al.* [2], consisted of a sol-gel method that involves two consecutive steps: an acidic and an alkaline hydrolysis. The silicon and aluminum sources were a solution of tetraethyl orthosilicate (TEOS, 20.88 mL) and aluminum isopropoxide respectively. This solution was mild stirred and a dodecylamine in a hydrochloric-alcoholic solution was added dropwise. This latter solution was prepared by dissolving 5 g of dodecylamine in 20 mL of ethanol, adding HCl up to pH 2 and shaking for 10 minutes. The acidic hydrolysis was carried out by stirring for 90 minutes and, then, the alkaline hydrolysis was accomplished by adjusting the pH to 10 through addition of an ammonia solution. This alkaline step favors the condensation of silicate groups. The resulting gel was aged at room temperature for 20

hours under static conditions and filtered, and the resulting solid was then washed with deionized water and dried overnight at 100 ºC. Then, the structure-directing agent was extracted with nitric acid 0.1 M ethanolic solution for 4 h , and subsequent calcination at 550 ºC for 3 h (heating rate of 1 ºC min^{-1}).

5.1.3. Al-KIT-6

Chemicals

- Poly(ethylene glycol)-block-poly(propylene glycol)-block-poly(ethylene glycol) average Mn~5800, PEG-PPG-PEG, Pluronic® P-123 (Sigma-Aldrich)
- Hydrochloric acid (VWR Chemicals, 37%)
- 2-Propanol (VWR Chemicals)
- 1-Butanol (Sigma-Aldrich, 99.8%)
- Tetraethyl orthosilicate, TEOS (Sigma-Aldrich, 98%)
- Ethanol absolute (VWR Chemicals)
- Aluminum chloride hexahydrate (Sigma-Aldrich, 99%)
- Tetramethylammonium hydroxide (Sigma-Aldrich, 25wt.% solution in water)

Synthesis procedure

Three similar methods were followed for the synthesis of KIT-6-type mesoporous silicas (KIT6-A, KIT6-B and KIT6-C), based on the works published by Aranda *et al.* [3] and Jo *et al.* [4].

KIT6-A and KIT6-B mesoporous silica materials were synthesized by adding Pluronic® P-123, as template (9.7 g), to an acidic solution prepared from deionized water (850 mL) and hydrochloric acid 35 % (31 mL). The mixture was stirred at 35 ºC for 4.5 h, until complete dissolution of the surfactant. Then, n-butanol (24 mL) was added, and the resulting solution was stirred for another 1 h at the same temperature. After stirring, it was divided into two equal portions, and 27.8 mL of TEOS were added to each, being one part stirred at 35 ºC for 24 hours (A) and for 72 hours the other one (B). Both mixtures were subjected to hydrothermal treatment at 120 ºC for 24 hours, filtrated, washed with deionized water and dried at 120 ºC. Thereafter, the obtained products were calcined at 550 ºC in air for 6 hours (heating rate 2 ºC min^{-1}) to obtain KIT6-A and KIT6-B silica materials.

The KIT-C synthesis was carried out starting from the same products and conditions, but adding isopropanol (25 mL) instead of n-butanol and stirring at 35 ºC for 36 hours. The rest of the experimental conditions were the same as for the other catalysts.

KIT6-C post-synthesis alumination

The synthesized KIT6-C silica was modified by two different post-synthesis treatments to incorporate aluminum in order to enhance the acidity and consequently the catalytic activity. In this sense, following the procedure reported by Luan *et al.* [5], 2 g of KIT6-C silica were added under stirring to 200 mL of a dry ethanol solution containing aluminum chloride (Si/Al molar ratio of 10), at room temperature for 12 hours. After filtration and washed with dry ethanol, the solid was

dried at room temperature and, finally, calcined at 550 ºC for 6 hours (heating rate 10 ºC min^{-1}). The obtained catalyst was labeled as Al-KIT6-C1. The latter procedure, based on the one reported by Gómez-Cazalilla *et al.* [6], combined the KIT6-C silica (2 g) with a solution of aluminum chloride (Si/Al molar ratio of 10) into tetramethylammonium hydroxide (20 mL), maintaining a molar ratio [TMAOH]/[Al] molar ratio of 2.5. This ratio was chosen based on a previous study, where it was found that the amount of incorporated Al was higher at this value [7]. The acidic solution and the mixture were prepared at 80 ºC under stirring, taking 30 minutes and 3 hours, respectively. After filtration and washing with deionized water, the solid was dried overnight at 60 ºC and calcined (550 ºC, 6 hours, 10 ºC min^{-1}). The obtained catalyst was named as Al-KIT6-C2.

The labels of all these synthesized catalysts are listed in Table 1.

Table 1. Synthesized materials

	catalyst
Mesoporous tantalum oxide	Ta_2O_5
Aluminum doped MCM-41 silicas	10Al-MCM-41
	5Al-MCM-41
Mesoporous KIT-6 silicas	KIT6-A
	KIT6-B
	KIT6-C
Aluminum doped KIT-6 silicas	Al-KIT6-C1
	Al-KIT6-C2

5.1.4. Protonated zeolites

- CBV3024E ZSM-5 type zeolite (Zeolyst International). SiO_2/Al_2O_3 molar ratio: 30. Nominal cation form: ammonium.
- CBV712 Y type zeolite (Zeolyst International). SiO_2/Al_2O_3 molar ratio: 12. Nominal cation form: ammonium.
- CBV720 Y type zeolite (Zeolyst International). SiO_2/Al_2O_3 molar ratio: 30. Nominal cation form: hydrogen.
- CP814E Beta type zeolite (Zeolyst International). SiO_2/Al_2O_3 molar ratio: 25. Nominal cation form: ammonium.
- CP814C Beta type zeolite (Zeolyst International). SiO_2/Al_2O_3 molar ratio: 38. Nominal cation form: ammonium.
- CBV21A Mordenite type zeolite (Zeolyst International). SiO_2/Al_2O_3 mole ratio: 20. Nominal cation form: ammonium.

CBV3024E (ZSM-5), CBV712 (Y), CP814E (Beta), CP814C (Beta), and CBV21A (Mordenite) zeolites, with ammonium as nominal cation form, were calcined in air at 550ºC for 6 hours (1 ºC min^{-1}) to obtain the corresponding protonated forms (H-Z). CBV720 Y, commercial as hydrogen form, was used as supplied. These H-zeolites were labeled according to the nomenclature shown in Table 2.

Table 2. Commercial materials

	treatment	**Si/Al ratio**	**catalyst**
CBV3024E (NH_4-ZSM-5)	calcination	15	H-ZSM5-15
CBV712 (NH_4-Y)	calcination	6	H-Y-6
CBV720 (H-Y)	-	15	H-Y-15
CP814E (NH_4-Beta)	calcination	12.5	H-Beta-12.5
CP814C (NH_4-Beta)	calcination	19	H-Beta-19
CBV21A (NH_4-Mordenite)	calcination	10	H-MOR-10

5.1.5. Iron-containing zeolites

Commercial zeolites were modified by incorporating Fe^{2+} ions by an ion exchange process, using iron(II) sulphate heptahydrate (Sigma-Aldrich, 98%).

CBV3024E (NH_4-ZSM-5) zeolite (2 g) was treated with a 0.1 M $FeSO_4$ aqueous solution (60 mL) under a nitrogen atmosphere [8]. After stirring for 24 hours, the resulting zeolite was filtered and washed with deionized water, dried at 60 ºC overnight and, finally, calcined at 550 ºC for 5 hours (10 ºC min^{-1}). The exchange process, with a duration of 24 h each, was repeated two and three times, following the same post-treatment. The CHNS/O analysis revealed 27, 84 and 88% of ammonium groups removed after the first, second and third exchange process, respectively. Thus, three subsequent exchange steps with fresh iron(II) sulfate aqueous solutions, under the same experimental conditions, were used for facilitating the NH_4^+-Fe^{2+} exchange in CBV3024E (NH_4-ZSM-5), CBV712 (NH_4-Y), CP814E (NH_4-Beta) and CBV21A (NH_4-Mordenite) zeolites, and also H^+_{aq}-Fe^{2+} exchange

with the CBV720 (H-Y) zeolite. The adopted nomenclature is indicated in Table 3.

Table 3. Iron-containing zeolites.

Commercial (precursors)	Si/Al molar	Catalyst
CBV3024E (NH_4-ZSM-5)	15	Fe-ZSM5-15
CBV712 (NH_4-Y)	6	Fe-Y-6
CBV720 (H-Y)	15	Fe-Y-15
CP814E (NH_4-Beta)	12.5	Fe-Beta-12.5
CBV21A (NH_4-Mordenite)	10	Fe-MOR-10

5.1.6. Copper-containing zeolites

Commercial zeolites were also modified by incorporation of Cu^{2+} ions, using copper(II) acetate monohydrate (Merk Millipore).

2 g of CBV3024E (NH_4-ZSM-5) zeolite were put in contact with 20 mL of a $Cu(CH_3COO)_2$ 0.005 M aqueous solution [9]. The exchange process was similar to that applied to synthesize the iron-containing zeolites, and it was repeated twice. The CHNS/O analysis revealed 60 and 66% of ammonium groups removed after the first and second treatment, respectively, and the treated zeolites were CBV3024E (NH_4-ZSM-5), CBV712 (NH_4-Y) and CP814E (NH_4-Beta), whose final nomenclature was as referenced in Table 4.

Table 4. Copper-containing zeolites.

Commercial (precursors)	Si/Al ratio	Catalyst
CBV3024E (NH_4-ZSM-5)	15	Cu-ZSM5-15
CBV712 (NH_4-Y)	6	Cu-Y-6
CP814E (NH_4-Beta)	12.5	Cu-Beta-12.5

5.1.7. Porous carbons

Two groups of acidic porous carbons. synthesized by the group headed by Prof. Cordero [10], were provided to be tested for the glucose dehydration to HMF. The first group, HA- carbons, were prepared from olive stones from local olive manufacturers, whereas the second group, L- carbons, from commercial lignin (ALCELL®). All of them were activated through a chemical treatment with phosphoric acid to obtain acidic catalysts [11,12], being labeled as shown in Table 5.

Table 5. Carbon-based catalysts.

Catalysts	
HA3500	Olive stones derived
HA31500	
HA31800	
L3500	Alcell lignin derived
L31500	
L31800	

5.1.8. Homogeneous catalysts

The dehydration of glucose under homogeneous catalysis was also studied by using phosphoric acid aqueous solutions (0.14 and 0.25 M), prepared from commercial phosphoric acid (Sigma-Aldrich, 85 wt.%). These homogeneous catalysts were labeled accordingly in Table 6.

Table 6. Homogenous catalysts

	Catalyst
H_3PO_4-0.14M	PA-0.14
H_3PO_4-0.25M	PA-0.25

5.2. Chemical reagents and solvents

In the different catalytic reactions, the following chemicals were used:

- D-(+) Glucose (Sigma-Aldrich, 99%)
- D-(-) Fructose (Sigma-Aldrich, 99%)
- Methyl isobutyl ketone (Sigma-Aldrich, 98.5%)
- Cyclopentyl methyl ether (Sigma-Aldrich)
- Tetrahydrofuran (99.9%, Sigma-Aldrich)
- Silicon oils for heating baths LBSil 100 Aux (Labkem)
- Lithium chloride (Sigma-Aldrich, 99.99%)
- Sodium chloride (VWR Chemicals)
- Potassium chloride (WVR Chemicals)
- Calcium chloride dihydrate (Sigma-Aldrich)
- Sodium bromide (Sigma-Aldrich, 99%)
- Sodium sulfate (Sigma-Aldrich, 99.99%)

Reaction products were analyzed by High Performance Liquid Chromatography (HPLC) , and the following chemicals were needed:

- Methanol for UV, IR, HPLC, ACS (Panreac)
- 2-Propanol for HPLC (WVR Chemicals)
- D-(+) Glucose (Sigma-Aldrich, 99%)
- D-(-) Fructose (Sigma-Aldrich, 99%)
- 5-(hydroxymethyl)furfural (Sigma-Aldrich, 99%)
- Levulinic acid (Sigma-Aldrich, 98%)
- Formic acid (Sigma-Aldrich)

Deionized water was used throughout all the experimental procedures.

5.3. Catalyst characterization techniques

Different techniques were used for the physico-chemical characterization of fresh and spent catalysts.

5.3.1. X-ray diffraction analysis

X-ray diffraction (XRD) is a useful technique for the study of polycrystalline and amorphous materials, allowing the identification of the nature and composition of crystalline phases, the determination of unit cell lattice parameters and average crystallite sizes, among others. In this sense, it is also employed for the analysis of ordered nanostructured solids.

This technique is based on the phenomenon that occurs when a monochromatic X-ray beam (with a characteristic wavelength, λ) is incident on the lattice planes in a crystal (distanced d) at an angle θ. The diffraction appears only when the distance travelled by the rays reflected from successive planes differs by a complete number n of wavelengths ($n\lambda$), Figure 1. This condition was established by Bragg in 1912 as:

$$n\lambda = 2d \sin\theta$$

Plotting the angular positions and intensities of the resultant diffraction peaks, a characteristic pattern of the sample is produced. If a mixture of crystalline phases is present, the resulting diffractogram is formed by addition of the individual patterns [13].

Powder XRD patterns of the catalysts were recorded on an EMPYREAN PANanalytical diffractometer, using strictly

monochromatic $CuK_{\alpha 1,2}$ radiation (λ= 1.54059 Å, Ge (1 1 1)) primary monochromator and working in reflection geometry ($\theta/2\theta$). The X-ray tube worked at 45 kV and 40 mA. The optical configuration consisted on a fixed divergence slit (1/2°), a fixed incident antiscatter slit (1°), a fixed diffracted anti-scatter slit (1/2°) and a PIXCEL detector, working in scanning mode with maximum active length. Data were collected from 2 to 80° for 30 minutes.

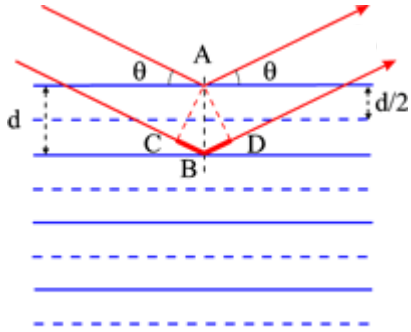

Figure 1. Bragg's law. Adaption from the Online Dictionary of Crystallography [42].

5.3.2. X-ray photoelectron spectroscopy

X-ray photoelectron spectroscopy (XPS) is a powerful technique to analyze the surface chemistry of materials, providing data on the elemental composition, the chemical and electronic states of elements present of the outer layer of a material. By irradiating the surface with a X-ray beam, spectra are obtained, appearing electrons emission peaks at energy values characteristic of each element and state. While

the material is being irradiated, the kinetic energies and the amount of emitted electrons are measured [14]. The energy values and the intensities of the peaks enable the identification and quantification of elements in the surface. Taking into account the importance of the physical and chemical interactions at the catalyst surfaces, XPS can be considered as a fundamental technique in the present PhD work.

XPS analyses were collected using a Physical Electronics PHI 5700 spectrometer with a non-monochromatic Mg K_α radiation (300 W, 15 kV, 1253.6 eV) for the analysis of the core level signals. Charge referencing was measured against adventitious carbon (C 1*s*, 284.8 eV). A PHI ACCESS ESCA-V6.0 F software package was used for acquisition and data analysis. A Shirley-type background was subtracted from the signals. The modified Auger parameter of Al (α') was calculated using the equation:

$$\alpha' = 1253.6 + KE(Al_{KLL}) + KE(Al_{2p})$$

where KE corresponds to the kinetic energy of the Auger electron (KLL) or the photoelectron (2*p*).

5.3.3. Differential thermal analysis and thermogravimetry

The most used thermal techniques to characterize catalysts are Differential Thermal Analysis (DTA), Thermogravimetry (TG), Differential Thermogravimetry (DTG) and Differential Scanning Calorimetry (DSC), used either by themselves, or combined with other

techniques, such as TG-DSC. These techniques study the thermal behavior of a material when it is heated at a constant rate, or by steps of temperature, and are particularly adapted for studying the decomposition of catalyst precursors or for desorption studies of poisoned catalysts. The measured properties are mass, temperature and enthalpy in TG, DTA and DSC analysis, respectively [15,16]. A sample mass loss (TG) can be associated to decomposition, oxidation, vaporization, sublimation or desorption. The different temperatures between the sample and the reference in DTA analysis indicate chemical reactions, desorption or phase transitions. Enthalpy values provided by DSC analysis can be useful for characterizing the oxidation, decomposition or phase transition occurred in the material.

The TGA-DSC curves were registered with a thermobalance (Mettler Toledo, TGA-DSC1) in synthetic air (50 mL min^{-1}) with a heating rate of 10 ºC min^{-1}, in the 30-900 ºC temperature range. The analyzer was connected to a mass spectrometer (Pfeiffer Vacuum, ThermoStar GSD 320) to determine the gas composition, and gas evolution profiles as a function of temperature.

5.3.4. Nitrogen sorption analysis

The determination of textual parameters is a key step in the physico-chemical characterization of catalysts, and, in this context, the distinction between the external and the internal surface can be relevant. The external surface includes prominences, pores, cracks and cavities which are wider than deep, whereas the internal surface comprises the walls of the rest of pores, cavities and cracks. The total

surface area is the sum of the external and internal surface areas. This porous framework can be of many different kinds. The pore width is of special interest for the catalytic phenomenon, and solids are classified according to them in microporous (pores up to 2 nm), mesoporous (between 2 and 50 nm) and macroporous (wider than 50 nm). The total pore volume (specific) is the total internal volume per unit mass of the catalyst, but it can be enclosed and inaccessible to molecules in a catalytic process. The pore size distribution is the distribution of pore volume with respect to pore size, and it is an important factor controlling the diffusion of reactants and products in the porous catalysts. Gas adsorption methods are used to determine the surface area and pore size distribution, being the Brunauer-Emmett-Teller (BET) method the most widely used procedure for the determination of specific surface area [17]. There are also empirical equations to adjust the adsorption data, such as the Freundlich model and the Sips isotherm. About the micropore filling, Dubinin theory and its modifications were used [17–21].

The textural parameters were obtained from the nitrogen adsorption-desorption isotherms at -196 °C, as determined by an automatic ASAP 2020 V3.04H system from Micromeritics. Prior to nitrogen adsorption, these samples were evacuated overnight at 0.13 Pa and 350 °C.

5.3.5. Temperature-programmed desorption of ammonia

Physisorption appears when the adsorption (attractive interaction) is essentially due to van-der-Waals forces, and the physisorptive bonds

are characterized by dissociation energies below 50 kJ mol^{-1}. Nevertheless, when the overlap between the molecular orbitals of the adsorbed molecule and the surface atoms enables the formation of chemical bonds, which dissociation energies exceeding 50 kJ mol^{-1}, chemisorption takes place. This is often an activated process, requiring that an activation barrier is overcome. In the TPD analysis, the probe molecule (ammonia) is adsorbed on the material surface. The physisorbed amount is removed by a helium flow at low temperature (usually 100 ºC), remaining the chemisorbed ammonia. This is removed by heating the sample, and the analysis of desorbed ammonia by GC-TCD allows the determination of the ammonia chemisorbed and, therefore, the sample acidity.

Catalysts were heated from room temperature to 550 ºC (but up to 100 ºC in the case of carbon-based catalysts), with a heating rate of 10 ºC min^{-1}, under a helium flow (35 mL min^{-1}), and this temperature was maintained for 15 min. After cooling samples until 100 ºC under a helium flow, ammonia adsorption was undertaken. Finally, ammonia was desorbed from 100 to 550 °C and analyzed by an on-line gas chromatograph provided with a thermal conductivity detector (Shimadzu GC-14A).

5.3.6. Pyridine adsorption coupled to FT-Infrared spectroscopy

Different infrared (IR) spectroscopies (diffuse reflectance, emission, transmission-absorption, etc.) can be applied to study functional groups of materials. The transmission-absorption mode, with a variety

of cells, is very useful. Infrared spectra are produced through the absorption of infrared radiation by a molecule, caused by transitions between vibrational energy levels. A net change in the dipole moment of the molecule is needed to absorb the infrared radiation, and so, molecular asymmetry is required. The most useful IR radiation frequencies are between 4000 and 400 cm^{-1} (wavenumber values).

IR spectroscopy of adsorbed probe molecules is suitable for the study of the acid-base nature of catalysts. The determination of the acid properties requires probe molecule with basic properties, such as ammonia and most amines, including pyridine. Particularly, the nitrogen center of pyridine features a basic lone pair of electrons which interacts with Lewis acids, such as aluminosilicates or transition metal oxides. Besides, because this lone pair of electrons is not part of the aromatic ring, it can be protonated by reaction with protonic acids, forming the pyridinium ion. Typical IR absorption bands of pyridine adsorbed on Brönsted type acid sites are found around 1491, 1545, 1578, and 1640 cm^{-1}, whereas Lewis acidity gives rise to pyridine bands around 1450, 1491, 1578, and 1612 cm^{-1}. The most characteristic bands appear at 1545 (Brönsted acid sites) and 1450 (Lewis acid sites) cm^{-1}. Moreover, the exact positions of the bands located at 1450 and 1612 cm^{-1} (L-Py bands) are sensitive to the strength of the Lewis acid sites [22–24]. From the integral intensities of these bands, the concentration of both types of surface acid sites can be determined by using the Lambert-Beer law and the molar extinction coefficients (or molar absorptivities) for pyridine adsorbed on Brönsted and Lewis acid sites [25]:

$$A = C\varepsilon$$

where A is the integrated absorbance (cm^{-1}), C is the concentration of absorbate ($\mu mol\ cm^{-2}$). The molar extinction coefficient ε has been calculated in different works, depending the obtained values on the experimental conditions. Values of 0.73 and 1.11 ($cm\ \mu mol^{-1}$) for the bands at 1545 cm^{-1} (PyH^+) and 1455 cm^{-1} (PyL) have been reported by Datka *et al.* [26]. Other values have been reported later and used as well [27,28].

FTIR spectra of adsorbed pyridine were recorded on a Shimadzu Fourier Transform Infrared Instrument (FTIR-8300). Self-supported wafers of the samples (with weight/surface ratio in the range 10-20 $mg\ cm^{-2}$) were placed in a vacuum cell with greaseless stopcocks and CaF_2 windows. Samples were previously evacuated at 250 ºC and 10^{-2} Pa overnight, and then exposed to pyridine vapors at room temperature for 15 min. Thereafter, they were outgassed at different temperatures (100-300 °C). The IR spectra of the evacuated, exposed to pyridine and outgassed samples, were registered and the Hyper IR software package (LabControl®) was used for acquisition and data analysis.

5.3.7. Solid-state nuclear magnetic resonance (MAS-NMR)

High resolution NMR spectra of solids are useful to characterize the structural and chemical environment of their lattice atoms. This is because the transition frequency measured in the NMR spectrum of an atomic nucleus in a particular chemical or structural environment is a very sensitive probe of that environment. The Magic Angle Spinning

(MAS) rotation application to this technique has meant its applicability to micro and mesoporous materials. In MAS-NMR, by spinning the sample at a very high speed and at the magic angle (54.7º with respect to the direction of the magnetic field), dipolar, chemical shift anisotropy and quadrupolar interactions, can be averaged, leading to much narrower signals [29][30].

In the framework of zeolites or other aluminosilicates, silicon, aluminum and oxygen are the main atomic constituents. ^{17}O isotope is lacking in natural abundance (0.037%) and it also has a nuclear quadrupole moment which produces the line broadening, making its application difficult. The ^{27}Al isotope is 100% abundant, but its nuclear quadrupole moment may give rise to broadened lines. In contrast, the ^{29}Si isotope has no quadrupole moment, leading to narrow resonance lines, and its natural abundance is 4.7%. Other elements which can replace silicon or aluminum in the tetrahedral sites of the aluminosilicate framework, such as ^{51}V or ^{31}P, can also be studied by MAS-NMR [31,32]. Moreover, most of cations acting as charge balancing species possess isotopes suitable for NMR studies, e.g. ^{23}Na [33–35].

The chemical shift of ^{29}Si in silicates or aluminosilicates depends on the number and type of T-atoms (tetrahedral framework atoms) connected with a SiO_4 tetrahedron. Increasing the degree of SiO_4 polymerization, high-field shifts are observed, whilst the degree of tetrahedral Al substitution leads to low-field shifts of resonances. In the particular case of zeolites and other aluminosilicates, the silicon atoms are connected with other T atoms through oxygen bridges,

within a 3D framework, and five types of structural units types can be present as:

$$Si(OSi)_{4-n}(OAl)_n, \qquad n=0, 1, 2, 3, 4$$

and thus, the ^{29}Si NMR spectrum may content from one to five peaks, and increasing "n", the peaks shift to lower field, about 5 ppm for each Al substitution () [36].

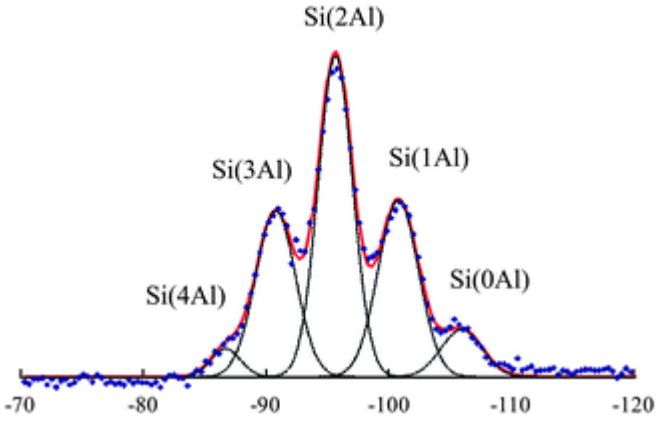

Figure 2. High-resolution ^{29}Si MAS-NMR spectrum for a Na-Y zeolite collected at 39.75 MHz. Experimental spectrum – blue symbols, red line corresponds to computer simulated spectrum, fitted with pseudo-Voigt peak profiles, deconvoluted peaks, to black dotted lines [41].

High sensitivity of ^{27}Al MAS-NMR allows the identification of different aluminum species. Tetrahedrally coordinated Al in zeolites and other aluminosilicates appears at about 60 ppm, whereas the octahedrally coordinated one does at about 0 ppm. Non-framework Al species can be identified by MAS-NMR, since they produce a broad

^{27}Al band between the tetrahedral and the octahedral Al signals (shown in Figure 3, [37,38]).

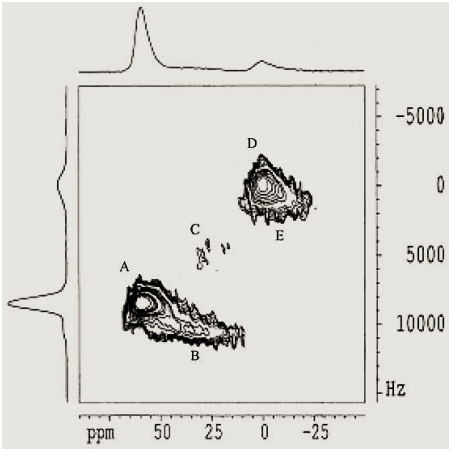

Figure 3. ^{27}Al 3Q MAS-NMR spectrum of an USY zeolite. Tetrahedral framework (A), tetrahedral distorted framework (B), penta-coordinated (non framework) (C), octahedral framework (D) and distorted.-tetrahedral (B), octahedral framework (D) and octahedral non framework (E) aluminums, from Yan et al. [38].

These extra-framework Al species usually present disadvantages for the catalysis and the transport phenomenon ought to they may compensate the framework charge, decreasing the Brönsted acid sites concentration, or they can difficult the access to the acid sites by blocking the pores [39,40].

Not only are them the main components of zeolites and other aluminosilicates or have them an important role as framework constituents, also because of their favorable properties in MAS-NMR experiments, and especially due to the high sensitivity of their spectra against structural effects, ^{29}Si and ^{27}Al nuclei have an important role in MAS-NMR studies.

^{27}Al solid-state NMR spectra were recorded under magic angle spinning at ambient temperature on a Bruker AV 400 WB spectrometer equipped with a 4 mm MAS probe.

5.3.8. Elemental analysis (CHNS/O)

Quantitative elemental analysis of materials allows the determination of carbon, hydrogen, nitrogen, sulfur and oxygen contents. The most common form of elemental analysis is accomplished by combustion, burning the sample in an excess of oxygen and collecting the combustion products: carbon dioxide, water, nitrogen and sulfur dioxide. The masses of these combustion products can be used to calculate the composition of the unknown sample.

The CHNS/O analyzes were carried out in a Leco TruSpec® Micro analyzer, under optimal conditions (950 – 1300 ºC, pure oxygen).

5.4. Reaction system and procedures

All the catalytic experiments were performed in 15 mL thick-walled glass reactors (Sigma-Aldrich) provided with screw tops of poly of polytetrafluoroethylene (PTFE), heated in temperature-controlled oil baths placed on top of magnetic stirrer hot plates (IKA). The reaction temperatures of the experiments were set in the temperature range 155-195 ºC. In a typical experiment, 1.5 mL of an aqueous solution composed of hexose (10 wt.%) and 50 mg of catalyst was combined with 3.5 mL of the extracting organic solvent . When inorganic salts were added, the aqueous-phase was saturated with the corresponding salt. The reactor was placed in the oil bath, stirred at 600 rpm and removed after time reaction had expired. The reaction was stopped by cooling the reactor in an ice bath. Reaction procedure is displayed in **Image 2. .**

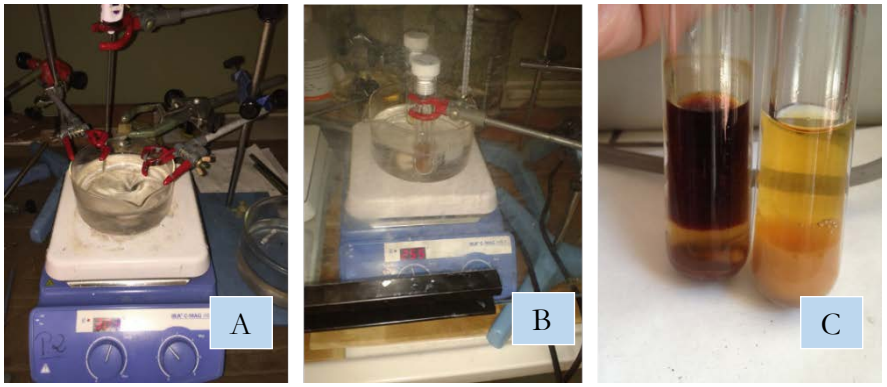

Image 2. Reaction procedure: magnetic stirrer hot place (A), oil bath (B) and glass reactors containing the extracting organic solvent, the aqueous phase, the reactant and the catalyst (C).

After reaction, both reaction phases were handled separately before their analysis. 116 μL of aqueous layer were diluted to 2 mL with deionized water, whereas 83.6 μL of the organic phase were to 10 mL with methanol. Both were filtered through 0.45 μm syringe filters (VWR), degassed with nitrogen and bottled in glass autosampler vials (VWR), prior to the chromatographic analysis. The procedure for the sample analysis is displayed in Image 3.

Image 3. Sample analysis procedure.

5.5. Reaction products analysis

Sample analyses were performed by means of high performance liquid chromatography (HPLC) using a JASCO system equipped with a quaternary gradient pump (PU-2089), an autosampler (AS-2055), a column oven (CO-2065), a reversed-phase column (PHENOMENEX LUNA C18) and a monosaccharide column (PHENOMENEX REZEX RHM-Monosaccharide H+ 8% C18), coupled to a multiwavelength (MD-2015-Plus) and a refractive index (RI-2031-Plus) detectors. HPLC equipment is shown in Image 4.

Image 4. HPLC equipment.

Sugars and their derived products (mainly, HMF) in the aqueous phase were monitored using the monosaccharide column at 80 ºC with deionized and filtered water, as the mobile phase, at a flow rate of 0.6 mL min^{-1} for 35 minutes. Sugar concentrations were measured with the refractive index detector and the HMF in this aqueous phase was measured with the multiwavelength detector at 278 nm, with an injection volume of 6 µL. The HMF content in the organic phase was

monitored with the multiwavelength detector at 290 nm, with the reversed-phase column. Methanol was the mobile phase at a flow rate of 0.5 mL min^{-1} for 11 minutes, also with an injection volume of 6 μL.

Reactant (R) conversion, selectivity, and yield of products (P) were defined as follows:

$$Conversion\ (\%) = X(\%) = \frac{moles\ of\ R\ reacted}{moles\ of\ R\ initial} \times 100$$

$$Selectivity\ (\%) = S(\%) = \frac{moles\ of\ P\ produced}{moles\ of\ R\ reacted} \times 100$$

$$Yield\ (\%) = Y(\%) = \frac{moles\ of\ P\ produced}{moles\ of\ R\ initial} \times 100$$

5.6. List of Figures

5.7. List of Tables

5.8. References

[1] L. Xu, J. Guan, W. Shi, L. Liu, Heterostructured mesoporous In2O3/Ta2O5 composite photocatalysts for hydrogen evolution: Impacts of In2O3 content and calcination temperature, J. Colloid Interface Sci. 377 (2012) 160–168. https://doi.org/http://dx.doi.org/10.1016/j.jcis.2012.04.010.

[2] J. Aguado, D.P. Serrano, J.M. Escola, A sol–gel approach for the room temperature synthesis of Al-containing micelle-templated silica, Microporous Mesoporous Mater. 34 (2000) 43–54. https://doi.org/10.1016/S1387-1811(99)00154-7.

[3] A. Aranda, B. Puértolas, B. Solsona, S. Agouram, R. Murillo, A.M. Mastral, S.H. Taylor, T. Garcia, Total Oxidation of Naphthalene Using Mesoporous CeO2 Catalysts Synthesized by Nanocasting from Two Dimensional SBA-15 and Three Dimensional KIT-6 and MCM-48 Silica Templates, Catal. Letters. 134 (2010) 110–117. https://doi.org/10.1007/s10562-009-0203-9.

[4] C. Jo, K. Kim, R. Ryoo, Syntheses of high quality KIT-6 and SBA-15 mesoporous silicas using low-cost water glass, through rapid quenching of silicate structure in acidic solution, Microporous Mesoporous Mater. 124 (2009) 45–51. https://doi.org/10.1016/j.micromeso.2009.04.037.

[5] Z. Luan, Alumination and ion exchange of mesoporous SBA-15 molecular sieves, Chem. Mater. 11 (1999).

[6] M. Gómez-Cazalilla, J.M. Mérida-Robles, A. Gurbani, E. Rodríguez-Castellón, A. Jiménez-López, Characterization and acidic properties of Al-SBA-15 materials prepared by post-synthesis alumination of a low-cost ordered mesoporous silica, J. Solid State Chem. 180 (2007) 1130–1140. https://doi.org/http://dx.doi.org/10.1016/j.jssc.2006.12.038.

[7] S. Zeng, J. Blanchard, M. Breysse, Y. Shi, X. Shu, H. Nie, D. Li, Post-synthesis alumination of SBA-15 in aqueous solution: A versatile tool for the preparation of acidic Al-SBA-15 supports, Microporous Mesoporous Mater. 85 (2005) 297–304.

https://doi.org/10.1016/j.micromeso.2005.06.031.

[8] L. WG, Y. Zhou, G. FN, Z. SL, Z. JH, Catalytic degradation of tobacco-specific nitrosamines by ferric zeolite, Appl. Catal. B Environ. 129 (2013) 301–308. https://doi.org/10.1016/j.apcatb.2012.09.039.

[9] P.N.R. Vennestrøm, T.V.W. Janssens, A. Kustov, M. Grill, A. Puig-Molina, L.F. Lundegaard, R.R. Tiruvalam, P. Concepción, A. Corma, Influence of lattice stability on hydrothermal deactivation of Cu-ZSM-5 and Cu-IM-5 zeolites for selective catalytic reduction of NOx by NH3, J. Catal. 309 (2014) 477–490. https://doi.org/10.1016/j.jcat.2013.10.017.

[10] Universidad de Málaga, Grupo Terma, (2017). http://www.grupoterma.uma.es/index.php/es/personal/tomas-cordero-alcantara/

[11] J. Bedia, J.M. Rosas, J. Márquez, J. Rodríguez-Mirasol, T. Cordero, Preparation and characterization of carbon based acid catalysts for the dehydration of 2-propanol, Carbon N. Y. 47 (2009) 286–294. https://doi.org/10.1016/j.carbon.2008.10.008.

[12] J.M. Rosas, R. Ruiz-Rosas, J. Rodríguez-Mirasol, T. Cordero, Kinetic study of the oxidation resistance of phosphorus-containing activated carbons, Carbon N. Y. 50 (2012) 1523–1537. https://doi.org/10.1016/j.carbon.2011.11.030.

[13] H.P. Klug, L.E. Alexander, X-Ray Diffraction Procedures: For Polycrystalline and Amorphous Materials, 1956. https://doi.org/10.1016/0001-6160(56)90124-9.

[14] J.F. Watts, J. Wolstenholme, An Introduction to Surface Analysis by XPS and AES, John Wiley & Sons, Ltd, 2003.

[15] F.J. González Benito, Caracterización de Materiales y defectos. Técnicas de Análisis Térmico, n.d. http://ocw.uc3m.es/ciencia-e-oin/caracterizacion-de-materiales/material-de-clase-1/Analisis_termico.pdf.

[16] P.K. Gallacher, Handbook of thermal analysis and calorimetry, 1998. https://doi.org/10.1017/CBO9781107415324.004.

[17] S. Brunauer, P.H. Emmett, E. Teller, Adsorption of gases in multimolecular layers, J. Am. Chem. Soc. 60 (1938) 309–319. http://www.scopus.com/inward/record.url?eid=2-s2.0-12444272525&partnerID=40&md5=cedc5a23cb60bbe15ae74ceb04bc4ccf.

[18] H.M.F. Freundlich, Über die adsorption in losüngen, Z. Phys. Chem. 57 (1906) 385–470.

[19] R. Sips, On the Structure of a Catalyst Surface, J. Chem. Phys. 16 (1948) 490–495. https://doi.org/10.1063/1.1746922.

[20] H.F. Stoeckli, J.P. Houriet, The Dubinin theory of micropore filling and the adsorption of simple molecules by active carbons over a large range of temperature, Carbon N. Y. 14 (1976) 253–256. https://doi.org/10.1016/0008-6223(76)90127-5.

[21] H.. Stoeckli, A generalization of the Dubinin—Radushkevich equation for the filling of heterogeneous micropore systems, J. Colloid Interface Sci. 59 (1977) 184–185. https://doi.org/10.1016/0021-9797(77)90355-1.

[22] J.W. Ward, The nature of active sites on zeolites: I. The decationated Y zeolite, J. Catal. 9 (1967) 225–236. https://doi.org/10.1016/0021-9517(67)90248-5.

[23] S. Rajagopal, J.A. Marzari, R. Miranda, Silica-Alumina-Supported Mo Oxide Catalysts: Genesis and Demise of Brønsted-Lewis Acidity, J. Catal. 151 (1995) 192–203. https://doi.org/10.1006/JCAT.1995.1021.

[24] S. Damyanova, P. Grange, B. Delmon, Surface Characterization of Zirconia-Coated Alumina and Silica Carriers, J. Catal. 168 (1997) 421–430. https://doi.org/10.1006/JCAT.1997.1671.

[25] T.R. Hughes, H.M. White, A study of the surface structure of decationized Y zeolite by quantitative infrared spectroscopy, Phys. Chem. 71 (1967).

[26] J. Datka, A.. Turek, J.M. Jehng, I.. Wachs, Acidic properties of supported niobium oxide catalysts: An infrared spectroscopy investigation, J. Catal. 135 (1992) 186–199. https://doi.org/10.1016/0021-9517(92)90279-Q.

[27] K. Góra-Marek, J. Datka, S. Dzwigaj, M. Che, Influence of V Content on the Nature and Strength of Acidic Sites in VSiβ Zeolite Evidenced by IR Spectroscopy, J. Phys. Chem. B. 110 (2006) 6763–6767. https://doi.org/10.1021/jp0582890.

[28] C.A. Emeis, Determination of Integrated Molar Extinction Coefficients for Infrared Absorption Bands of Pyridine Adsorbed on Solid Acid Catalysts, J. Catal. 141 (1993) 347–354. https://doi.org/10.1006/jcat.1993.1145.

[29] E.R. Andrew, A. Bradbury, R.G. Eades, Nuclear Magnetic Resonance Spectra from a Crystal rotated at High Speed, Nature. 182 (1958) 1659. http://dx.doi.org/10.1038/1821659a0.

[30] I.J. Lowe, Free Induction Decays of Rotating Solids, Phys. Rev. Lett. 2 (1959) 285–287. http://link.aps.org/doi/10.1103/PhysRevLett.2.285.

[31] G. Lischke, R. Eckelt, H.-G. Jerschkewitz, B. Parlitz, E. Schreier, W. Storek, B. Zibrowius, G. Öhlmann, Spectroscopic and physicochemical characterization of P-Modified H-ZSM-5, J. Catal. 132 (1991) 229–243. https://doi.org/10.1016/0021-9517(91)90259-7.

[32] G. Seo, R. Ryoo, 31P, 27Al, and 129Xe NMR study of phosphorus-impregnated HZSM-5 zeolite catalysts, J. Catal. 124 (1990) 224–230. https://doi.org/10.1016/0021-9517(90)90117-3.

[33] M. Feuerstein, M. Hunger, G. Engelhardt, J.P. Amoureux, Characterisation of sodium cations in dehydrated zeolite NaX by 23Na NMR spectroscopy, Solid State Nucl. Magn. Reson. 7 (1996) 95–103. https://doi.org/10.1016/S0926-2040(96)01246-5.

[34] M. Hunger, G. Engelhardt, H. Koller, J. Weitkamp, Characterization of sodium cations in dehydrated faujasites and zeolite EMT by 23Na DOR, 2D nutation, and MAS NMR, Solid State Nucl. Magn. Reson. 2 (1993) 111–120. https://doi.org/10.1016/0926-2040(93)90029-M.

[35] M. Hunger, P. Sarv, A. Samoson, Two-dimensional triple-quantum 23Na MAS NMR spectroscopy of sodium cations in dehydrated zeolites, Solid State Nucl. Magn. Reson. 9 (1997) 115–120. https://doi.org/10.1016/S0926-2040(97)00051-9.

[36] G. Engelhardt, Solid state NMR spectroscopy applied to zeolites, in: H. van Bekkum, E.M. Flanigen, P.A. Jacobs, J.C. Jansen (Eds.), Stud. Surf. Sci. Catal., 2001: pp. 387–418. https://doi.org/10.1016/S0167-2991(01)80251-2.

[37] F.. Chen, J.. Davis, J.. Fripiat, Aluminum coordination and Lewis acidity in transition aluminas, J. Catal. 133 (1992) 263–278. https://doi.org/10.1016/0021-9517(92)90239-E.

[38] Z. Yan, D. Ma, J. Zhuang, X. Liu, X. Liu, X. Han, X. Bao, F. Chang, L. Xu, Z. Liu, On the acid-dealumination of USY zeolite: a solid state NMR investigation, J. Mol. Catal. A Chem. 194 (2003) 153–167. https://doi.org/10.1016/S1381-1169(02)00531-9.

[39] A. Corma, A. Martinez, C. Martinez, The role of extraframework aluminum species in USY catalysts during isobutane/2-butene alkylation, Appl. Catal. A Gen. 134 (1996) 169–182. https://doi.org/10.1016/0926-860X(95)00228-6.

[40] J. Xia, D. Mao, W. Tao, Q. Chen, Y. Zhang, Y. Tang, Dealumination of HMCM-22 by various methods and its application in one-step synthesis of dimethyl ether from syngas, Microporous Mesoporous Mater. 91 (2006) 33–39. https://doi.org/10.1016/j.micromeso.2005.11.014.

[41] A. Sartbaeva, N.H. Rees, P.P. Edwards, A.J. Ramirez-Cuesta, E. Barney, Local probes show that framework modification in zeolites occurs on ammonium exchange without calcination, J. Mater. Chem. A. 1 (2013) 7415–7421. https://doi.org/10.1039/C3TA10243B.

[42] Online Dictionary of Crystallography, Comm. Crystallogr. Nomencl. Int. Union Crystallogr. (n.d.). http://reference.iucr.org/dictionary/Main_Page.

Results and Discussion

6. Results and Discussion

6.1. Physico-chemical characterization of the catalysts

The main parameters determining the catalytic activity of the heterogeneous catalysts studied in the present PhD work are:

- structural and morphological properties
- chemical composition and Si/Al molar ratios
- total acidity, type (Brönsted or Lewis) and strength of acid sites
- thermal, physical and chemical stabilities

Thus, once the catalysts had been synthesized, they were characterized to determine these parameters, by using the techniques described in Section 5.3. Next, the characterization results are shown and discussed to explain the catalytic performance and to stablish the corresponding structure-activity-stability relationships. Thermal, physical and chemical stabilities of the catalysts are included in Section 6.2 referred to the catalytic activity study.

6.1.1. Structural and morphological properties: XRD and N_2 sorption analyses

X-ray diffraction and nitrogen sorption analysis were carried out to determine the structural and textural properties of catalysts. XRD is a suitable tool for the study of both mesoporous solids and crystalline zeolites. As regards nitrogen sorption, it can be regarded as the first stage in catalyst characterization, as the obtained isotherms as well as the BET specific surface areas and pore sizes are very useful as "fingerprints" of microporous and mesoporous solids.

Mesoporous tantalum oxide

The first mesoporous tantalum oxide, synthesized by Antonelli and Ying by a methodological approach involving the careful hydrolysis of long-chain primary amine complexes of $Ta(OEt)_5$, exhibited a hexagonal array of pores, with an average pore size of 3.5 nm [1]. Yang *et al.* [2] prepared another mesoporous tantalum oxide through an amphiphilic poly(alkylene oxide) block copolymer, such as Pluronic® P-123, and $TaCl_5$, with a poorly ordered two-dimensional hexagonal mesostructured, as deduced from its diffraction peaks. They also used Transmission Electron Microscopy (TEM) to confirm the proposed structure and calculate the mean thickness of the pore/channel walls, resulting in 4 nm. Another 3D cubic mesoporous tantalum pentoxide with a space group $I\,m\bar{3}m$ was synthesized by Brezesinski *et al.* [3].

To enhance the catalytic activity, crystallization of an amorphous framework without losing the ordered mesostructured is a key issue.

The XRD pattern of the mesoporous Ta_2O_5 synthesized in the present work, by following the method proposed by Xu *et al.* [4], shows three broad bands at 2θ: 25, 33 and 55º, which reveal its low crystallinity. Moreover, the intense band centered at 2θ: 1.2º (Figure 1) is characteristic of a mesoporous structure, being 7.36 nm the corresponding d_{100} interplanar distance (Bragg's Law).

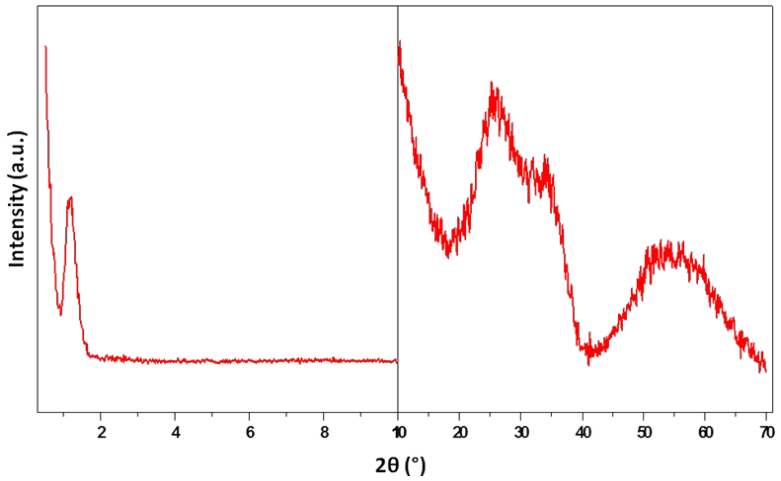

Figure 1. XRD patterns of mesoporous tantalum oxide: small-angle 2θ (º)= 0-10 (left) and high-angle 2θ (º)= 10-80 (right).

The tantalum oxide prepared by Xu *et al.* [4] exhibited an orthorhombic structure, associated to diffraction peaks located at d_{hkl} values of 3.88, 3.15, 2.45, 1.94 and 1.66 Å. Aleshina *et al.* [5] also reported an orthorhombic Ta_2O_5 structure.

In order to elucidate the thermal stability of the mesoporous tantalum oxide prepared in the present work, whose catalytic performance would be tested up to 200 ºC, a thermodiffraction study was undertaken between room temperature and 1000 ºC. Up to 500 ºC, the diffractograms do not change, but above 600 ºC, narrow and well defined diffraction peaks, corresponding to the cited orthorhombic structure [4,5] are clearly observed (Figure 2).

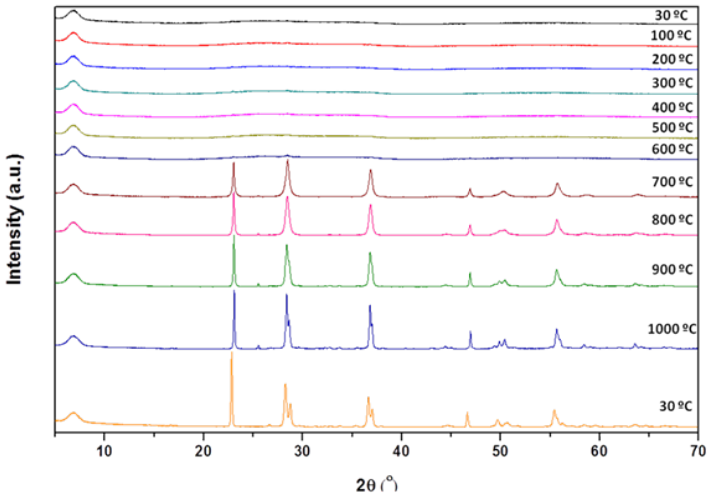

Figure 2. XRD patterns of mesoporous Ta_2O_5 from room temperature up to 1000 ºC and that of the orthorhombic phase reported by Aleshina *et al.* [5].

Considering that the mesoporous tantalum oxide was calcined at 550 ºC and assuming that a hexagonal structure was adopted, similar to other families of mesoporous inorganic solids, such as MCM-41 or SBA-15, the lattice parameter *a* was calculated by using the equation:

$$\frac{1}{d^2} = \frac{4}{3}\left(\frac{h^2 + hk + k^2}{a^2}\right) + \frac{l^2}{c^2}$$

obtaining "a" value of 8.49 nm. This periodic dimension of the unit cell includes the pore diameter and the wall thickness, hence the wall thickness resulted in being 4.79 nm considering the DFT pore size distribution (vide infra). The use of templates with high molecular

weight, such as Pluronic® P-123, led to thicker pore walls with ordered mesostructures during the synthesis procedure.

This catalyst exhibited a N_2 adsorption-desorption isotherm of Type IV(a), according to the IUPAC classification [6], typical of mesoporous solids, in which hysteresis is associated with capillary condensation. The shape of the hysteresis loop, classified as H2(b) by the IUPAC, indicated pore blocking in a wide range of pore necks. In fact, Density Functional Theory (DFT) method was used to calculate the pore size distribution, which resulted to be extended from 2 to 6 nm () [7,8].

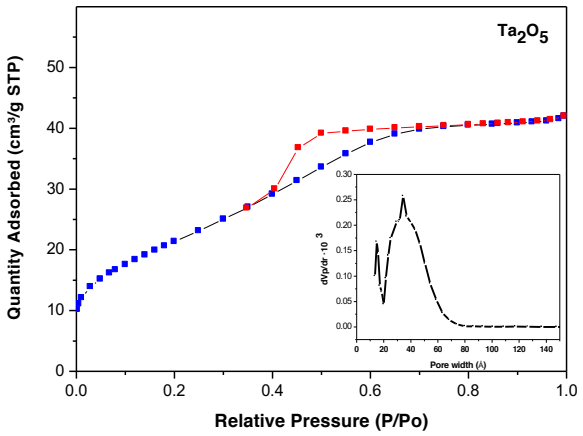

Figure 3. Nitrogen adsorption-desorption isotherm and pore-size distribution of mesoporous tantalum oxide.

The use of BJH method for this mesoporous material with pores narrower than 10 nm tends to underestimate the pore diameter by 20-30%, whereas DFT methods had resulted applicable and

recommended [7]. Surface area, evaluated with the BET method [9], was 79 $m^2\ g^{-1}$, with a total pore volume of 0.065 $cm^3\ g^{-1}$ (0.057 $cm^3\ g^{-1}$ DFT datum) (Table 1).

Table 1. Textural parameters from nitrogen sorption at -196 ºC of mesoporous Ta_2O_5 and mesoporous silica-based catalysts

Material	S_{BET} $m^2\ g^{-1}$	V_P $cm^3\ g^{-1}$	D_P (nm) (max. DFT)	S_{micro} t-plot $m^2 g^{-1}$	V_{micro} t-plot $cm^3 g^{-1}$
Ta_2O_5	79	0.065	3.3	1	0.001
10Al-MCM-41	587	1.450	1.3	197	0.112
5Al-MCM-41	734	1.700	3.3	454	0.251
KIT6-A	589	1.091	8.6	140	0.058
KIT6-B	661	1.192	8.6	126	0.049
KIT6-C	826	1.062	8.6	303	0.133
Al-KIT6-C1	714	0.953	7.4	228	0.099
Al-KIT6-C2	467	0.711	7.4	88	0.035

Mesoporous tantalum oxide synthesized by Xu *et al.* [10] possessed wider pore diameter and pore volume (9 nm and 0.092 $cm^3\ g^{-1}$) and, consequently, a lower S_{BET} (29.3 $m^2\ g^{-1}$), whereas the material synthesized by Yang *et al.* [11] showed the opposite tendency, with mesopores smaller than 4 nm and larger S_{BET} (165 $m^2\ g^{-1}$), providing further evidence of the importance of the synthesis method.

The low- and high-angle XRD patterns of both synthesized aluminum-doped MCM-41 silica samples are displayed in Figure 4.

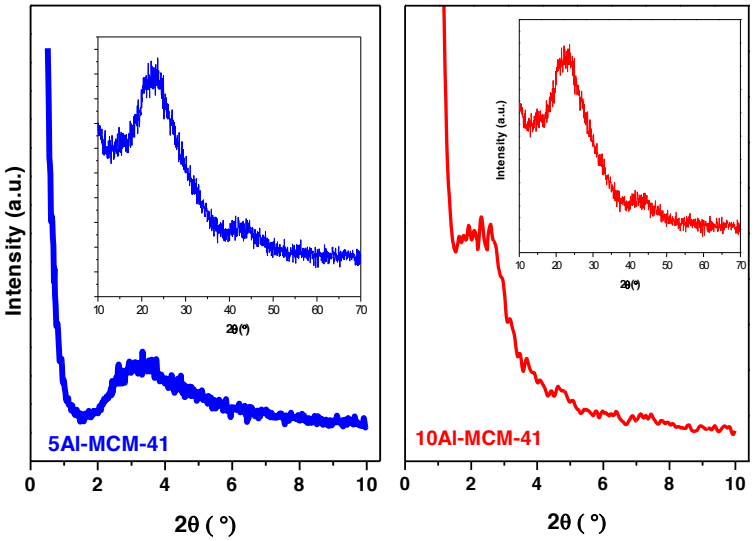

Figure 4. XRD patterns of aluminum-doped MCM-41silicas with Si/Al molar ratio of 5 (left) and 10 (right).

A broad diffraction peak can be observed at 1.5º< 2θ< 3.5º in the diffraction pattern of the 10AlMCM-41 catalyst, being broader in the case of 5Al-MCM-41 (1.5º< 2θ< 6º), with a higher aluminum content. These are associated with the (100) reflection of a hexagonal structure. Small-angle reflections reported for other aluminum-doped MCM-41 materials also appeared below 2θ= 2º ([12], while Araújo *et al.* [13] reported a broad peak extending up to 2.2º.

On the other hand, in the high-angle region (inset of Figure 4), only typical broad bands associated to the amorphous silica walls are observed, without any diffraction peak pointing out the presence of crystalline phases, even when the aluminum content was higher (5Al-MCM-41). The most ordered hexagonal structure for Al-MCM-41 materials has also been reported for a Si/Al molar ratio of 10 [14].

Low-angle XRD patterns of KIT6-A, B and C samples confirmed the formation of ordered mesostructures, resulting B and C in better long-range ordering, due to the longer synthesis periods which favored the condensation of silanol groups in the walls ().

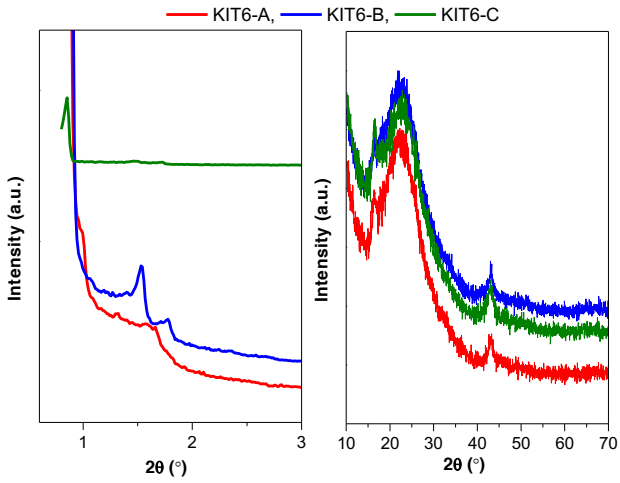

Figure 5. XRD patterns of KIT6-A, B and C catalysts.

KIT-C showed a well resolved diffaction signal associated with (211) planes in a body centered cubic *Ia3d* structure, with a d_{211} value of 10.5 nm and an unit cell parameter "*a*" of 25.7 nm ($a = d_{211} \times \sqrt{6}$). With

respect to the broad bands centered at 2θ= 22º, as previously noted, they are typical of amorphous silica-based materials. All these values are in good agreement with the data reported in the literature [15,16].

Considering these XRD data and textural characterization, KIT6-C was selected to post-synthesis alumination by two different methods (Section 5.1.3.), resulting in Al-KIT6-C1 and Al-KIT6-C2 materials. Low-angle XRD data showed sharper diffraction peaks for the aluminated samples, in comparison with the siliceous precursor, maintaining the position of diffraction signal associated with (211) planes with the body centered cubic *Ia3d* group. Moreover, both catalysts exhibited a very small shoulder at 2θ> 1º and small peaks at 1.5< 2θ< 1.8º, similarly to other aluminum KIT-6 silicas [16]. The high-angle region remained unchanged, meaning nonstructural changes and well aluminum dispersion after the heteroatom incorporation ().

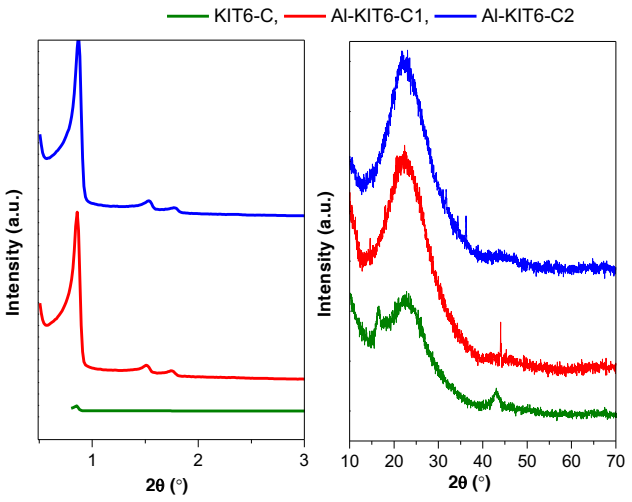

Figure 6. X-ray diffractograms of KIT6-C, Al-KIT6-C1 and Al-KIT6-C2 mesoporous silicas.

XRD patterns of 10Al-MCM-41 and Al-KIT6-C2 silicas containing a theoretical Si/Al molar ratio of 10 (Figure 7), in the high-angle region, were similar and characteristic of mesoporous silicas, whereas the low-angle region is different, with a better long-range ordering with a body centered cubic *Ia3d* space group for Al-KIT6-C2.

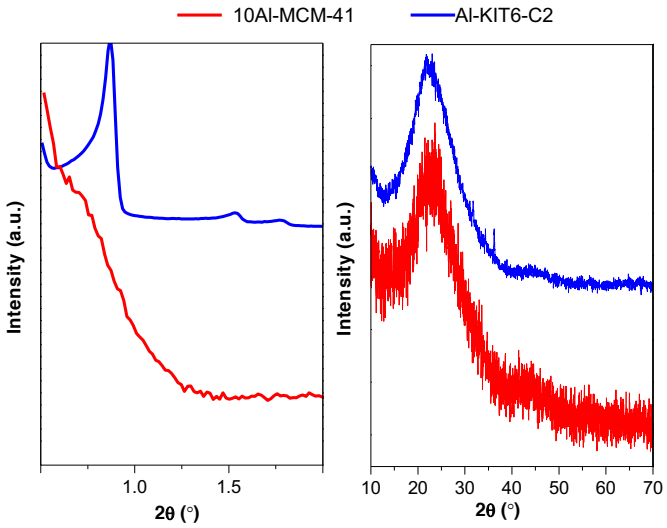

Figure 7. XRD patterns of 10Al-MCM-41 and Al-KIT6-C2.

Aluminum was incorporated during the synthesis in the MCM-41 silica and through post-synthesis in the KIT-6 one, and this fact could have poduced differences concerning the ordering, as in the second case aluminum species are mainly present on the catalyst surface, whereas, in the first case, aluminum atoms substituting silicon could cause more disorder. This fact is in agreement with the well-defined and sharper peaks at low 2θ angle shown for a KIT-6 silica with Si/Al molar ratios varying from 33 to 110, where Al was incorporated by post-synthesis

[16] in comparison with an as-synthesized Al-KIT-6 with Si/Al molar ratios from 20 to 150 [17].

Although these silicas are mostly mesoporous, however, it should be noted that the presence of a small contribution of microporosity should be expected in some of them. Nitrogen adsorption-desorption isotherms of 10Al-MCM-41 and 5Al-MCM-41 (Figure 8) can be classified as Type IV(a), according to the IUPAC [6], typical of mesoporous adsorbents. H1 hysteresis loop type, very narrow, indicated delayed condensation ought to uniform cylindrical pores.

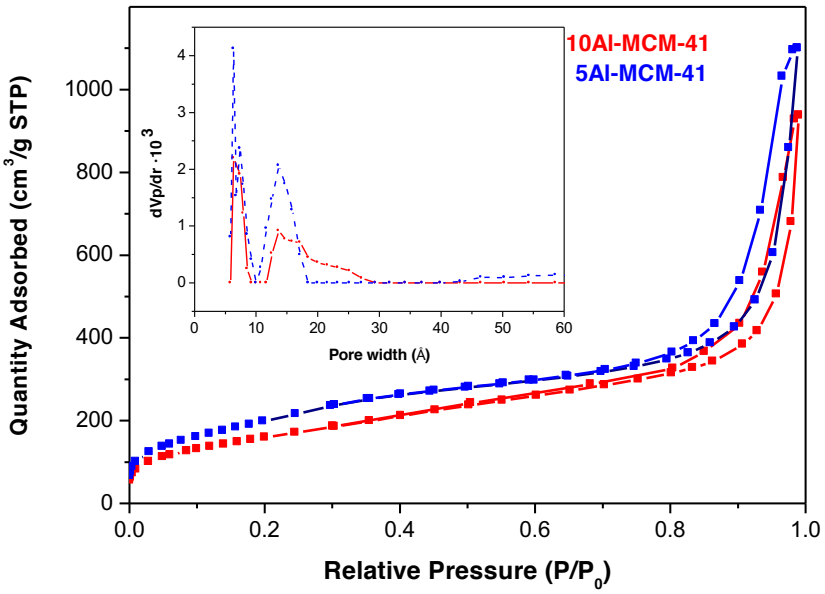

Figure 8. Nitrogen adsorption-desorption isotherms and pore size distributions (DFT method) of MCM-41 catalysts.

The notable increase in the adsorbed volume at high relative pressures pointed out the existence of wide pores, which according to the DFT

analysis, were within the interval 1-3 and 1-2 nm in 10Al-MCM-41 and 5Al-MCM-41 catalysts, respectively. BET surface areas increased with the amount of aluminum, from 587 to 734 $m^2\ g^{-1}$ for 10Al-MCM-41 and 5Al-MCM-41, respectively, which could be justified by the presence of extra-framework amorphous alumina in the more aluminum enriched catalyst, and endorsed by the higher abundance of octahedral aluminum (Section 6.1.2.). The presence of alumina increased the micropore volume to the detriment of mesoporosity, corresponding the 33% of the surface to micropores in 10Al-MCM-41, compared to the 66% in 5Al-MCM-41 (Table 1). MCM-41 with high aluminum content, without loss of mesoporosity, have been prepared through post-synthesis methods instead of direct hydrothermal ones [18]. Both, the aluminum content and the experimental conditions used in the synthesis, determine the textural properties of these materials [19], but in this case, both possess mesoporous structures which seemed to be suitable for catalytic purposes.

The nitrogen adsorption-desorption isotherms of KIT6-A, KIT6-B and KIT6-C silicas (previously to aluminum incorporation) are compared in , and textural parameters are displayed in Table 1 [9,20]). Sorption isotherms are also Type IV(a) (IUPAC classification [6]), characteristic of mesoporous materials. The surface development undergone during the synthesis procedure in KIT6-B (stirred for longer time) led to a higher surface than in KIT6-A (661 *versus* 589 $m^2 \cdot g^{-1}$), but with a very similar porosity. KIT6-C developed the largest BET surface, 826 $m^2 \cdot g^{-1}$, but different porosity. While all of them possessed mesopores between 7 and 10 nm, and, mainly, around 8.6 nm, KIT6-C, on the contrary, developed more micropores and less

mesoporosity. The wide mesopores in these KIT-6 materials caused capilar condensation during the desorption, producing hysteresis. But, even though these silicas with ordered three dimensional pore networks use to lead to type H1 hysteresis, KIT6-A, B and C seemed to have a wide distribution of pore sizes, according to the hysteresis loop shapes, with steep desorption branches, which corresponded with a H2(b) (IUPAC type) [21]. Horizontal plateaus in the isotherms at high relative pressures revealed the absence of macropores.

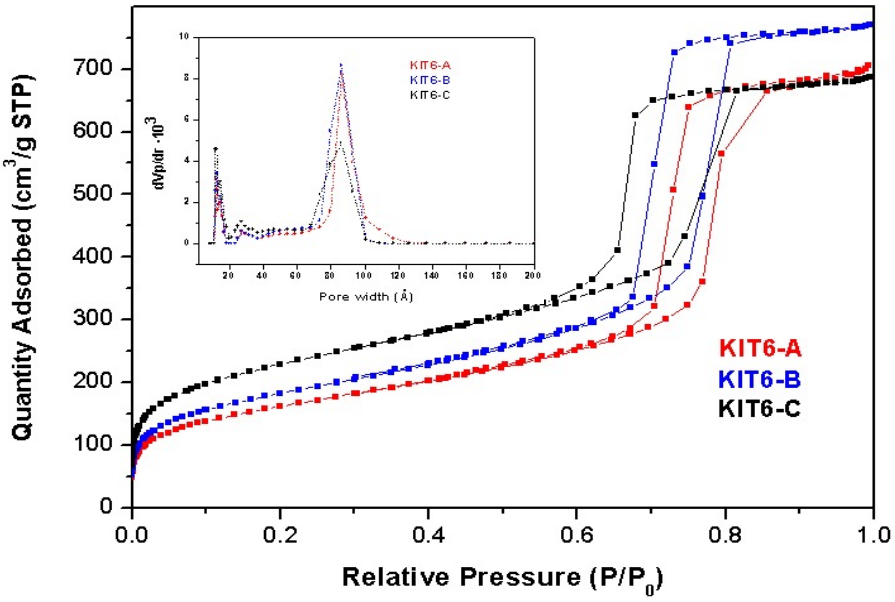

Figure 9. Nitrogen adsorption-desorption isotherms and pore-size distributions (DFT) of KIT6-A, B and C silicas.

KIT-6-10-0 silica reported by Wang *et al.* [22] and KIT-6-100 silica from Vinu *et al.* [23], synthesized similarly to KIT6-A, but being hydrothermal treated at 100 ºC instead of 120 ºC, resulted in similar porosity but with different BET surfaces, whereas KIT-6 synthesized

by Soni *et al.* [15], under similar experimental conditions to those KIT-6-10-0 (Wang, [22]) and KIT-6-100 (Vinu, [23]), possessed narrower pores and an intermediate surface (589 $m^2 g^{-1}$ for KIT6-A, 800 $m^2 g^{-1}$ for KIT6-10-0 (Wang), 728 $m^2 g^{-1}$ KIT-6-100 (Vinu) and 625 $m^2 g^{-1}$ KIT-6 (Soni)). On the one hand, synthesis temperature affects the hydrophilicity of the polyethylene oxide chains of the micelles in the sense that an increase in temperature reduces the hydrophilicity, enlarging the micelle size and, consequently, the pore diameter, but also large micelles can be broken as temperature increases. On the other hand, the copolymer dissolution process, which varies with the selected solvent, modifies the structure-directing agent intervention and thus, the textural properties of the resulting solid.

Al-KIT6-C1 and Al-KIT6-C2 were prepared from KIT6-C silica by two different methods, starting from identical amount of silica and aluminum precursor, but providing different textural parameters instead (Table 1). After aluminum incorporation, the narrow pore size distribution remained, but reduced the BET surface area and pore volume, as expected (Figure 10). Other authors have reported similar trends for Al-KIT-6 silicas with decreasing aluminum contents [16,17]. Al-KIT6-C2 differed from KIT6-C silica in a larger extent than Al-KIT6-C1, reducing the BET surface area in 43.5%, total pore volume from 1.062 to 0.711 $cm^3 g^{-1}$, micropore volume (t-plot method) from 0.133 to 0.035 $cm^3 \cdot g^{-1}$ and pore width from 8.6 to 7.4 nm (Table 1). These particularly marked differences in Al-KIT6-C2 catalyst suggested a higher aluminum incorporation into the structure and not superficially deposited on this catalyst and, therefore, a more effective post-synthesis procedure. The concentration and nature of aluminum

species in these catalysts were also studied by XPS, MAS-NMR and chemical analysis (Section 6.1.2.), for supporting these assumptions.

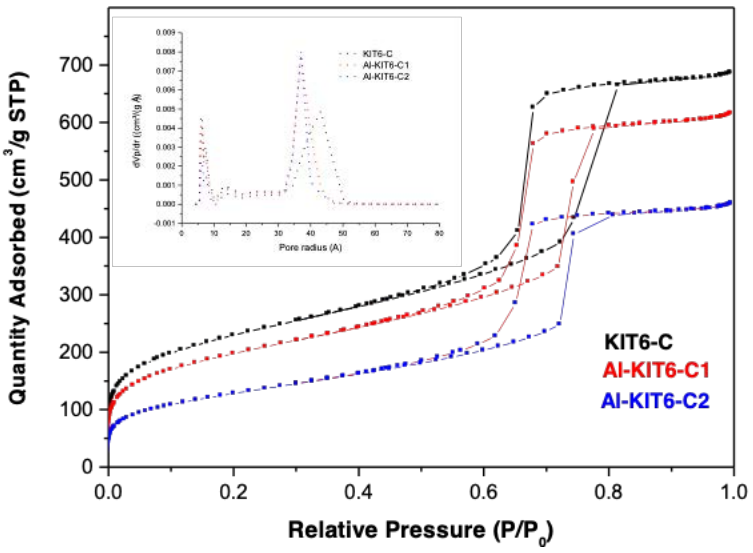

Figure 10. Nitrogen adsorption-desorption isotherms and pore-size distribution (DFT) of KIT6-C silica and both aluminum doped KIT6-C silicas (Al-KIT6-C1 and Al-KIT6-C2).

Zeolites: ZSM-5, Y, Beta

Three ZSM-5 zeolites with a theoretical Si/Al atomic ratio of 15 (H-ZSM5-15, Fe-ZSM5-15 and Cu-ZSM5-15), as well as the commercial NH_4-ZSM-5 precursor, were characterized by powder X-ray diffraction. ZSM-5 zeolite framework is MFI-type and contains one set of similar 10-sided channels intersected orthogonally by a set of nearly circular tortuous channels (5.4 Å diameter). All the diffractograms resulted similar, with main diffraction peaks at 2θ: 23.10, 7.8, 8.7, 23.32, 23.95, 23.72 and 24.42º, ordered according to

their intensity from high to low values (), which matched well with the reported data of this type of zeolite [24].

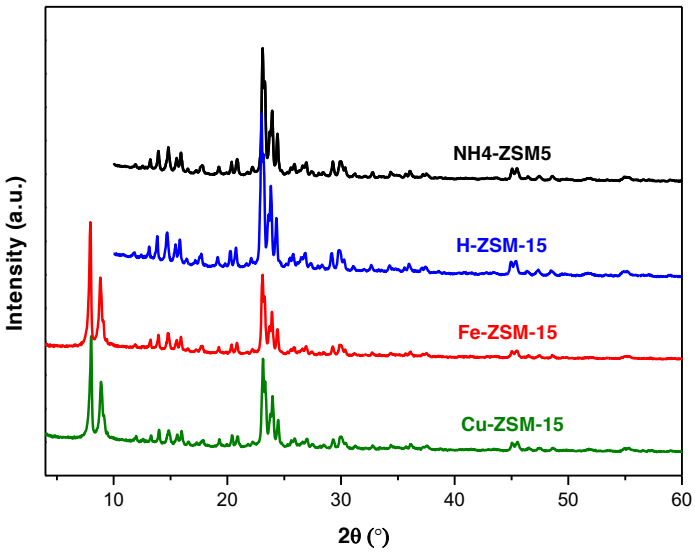

Figure 11. DRX patterns of ZSM-5 zeolites.

d spacing calculated from the main diffraction peak was 3.85 Å. Reported values of the unit cell of ZSM-5 zeolite, with an orthorhombic system , were *a:* 20.09 Å, *b:* 19.74 Å, *c:* 13.14 Å, α=ß=Ɣ: 90º, and channels dimensions {[100] 10 5.1 x 5.5 <-> [010] 10 5.3 x 5.6}*** (3-dimensional)[25]. After iron and copper incorporation, followed by thermal treatment at 550 ºC, structures stayed well preserved. No diffraction signals associated to iron oxides, such as hematite (Fe_2O_3, reference pattern 00-024-0072), burnt ochre (00-033-0664) or iron(II) oxide (00-003-0968) were detected in the Fe-ZSM-15 diffractogram, as can be observed in [26].

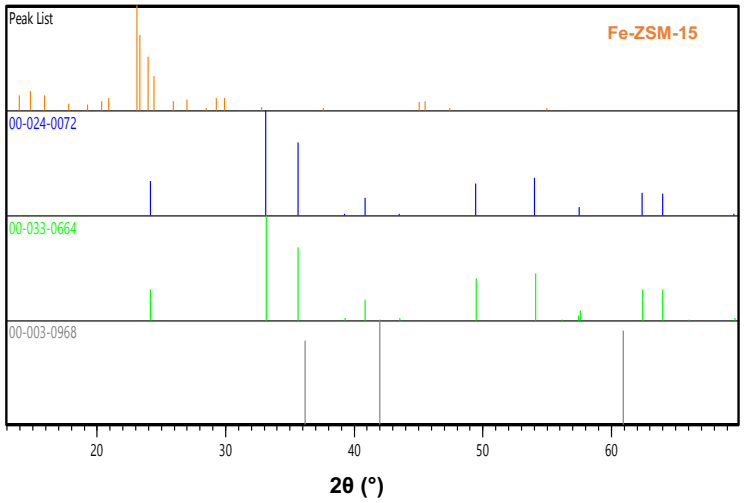

Figure 12. XRD patterns of Fe-ZSM-15 zeolite and some iron oxides.

For Cu-ZSM-15, diffractogram was just like other similar zeolites [27] and there were not detected copper oxide either (Figure 13), in which main CuO diffraction peaks have also been included (reference patterns 00-005-0661, 00-041-0254, 00-044-0706 and 01-078-0428 [26]). Nevertheless, the invariability of the position of the main diffraction peaks would suggest that these cations are predominantly in extra-framework positions.

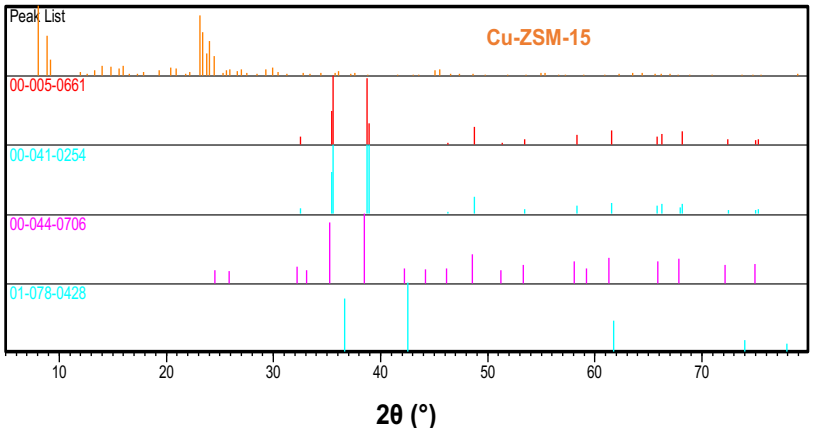

Figure 13. XRD patterns of Cu-ZSM-15 zeolite and some copper oxides.

On the other hand, all the Y zeolites (H-Y-6, Fe-Y-6 and Cu-Y-6 with a Si/Al molar ratio of 6, and H-Y-15 with 15) possessed faujasite frameworks, with a cubic structure and wider channels than ZSM-5 zeolites, with dimensions <111> 12 7.4 x 7.4*** (3-dimensional) [25]. In this sense, diffraction patterns showed main diffraction peaks at 6.33, 10.34 and 15.97 (*2θ* degrees), corresponding a value for *d* spacing of 13.96 Å from the first and most intense peak. All these values match well with those of a FAU structure (reference pattern 01-077-1151) (Figure 14). Iron and copper incorporation by cationic exchange seemed to be appropriated regarding the absence of iron or copper oxide diffraction peaks, although the incorporation of copper oxide nanoparticles in Cu-zeolites has demonstrated to enhance their catalytic activity in selective catalytic reduction of nitrogen oxides by propane ($DeNO_x$) [28].

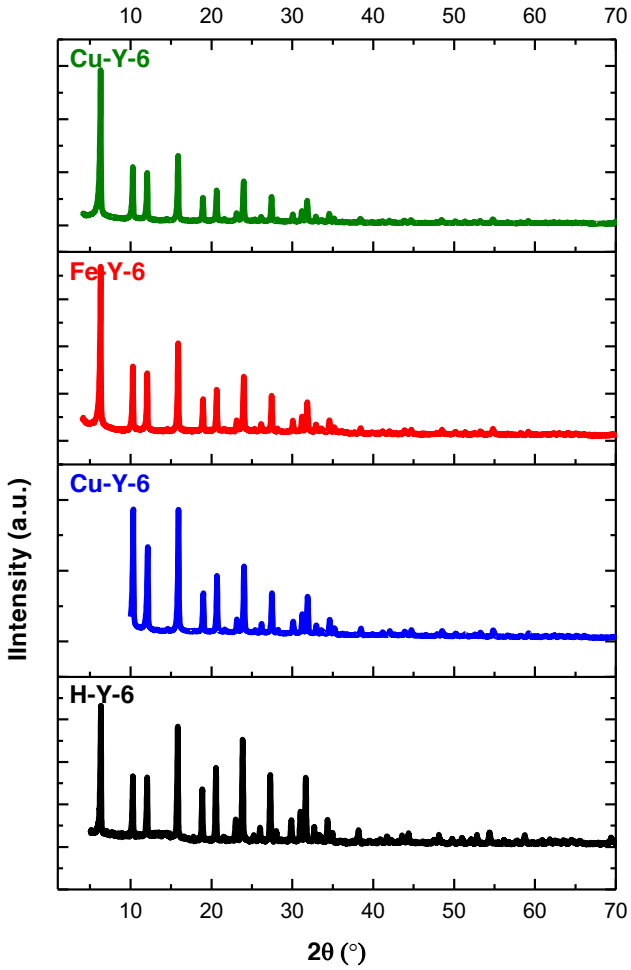

Figure 14. X-ray diffraction patterns of Y zeolites.

Beta zeolites exhibit a BEA framework type, with 3D channels and tetragonal atoms arrangement with approximate cell dimensions $a = b = 12.63$ Å, $c = 26.19$ Å. X-ray diffraction patterns are shown in . H-Beta-19 showed only one main peak, as data were collected from 2θ=

10º, but two main peaks in the other Beta zeolites, wider than those of the other ZSM-5 and Y zeolites, could be distinguished.

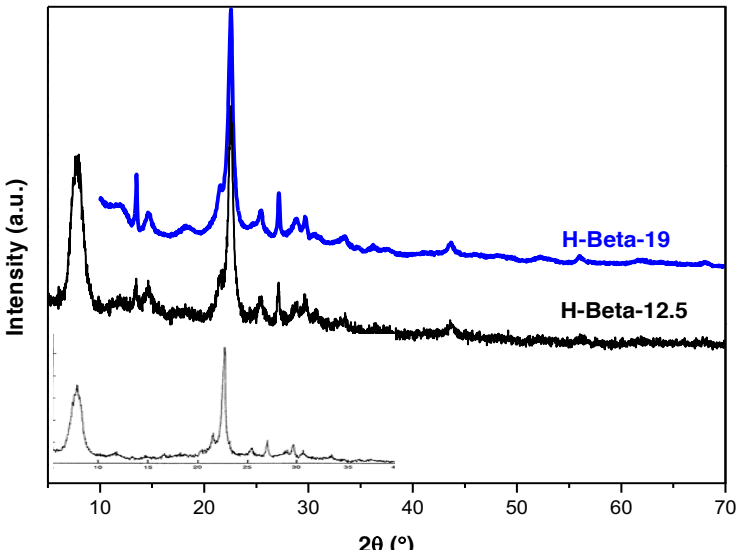

Figure 15. X-ray diffraction patterns of prepared (19, 12.5) and reported (5.2, [30]) H-Beta zeolites.

This fact means a lower crystallinity, which is associated with the presence of structural defects due to the incorporation of aluminum species [29], although there were no notable differences between the diffractograms of H-Beta-12.5 and 19, with different Al content. Main peaks at 2θ= 7.97 and 22.57º (Figure 15) correspond to the characteristic reflections of the BEA topology [29,30]. Fe and Cu were incorporated into H-Beta 12.5 zeolite for the purpose of modifying its acidic properties. After the cation exchange, no significant differences were observed in the diffractograms when comparing with the precursor H-Beta-12.5, not being found evidences of formation of

extra-framework crystalline iron or copper species, or long-range amorphization of the zeolite (), according to the data reported by other authors for iron- and copper-exchanged zeolites [31,32].

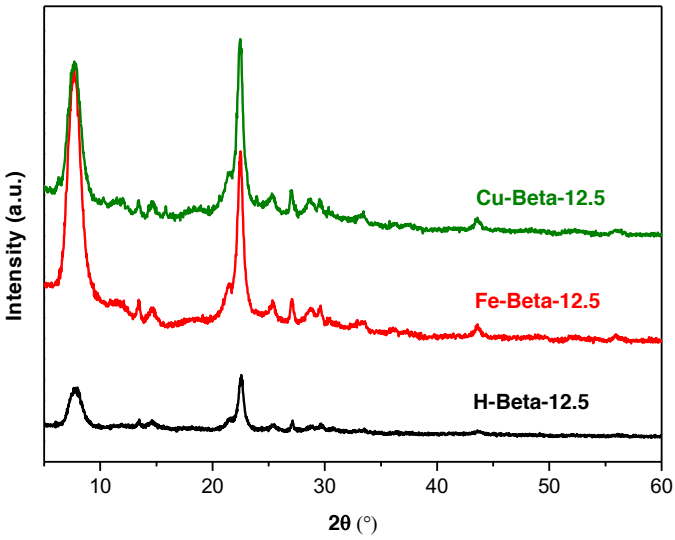

Figure 16. X-ray diffraction patterns of H-Beta-12.5, Fe-Beta-12.5 and Cu-Beta-12.5 (cation-exchanged) zeolites.

Regarding textural properties, ZSM-5 zeolites showed typical Type I isotherms, characteristic of microporous solids (**¡Error! No se encuentra el origen de la referencia.**).

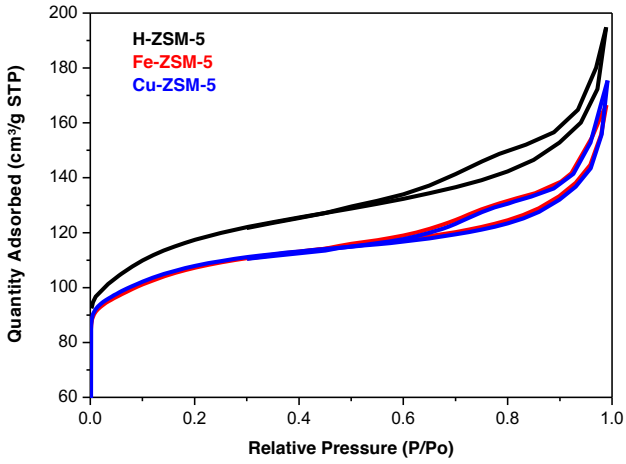

Figure 17. Nitrogen adsorption-desorption isotherms of catalysts based on ZSM-5 zeolite.

BET surfaces were slightly larger than the microporous surface areas determined from the t-plot method, and in agreement with other ZSM-5 zeolites [27,33]. On the one hand, the adsorbed amount of nitrogen diminished for the cation-exchanged zeolites with respect to the protonated form, being the isotherm moved downwards. The presence of iron and copper as very small nanoparticles, not detected by XRD, could be responsible for the external surface lowering [34]. On the other hand, the iron and copper contents, determined by ICP-AES, were found to be 1.8 and 1.9 wt.% for Fe-ZSM-5 and Cu-ZSM-5, respectively, which were low in comparison with other similar Fe-ZSM-5 zeolites, also with Si/Al molar ratios around 15 [35]. Although iron and copper metal cations incorporation did not affect the textural parameters considerably, and lower amounts of metals were incorporated into the zeolites, the nitrogen isotherms pointed out a

small and partial blockage of micropores due to the presence of cations.

Figure 18 shows the nitrogen adsorption-desorption isotherms of H-Y-6, H-Y-15, Fe-Y-6, Cu-Y-6 and H-ZSM5-15, and the corresponding textural parameters are listed in .

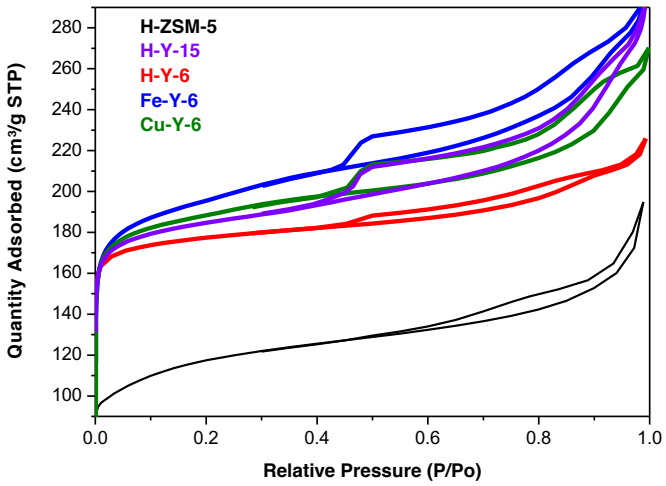

Figure 18. Nitrogen adsorption-desorption isotherms of catalysts based on Y zeolites.

Table 2. Textural parameters (nitrogen sorption) of catalysts based on zeolites.

Material	S_{BET} ($m^2 g^{-1}$)	V_P ($cm^3 g^{-1}$)	$S_{micro\ t\text{-}plot}$ ($m^2 g^{-1}$)	$V_{micro\ t\text{-}plot}$ ($cm^3 g^{-1}$)
H-ZSM-5	404	0.301	344	0.160
Fe-ZSM-5	365	0.258	327	0.153
Cu-ZSM-5	365	0.271	332	0.157
H-Y-6	595	0.349	551	0.256
H-Y-15	$823_{(LANGMUIR)}$	0.451	727	0.244
Fe-Y-6	659	0.453	570	0.273
Cu-Y-6	627	0.418	568	0.272
H-B-12.5	441	0.853	279	0.126
Fe-B-12.5	547	1.002	380	0.173
Cu-B-12.5	465	0.855	302	0.140

B = Beta

For H-Y-15, data were fitted better to a Langmuir equation instead of a BET one, thus providing a larger specific surface area, which is over-estimated. Langmuir equation is based on a monolayer filling, which cannot be exceeded, but this premise in not true in this kind of materials in which the plateau observed in isotherms is associated to micropore filling, and the limiting value is reached when micropores are filled. In comparison with ZSM-5 catalyst, higher quantities were adsorbed in the micropores by Y-type zeolites. All the Y catalysts also exhibited Type I isotherms [6]. Nevertheless, ZSM-5 type materials presented a H3 hysteresis loop type which could be attributed to aggregates of particles which caused medium and wide sized cavities, whereas Y-type materials showed a H4 (hysteresis loop) type, with a

steeper ending of the desorption branch, typical of zeolites with micro and mesopores. Textural data of H-Y-6 and its exchanged Fe and Cu-Y-6 zeolites resulted to be very similar and the main differences were due to the introduction of larger cations in the zeolitic structure, resulting in larger external surfaces and pores width enlargement.

Finally, the nitrogen adsorption-desorption isotherms for Beta zeolites showed high-rise adsorption at high relative pressures. H-Beta-12.5 and H-Beta-19 isotherms resulted intermediate between H-Y-6 and 10Al-MCM-41 ones. BJH pore size distribution applied to the desorption branch yielded an average diameter around 12 nm, typically in the mesopore range, in addition to the micropores from the zeolitic structure (Figure 19 and 20) [28,29]. H-Beta-19 possessed similar nitrogen adsorption capacity, but a lower microporosity. With respect to the incorporation of Fe and Cu in the Beta-12.5 zeolite (post-synthesis), Fe cation exchange led to better textural properties with both larger external surface area and microporosity ().

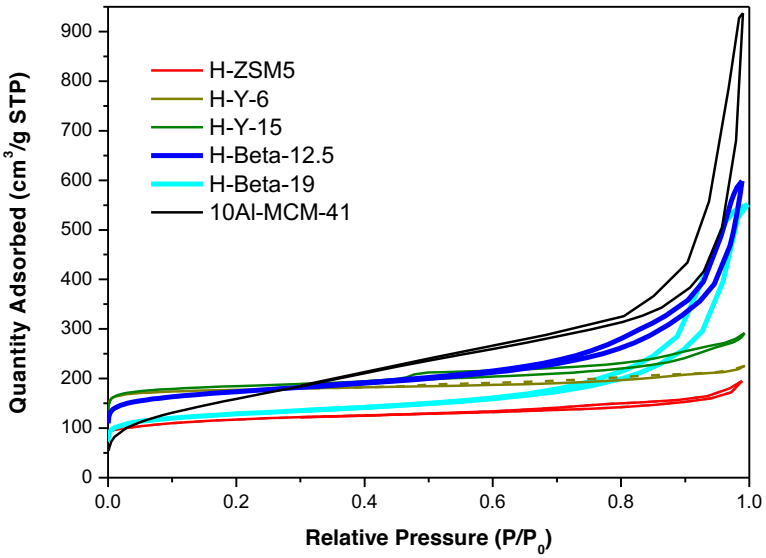

Figure 19. Nitrogen adsorption-desorption isotherms of catalysts based on zeolites and MCM-41.

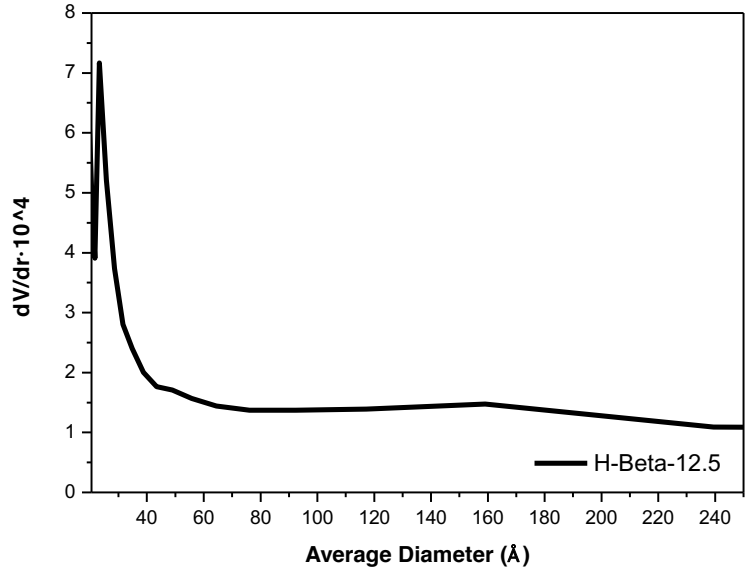

Figure 20. Pore size distribution of H-Beta-12.5 calculated by BJH method.

Copper-exchanged zeolites showed similar structures than their precursors, which indicated that they contained very little copper and no oxides were detected, even though they had synergic effect on the catalytic activity of some zeolites [28].

Although the incorporation of iron into zeolites reduces the specific surface area and micropore volume, in Beta-zeolites the addition of iron produces the opposite effect, increasing the surface area as well as the micropore volume. Campisi *et al.* studied iron cation-exchanged ZSM-5 and Beta type zeolites, observing that textural properties of ZSM-5 decreased due to the partial blockage of the pores by iron species, while in the Beta zeolite, they were increased, which could be due to the presence of iron aggregates [36]. Fe-Beta-12.5 would possess iron aggregates on surface, confirmed by a Fe/Al atomic ratio determined by XPS higher than that obtained by XRF (18.6 *vs* 0.4 %). These aggregates reduced the acidity by the presence of iron, as only a fraction of iron loading was as isolated iron in the zeolite pores, while in Fe-ZSM5-15, iron would be mainly as isolated in pores, and Fe/Al was lower on surface, as observed by XPS, than the ratio measured by XRF (0.2 *vs* 0.33).

Acidic carbons

The textural parameters of carbons used as solid acid catalysts in the present PhD work are summarized in Table 3. HA- and L-carbons presented BET surface areas between 1269 - 2081 m^2 g^{-1}, with an important contribution of micropores.

Table 3. Textural parameters from nitrogen adsorption-desorption isotherms of carbon-based catalysts.

Material	S_{BET} $m^2 g^{-1}$	V_P cm^3 g^{-1}	V_{meso} $cm^3 g^{-1}$	S_{micro} t-plot m^2 g^{-1}	V_{micro} t-plot cc g^{-1}	S_{micro}/S_{BET}	V_{micro}/V_P
HA3500	1278	2.11	1.84	707	0.27	0.6	0.1
HA31500	2011	3.10	2.56	951	0.54	0.5	0.2
HA31800	1671	1.30	0.72	482	0.58	0.3	0.4
L3500	1269	1.28	1.08	860	0.20	0.7	0.2
L31500	2081	1.88	1.52	1407	0.36	0.7	0.2
L31800	1889	1.10	0.38	442	0.72	0.2	0.6

In addition to these well-developed microporous structures, a significant contribution of mesoporosity was observed for all of them. Specially for the carbons activated at 500 ºC, volume of mesopores were about 80% of total pore volume, whereas for the carbons activated at 800 ºC (HA31800 and L31800), were 54 and 34 %, respectively. Nevertheless, external surface areas associated to mesopores were higher than 70% in both carbons activated at 800 ºC. These facts could indicate that activation at 800 ºC generates wider pores, while activation at 500 ºC favors the mesopores development. In general, surface areas decreased with the activation temperature, in line with previous studies (due to wider mesopores), and higher impregnation ratios raise the external surface area and mesopore volume [37]. Thus, HA31500 possessed a surface area of 2011 $m^2 g^{-1}$, whereas HA31800, activated at 800 ºC, resulted in 1671 $m^2 g^{-1}$ More obvious relation between textural parameters and synthesis conditions

were found with the impregnation ratio (H_3PO_4/precursor mass ratio) than with the activation temperature, comparing the HA-carbons from the present PhD work and data previously reported [37,38]. BET surface area increased linearly, whereas mesopore volume did exponentially with the impregnation ratio. As previously mentioned, the increase in the impregnation ratio resulted in carbons with a wider porous structure due to the incorporation of a higher amount of phosphate species, dilating the carbon structures. L3500, L31500 and HA3500 possessed the highest proportion of micropores and the smallest ones ($S_{micro\ t\text{-}plot}/S_{BET}$ and $V_{micro\ t\text{-}plot}/V_p$). Synthesis modifications from HA3500 to HA31500 and from LA3500 to LA31500 produced evident increases in BET surface area and better textural parameters, having obtained really mesoporous material from biomass.

6.1.2.

6.1.2. Chemical composition: XPS and MAS-NMR

To get insights into the surface characteristics and composition of catalysts, X-ray photoelectron spectroscopy was employed, providing binding energy (BE) values and surface elemental composition (including the surface Si/Al atomic ratio), which can be compared with bulk values (obtained from X-ray fluorescence analysis) in order to elucidate the dispersion of different species in solids.

Solid-state nuclear magnetic resonance (MAS-NMR) was used to characterize the chemical and structural environment of the lattice atoms. Well separated signals appear for ^{27}Al in tetrahedral framework and octahedral non-framework aluminum, which are associated to different types of acid sites. Thus, Brönsted acid sites are generated by

tetrahedrally coordinated Al forming Si-OH-Al bonds, whereas aluminum oxide clusters inside pores may act as Lewis acid sites, but also, may enhance Brönsted acidity. Moreover, MAS-NMR provides Si/Al (framework) atomic ratios.

Mesoporous tantalum oxide

Surface composition of mesoporous Ta_2O_5 obtained from XPS resulted in 57.2 at.% O and 24.1 at.% Ta, near to the stoichiometric composition of Ta_2O_5. In the core level region of Ta *4f,* two peaks were observed: Ta $4f_{7/2}$ and Ta $4f_{5/2}$, at 26.1 and 28.0 eV, respectively, with a separation of 1.9 eV. These values and the area ratio (1.36) confirmed that tantalum was only present as Ta(V). The O *1s* region evidenced an intense band centered at 531.6 eV with a large tail, which can be deconvoluted in two contributions: at 530.5 and 531.9 eV, which could be attributed to the Ta_2O_5 network and coordinated water or OH groups, respectively [39] (and 22).

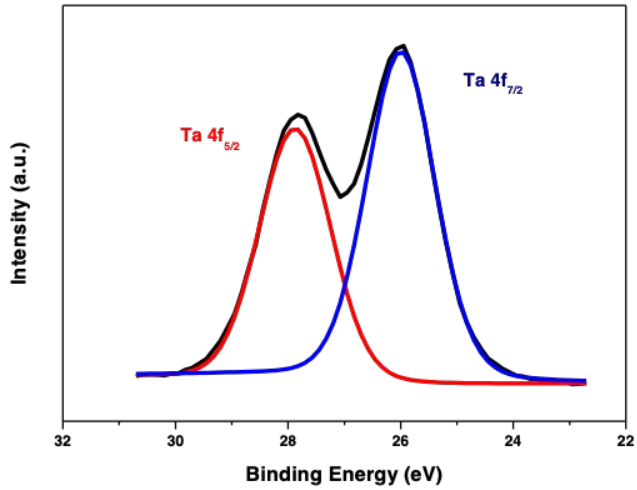

Figure 21. Ta 4f core level spectrum of mesoporous tantalum oxide.

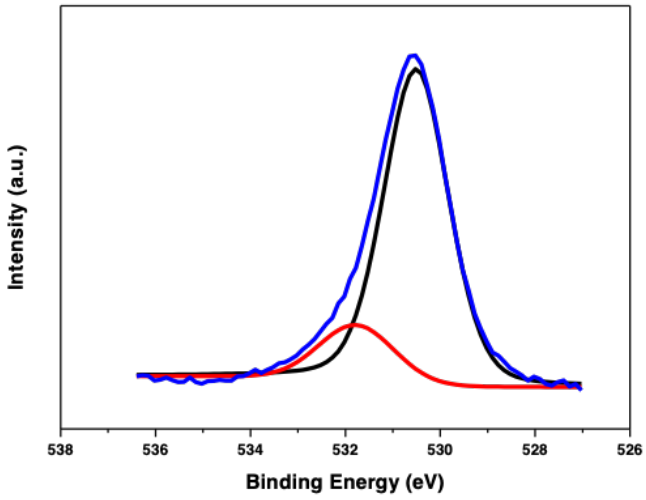

Figure 22. O 1s core level spectrum of mesoporous tantalum oxide.

Mesoporous silica-based catalysts: MCM-41, KIT-6

The Si/Al atomic ratio for 10Al-MCM-41 obtained from XPS (surface) and EDX analysis were 12.3 and 10.1, respectively, whereas

for 5Al-MCM-41, Si/Al determined by XPS was 5.4, matching very well with the EDX data (5.7). Binding energies for Si 2p and O 1s were very similar: 102.9-103.1 and 532.3-532.5 eV, respectively, typical of silica and/ or alumina. Characteristic Al 2p binding energy in aluminosilicates and alumina are around 74.6 eV, whereas in the aluminum-doped mesoporous silica appeared at 74.9-75.0 eV, slightly higher, but similar to other Al-MCM-41 compounds [40]. To get information about Al coordination, Auger spectra were obtained and the Auger parameters (α´) for both catalysts were calculated [41]. Both Al_{KLL} Auger spectra exhibited an asymmetric band which can be deconvoluted in two peaks: 1383.7 and 1385.5 eV ().

Table 4. Core level binding energies and Auger kinetic energies of Al-MCM-41

	Binding energy (eV)			**Auger parameter α´ (eV)**	
Catalyst	**Al 2p**	**Si 2p**	**O 1s**	**Al $2p_t$**	**Al $2p_o$**
10Al-MCM-41	75.0	103.3	532.5	1458.7	1460.4
5Al-MCM-41	74.9	102.9	532.3	1458.6	1460.6

Both catalysts had two Auger parameters for Al, one nearly 1461 eV, typical of octahedral Al and the other at lower energy, corresponding to tetrahedral Al [42,43]. Aluminum incorporated into the siliceous structure was supposed to be tetrahedral, but some aluminum remained on the external surface, as aluminum oxide, in octahedral coordination, being majority in 5Al-MCM-41.

The presence of both tetrahedral and octahedral aluminum was confirmed by ^{27}Al NMR of 10Al-MCM-41, with two main signals at about 60 and 0 ppm. Strongly overlapped lines could be considered in both signals (Figure 23). Non-framework tetrahedral aluminum has been suggested to be responsible for these contributions, shifted to lower chemical shifts, but they had not been studied [44]. The intensity Al^T:Al^O ratio gave a value of 2. These data indicated a higher proportion of framework aluminum than in other Al-MCM-41 materials synthesized with similar methods. Vaschetto *et al.* prepared Al-MCM-41 with Si/Al molar ratios of 20 by hydrothermal synthesis, under different experimental conditions, and achieved 19.35% Al^T (tetrahedral) at most [12]. The aluminum oxide on the pore walls (Al^O) could be responsible for the X-ray scattering, which produced the broadening of the low-angle diffraction peak (Figure 23).

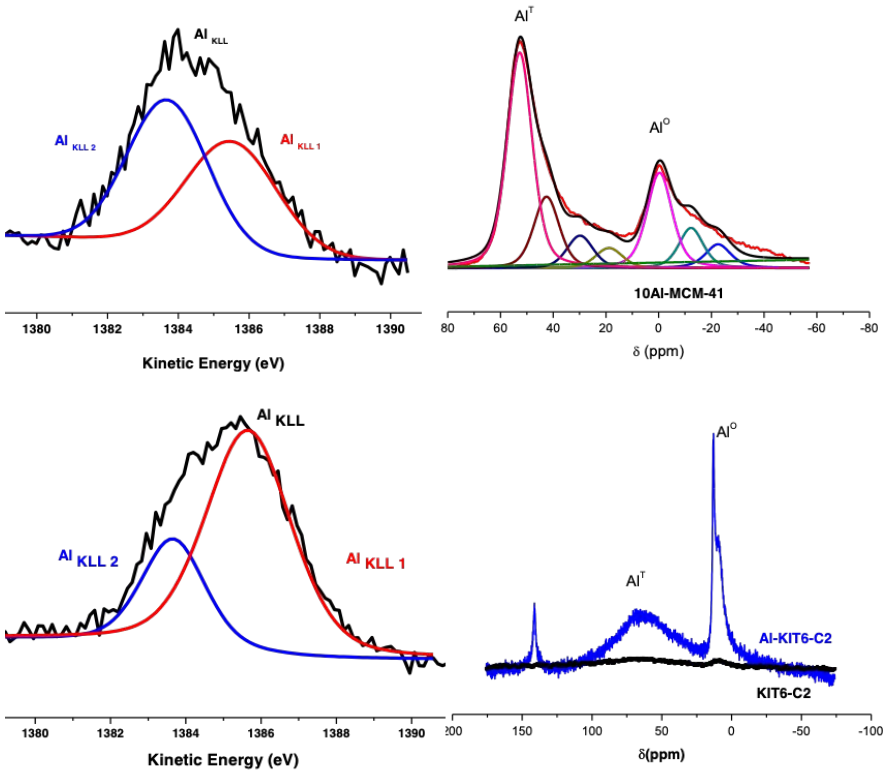

Figure 23. Auger kinetic energies for Al KLL of 10Al-MCM-41 (left-up) and 5Al-MCM-41 (left-down) and ^{27}Al NMR spectrum of 10Al-MCM-41 (right-up). ^{27}Al NMR spectra of KIT6-C and Al-KIT6-C2 silicas (right-down).

Regarding KIT-6 silicas, surface composition of KIT6-B was nearly the stoichiometric. The surface Si/Al atomic ratios (Table 5), as deduced from XPS data, were decisive to support the aluminum post synthesis incorporation into the KIT6-C silica. Al-KIT6-C1 barely contained surface aluminum, according to XPS data, and XRF analysis confirmed the scarcity of Al, giving a Si/Al atomic ratio of 82. On the contrary, Al-KIT6-C2 possessed a Si/Al atomic ratio of 9.5, near to the value used in the synthesis step (10) (Figure 23), as much

tetrahedral framework aluminum (Al^{T}) as octahedral non-framework (Al^{O}), according to the MAS-NMR data, and even other contributions, as could be deduced from the broadness of both main peaks (Figure 23). Owing to this better incorporation of aluminum into Al-KIT6-C2 with respect to Al-KIT6-C1, this silica was chosen for the catalytic study.

Table 5.Surface atomic composition of KIT-6-based catalysts from XPS analysis

Material	C 1s	O 1s	Al 2p	Si 2p	Si/Al
KIT6-B	3.4	63.9	-	32.7	-
KIT6-C	0.1	72.1	-	27.8	-
Al-KIT6-C1	1.5	70.4	0.4	27.7	69.2
Al-KIT6-C2	3.3	69.3	2.6	24.8	9.5

Karthikeyan *et al.* made a post-synthesis alumination of KIT-6 materials with Si/Al ratios from 25 to 100, and the obtained ^{27}Al NMR spectra showed aluminum in both tetrahedral and octahedral environments, but mainly in tetrahedral sites, with was supported by some de-alumination occurred during the acid treatment, which removed extra-framework aluminum species [16]. On the other hand, Luan *et al.* carried out the alumination of SBA-15 silica materials by three different post-synthesis routes: i) treatment of silica with an aqueous solution of sodium aluminate only gave rise to a line corresponding to tetrahedral aluminum, even before calcination, ii) the use of aluminum isopropoxide in dry hexane produced both

prominent signals of Al^{T} and Al^{O}, even broader for Al^{O} than in Al-KIT6-C2 silica, and iii) starting from silica and $AlCl_3$ in dry ethanol, gave lines at 53 and 0 ppm (δ) from tetrahedral and octahedral aluminum species [45]. For Al-KIT6-C2, $AlCl_3$ was also employed (in tetramethylammonium hydroxide, [TMAOH]/[Al] molar ratio of 2.5). Although the aluminum dissolution was tried to be completed before the silica structure formation, both seemed to occur simultaneously at some point of the synthesis, leaving part of the aluminum as extra-framework species, even though the subsequent washing and calcination produced some surface dealumination.

Zeolites: ZSM-5, Y, Beta and Mordenite

In the case of ZSM-5 catalysts, the surface Si/Al atomic ratio values were close to that of the parent NH_4-ZSM5-15 zeolite (18.6). The H-ZSM5-15 zeolite possessed a surface Si/Al atomic ratio of 18.9, higher than the theoretical one (15) and the value obtained from EDXRF analysis (16). In Fe-ZSM5-15 and Cu-ZSM5-15, Si/Al ratio differed from their precursor (H-ZSM5-15) in opposite ways: whereas the surface of Fe-ZSM5-15 diminished the aluminum content (Si/Al atomic ratio= 22.8), in Cu-ZSM-15 aluminum enhanced (14.3), pointing out different preferential location of these cations after ion-exchange and calcination stages (,). Si 2p binding energies values (103.1-103.2 eV) were typical of silica, whereas Al 2p core level spectra exhibited bands at 74.5-74.7 eV, typical values of Al(III) in silicates or oxides. For Cu-ZSM5-15 zeolite, two peaks could be observed in the Al 2p spectrum: 74.7 and 76.2 eV. However, this was due to Cu $3p_{3/2}$ overlapped with Al 2p signal [46,47].

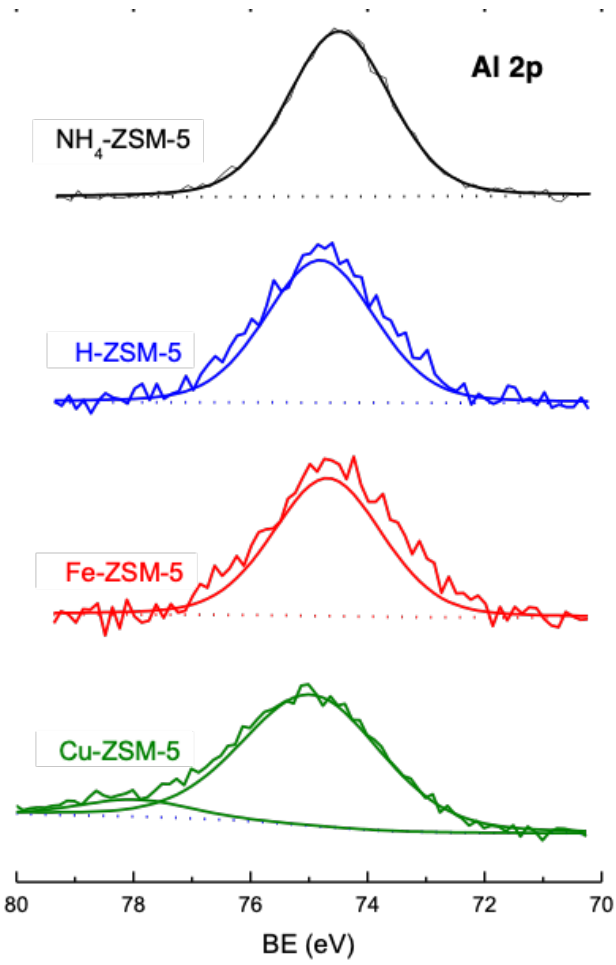

Figure 24. Al 2p core level spectra of ZSM-5 zeolite-based catalysts.

Table 6. Photoelectron emission and Auger data from XPS analyses of zeolite-based catalysts.

Sample	Binding energies (eV)							
	Si 2p	**Al 2p**	**O 1s**	**Fe $2p_{3/2}$**	**Cu $2p_{3/2}$**	**Cu $_{LMM}$**	**Si/Al (atom)**	**Me/Al (atom)**
H-Z	103.2	74.5	532.5	-	-	-	18.9	-
Fe-Z	103.1	74.5	532.5	710.8	-	-	22.8	0.2
Cu-Z	103.2	75	532.6	-	933.5	*	14	0.2
H-Y6	102.6	74.5	531.9	-	-	-	1.4	-
Fe-Y6	103.1	74.5	532.4	710.7	-	-	6.2	0.8
Fe-Y15	103.1	74.5	532.3	710.6	-	-	15.2	0.5
Cu-Y6	102.9	74.9	532.2	-	933.3	**	4.3	0.1
H-B12.5	103.5	75.2	532.8	-	-	-	12.7	-
Fe-B12.5	103.5	75	532.8	710.3	-	-	15.1	0.2
Cu-B12.5	103.3	74.9	532.6	-	933.3	339.6	8.2	0.1
H-M10	103.1	74.6	532.4	-	-	-	12.4	-
Fe-M10	103.5	74.8	532.7	710.6	-	-	23.4	0.3

Z: ZSM-5, B: BETA, M: MOR *341.1>338.6 **340.5>337

^{27}Al MAS-NMR spectra of these ZSM-5 zeolites showed both tetrahedrally and octahedrally coordinated aluminum atoms, being higher the tetrahedral contribution, corresponding to framework species. These species are associated to broad resonance lines at 54 (H- and Fe-ZSM5-15) and 52 ppm (Cu-ZSM5-15), .

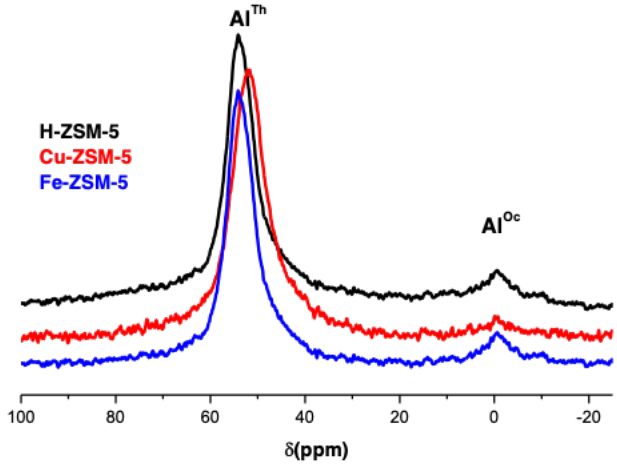

Figure 25. ^{27}Al MAS-NMR spectrum of ZSM-5-based catalysts.

Not other environments of aluminum atoms, such as distorted tetrahedrally coordinated or tetrahedrally coordinated but not connected to the framework, which gives peaks in the range 30-50 ppm [48], were detected. The intensity of the peak at 54 ppm was similar for the three ZSM-5 zeolites, indicating similar Al content, but the slight shift from 54 to 52 ppm in Cu-ZSM5-15 could confirm a different preferential location of metal cations in this catalyst, which enhanced surface aluminum atoms with respect to the zeolitic framework. Cu-ZSM5-15 possessed the most intense peak at 0 ppm, thus, more aluminum in extra-framework positions, although these extraframework Al atoms represented a small amount. Fe-ZSM-15 catalysts, with 0.8 wt.% Fe, showed a ^{27}Al MAS-NMR spectrum similar to that of a Fe-ZSM-5 zeolite with 0.64 wt.% Fe (Fe-ZSM5*c*) reported by Pérez-Ramírez *et al.*, prepared by similar ion-exchange

treatment, with small amount of extraframework Al, mainly produced after calcination [49].

With reference to Y zeolites, the surface Si/Al atomic ratio of H-Y-6 zeolite was 1.4, indicating an aluminum enrichment, while EDXRF analysis gave a value of 4.8. Bare *et al.* [50] reported that XPS of aluminosilicates zeolites does not provide a true measurement of the surface stoichiometry, resulting better variable kinetic energy than binding energy results. Then, the Si/Al atomic ratio of this zeolite was reinterpreted with complementary MAS-NMR measurement. ^{29}Si and ^{27}Al MAS-NMR spectra were obtained, quantified and deconvoluted. The majority of ^{29}Si NMR shifts are found in a range between +50 and -200 ppm, and particularly silicates around -100 ppm. The number of signals in the spectrum gives the number of different structural environments of Si atoms, and the relative (integrated) signal intensities correspond to the relative occupancies of the different environments. Thus, taking into account both ^{29}Si and ^{27}Al spectra and the intensities of each peak, the Si/Al ratio in framework were obtained, [2] resulting accurate values, close to the synthesis ratios: 8.8 for H-Y-6 and 2.67 for H-Y-2.6. Whereas H-Y-6 possessed 73% of the aluminum in the zeolitic framework, in H-Y-2.6, the 98% of the aluminum was incorporated. Moreover, in H-Y-6, aluminum atoms were mainly in Si(1Al) units, and, in H-Y-2.6, in Si(2Al) units, owing to its higher aluminum content (and 27).

---

[2] $\frac{Si}{Al} = \frac{\sum_{n=0}^{n=4} I_{Si(nAl)}}{\sum_{n=0}^{n=4} \frac{n}{4} I_{Si(nAl)}}$

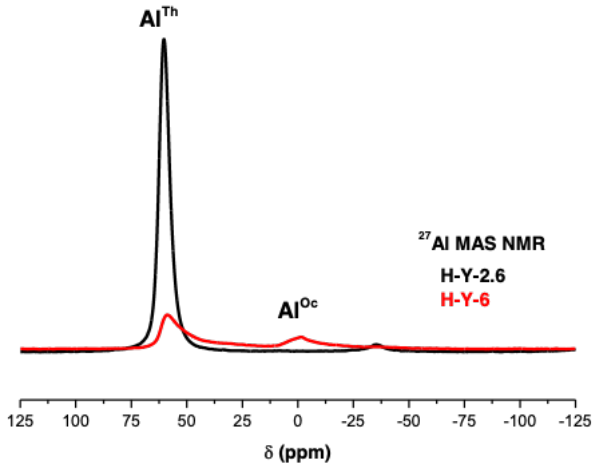

Figure 26. [27]Al MAS-NMR spectra of H-Y-2.6 and H-Y-6 catalysts.

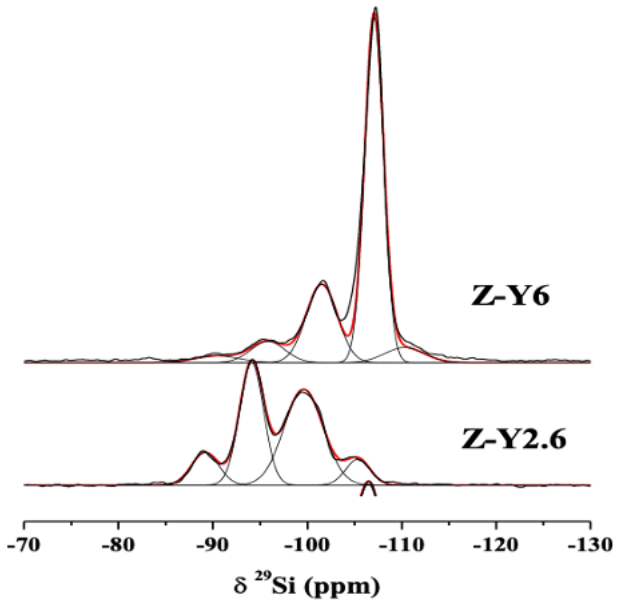

Figure 27. [29]Si MAS-NMR spectra of H-Y-2.6 and H-Y-6 catalysts.

It has previously reported for H-Y-2.6 zeolite that aluminum was also mainly as Si(2Al) units, but for H-Y-3.3 and H-Y-3.6, Si(1Al) dominated [51]. The Si/Al ratio below 3.3 seemed to be the limit from Q^1, or Si(1Al), to Q^2 (or Si(2Al) predominance. The Si/Al atomic ratio of Fe-Y-6 calculated by XPS resulted 6.2 and by EDXRF was 7.8, whereas for Cu-Y-6 were 4.3 and 6, respectively (). Those values obtained for iron zeolite were close to the precursor ratio (6), but slightly higher, which have been observed in other Fe-Y zeolites such as a Fe-Y zeolite obtained by sublimed $FeCl_3$ at 320 ºC [52]. Al 2p core level spectra for all these catalysts also showed the typical peak at 74.5 eV. In Cu-Y-6 zeolite, two peaks were observed in the Al 2p spectrum, as previously observed for Cu-ZSM5-15, due to overlapping of Cu $3p_{3/2}$ and Al 2p signals ()[46,47].

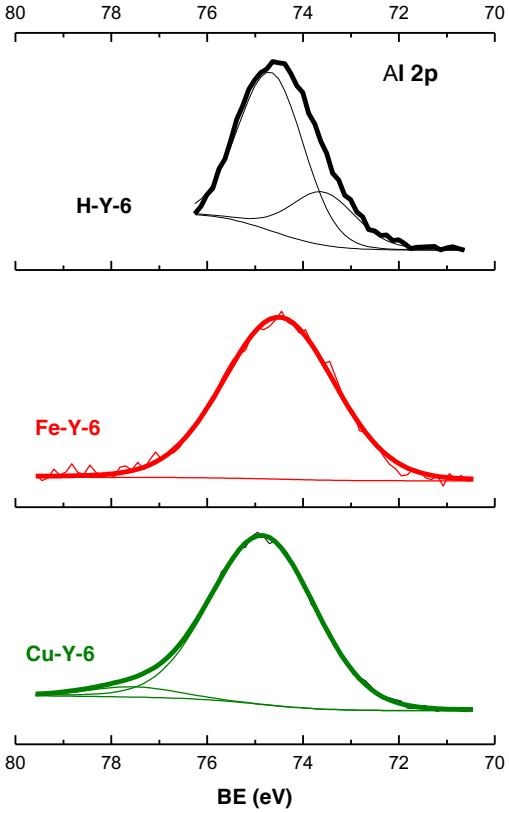

Figure 28. Al 2p core level spectra of Y-6 zeolites.

Concerning Beta zeolites, the surface Si/Al atomic ratio of H-Beta-12.5 resulted to be very similar to the synthesis ratio (12.7 *versus* 12.5), whereas in iron-exchanged Beta zeolite (Fe-Beta-12.5) increased to 15.1 and in copper-exchanged one (Cu-Beta-12.5) decreased to 8.23. EDXRF analysis reported a Si/Al atomic ratio of 12.2 for Fe-Beta-12.5, and 10.4 for Cu-Beta-12.5, close to synthesis values. Al 2p core level spectra of Beta-12.5-based zeolites were around 75 eV, typical of Al(III) (), together with the characteristic Si 2p values around 103.1

eV, similar to those reported for other BEA, MFI and MOR zeolites [53–55]. These zeolites were not studied by MAS-NMR, but a H-Beta zeolite with Si/Al atomic ratio of 13.7 (MAS-NMR) showed mainly Q1 (Si(1Al)) units and two broad resonance lines, around 53 and -2.5 ppm in ^{27}Al MAS-NMR spectrum, with mainly tetrahedral aluminum, but also octahedral because of the calcination process [56].

O 1s core level spectra exhibited a band at 532.5 eV, which can be deconvoluted in three contributions: i) the main around 532.6 eV, from O-Si bounds into the zeolitic framework [57,58], ii) 531.1 eV from O-Metal bounds [59], and iii) at highest binding energy and with the lowest intensity, around 534.3 eV, originated by carbonaceous contamination [60,61] (Figure 29).

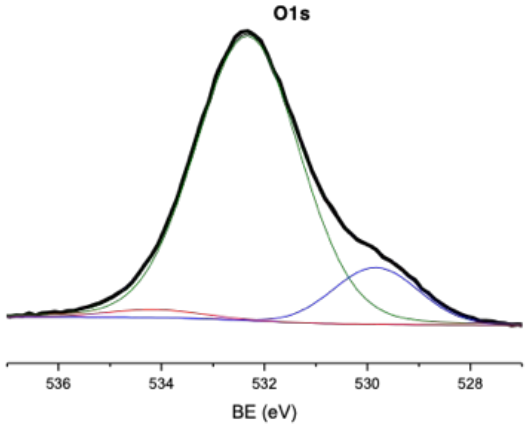

Figure 29. O 1s core level spectrum of H-Beta-12.5 zeolite.

Iron-containing zeolites

The nature and environment of iron species can be well studied by diffuse reflectance UV-vis and Mössbauer spectroscopies, as well as by MAS-NMR and XPS. In the present PhD work, XPS was used for this purpose. Si 2p and O 1s core level spectra had similar signals to the ones reported values for MFI, Y and MOR zeolites: O is around 532 eV and Si 2p around 108 eV, which correspond to tetrahedral silica [62]. XPS Fe core level spectra are complex and consist of many peaks contributions, depending on the oxidation state, and peaks can also be deconvoluted. Fe 2p and Fe 3p photoelectronic spectra of iron zeolites are represented in Figure 30, which show clear differences. The Fe 2p core excitations ($2p_{3/2}$ and $2p_{1/2}$ peaks) had a relative intensity of 2:1. In Fe-ZSM5-15 zeolite, Fe $2p_{3/2}$ and Fe $2p_{1/2}$ signals appeared at 710.5 and 724.6 eV, respectively, and no satellite was observed. However, a small peak at 714.3 eV could correspond to the Fe^{2+} satellite, and the Fe 3p signal, around 55.1 eV, could confirm the presence of Fe(II) [63,64]. Fe-Y-6 had similar binding energies for the Fe 2p, but higher intensities due to its higher iron content. With respect to Fe 3p spectrum, the presence of Fe(III) was suggested, with signals around 55.6 eV [64]. Fe-Beta-12.5 spectrum matched well with Fe 2p of Fe-ZSM5-15, but slightly more intense. Fe-Y-6, with the narrowest Fe $2p_{3/2}$, confirmed the presence of Fe(II), and Fe 3p at 55.7 eV suggested the existence of Fe(III). In Fe-Y-15 and Fe-MOR-10, prepared with the same synthesis method, two small satellites could be appreciated, one at about 718 eV and the other at about 729 eV, which indicated the presence of Fe(II), whereas Fe 3p at 55.9 eV, could correspond to Fe(III). Then, all these Fe 2p spectra, together Fe 3p ones, could point out the partial oxidation of Fe(II) to Fe(III) [64–

67], despite having exchanged Fe(II) under a nitrogen atmosphere during the preparation.

With regard to the Fe/Al content, the theoretical limits are up to 0.50 in Fe(II)-zeolites and 0.33 in Fe(III)-zeolites. The values obtained were 0.33, 0.47 and 0.41 for iron-exchanged ZSM-5, Y-6 and Beta-12.5 zeolites. The channel size and the iron type determine the final loading in the zeolite. Fe^{2+}cation-exchange in aqueous solution at the exchange pH could be as hydrated ferrous ion, with a similar size than Y and Beta zeolites channels, but wider than ZSM-5 channel, diffusing less easily and leading to lower exchange ratio.

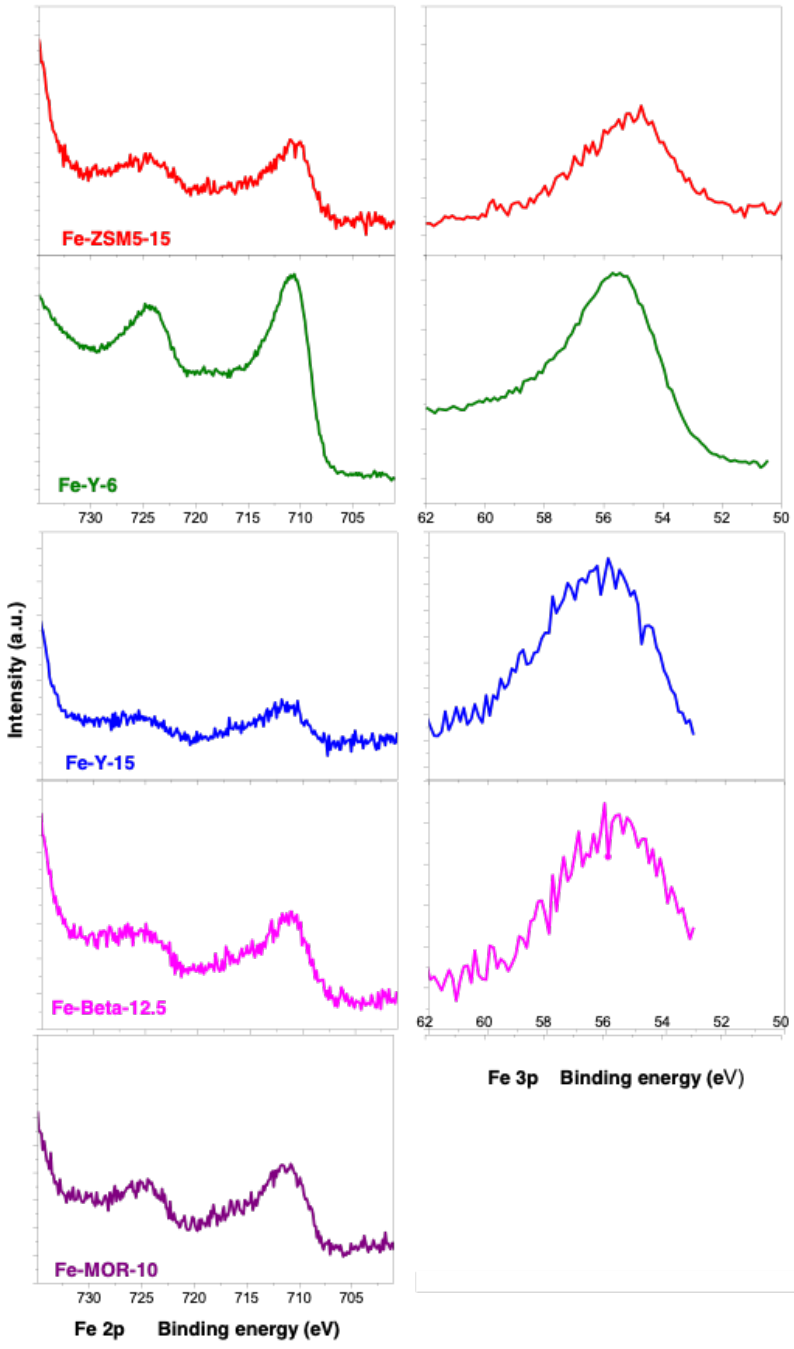

Figure 30. Fe 2p and Fe 3p core level spectra of iron-zeolites.

Gurgul *et al.* prepared three iron-containing Beta zeolites and studied the nature and influence of iron species by DR UV–vis, XPS and Mössbauer spectroscopy [31]. $Fe_{3.8}$SiBea, with an iron content of 3.8 wt.%, was similar to Fe-Beta-12.5 catalyst (3 wt.%). Nevertheless XPS Fe $2p_{3/2}$ signals of Fe_{15}SiBEA were around 712 eV, higher than 710.5 eV, strongly indicating the presence of Fe(III) species, whereas Fe $2p_{3/2}$ signals of Fe-Beta-12.5 catalysts Fe $2p_{3/2}$ signals appeared below 710.5 eV.

Pérez-Ramírez *et al.* studied the influence of the preparation method on Fe-MFI zeolites, confirming the heterogeneous distribution of iron species and the degree of iron clustering in Al-containing Fe zeolites [68].

Si/Fe atomic ratios increased with the Si/Al ratio, as expected. The zeolite with the highest aluminum content possessed also the highest iron content, so the catalyst with the highest iron loading was Fe-Y-6 , which possessed a Fe/Si ratio of 7.75, whereas Fe-ZSM-5, a silicon-rich zeolite type, possessed a Fe/Si ratio of 114.

Copper-containing zeolites

The copper in exchanged zeolites can vary its oxidation state, and most studied Cu-Y zeolites include Cu(I) and Cu(II), which can occupy three different sites in the Faujasite framework structure, which were referred as I(I'), II(II') and III(III') [69], and being the most effective for catalysis Type III sites, because of easier accessibility [70]. These sites are illustrated in Figure 31.

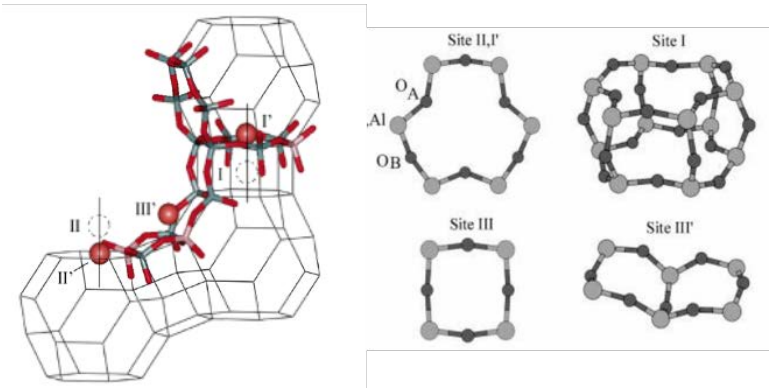

Figure 31. I, II, III type sites for Cu cations in the Faujasite framework [70].

Cu 2p peaks have significantly split spin-orbit components, with Δ= 19.75 eV, being in the range 19.3-20.1 for Cu-ZSM5-15, Y-6 and Beta-12.5 catalysts. Cu(II)spectra exhibited observable shake-up satellites around 943-945 eV. In the prepared copper zeolites, satellites are near 945 eV. With respect to copper cations in Cu-ZSM5-15 zeolite, Cu $2p_{3/2}$ at 933.5 eV binding energy (shifted from 933 eV) as much as two broader shake-off bands (around 940-945 and 960-965 eV regions), confirmed the presence of Cu (II). A similar behavior was observed for Cu-Y-6 and more evident for Cu-Beta-12.5 zeolites (). For copper zeolites, Auger spectra were also obtained. In Cu-ZSM5-15, Auger Cu LMM spectrum could be deconvolved into two bands at 338.6 and 341.1 eV ().

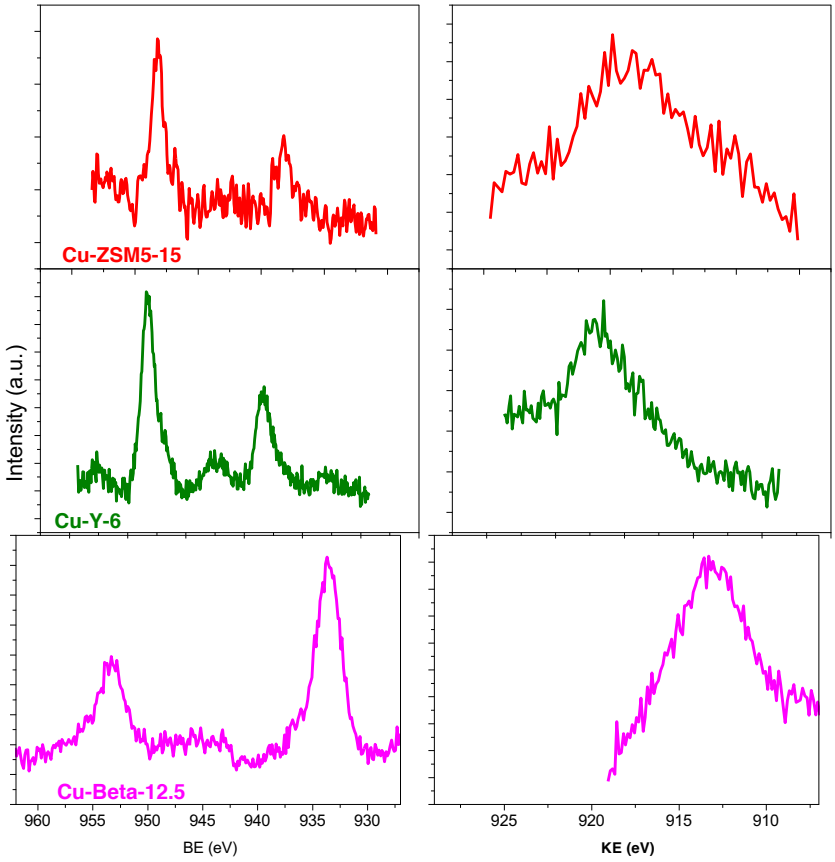

Figure 32. Cu 2p core level spectra (left) and Cu LMM Auger spectra (right) of copper containing zeolites.

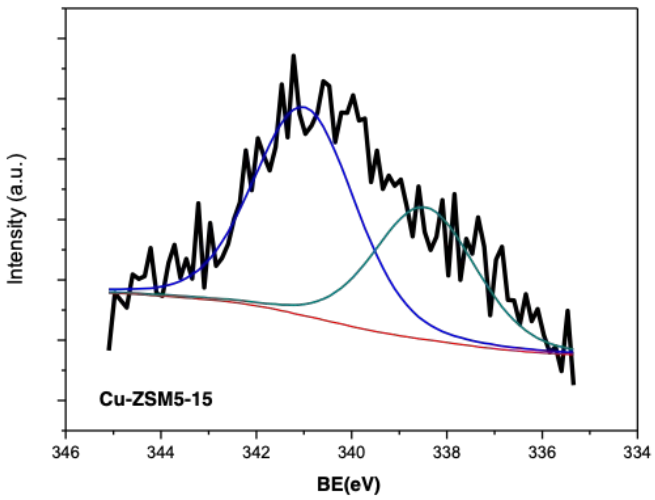

Figure 33. Cu LMM Auger spectrum in Cu-ZSM5-15 zeolite.

Taking into account the kinetic energy (KE Cu LMM) and the binding energy of the photoelectron (BE Cu $2p_{3/2}$), the corresponding modified Auger parameter, α´, were calculated[3] (α´= KE Cu LMM + BE Cu $2p_{3/2}$), obtaining the values of 1853.2 and 1850.7 eV, confirming not only the presence of Cu(II) but also the formation of Cu(I), which, in this case, should have been produced by photo-reduction during the X-ray exposure [71–73]. Another cause of the presence of Cu(I) in this silicon rich zeolite could be the interaction between Cu cations and the zeolite structure, which would be capable to maintain at higher temperature Cu cations as Cu(I) [74]. Cu $2p_{3/2}$ binding energy and Cu LMM kinetic energy represented in a Wagner

[3] $\alpha' = KE_{CuLMM} + BE_{Cu\ 2p3/2}$

plot contributed to distinguish copper oxidation states. The respective values for the copper zeolites were represented, confirming the presence of both Cu(I) and Cu(II), being the amount of Cu(II) higher in Cu-Beta-12.5 catalyst(Figure , [71]).

The more aluminum content, the more copper content, in the same way than in iron-exchanged zeolites. Thus, Cu-Y-6, Cu-Beta-12. 5 and Cu-ZSM5-15 possessed Si/Cu atomic ratios of 43, 68 and 70, respectively. There was a noticeable difference between copper- and iron-exchanged zeolites: the enrichment of aluminum on surface compared to the respective precursors, which were probably due to aluminum gradients from the inner to outer regions of zeolites [47,75].

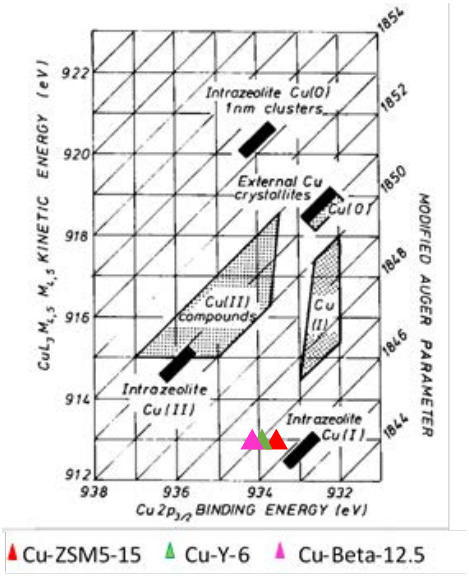

Figure 34. Wagner plot: Cu $2p_{3/2}$ binding energy and Cu LMM kinetic energy for copper containing zeolites.

Acidic carbons

The surface chemistry analysis were reported by Rosas *et al.* [38]. Main elements on the carbon surfaces were carbon and oxygen, and lower amounts of phosphorous. Surface phosphorus compounds formed in the activation step were stably bonded to carbon, as did not leach with acids or hot water. The acidic carbons possessed high surface oxygen from phenolic, lactonic, carboxylic and phosphorous-containing groups.

6.1.3. Acidity characterization: NH_3-TPD and Pyr-FTIR spectroscopy measurements

The total acidity of catalysts was determined by temperature-programmed desorption of ammonia, which also allows to determine both the quantity and the strength of acid sites. Acidity strength was referred to temperature at which maximum ammonia desorption occurred, or to the amount of ammonia which remains adsorbed in a determined temperature range. The ammonia desorption was measured in the range 100-550 ºC. The interval chosen to compare the acid strength of different materials was 200-300 ºC, because reaction temperature was between 175 and 205 ºC, but it is also necessary to take into account that the catalytic process were carried out under autogenous pressure due to the boiling points of water and organic solvents, which can influence on the acidity.

Once calculated strength and total acidity of catalysts, pyridine as probe molecule was also adsorbed to calculate available acid sites to large sugar molecules and, coupled to FTIR spectroscopy, allows to

distinguish between Brönsted and Lewis acid sites, as both of them condition the catalytic behavior.

Data obtained from ammonia-TPD and pyridine-FTIR analyses are reported in and .

Table 7. NH_3 temperature-programmed desorption data of catalysts

Sample	Total NH_3	Tmax. desorp.	100-200 ºC (weak)	200-400 ºC (medium)	400-550 ºC (strong)
	µmo l g^{-1}	ºC		µmo l g^{-1}	
Ta_2O_5 mes.	228	297	16	141	57
5Al-M-41	956	161	300	555	101
10Al-M-41	522	267	64	309	109
KIT6-C	34	164	11	12	11
10Al-KC1	146	140	132	5	9
10Al-K-C2	291	164	116	161	14
H-Z-15	1259	167	308	636	249
Fe-Z-15	1131	178	347	673	101
Cu-Z-15	1126	173	286	681	144
H-Y-6	1676	185	337	1004	273
Fe-Y-6	888	175	293	489	105
Cu-Y-6	1169	169	423	644	101
H-B-12.5	1217	160	393	634	207
Fe-B-12.5	771	172	307	459	63
Cu-B-12.5	971	171	400	527	46
HA3500	622	174	309	208	105
HA31500	534	171	253	250	31
HA31800	343	158	157	166	20
L3500	806	172	247	507	52
L31500	256	161	112	61	54
L31800	244	155	114	115	16

M: MCM-41, Z: ZSM5, B: BETA-12.5

Table 8. Adsorbed pyridine on Brönsted and Lewis acid sites and adsorbed ammonia after evacuation at different temperatures on tantalum oxide, MCM-41 types and zeolite-based catalysts.

	Pyridine μmol g^{-1} Brönsted/Lewis				NH_3 μmol g^{-1}
Sample	**r.t.**	**100 ºC**	**200 ºC**	**300 ºC**	**200 ºC**
Ta_2O_5	-/94	-/68	- / 22	- / -	142
5Al-M	193/64	213/66	136 /64	109 /60	328
10AlM	254/137	280/149	223/165	100/254	292
H-Z15	24/143	29/143	27 /103	21 /91	503
FeZ15	76/167	183/272	235/171	289/129	260
CuZ15	63/746	50/644	132/334	93 /80	408
H-Y-6	50/613	60/426	105/276	92 /113	726
Fe-Y-6	- /732	-/459	- /205	- / -	292
Cu-Y6	33/1532	39/1183	161/717	252/249	317
H-B	27/833	40/772	- /742	- /236	445
Fe-B	- /684	- / 591	- / 410	- /177	162
Cu-B	- /1359	- / 858	- / 453	- / -	239

M: MCM-41, Z: ZSM5, B: BETA-12.5

Mesoporous Ta_2O_5, MCM-41 and KIT-6

The strength of acid sites was studied by considering the desorption temperature at which ammonia molecules are desorbed, and they were classified into weak (below 200 ºC), medium (200-350 ºC) and strong

(higher than 350 ºC). Mesoporous Ta_2O_5 and 10Al-MCM-41 exhibited maxima desorption temperatures at 297 and 267 ºC, respectively, remaining 62% and 56% of ammonia adsorbed below 300 ºC, as is shown in Figure 34.

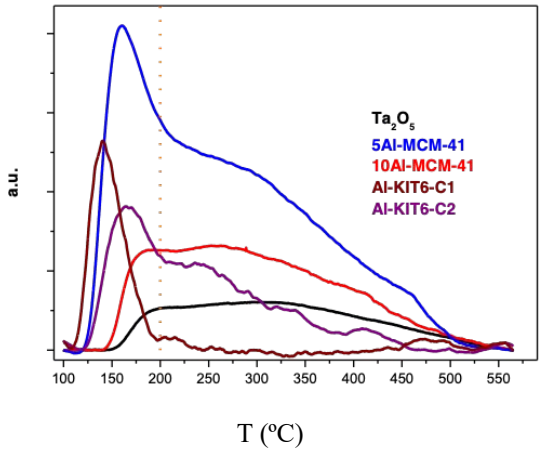

Figure 34. Ammonia-TPD of mesoporous tantalum oxide, MCM-41 and KIT6-C based catalytsts from room temperatura to 550 ºC.

Al-KIT6-C2 and 5Al-MCM-41 showed lower desorption temperatures (161 and 164 ºC, respectively), remaining less than 40% of ammonia adsorbed above 200 ºC. Al-KIT6-C2 was the weakest, loosing most of ammonia molecules (90%) below 200 ºC and with maximum desorption at 140 ºC (Figure 35). The order in total acidity was: 5Al-MCM-41 (956 μmol g^{-1}, 1.3 μmol m^{-2}) > 10Al-MCM-41 (528 μmol g^{-1}, 0.9 μmol m^{-2}). The amount of ammonia increased with the aluminum content in MCM-41 and KIT-6 catalysts, as expected [16,76,77]. Al-KIT6-C2 and mesoporous Ta_2O_5 desorbed 291 (0.6) and 228 μmol g^{-1} (2.9 μmol m^{-2}), respectively. This high density of acid sites of mesoporous tantalum oxide must be highlighted, having found similar values in the literature (3.1 μmol m^{-2}) [78].

Comparing the ammonia values desorbed from Al-KIT6-C1, Al-KIT6-C2 and other reported aluminated KIT -6 silicas [16], it was observed that the acidity was maximum when Si/Al molar ratios were between 10 and 33. Taking into account both, strength and amount of acid sites (calculated from ammonia adsorption), 10Al-MCM-41 could be considered the more acidic catalyst, due to high number of acid sites as well as to its high strength [13], followed by mesoporous tantalum oxide and 5Al-MCM-41. This one, despite of having the highest aluminum content and, therefore, the highest number of acid sites, resulted weaker. This weakness could be conditioned by the presence of extra-framework octahedral aluminum on the outer surface.

Considering the pretreatment at 550 ºC with He gas, previous to ammonia adsorption, the majority of the coordinated water molecules were desorbed and the adsorbed ammonia could be coordinated to the aluminum or tantalum atoms. The total amount of desorbed ammonia could facilitate the calculation of available acid sites, resulting for the mesoporous tantalum oxide a $1Ta_2O_5$: 0.16 NH_3 ratio, which was a value near to the one found for the coordinated water ($1Ta_2O_5$: 0.19 H_2O), thus confirming that the acidity of this catalyst was mainly originated by the presence of coordinated water molecules and coordinated OH groups to tantalum ions. Acidic properties of tantalum oxide are influenced by the symmetry and oxidation state of metal cation, which was Ta(V) in the mesoporous tantalum oxide [79]. For 10Al-MCM-41 and 5Al-MCM-41, the ratio were 1Al : 0.3 NH_3, which meant that one third of the aluminum atoms in the MCM-41 mesoporous structure provided acid sites.

In mesoporous tantalum oxide, the pyridine adsorbed was 94 μmol g^{-1} at room temperature and 22 μmol g^{-1} at 200 ºC, and only Lewis acid sites were detected (Figure 35). The comparison between coordinated water ($1Ta_2O_5$: 0.19 H_2O) and adsorbed ammonia ($1Ta_2O_5$: 0.16 NH_3) confirmed that this acidity came mainly from coordinated water molecules and OH groups to tantalum ions, as Brönsted acid sites. From pyridine adsorption the ratio resulted to be 0.08 Pyr : 1Ta, which meant that all Brönsted acid sites, after outgassing at 250 ºC under vacuum, were transformed into Lewis type acid sites because of water and OH groups loose. The presence of these groups was also confirmed by Raman and FTIR spectroscopies. In the range 200 – 1200 cm^{-1}, a characteristic Raman band at 660 cm^{-1} corresponded to Ta–O stretching vibrations of octahedral TaO_6, also detected in the FTIR spectrum at 2235 cm^{-1}, and a shoulder at 940 cm^{-1} in the Raman spectrum corresponded to the symmetric stretching mode of terminal Ta=O bonds. Peaks at 1615 and 3400 cm^{-1} (FTIR) could be associated to the vibration modes of water molecules and OH groups. Lewis character predominant in acid sites of tantalum oxide had been previously reported by Baltes *et al.* [80].

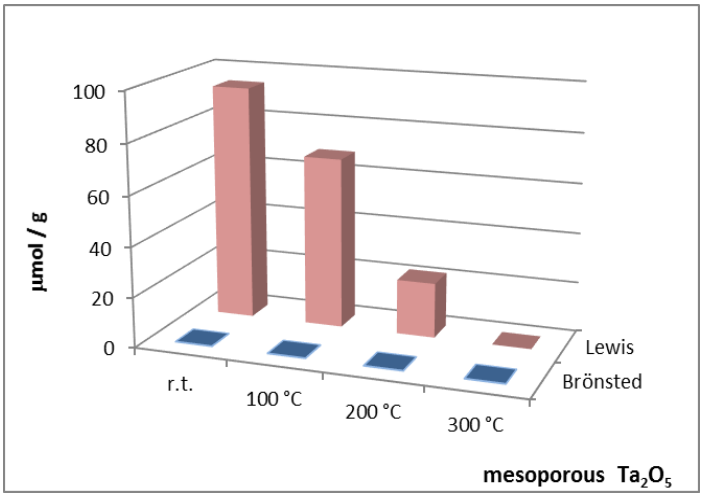

Figure 35. Adsorbed pyridine after evacuation at different temperatures on mesoporous tantalum oxide.

With regard to MCM-41 silicas, the corresponding Pyr-FTIR spectra showed both strong bands at 1450 and 1550 cm^{-1}, indicating the presence of both Lewis and Brönsted acid sites. They remained even after pyridine evacuation at 300 ºC, primarily in 10Al-MCM-41, evidencing the acidity strength already observed. Brönsted acid sites, associated to silanol and isolated Si(OH)Al hydroxyl groups, were mainly responsible for the total acidity, but it was remarkable the presence of both Lewis and Brönsted acid sites [13] (). Several types of surface silanol groups with different acidic properties can be present: terminal, geminal, vicinal and nests [81–83]. Vicinal and nests, generated at framework defect sites, had been observed around 3700 and 3590–3600 cm^{-1}, respectively, by Vaschetto *et al.* [12] in Al-MCM-41 with Si/Al molar ratios 20 and 60, lower than the present materials, although they did not detected terminal silanol groups (around 3740 cm^{-1}).

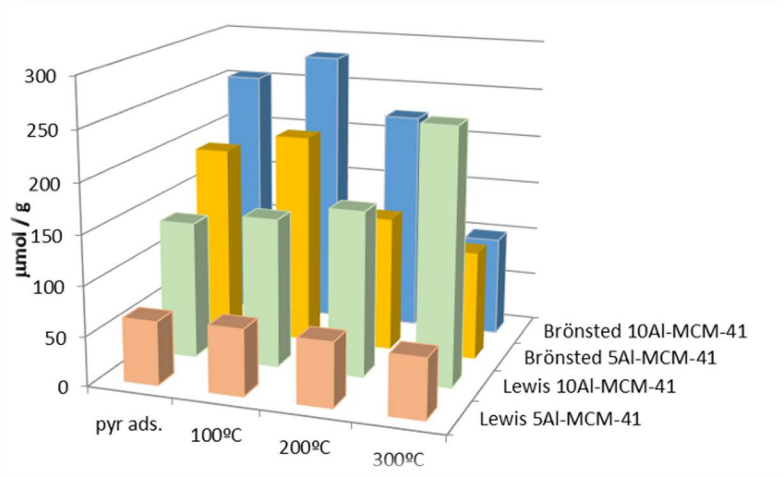

Figure 36. Adsorbed pyridine after evacuation at different temperatures on MCM-41-based catalysts.

The acidity of different silanol species were also studied by Sato *et al.* [84], who found the ease of proton escape from silanol was in the order: nest, vicinal, geminal and terminal. Therefore, nest silanol groups can give a proton to a basic molecule easily, providing the strongest Brönsted acid sites. In relation to Lewis acidity on Al-MCM-41 material, they are provided by two different species: intra-framework $Al(OSi)_3$ and extra-framework alumina, formed during calcination. The introduction of aluminum into the framework not only increases Lewis acidity, but also Brönsted one, because of the increase of nest silanol groups. 5Al-MCM-41 had a higher aluminum content, but Lewis and Brönsted acidities were lower than in 10Al-MCM-41. Pyridine coordinated to Lewis acid sites remained around 60 µmol g^{-1} in 5Al-MCM-41, whereas more than 150 µmol g^{-1} was measured for 10Al-MCM-41, and even 254 µmol g^{-1} at 300 ºC.

Moreover, the amount of Brönsted acid sites was higher in 10Al-MCM-41, excepting at 300 ºC, which were almost the same. This could be due to silanol groups, whose hydroxyl groups are not capable to protonate pyridine, but can form H bonds with it, disappearing at 200 ºC.

Zeolites: ZSM-5, Y and Beta.

The values of total acidity of protonated zeolites were much higher than those of mesoporous catalysts: 1217, 1259 and 1676 μmol $NH_3 g^{-1}$ for H-Beta-12.5, H-ZSM5-15 and H-Y-6, respectively, although the surface density of desorbed ammonia was similar, and even the maxima desorption temperatures, from 160 to 185 ºC, and the ammonia remaining above 200 ºC (around 40%), as can be observed in . Taking into account the surface molar ratio between adsorbed ammonia and aluminum content, H-ZSM5-15 headed with a ratio 1Al : 1.2 NH_3, whereas H-Y-6 and H-Beta-12.5 showed ratios of 0.5 and 0.7, respectively. The high ratio in H-ZSM5-15 could involve acidity from hydroxyl groups besides aluminum atoms. The acidic strength of the bridging hydroxyl groups in H-ZSM5-15 had been previously reported, confirming that its strength remained constant at Si/Al molar ratios higher than 10 [85].

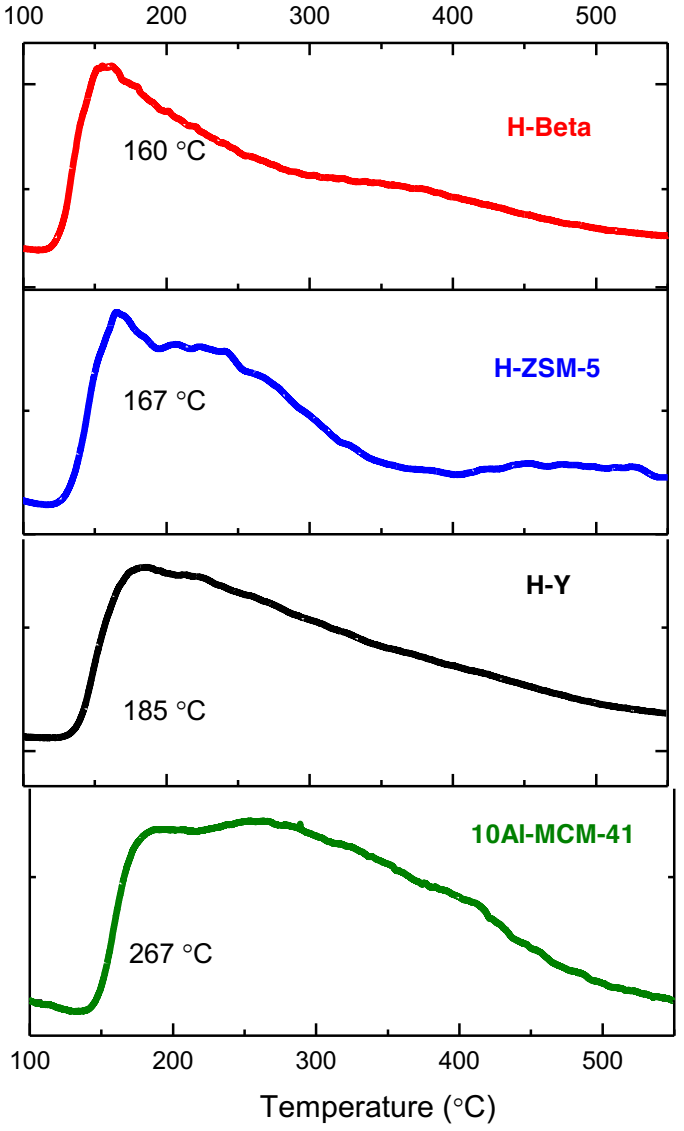

Figure 37. Ammonia temperature-programmed desorption in the range 100-500 ºC of protonated zeolites and 10Al-MCM-41.

H-Y-6 zeolite (Si/Al molar ratio of 6) showed 426 Pyr μmol g^{-1} of Brönsted acid sites at 100 ºC, and decreasing until 276 Pyr μmol g^{-1} at

200 ºC, similar to other reported H-Y zeolites [51]. Besides, in these reported USY zeolites, Brönsted acidity increased with aluminum content, whereas Lewis type decreased. The amount of Lewis acid sites decreased from 613 to 566 Pyr μmol g^{-1} at room temperature and from 276 to 48 Pyr μmol g^{-1} at 200 ºC as the aluminum content increased (for H-Y-6 to H-Y-2.6, respectively) ().

Regarding metal-exchanged zeolites, the acidity kept constant for ZSM-5 zeolites (1Al:1.2NH_3), but diminished slightly in the other cases: from 0.5 to 0.4 and from 0.7 to 0.6 mol NH_3 per atom of aluminum, in the Y and Beta zeolites, respectively. Thus, around 50% of the aluminum is associated with acid sites. In relation to iron-exchanged zeolites, the presence of this transition metal lowered total acidity, in general, but peaks were shifted to higher desorption temperatures (). The peaks with maxima at 160-180 ºC could correspond to Lewis acid sites [86], which was confirmed by Pyr-FTIR spectroscopy (). The observed shift had also been reported for other iron-containing zeolites with lower iron content than Fe-ZSM5-15 (1.7 wt%) and Fe-Beta-12.5 (3 wt%) by Borón *et al.*[31], but they suggested that iron ions could also adsorb ammonia molecules, which we did not observe. With respect to copper, not only copper ions into the framework can be considered as active sites for catalysts, but also isolated copper ions [87,88], copper ion structures with extra-lattice oxygen [89,90] and even copper oxide nanoparticles [91] have been reported as so. They act mainly as Lewis acid sites.

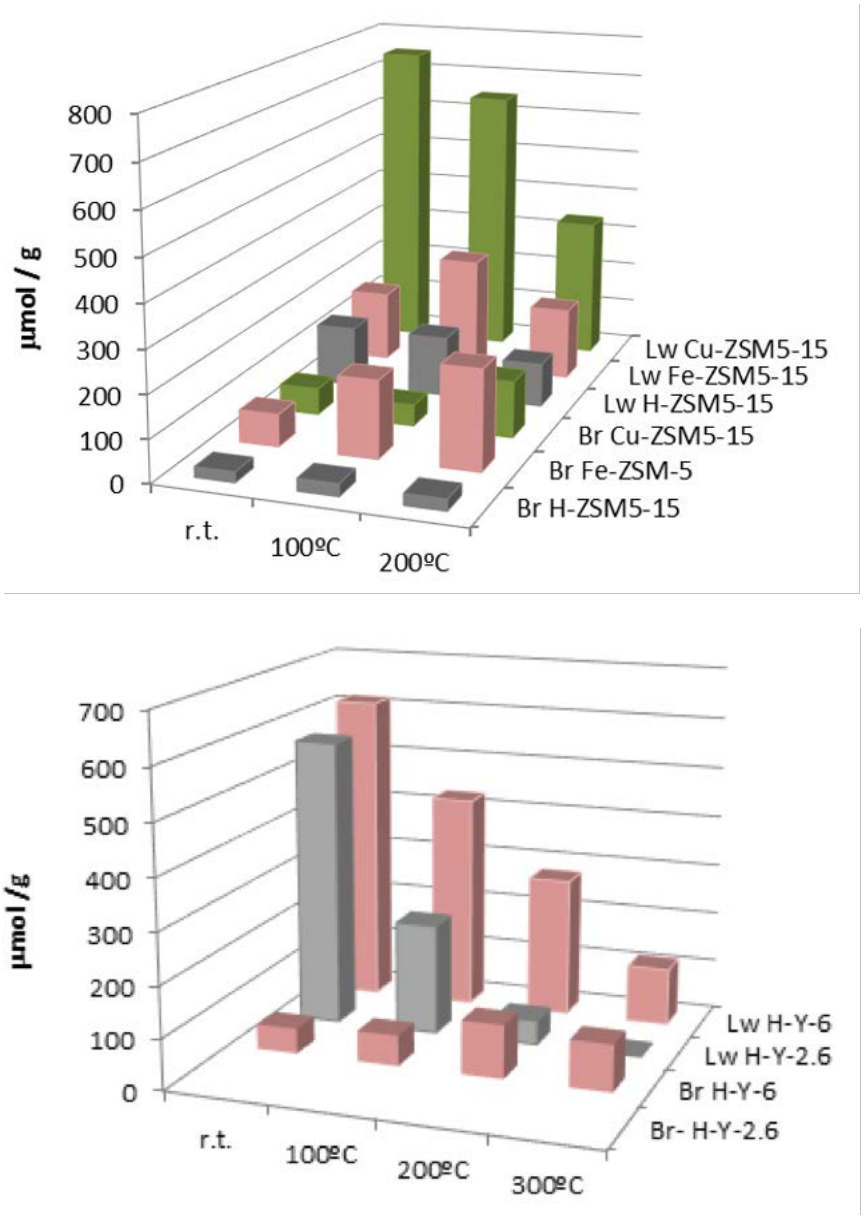

Figure 39. Adsorbed pyridine on ZSM-5 (above) and Y (below) zeolites, after evacuation at different temperatures.

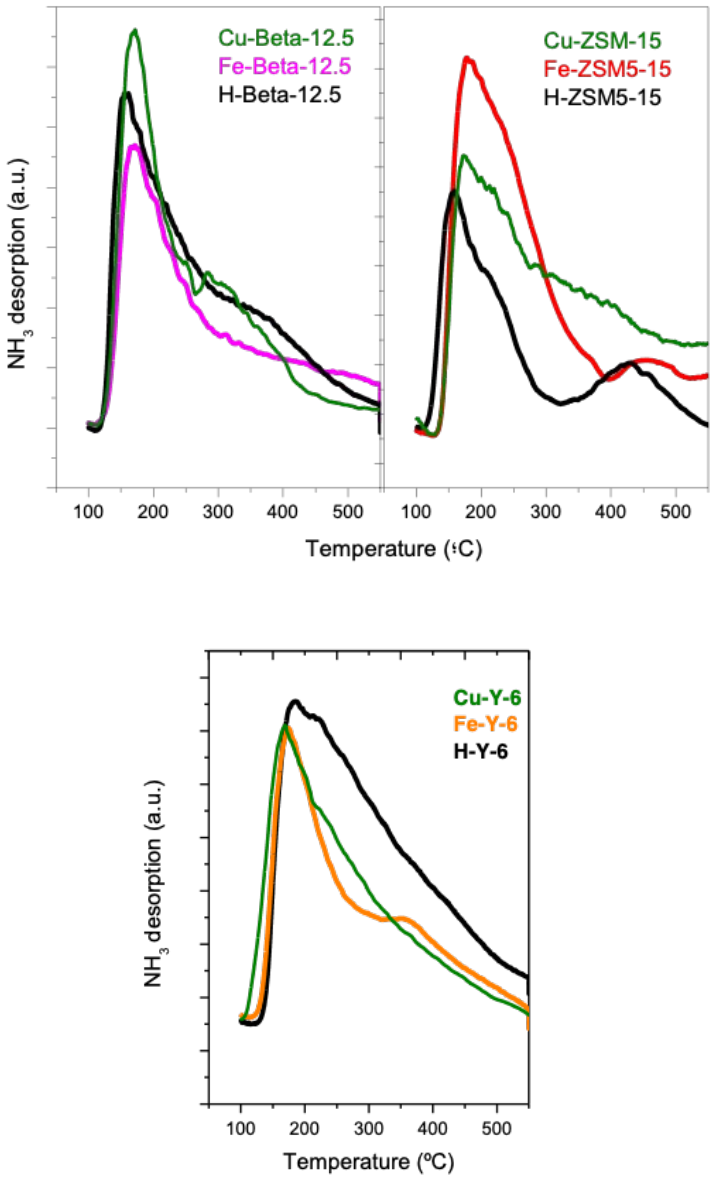

Figure 40. Ammonia TPD of catalysts based on Beta, ZSM-5 and Y zeolites.

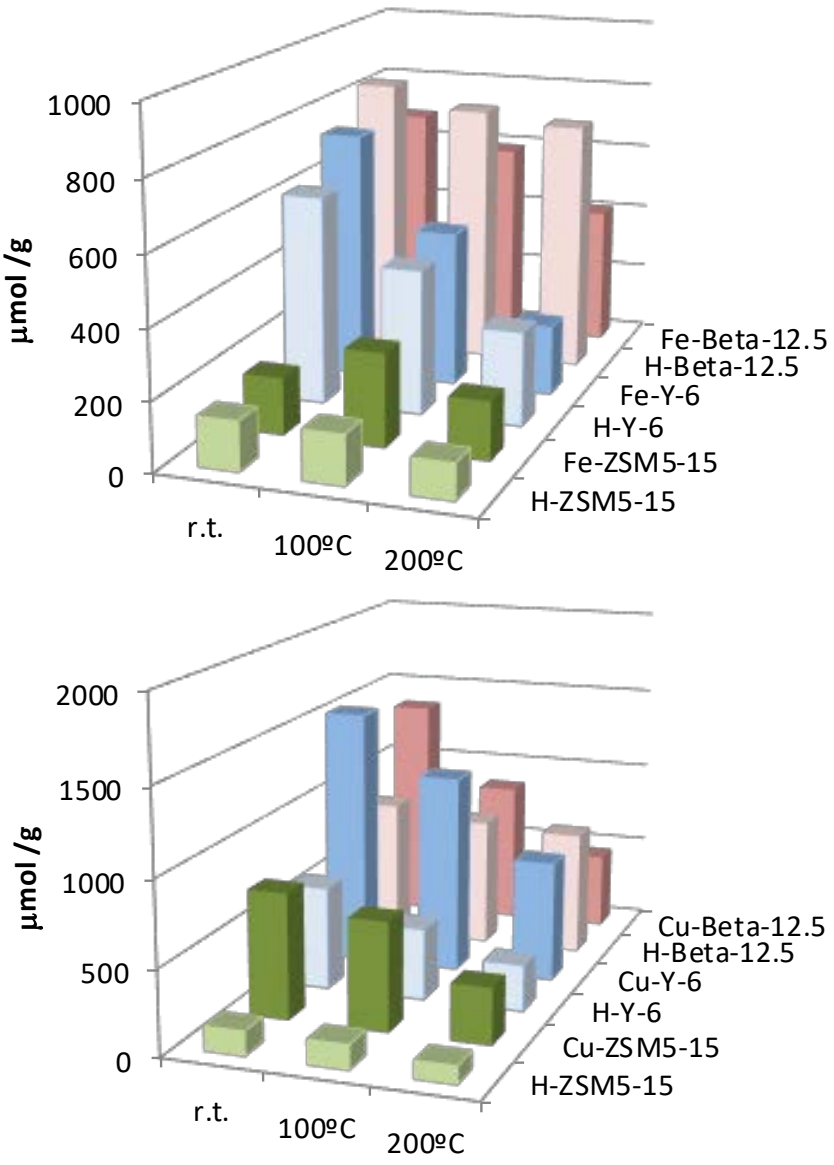

Figure 38. Adsorbed pyridine from r.t. to 200 ºC on Lewis acid sites in protonated, iron and cupper exchanged (H-, Fe- and Cu-) zeolites.

In Fe- and Cu-ZSM5-15 catalysts, Brönsted acidity increased with the metal cation-exchange, because of nest silanol groups are generated by modification of the zeolitic framework. These Brönsted acid sites areassociated to bridging Al-O(H)-Si groups located at the internal surface of channels and cavities of zeolite structure. The increase in Brönsted acidity came from iron-exchanged cations, whereas copper cations specially altered Lewis acidity. Acid sites concentration can be attributed to higher proton activities due to the lower negative charge density of the zeolitic framework after the cation-exchange processes [92]. Lewis acid sites concentration also increased with the metal cation. Despite H-ZSM-5 possessed protons, its Lewis to Brönsted ratio was the highest, decreasing from 3.8 to 0.7 and 2.5 in Fe-ZSM-5 and Cu-ZSM-5, respectively (at 200 ºC), because of stronger modifications of the Brönsted acidity than on the Lewis one, and, mostly, because of Al atoms in the ZSM-5 zeolites were responsible for acidity (). Ammonia TPD showed similar total acidity for H-, Fe- and Cu-ZSM5-15 catalysts, but Pyr-FTIR spectroscopy data pointed out their different acidities ().

Regarding Beta zeolites, both ammonia TPD () and pyridine FTIR spectroscopy data () showed lower and weaker acidity of Fe-Beta-12.5 in comparison with H-Beta-12.5, being only Lewis type. Copper introduction increased notably Lewis acidity, but became weaker, with only 453 μmol g^{-1} adsorbed at 200 ºC, whereas the protonated zeolite adsorbed 742 μmol g^{-1}. No formation of an additional amount of Brönsted acid sites occurred. Copper in extra-framework positions, deduced from XRD patterns, resulted in formation of more Lewis acid centers. Similar behavior was reported for other Cu-BEA (Beta) zeolites [32]. For Y zeolites, iron exchange affected to the acid

character below 200 ºC, weakening Lewis acid sites. Copper exchange increased remarkably the concentration of Lewis acid sites, although keeping the same strength, loosing 50% of them below 200 ºC.

All these data show that it is feasible to modify the nature of the acid sites of zeolites by thermal or ion-exchange treatments.

Acidic carbons

Acidity measurements of carbons can be determined by pyridine adsorption [37], titration with NaOH [93] or ammonia TPD [94]. Similar acidic carbons impregnated with phosphoric and nitric acids were treated under a He flow at 300 ºC for 60 min., prior to ammonia adsorption. The L- and HA- carbons exhibited low total acidities, as inferred from desorbed ammonia (μmol g^{-1}): 158 (HA3500), 225 (HA31500), 60 (L3500) and 224 (L31500). The ammonia TPD study was also carried out by using a milder pretreatment (100 ºC) [95]. An evident loss of acid sites occurred after the pre-treatment at higher temperature (). L31500 and HA31500, prepared by using a similar impregnation method and ratio, resulted as the most acidic carbons, followed by HA3500 and L3500. The thermal treatment at 800 ºC during the synthesis did not improve the acidity, and each carbon type activated at 800 ºC resulted in lower acidity than the ones activated at 500 ºC in their respective series (HA- or L-). Acid sites remaining over 200 ºC were around 50 % in HA3500, HA31500 and LA31500, and higher L3500, HA3500 and HA31500, and lower in the other carbons (Figure 40). As for the acid sites surface density, L3500 and HA3500 led again, with 0.6 and 0.5 NH_3 μmol g^{-1}.

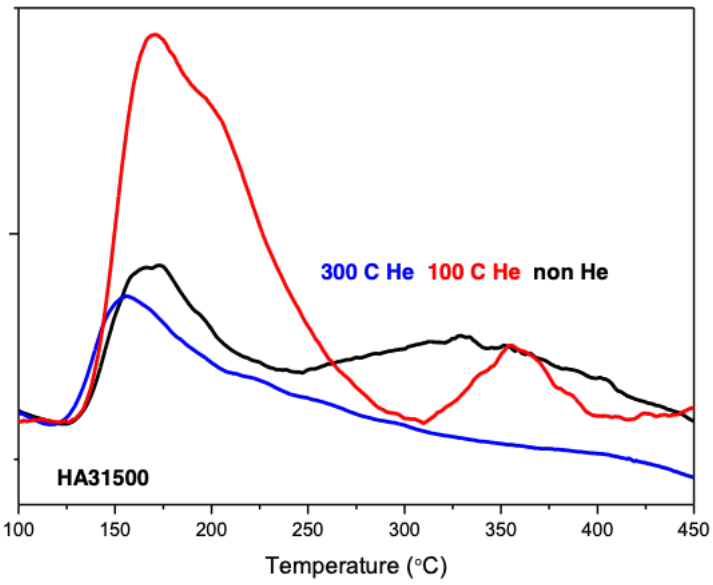

Figure 39. Ammonia TPD on HA31500 acidic carbon without previous gasification (black), after degasification in He at 100 ºC (red) and at 300 ºC (blue).,

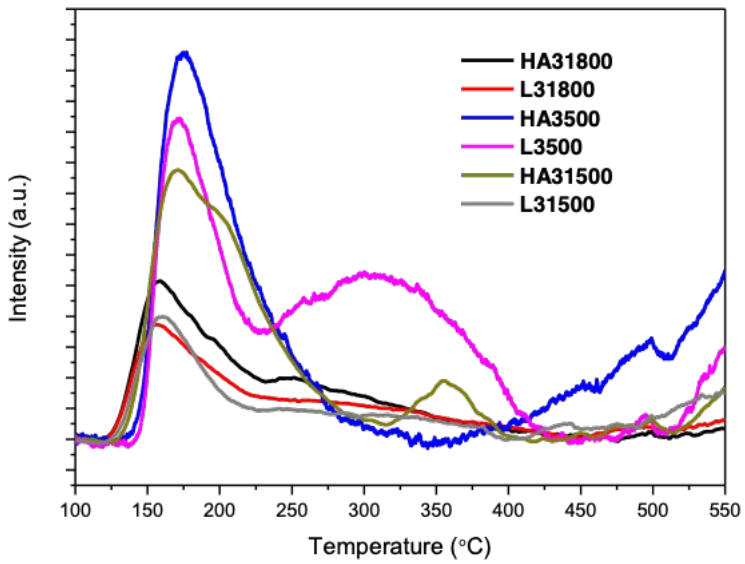

Figure 40. Comparison of ammonia TPD of the acidic carbons.

In general, carbons treated with higher phosphoric acid concentrations possessed higher concentration of acid sites [94], but in the present phosphorylated carbons, similar acid concentrations led to different acidities.

Zhao *et al.* studied sulphonated carbons, and the ones impregnated with more concentrated sulfuric acid solutions resulted the least acidic of all [93]. Other reported carbons from hemp residues, activated at 450 ºC with impregnation ratios of 1 and 2, desorbed 1850 and 1020 NH_3 μmol g^{-1}, respectively [96]. A similar carbon to HA3500, prepared by Bedia *et al.* [95], also from olive stone, impregnated with phosphoric acid with a ratio of 1 and treated at 500 ºC possessed 956 NH_3 μmol g^{-1}, with 390 NH_3 μmol g^{-1} as weak acidity and 303 NH_3 μmol g^{-1} as moderate acidity. They assigned weak acidity to

hydroxyphenolic groups and pointed out that surface acidity of this type of carbons was mainly Brönsted type, being originated by the most oxidized phosphorus groups, C–O–PO_3, $(C–O)_3PO$, C–PO_3 and C_2PO_2. Temperatures of maximum ammonia desorption were in the 155-174 ºC range, confirming weak and moderate acidity strength in these catalysts, while L3500 showed a second maximum at 305 ºC, which indicated stronger acidity (Figure 40).

The acidity was also dependent on the amount of phosphorus retained on the surface, then, impregnation labelled as "3" (L3500 and HA3500) could produce better phosphorous retention than -31500 or -31800 materials [97,98]. L3500 could be quite suitable for acid catalysis because of a large surface BET area, wide mesopores which represented over 80 % of the pore volume, acidity and weak, medium and strong acid sites.

6.2. Catalytic Activity in glucose and fructose dehydration to 5-hydroxymethylfurfural.

Once the physicochemical characterization of the catalysts was carried out, their catalytic activity was evaluated in the fructose and glucose dehydration to 5-hydroxymethylfurfural (HMF). A large number of reactions were carried out, varying the experimental conditions, in order to optimize the main variables to attain HMF yields. Likewise, the reuse capability of these catalysts, according to the principles of heterogeneous catalysis and Green Chemistry, was evaluated. Research was organized mostly varying the following parameters to study their influence:

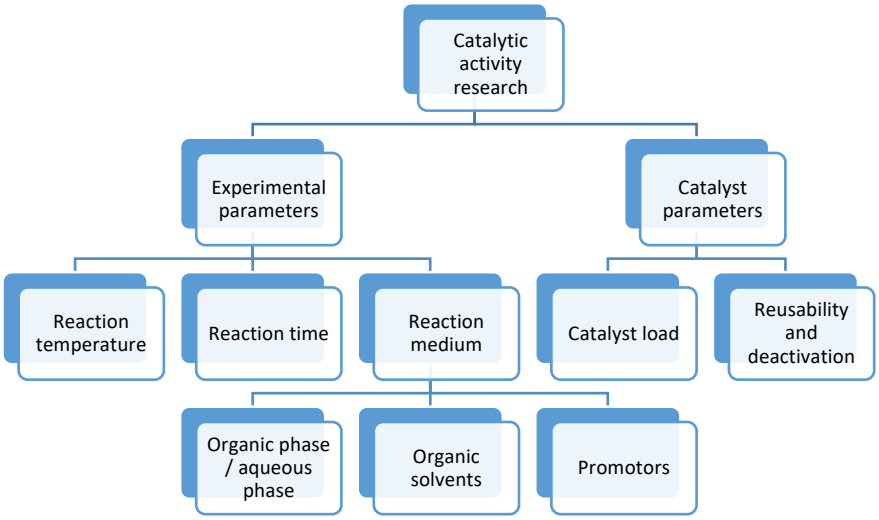

6.2.1. Mesoporous tantalum oxide

Previous works dealing with tantalum-based catalysts have been performed by the Research Group "Nuevos Materiales Inorgánicos" (Departamento de Química Inorgánica, Cristalografía y Mineralogía. Universidad de Málaga), mainly on: i) the synthesis and application of acidic tantalum oxide supported on SBA-15 for the methanolysis of sunflower oil for biodiesel production [99], ii) mesoporous tantalum phosphate for the same catalytic process [100] and iii) mesoporous tantalum phosphate for glucose dehydration to 5-(hydroxymethyl)furfural [101]. Thus, the preparation of mesoporous tantalum oxide, instead of supported on a mesoporous material, was the first objective of this PhD work. Once synthesized and characterized, mesoporous tantalum oxide was tested as catalyst in the glucose dehydration to 5-(hydroxymethyl)furfural.

Reaction temperature

To study the influence of the reaction temperature, the settled experimental conditions were 150 mg of glucose in 1.5 mL of water, in contact with 50 mg of catalyst, 3.5 mL of methyl isobutyl ketone (MIBK) as organic phase and 90 min. as reaction time. Several catalytic reactions were carried out at 155, 165, 175 and 185 ºC. The catalytic results (Figure 41) revealed that glucose conversion rose with temperature, achieving a maximum value close to 76.5% at 185 ◦C. Only fructose and HMF were detected and quantified as reaction products, being fructose favored at lower temperatures (16.3% selectivity at 155ºC), whereas HMF selectivity increased up to 175 ºC (33.5%) and decreased at 185 ºC (31.1%).

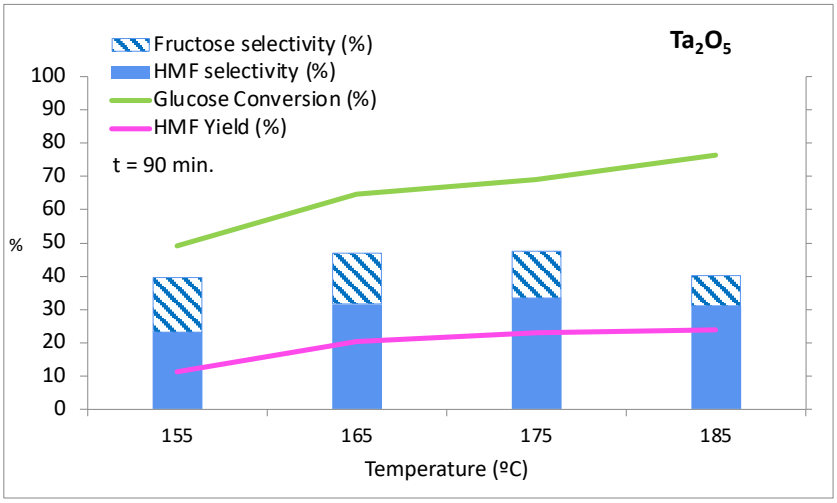

Figure 41. Influence of reaction temperature on glucose conversion to HMF over mesoporous tantalum oxide, after 90 min., in biphasic system water/MIBK with S/C ratio 3.

Levulinic acid was not detected, but at higher temperatures, insoluble humins could be clearly observed. The formation of these humins and soluble polymers in the medium of reaction and on the surface of the catalyst caused the HMF selectivity to drop slightly but in a longer reaction time. The detection of fructose, mostly at lower temperatures, agreed with the two-stages process proposed by Ordomsky *et al.* [102], with a first step in which glucose isomerized into fructose and a second step in which fructose was dehydrated to HMF. Nevertheless, a direct dehydration of glucose to HMF cannot be ruled out. The hexose isomerization was carried out on Lewis acid sites, whereas the dehydration occurred on Brönsted acid sites. In the catalytic reaction with mesoporous tantalum oxide, both acid sites types had been previously detected and analyzed, resulting that the acidity of this catalyst was initially and mainly from coordinated water molecules and OH groups bonded to Ta ions, as Brönsted acid sites. The ammonia TPD analysis gave a ratio of 0.08NH_3 : 1Ta, and from pyridine adsorption, the ratio resulted 0.08Pyr : 1Ta. This difference could mean that all Brönsted acid sites were transformed into Lewis type acid sites because of water and OH groups loose. Moreover, Brönsted acid sites were not detected after heating the catalyst at 125 ºC under vacuum, due to the elimination of most coordinated water molecules, which matched well with the thermal analysis results ().

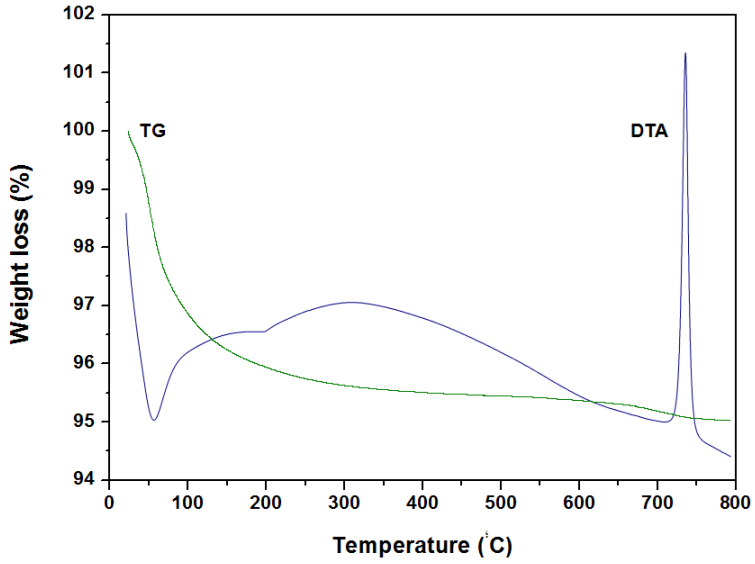

Figure 42. DTA and TG analysis of mesoporous Ta_2O_5.

The detected Lewis acid sites were weak, since they diminished considerably at 200 ºC, from 98.1 to 22 mol g^{-1}, and disappeared after evacuation at 300 ºC. In the catalytic reaction, both types of acid sites were desirable to participate in. Nevertheless, the presence of OH groups at room temperature was confirmed by FTIR spectroscopy, with signals at 1615 and 3400 cm^{-1} from O-H bonds and O-H stretching, respectively, Figure 43. CO_2 temperature programmed desorption was carried out, not detecting basic centers.

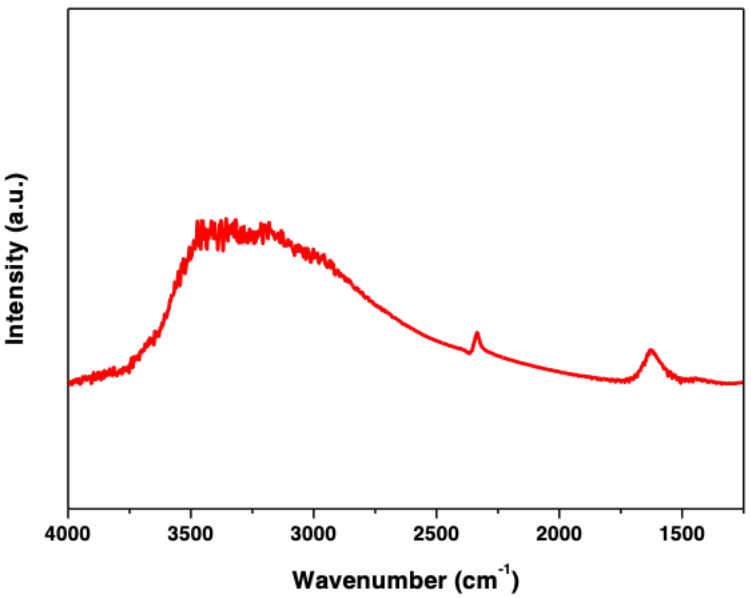

Figure 43. FTIR spectrum of mesoporous Ta_2O_5.

Kondo *et al.* performed an IR spectroscopy characterization of mesoporous tantalum oxide, neither detecting the presence of basic centers by CO_2 adsorption and finding Lewis acid centers, medium strength, by CO adsorption [103,104].

To check the participation of Brönsted acid sites in this catalytic process, the mesoporous tantalum oxide was treated with excess of KOH for one hour and, later, it was washed with water, in order to neutralize all the Brönsted acid centers. The modified catalyst was assayed in the catalytic reaction at 175 ºC, and maintaining the rest of experimental conditions, leading to a glucose conversion of 54.7% and a 24.6% of HMF selectivity, which were lower values than those

attained with the pristine catalyst, that is, a glucose conversion of 69% and HMF selectivity of 33%. The different catalytic performance could be attributed to the Brönsted acid sites participation.

Both types of acid sites taking part in this reaction with mesoporous Ta_2O_5 matched well with the results reported by Ordomsky *et al.* [105]. They carried out the selective elimination of Brönsted acidity by Na^+ treatment of phosphate catalysts (Al, Ti and Nb) and the results showed the synergism of nearby Lewis and Brönsted acid sites in glucose transformation to HMF. On the contrary, Nakajima *et al.* [106] studied the HMF production using $Nb_2O_5 \cdot nH_2O$ and $Nb_2O_5 \cdot H_2O$ exchanged with Na^+ to block the Brönsted acid sites, and obtained similar yields [106]. Niobic acid possesses acid strength enough to effective hydration or dehydration reactions, but this is strongly affected by thermal treatments due to crystallization of Nb_2O_5, and phosphoric acid has been used to suppress this crystallization, and enhance the acidity. Okazaki *et al.* [107] treated the catalyst with H_3PO_4 0.05-1 M during 48 hours, evaporating it at 120 ºC and calcining from 200 to 800 ºC to form an amorphous phosphate on the surface. In a similar way, mesoporous Ta_2O_5 (300 mg) was modified through a chemical treatment with phosphoric acid 1 M (20 mL) for 24 hours, followed by washing, drying and calcination (300 ºC). Once prepared, it was tested in glucose dehydration to HMF at 175 ºC for 120 min., not showing any catalytic improvement. When the chemical treatment with phosphoric acid was carried out, but the catalyst was not calcined, only dried, the glucose conversion increased up to 70 % and the HMF selectivity resulted 40 %. This enhancement could be explained because the modifications on the acidic active sites on the surface after the treatment with phosphoric acid.

Since neither levulinic acid nor furfural were never detected, the acidic strength of the mesoporous tantalum oxide (142 μmol NH_3 g^{-1} and 22 μmol Pyr g^{-1} at 200 ºC) was not enough to rehydrate HMF to levulinic acid. To check it, a reaction from HMF in a biphasic system (1.5 mL water/3.5 mL MIBK), with 50 mg of catalyst, was carried out under the same reaction conditions (175 ºC, 90 min.), and levulinic acid was not detected, and moreover, the HMF amount was kept. Lewis acidity favors the HMF degradation, but it was not detected, which could indicate that the temperature of 175 ºC was not high enough to degradate HMF [108,109]. But it could also indicate that these byproducts did not proceed directly from the HMF degradation, but from the condensation/polymerization of HMF with glucose, as proposed by Dee and Bell [110]. As HMF was totally recovered without having added glucose, the mechanism foregoing mentioned could be supported in this case.

Understanding the different processes involved in the HMF degradation would be desirable for HMF yield enhancement, but this will require additional experimental and theoretical research.

Reaction time

At 175 ºC, 13.9% fructose selectivity and 33.5% HMF selectivity were achieved after 90 min. reaction for a 69% glucose conversion, whereas at 185 ºC, 9.2 , 31.1 and 76.3% were, respectively, achieved. Despite higher glucose conversion and lower fructose selectivity at 185 ºC, the HMF selectivity diminished slightly because of the temperature, which favored the HMF degradation [108]. Thus, 175 ºC was prefixed to

study the influence of the reaction time, giving the results shown in Figure 44.

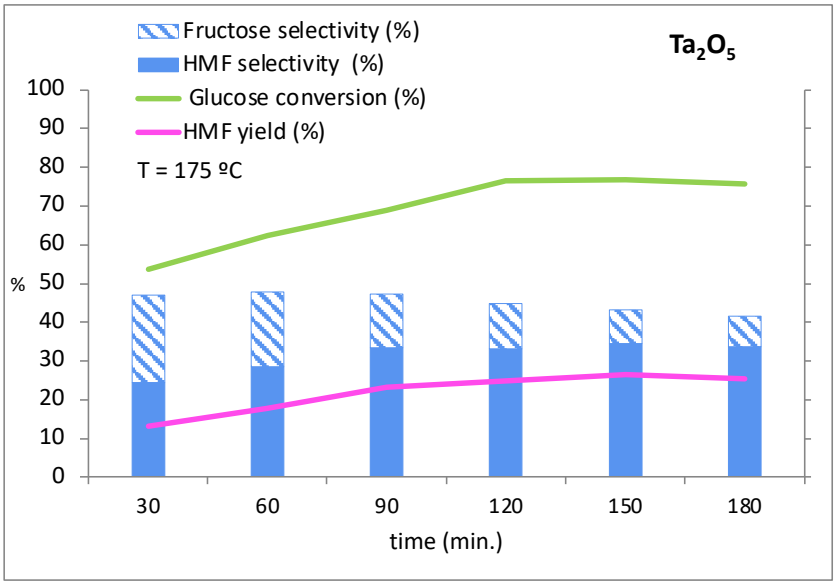

Figure 44. Catalytic activity of mesoporous Ta_2O_5 at 175 ºC after different reaction times in biphasic system water/MIBK system with S/C ratio 3..

These data revealed the fast isomerization of glucose to fructose with respect to glucose direct dehydration, since fructose selectivity was maximum (22.4%) after 30 min. of reaction, and diminished at longer reaction times. This decrease was due to fructose was dehydrated to HMF, although a direct transformation of glucose to HMF could be partially also considered. Longer reaction times than 90 min. led to similar HMF selectivity and yield (33.5 and 23.1%, respectively) because HMF production and degradation competed among them. Consequently, 90 min. resulted to be the optimal reaction time. In the

first 30 min., 50% of the maximum HMF yield and 70% of the highest glucose conversion were achieved, and this time resulted enough for isomerization to fructose, which was the limiting step in this reaction [111]. TOF number, as mol of desired product per mol of catalyst and hour, was calculated, and the first 30 min. displayed as the most active time reaction and reflected that the activity dropped at longer reaction times and that it was mostly because of the variations occurring at the catalyst surface. In addition, a modified TOF number, referred to mmol of desired product per m^2 of external surface of catalyst and hour, was determined to consider not the whole catalyst but the active sites. In this case, the observed tendencies considering mol of catalyst or surface were similar (Table 9. TOF values for mesoporous Ta2O5 at 175 ºC.

Table 9. TOF values for mesoporous Ta_2O_5 at 175 ºC.

Time (min.)	30	60	90	120	150	180
TOF (mol h^{-1} mol^{-1})	1.15	0.77	0.67	0.54	0.46	0.37
TOF^{m2} (mmol h^{-1} m^{-2})	0.056	0.038	0.032	0.026	0.022	0.018

Starting from fructose, the first step took 30 min. in a similar reaction using vanadyl phosphate (VOP) at 80 ºC , achieving a HMF yield of 40.2% in the first 30 min. and 41.9% after 60 min.. By increasing the Lewis acidity with iron (FeVOP) or aluminum (AlVOP), no higher yields were achieved in the first 30 min., resulting in 36.4 and 36.8%, respectively [112].

These data confirmed that Lewis acid sites were most important for glucose isomerization to fructose than for the dehydration step, and that glucose to fructose isomerization and dehydration from fructose took about 30 min.. Mesoporous tantalum phosphate at 170 ºC, under similar experimental conditions, led to maximum HMF selectivity after 60 min. (near 60%), but maximum HMF yield (near 35%) needed 120 min., due to higher glucose conversion [101]. The difference between mesoporous tantalum phosphate and mesoporous tantalum oxide related to specific surface area (255 vs. 79 $m^2 g^{-1}$) led to longer reaction times for maximum activity for the phosphate.

When niobium phosphate were used as catalyst in fructose dehydration to HMF, maximum catalytic activity was found between 20 and 40 min. [113]. From 150 to 180 min., a 1% lowering of HMF and glucose could support the possibility of reaction among them, producing humins [110]. In the range 30-120 min., the glucose conversion was linear, whereas a change of trend occurred at longer reaction times. The glucose conversion standstill starting up 120 min. of reaction time was caused by the presence of soluble polymers in the reaction medium and by the humins deposition on the catalyst surface, making difficult and even blocking the access of the reactants to the catalyst.

Catalyst loading

The initial experimental test was carried out with a catalyst loading consisting of a substrate (S) /catalyst (C) weight ratio of 3. Experimental series with others S/C ratios were done to study the influence of the catalyst loading, at 175 ºC and 90 min. ().

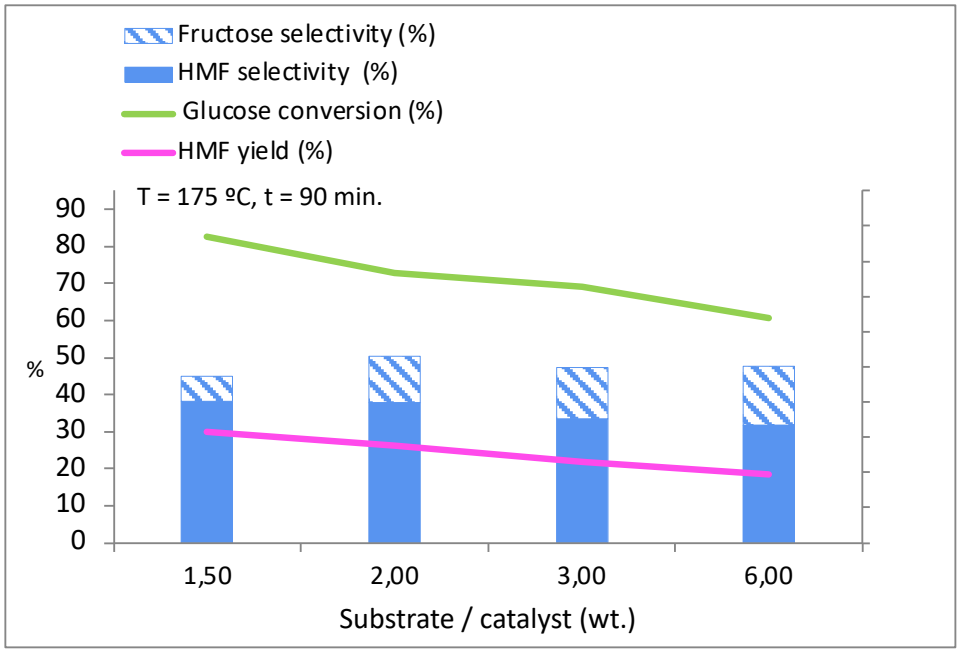

Figure 45. Influence of the substrate/catalyst ratio (S/C) with mesoporous Ta_2O_5 within 90 min. and 175 ºC, in biphasic system water/MIBK.

As expected, the glucose conversion and the HMF yield rose with the catalyst loading (lower S/C). On the contrary, the selectivity towards HMF remained constant for S/C ratios lower than 2. It was due to with such amount of catalyst, more activity was possible, not only towards the desirable dehydration products, but also towards the direct decomposition of hexoses or the cross-reaction between the formed HMF and hexoses, both producing humins.

Patil *et al.* [114] studied humin formation from glucose, fructose and HMF under acid catalysis, and concluded that the most likely pathways for humins formation were dehydration of glucose and/or

fructose to HMF, formation of 2,5-dioxo-6-hydroxyhexanal (DHH) from HMF, and aldol addition/condensation polymerization of DHH to humins. The direct conversion of cellobiose, glucose, or fructose to humins did not appear to be significant in their results.

Glucose conversion and HMF yield did not increase linearly in comparison to mesoporous tantalum phosphate used in glucose dehydration to HMF, with almost lineal increments with the catalyst weight. It means that there was some diffusional limitation in the glucose dehydration process, probably owing to a higher temperature of reaction and. moreover, to a longer reaction time (1 hour at 170º C for tantalum phosphate and 90 min. at 175 ºC for tantalum oxide) in which more glucose was transformed. S/C ratio of 6 consisted on 25 mg of catalyst with 150 mg of glucose and could be considered the most optimal because the double ratio (S/C = 3) did not lead to double catalytic activity, but for higher activity and low S/C ratios, a S/C ratio of 3 was fixed as optimum value.

Catalyst reusability and deactivation

As the reusability of the catalysts is one of the main advantages of the heterogeneous catalysis, it was studied in this PhD work. In these liquid-solid processes, reusability is conditioned by deactivation, which can be produced by different factors, such as physical (e.g. fouling), chemical (e.g. poisoning) or thermal (sintering) [115,116]. A second catalytic cycle with mesoporous tantalum oxide was carried out at 175 ºC for 90 min.. Previously, the spent catalyst was washed with water and calcined at 550 ºC for 2 hours (preheating rate 10 ºC min^{-1}). In

this second cycle, glucose conversion resulted only 4% lower than in the first cycle (64.9%), HMF selectivity 3% lower (30.4%) and HMF yield reached 20%. When this catalyst was tested in a second cycle but as spent, without any chemical or physical treatment, glucose conversion dropped by 60%. These meant catalyst lifetime for suitable work under the tested conditions was only 1 cycle.

In general, the acid catalyzed conversion of biomass gives rise to the formation of humins, which are complex carbonaceous materials, dark brown, insoluble in water at all pH's and non-homogeneous. Thus, fouling, which involves the deposition of chemicals on the surface of the catalyst, could be the main deactivation process in this reaction , because the mentioned humins as by-products were insoluble in the reaction medium and, besides, easily adsorbable on the catalyst surface, as could be checked visually with a turbid aqueous phase medium and a brown catalyst (white initially).

Lund *et al.* [117] considered that these humins are formed by the rehydration of HMF and that levulinic acid is not involved in the formation of them, whereas Zandvoort *et al.* [118] suggested that humins are formed from condensation reactions between sugar, HMF and dehydration intermediates. Tsilomelekis *et al.* [119] observed that humin formation are also influenced by the solvent, and that DMSO minimizes them. Eliminating or adding value to these humins are challenges in these catalytic processes starting from biomass.

6.2.2. Mesoporous silica: Al-MCM-41 and Al- KIT-6.

Both mesoporous silicas containing aluminum were tested in the dehydration reaction of glucose to HMF. The influence of several experimental variables, such as reaction temperature, reaction time and catalyst loading, was also studied, as well as other parameters such as the nature of the organic solvent, the addition of NaCl in the aqueous phase and the aluminum content in the synthesized catalysts.

Reaction temperature

Firstly, 10Al-MCM-41 was used to evaluate the influence of the reaction temperature, using 150 mg of glucose in 1.5 mL of water, in contact with 50 mg of catalyst, and 1.5 mL of methyl isobutyl ketone (MIBK) as organic phase, and 150 min. as reaction time. The reaction temperature was varied between 155 and 195 ºC. Glucose conversion resulted greatly dependent on the reaction temperature and achieved a maximum value of 86.5% at 195 ºC. Fructose, glucose and HMF were detected, being fructose favored at lower temperatures, achieving selectivities of 33% at 155 and even at 165 ºC, and decreasing above 165 ºC, whereas HMF selectivity increased specially from 175 ºC, being maximum at 195 ºC (41%) (Figure 46).

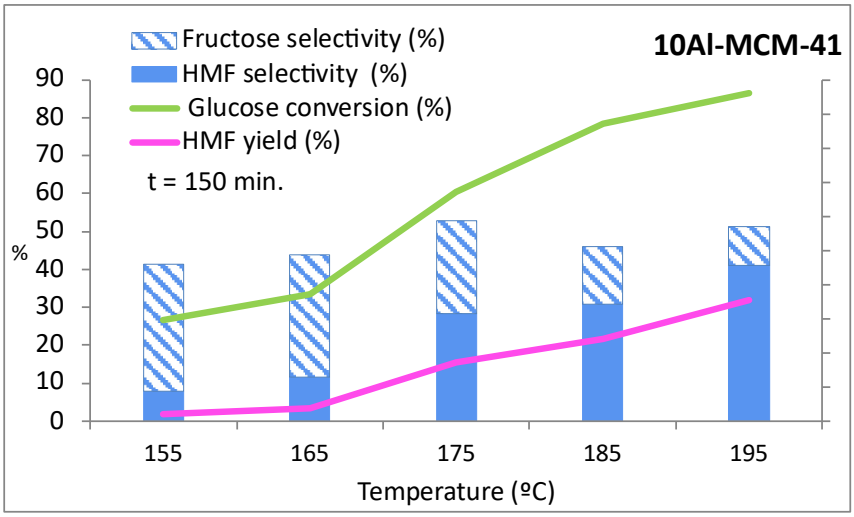

Figure 46. Glucose dehydration to HMF at different temperatures, using 10Al-MCM-41 in biphasic system water/MIBK with S/C ratio 3.

Maximum slope for glucose conversion and HMF yield occurred from 165 to 175 ºC, revealing the important effect of the reaction temperature, mainly between 165 and 185 ºC. At higher reaction temperatures, a lower rate was obtained, although slightly better catalytic results, indicating that other secondary reaction products affected the activity.

HMF yield far exceeded the one achieved with mesoporous tantalum oxide (35.6% versus 25.6%), demonstrating the better catalytic properties of 10Al-MCM-41, which can be attributed to its high concentration of Brönsted acid sites. Levulinic acid was not detected among the reaction products, revealing that the acid sites present on the catalyst surface were not strong enough to produce the HMF hydration. This fact was verified by putting in contact the same moles

of HMF as glucose used in previous studies with 10Al-MCM-41, also at 195 ºC for 150 min, and in the same biphasic system. Any levulinic acid was detected, pointing out that 10Al-MCM-41 was unable to rehydrate HMF. However, only 91% of HMF was recovered and thus a 9% of the HMF was transformed in other substances, such as soluble polymers or aldol condensation products, excluding humins, since the color of the catalyst remained. **Image 1 sh**ows two reactors after reaction with different conversion values, where the presence of humins is easily perceptible at first sight.

Image 1. Reaction medium after using 10Al-MCM-41 catalyst at 195 ºC (left) and at 155 ºC (right).

Al-KIT6-C2 mesoporous aluminosilicate, with a similar Si/Al ratio than 10Al-MCM-41 was also evaluated for glucose dehydration to HMF, showing remarkable differences. This KIT-6-based catalyst provided very low glucose conversion at different temperatures, while resulted to be very selective towards HMF (Figure 47). Its specific surface area was 20% smaller and acidity resulted even lower than in the MCM-41-based catalyst. These parameters were mainly responsible for the low conversion. Barely fructose formation and the

high selectivity towards HMF would agree with the Brönsted acidity and some synergy between Lewis and Brönsted acid sites.

Al-MCM-41 and Al-KIT6 aluminosilicates with similar Si/Al content have been synthesized and characterized by Kim et al., finding more Lewis acid sites in Al-MCM-41 and a high Brönsted acididty in Al-KIT6 materials [120].

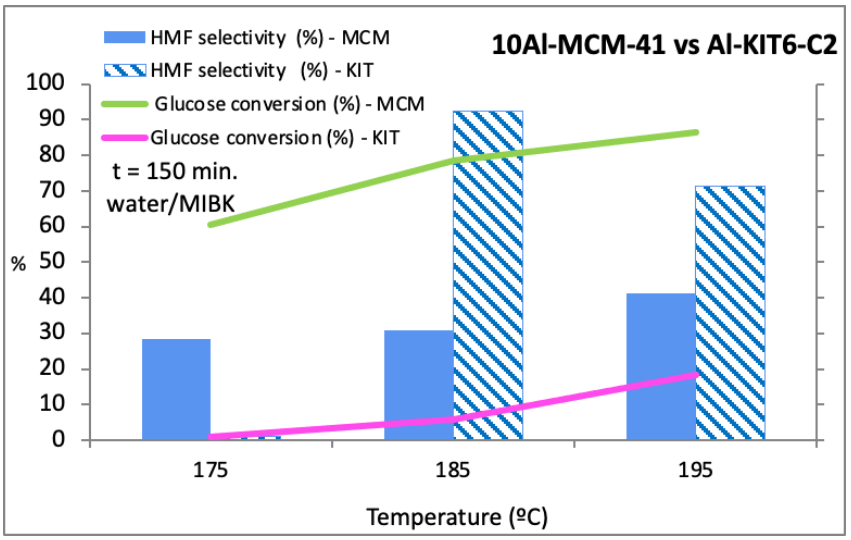

Figure 47. Comparison of glucose conversion and HMF selectivity between MCM-41 and KIT6-based catalyst with Si/Al ratio of 10 in biphasic reaction medium after 150 min with S/C ratio 3.

Reaction time

The reaction temperature with maximum HMF yield, 195 ºC, was fixed to study the kinetic of the reaction, from 30 to 150 min. with 10Al-MCM-41. The results revealed that glucose conversion and HMF yield increase linearly with the reaction time till 120 min. From 120 to

150 min., conversion and yield rose slightly, reaching maxima values of 86.5 and 31.9%, respectively (Figure 48).

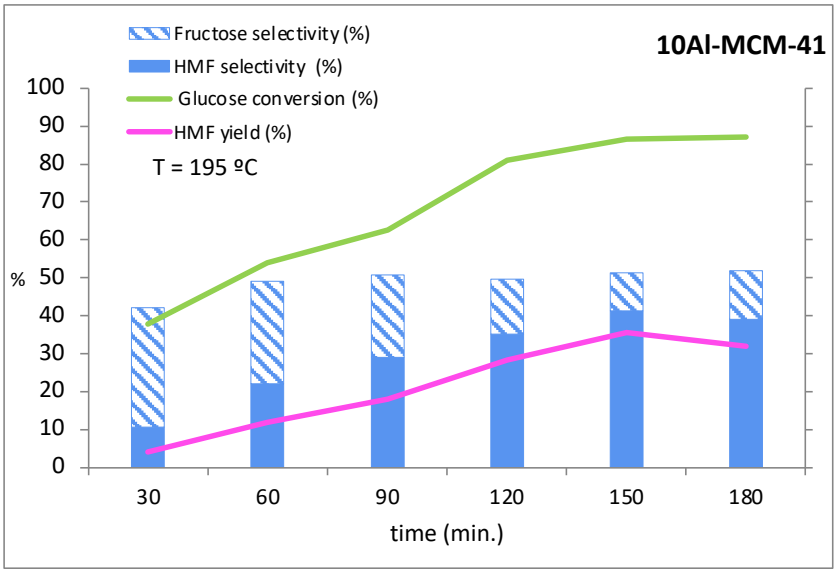

Figure 48. Influence of the reaction time on the catalytic activity using 10Al-MCM-41 at 195 ºC in biphasic system water/MIBK with Substrate/Catalyst ratio 3.

At longer reaction time, 180 min., these values diminished as the catalytic performance did not improve, possibly as a consequence of the deposition of insoluble polymers on the active sites of the catalyst. This different behavior would mean that secondary products, such as humins and soluble polymers become harmful for the catalytic process above 120 min., so this time could be considered as optimal. Within respect to mesoporous tantalum oxide, this catalyst reached much better selectivity towards HMF and its acidic properties did not favor the fructose presence, promoting its dehydration towards HMF. If

TOF values are considered (Table 10), also 120 min. could be considered as optimum under these experimental conditions.

Table 10. TOF values of 10Al-MCM-41 catalyst at 195 ºC

Time (min.)	30	60	90	120	150	180
TOF (mol h^{-1} mol^{-1})	0.08	0.12	0.12	0.14	0.14	0.11
TOF^{m2} (mmol h^{-1} m^{-2})	0.0023	0.0034	0.0034	0.0040	0.0040	0.0030

The obtained values were lower than those attained with mesoporous tantalum oxide, but they could not be compared at all because the other has a higher molecular weight and much lower specific surface area.

Marianou *et al.* [121] tested Sn10/Al-MCM-41 with similar aluminum content than 10Al-MCM-41 (4 and 4.5 wt.%, respectively) in glucose dehydration to HMF and lactic acid, in DMSO/water. Supporting SnO_2 on Al-MCM-41 increased the conversion of glucose (to 100%) and the HMF yield (from 8 to 18%) with respect to Al-MCM-41 at 150 ºC, with a substrate/catalyst ratio 1:1, after 60 min.. They also obtained lactic acid, but 10Al-MCM-41 possessed higher Brönsted acidity, which favored the formation of HMF over lactic acid, achieving higher HMF yields.

Jiménez-Morales *et al.* [122] carried out a similar catalytic process, using Zr-MCM-41 as catalyst, at 175 ºC. From 30 to 90 min. of reaction time, they attained higher conversion than the one achieved

with 10Al-MCM-41, but lower values from 120 min.. These results suggested the catalyst with Zr species would present lower activation energy requirements. HMF selectivity and yield resulted higher for 10Al-MCM-41 at the same reaction times, but it has to be taken into account that the experiments were carried out at higher temperatures: 195 ºC for 10Al-MCM-41 and 175 ºC for Zr-MCM41-550. In any case, similar fructose and HMF selectivities were observed for both MCM-41-based catalysts ().

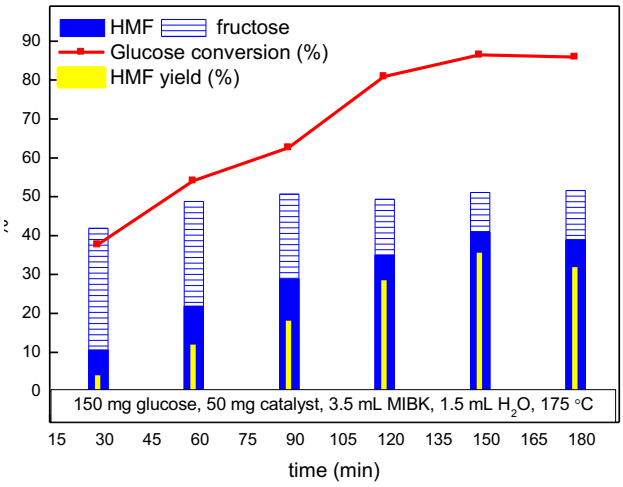

Figure 49. Catalytic activity along time of Zr-MCM-41 in a biphasic water/MIBK system, at 175 ºC. From reference [122].

Fructose selectivity decreased almost linearly with reaction time, while HMF selectivity enhanced (Figure 50). This could indicate the most of HMF was produced from fructose dehydration after glucose isomerization and also pointed out the formation of secondary products.

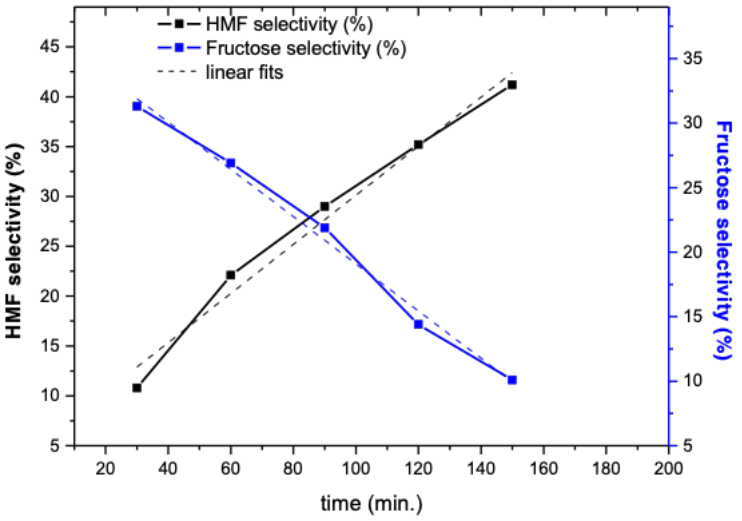

Figure 50. HMF and fructose selectivity values, after different reaction times, using 10Al-MCM-41 catalyst, at 195 ºC.

¡Error! No se encuentra el origen de la referencia. shows the quasi-linear dependency of HMF yield on glucose conversion along the reaction time, supporting this assumption. On the contrary, with respect to the reaction temperature, there was no linear dependency of HMF yield on glucose conversion, because glucose conversion was very sensitive to the temperature.

With regard to Al-KIT6-C2 aluminosilicate, it was also tested under the same conditions as 10Al-MCM-41, at 195 ºC, leading to a higher conversion. This catalyst also showed a very different behavior. While using 10Al-MCM-4, longer reaction times produced higher HMF yield and conversion, being optimum after 150 min., glucose conversion decreased when time increased while HMF yield kept at high values

using Al-KIT6-C2 as catalyst under the same experimental conditions (Figure 52). This behavior suggested a fast deactivation of the catalyst due to byproducts, mainly affecting the access of reactants, but without acidity variation because aluminum did not leach considerably.

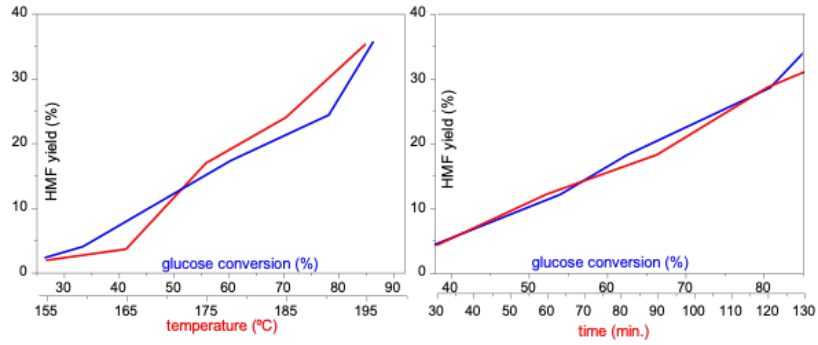

Figure 51. HMF yield (red) and glucose conversion (blue) at different temperatures, after 150 min. (left) and variation with time at 195 ºC (right) in biphasic system water/MIBK with S/C ratio 3.

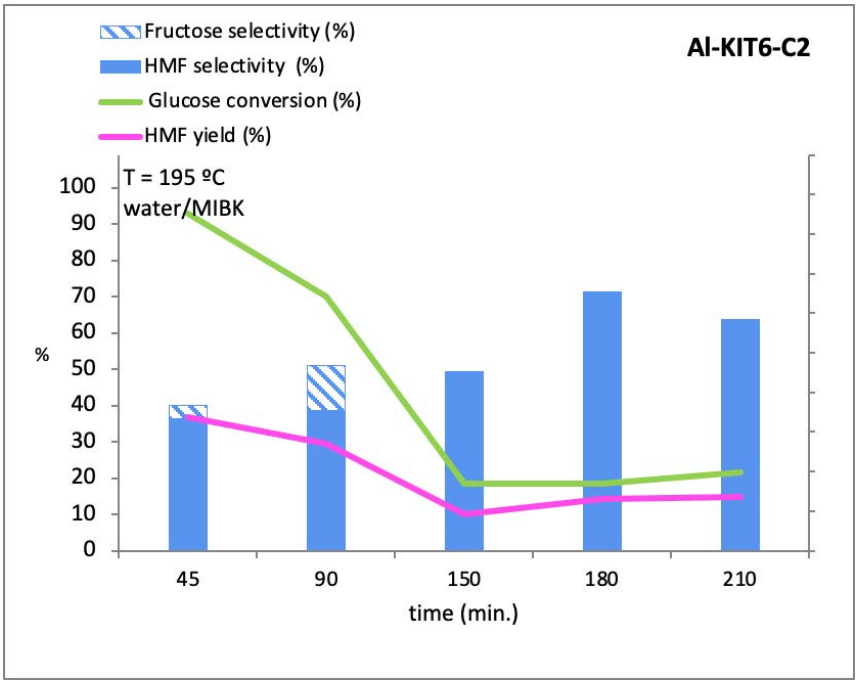

Figure 52. Influence of the reaction time on the catalytic activity of Al-KIT6-C2 catalyst in biphasic system water/MIBK with S/C ratio 3.

Karthikeyan *et al.* synthesized Al-KIT6 with different Si/Al ratios, whose textural properties were similar to those of Al-KIT6-C1 and -C2 catalysts and studied their catalytic performance in the synthesis of carbonitriles and carboxylates, also including their recovery and reusability. ICP analysis barely showed aluminum leaching, still existing a strong interactions between aluminum and silica [16].

Biphasic systems

In biphasic systems, the organic solvent acts extracting the HMF immediately after its formation and thus, its lower concentration in the aqueous phase limits side reactions, achieving higher HMF yields. The partition coefficient (R), which is the ratio of HMF (concentration) in the organic phase to that in the aqueous phase, allows to assess the effectiveness of a particular biphasic media. MIBK as organic solvent in a water:organic solvent volume ratio (mL/mL) of 1.5:3.5 had been previously used as biphasic systems with other catalysts [101,122], as well as in reactions with mesoporous tantalum oxide. Thus, with 10Al-MCM-41, reaction temperature and time studies were carried out with the above-mentioned volume ratio (1.5 mL water and 3.5 mL MIBK). At 195ºC, after 150 min., at which the highest conversion and yield values were reached, partition coefficient R resulted 2, and 72% of the HMF (mol) was in the organic phase. Maintaining the reaction conditions and the nature of the biphasic system, the volume of organic solvent MIBK was increased from 3.5 to 6.5 mL. The partition coefficient resulted to be similar, indicating almost the same solubility in both phases, and the catalytic results were kept almost invariable (88% glucose conversion *vs* 86.5% and 40% HMF selectivity *vs* 41%), with 81% of the HMF remained in the organic phase. When MIBK was increased from 3.5 to 5 mL, the partition coefficient increased, the HMF selectivity reached 40.1%, and 81% of the produced HMF remained in the organic phase, and for a subsequent supply in a biofuel production process or for HMF extraction, this higher quantity of HMF would be better. The whole catalyst always stayed in the aqueous phase, which makes its reutilization better. Thus, the ratio MIBK:water 5/1.5 mL could be considered as optimal under

these experimental conditions (Figure 53). This value would correspond to a V_{org}/V_{aq} = 3.3, which is near the one reported by Dumesic *et al.* [123] of 3.2.

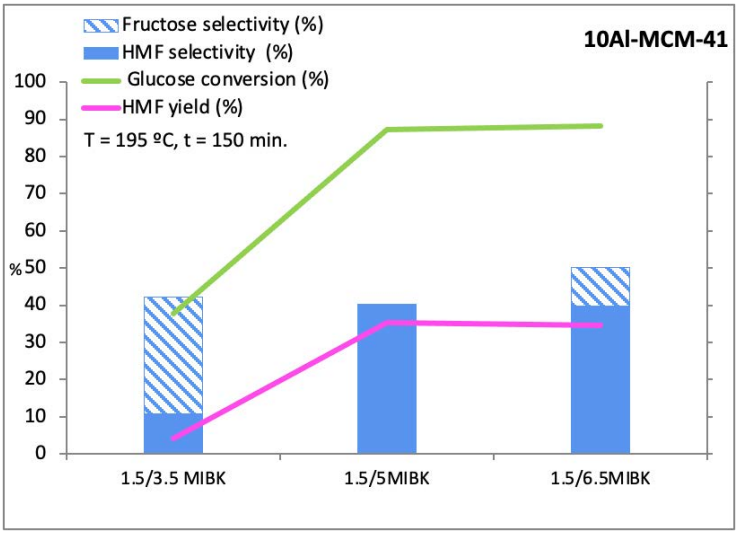

Figure 53. Catalytic activity using 10Al-MCM-41 in biphasic water/MIBK systems with S/C ratio 3, at 195 ºC after 150 minutes.

MIBK, with a low-boiling point (117 ºC), was compared with DMSO, with a high boiling point (189 ºC), through an Aspen model simulation for predicting the energy requirement for the separation of HMF. The vacuum evaporation method would evaporate 99.5% MIBK at 13 mbar and 70 °C with a 2.5% loss of HMF, whereas DMSO caused 30% HMF loss. The simulation also predicted that HMF separation from DMSO with minimal loss would require a more expensive vacuum distillation process and 40% more energy than that from MIBK [124].

A scheme of the HMF production via concurrent extraction and evaporation step from biphasic reactor reported by Saha *et al.* [125] is shown in Figure 54.

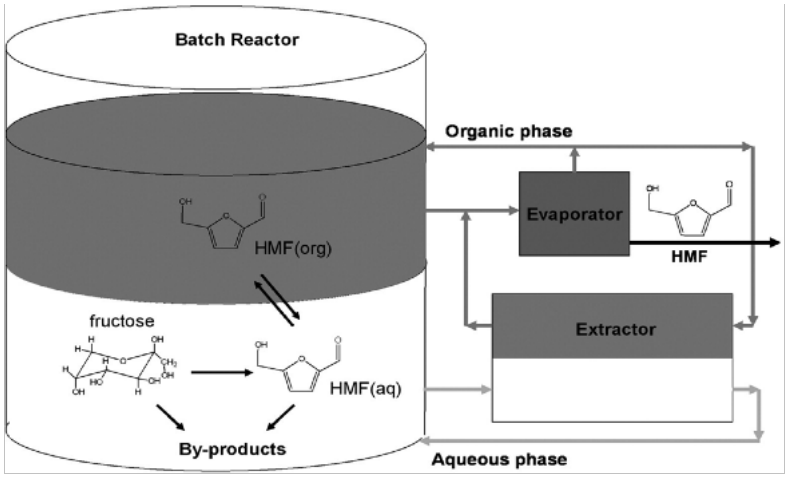

Figure 54. Schematic production of HMF via concurrent extraction and evaporation steps in a biphasic reactor [125].

De *et al.* [126] tested $AlCl_3$ as Lewis acid catalyst for glucose dehydration in a biphasic water/MIBK system, under microwave irradiation, with a volume ratio 1:2 (mL) and, under oil-bath heating, with a volume ratio of 2:8 (mL). Dutta *et al.* [127] also employed a biphasic water:MIBK system for fructose dehydration under microwave irradiation with a hierarchical macro/meso titanium phosphate, with a volume ratio 1:1, 0.5 mL for 50 mg substrate.

Other solvents such as toluene, 2-butanol, dimethylsulfoxide (DMSO), tetrahydrofuran (THF), and 1-butanol or cyclopentyl methyl ether

(CPME), which are "green solvents", have been employed for this reaction. Not only the highest HMF extraction (high partition coefficient) is a goal, but also, the ease of separation of HMF in the organic solvent for its supply to a subsequent processing.

In this way, $AlCl_3$ and a Brönsted acid (HCl), in a biphasic reactor consisting of water and an alkylphenol compound (2-*sec*-butylphenol), as organic phase, were used for glucose conversion, through a tandem pathway involving isomerization of glucose to fructose, followed by dehydration of fructose to HMF. The organic phase extracted 97% of the HMF produced, while both acid catalysts remained in the aqueous phase [128].

Dumesic *et al.* [123] used homogeneous catalysts (HCl, H_2SO_4) in biphasic systems with organic solvents, such as 2-pentanol and 2-methyltetrahydrofuran, for fructose dehydration at 150ºC, for 20 min., obtaining partition coefficients of 1.3 and 1.5, and HMF selectivities of 74 and 57%, respectively.

Ohara *et al.* [129] carried out the glucose dehydration to HMF with two catalysts, Amberlyst-15 to facilitate glucose dehydration and hydrotalcite to favor glucose to fructose isomerization. At 100 ºC, after 3 h, using only dimethylformamide (DMF) as solvent, 72% glucose conversion, 57% HMF selectivity and 4% fructose selectivity were reached. Adding water in a ratio organic:water of 3, HMF selectivity reached 64% and fructose diminished to 0%.

A promising eco-friendly solvent, stable under acidic and basic conditions, with a boiling point of 106 ºC, low solubility in water (1.1 g CPME/100 g) and applicable in biotechnology, biorefineries, bioeconomy or chromatography, is cyclopentyl methyl ether (CPME)

[130]. It is currently produced by petrochemical, but it could be produced from cyclopentanol or cyclopentanone derived from furfural or from adipic acid, respectively, both bio-based precursors. Its properties are suitable for reactions in biphasic media, such as furfural and HMF syntheses. Thus, cellulose from raw corncob has been simultaneously hydrolyzed to glucose and then catalytically converted to HMF in biphasic water/CPME and water/toluene systems, under heterogeneous catalysis by Qing *et al.* [131]. At 200 ºC, a HMF yield of 15.90% was reached in 20 min.. As this solvent is very suitable for the present reaction and bio-processes, it was tested as biphasic water/CPME medium (1.5 mL:3.5 mL) in glucose dehydration with 10Al-MCM-41, at 195 ºC and 150 min.. However, HMF selectivity resulted lower than with MIBK (22.5%) and fructose selectivity higher, 24.1% vs. 10.1%, at 52.9% glucose conversion. Partition coefficient resulted very low, 0.46, which disfavored HMF selectivity.

Biphasic system with sodium chloride

The partition coefficient not only depends on the nature of the solvents, but also on the presence of inorganic salts, such as NaCl, that improves the R value, as observed by Román-Leshkov and Dumesic in fructose dehydration to HMF [132]. They even observed that it is possible to form biphasic systems with solvents that are completely miscible with water in the absence of salt. Previously, Tyrlik *et al.* [133] studied glucose dehydration to levulinic acid in water solutions saturated with alkaline and alkaline earth metal salts.

Concentrated but unsaturated solutions of NaCl in water, by considering NaCl solubility in water (20 ºC) = 359 g/l, with

concentrations of 15 and 20 wt.% were employed as aqueous phase in glucose dehydration with 10Al-MCM-41, with the aim of reaching higher HMF yield through a higher partition coefficient. At 195 ºC, after only 30 min., very remarkable differences were observed: conversion changed from 37.7% with only water to 96.4% with $NaCl_{aq.}$ 20 wt.%, HMF yield reached the greatest value of 62.9% and fructose strongly diminished from 31.3 to 0.8% with $NaCl_{aq.}$ 20 wt.% (). These results are explained by the fast extraction of HMF from the aqueous phase to the organic phase promoted by the presence of sodium and chloride ions, which shifted the equilibrium of the reaction towards fructose dehydration to HMF. Partition coefficient, after 30 min. of reaction time, rose from 0.66 with pure water, as aqueous phase in the biphasic medium, to 1.92 with $NaCl_{aq}$ 20 wt.% instead. The equilibrium shift promoted by the presence of ions was remarkable even when a test without any catalyst was carried out under similar experimental conditions, since 27.6% glucose conversion and 22% HMF selectivity were attained.

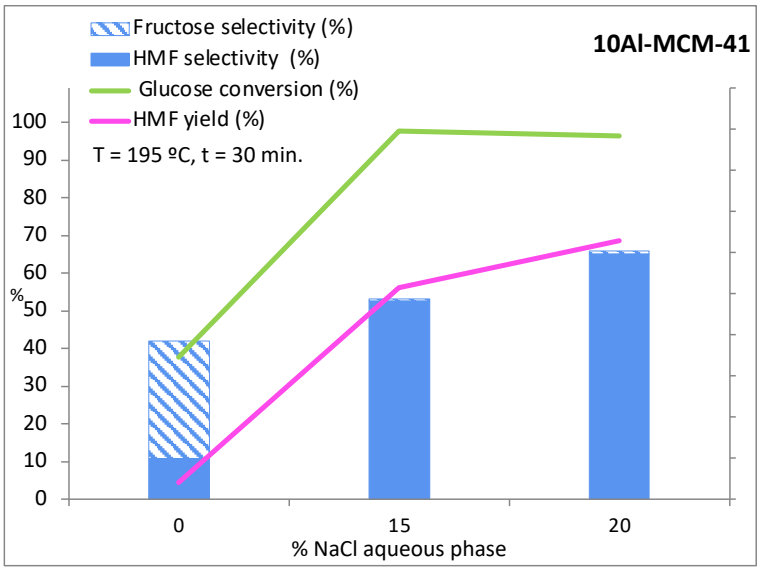

Figure 55. Catalytic activity of 10Al-MCM-41 in biphasic MIBK/sodium chloride aqueous solution systems, at 195 ºC after 30 min. with S/C ratio 3.

Observing the kinetic of the reaction (), glucose and fructose dehydration occurred in 15-30 min. period, and longer reaction times favored HMF degradation to secondary products, decreasing HMF yields. A test starting from HMF in the same biphasic medium, at 195 ºC and 30 min., was carried out and all the initial HMF stayed at the end of the reaction, which suggested HMF degradation needed other intermediates also produced in hexoses dehydration reactions. Besides, the same reaction medium was employed to dehydrate fructose directly at similar reaction conditions (195 ºC and 30 min.), achieving 99.4 % fructose conversion and 73.7 % HMF yield, which pointed out that glucose dehydration to HMF occurred preferentially to glucose to fructose isomerization. Starting from fructose, HMF yield resulted 85

% HMF, supporting the statement that the isomerization step is limitant.

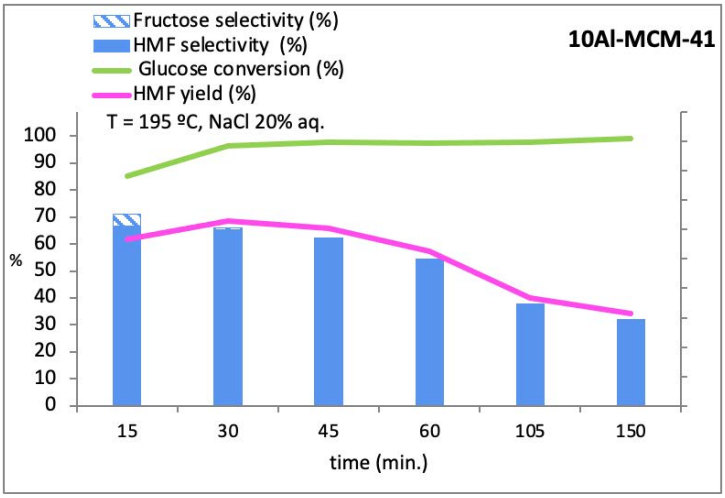

Figure 56. Kinetics of glucose dehydration to HMF with 10Al-MCM-41 in a biphasic MIBK/$NaCl_{aq}$ system at 195 ºC with S/C ratio 3.

Other biphasic systems consisting of CPME (3.5 mL)/NaCl (aq., 20 %wt.) and THF (3.5 mL)/NaCl (aq., 20 %wt.) were also employed with 10Al-MCM-41 at 195 ºC, achieving higher catalytic activity values than without NaCl solutions, but lower than those achieved with MIBK after 30 min., owing to lower partition coefficient, which facilitate subsequent side reactions (Figure 57).

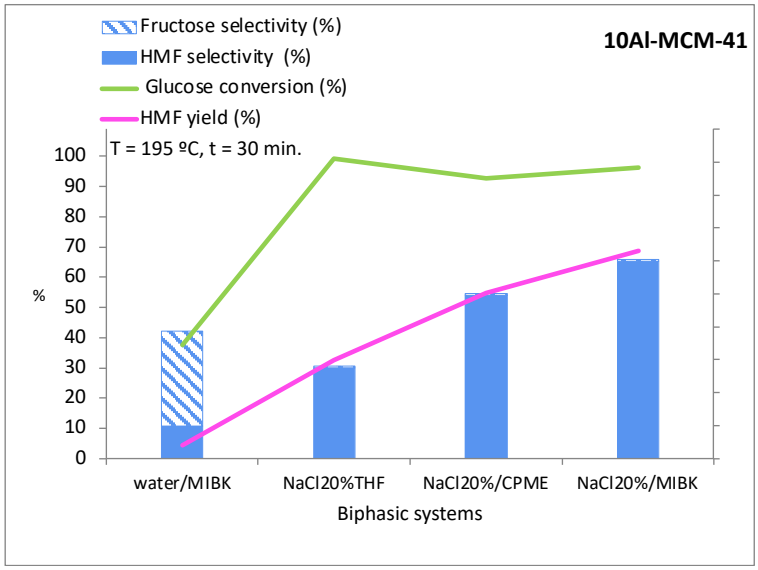

Figure 57. Catalytic activity using 10Al-MCM-41 in biphasic systems, at 195 ºC after 30 min. with S/C ratio 3.

In the same way that the volume of the organic phase was increased in previous experiments, finding 5 mL as optimal, additional experiments were carried out with 5 mL MIBK in the presence of $NaCl_{aq}$ 20 wt.% solutions instead of water as aqueous phase. Glucose conversion resulted 98.7%, HMF selectivity 61.1% and fructose selectivity 0.37%, essentially similar to those rose with 3.5 mL, and with a similar partition coefficient of 1.9, pointing out a preferential effect of the presence of ions from the salt than the effect of the volume increase on the partition coefficient (R).

Besides alkaline salts such as NaCl, alkaline earth metal chlorides have been evaluated in glucose dehydration to HMF. Tyrlik *et al.* [133] studied saturated and very concentrated alkaline and alkaline earth metal chlorides in glucose dehydration to HMF and levulinic acid,

concluding that simultaneous presence of magnesium chloride with hydrochloric acid in saturated water solution of salt provided the best catalyst for glucose dehydration, and that protons were not unique as catalysts for HMF, but complexes of magnesium-glucose were also active.

García-Sancho *et al.* used alumina with different acid-base properties for the dehydration of glucose to HMF and demonstrated that the presence of calcium chloride in the reaction medium notably improved the catalytic activity at shorter reaction times, which related to the interaction between Ca^{2+} cations and glucose molecules. They employed different calcium chloride concentrations, from 0.193 to 0.9 g salt per gram of aqueous solution, achieving the best results with the value of 0.65 [134].

Biphasic system with calcium chloride

Considering these previous studies, a $CaCl_2$ solution with the same cation concentration than in the tested NaCl solution, where used as aqueous phase in combination with MIBK for glucose dehydration to HMF, with 10Al-MCM-41 at 195ºC for 30 min.. Conversion resulted similar as the one achieved with $NaCl_{aq}$, but HMF yield increased with respect to the use of water as aqueous phase but not as much as with $NaCl_{aq}$ (35.1 %), resulting less effective. Identical reaction conditions were fixed in another reaction, with calcium chloride solution but without catalyst, and a high HMF selectivity was achieved, better than with catalyst, at lower glucose conversion (). This result agreed with the previous cited ones, which attributed to calcium a key role in

glucose conversion to HMF by interactions Ca-glucose instead of Ca-catalyst surface.

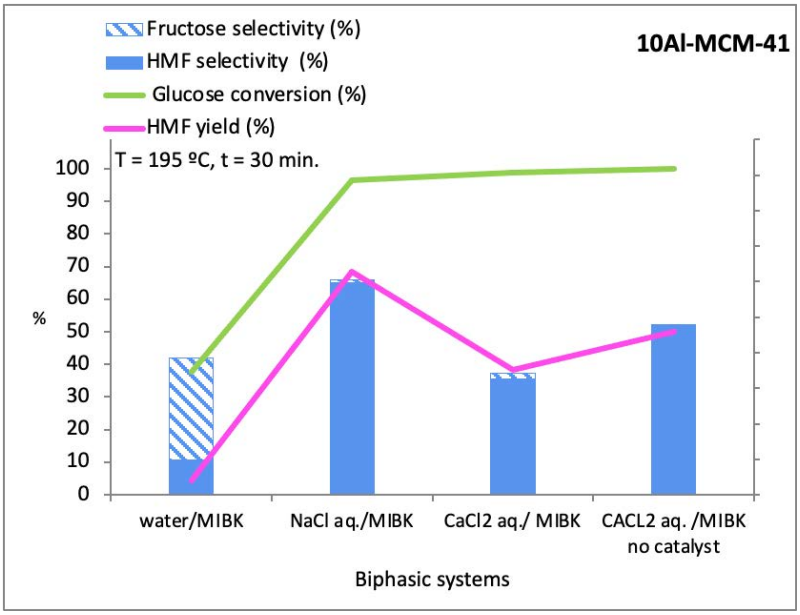

Figure 58. Catalytic activity in glucose conversion in biphasic MIBK and water or salts systems at 195 ºC after 30 min. with S/C ratio 3.

The maximum HMF selectivity and the minimum fructose selectivity also pointed out a main role of glucose instead fructose toward HMF production. The high activity observed in $CaCl_2$ (aq.)/MIBK reaction medium without catalyst would indicate completely different reaction pathways, competing the surface of the catalyst with calcium ions. $CaCl_2$(aq.) enhancement glucose conversion (100 %) was also studied without MIBK as organic solvent, only using the salt solution (195ºC) for 30 min., also achieving 100 % glucose conversion and not being

detected fructose. Nevertheless, HMF was barely found, supporting the role of calcium cations in the reaction mechanism through Ca-glucose species, specifically forming bidentate complexes involving the C-1 and C-3 hydroxyl groups of glucose, and further enhancing subsequent HMF degradation, according to Yang *et al.* [135]. The effect of calcium chloride does not seem to be only because of the Ca cation interactions, but also chloride anions seem to play an important role, donating electron density to glucose C-1, C-3, and C-5, also enhancing glucose conversion. Nevertheless the anion effect should be less determinant that calcium cation effect, as can be deduced by varying anions and cations, such as comparing NaCl and $CaCl_2$. The introduction of an organic phase to stabilize HMF is evidenced. The presence of alkaline or alkaline earth salts, although through different mechanisms of reaction, leads to better results than only water, but an organic phase is required to avoid subsequent reactions. The presence of salts also affect the organic phase by enhancing the partitioning coefficient of HMF. Thus, salt ions participate effectively in reactions.

Catalyst loading

All the previous studies have been performed with a substrate/catalyst (S/C) weight ratio of 3, but the effect of this ratio was also studied, by varying from 1.5 to 6, in a biphasic water/MIBK medium, at 195 ºC for 150 min., as well as in biphasic $NaCl_{aq.}$/MIBK medium, at 195 ºC for 30 min. (Figure 59).

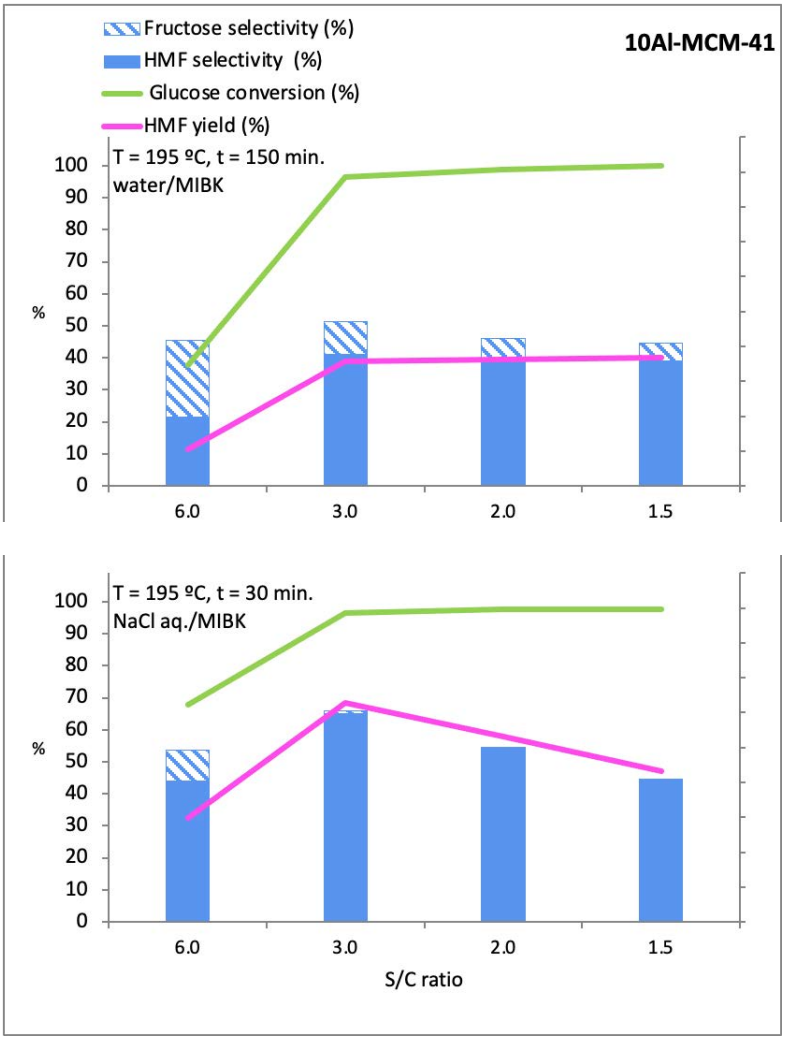

Figure 59. Effect of the substrate/catalyst ratio (S/C)) in glucose dehydration to HMF over 10Al-MCM-41, in biphasic water/MIBK (above) and NaCl (aq.)/MIBK (below) medium at 195 ºC.

Conversion increased notably from S/C ratios of 6 to 3, but decreasing when the amount of catalyst was increased to S/C= 1.5, while HMF selectivity was maximum with a S/C= 3, decreasing for a higher catalyst content. Thus, external diffusional limitations could be

the rate controlling step, limiting the adsorption and promoting the HMF reaction and degradation. This limitation is frequent at high reaction temperatures, with very small particles of catalysts. The reaction rate at the catalyst surface depend on the mass transfer coefficient k_c between fluid-solid phase, being the reaction rate expressed as follows:

$$(-r_A) = -\left(\frac{1}{S_{ex}}\right) g_A = k_C \left(C_{A_f} - C_{A_s}\right) \qquad [\text{kmol s}^{-1}\ \text{m}^{-2}]$$

S_{ex}: external surface of the catalyst particle, m^2

g_A: generation, kmol s^{-1}

k_C: individual mass transfer coefficient, (kmol s^{-1} m^{-2}) /(kmol m^{-3})

C_{Af}: concentration in the fluid, kmol m^{-3}

C_{As}: concentration at the surface, kmol m^{-3}

The amount of catalyst was also modified with NaCl 20% as aqueous phase instead of water, in the biphasic medium, resulting a full glucose conversion with more catalyst content than 50 mg (S/C = 3), but HMF selectivity was the highest with S/C of 3 (Figure 59). These results indicated more external diffusional control owing to the presence of the salt ions, supporting that external diffusion was the limiting step.

Jiménez-Morales *et al.* synthesized Zr-MCM-41 with a Si/Zr ratio of 5 for glucose dehydration to HMF reaction, which resulted quite selective and achieved 23 % HMF yield at 175 ºC after 150 min.. TOF expressed as mmol HMF per gram of catalyst and per hour, varied between 1.3 and 1.8 [136]. For 10Al-MCM-41, TOF expressed in similar terms, varied from 1.22 by employing a substrate/catalyst

(S/C) ratio of 1.5, to 2.36 with S/C = 3, being around 1.4 with S/C ratios of 2 and 6. When NaCl (aq. 20 %wt.) was incorporated and S/C ratio was set at 3 and the time at 30 min., HMF yield went up by a factor of 1.77, but in terms of TOF, the factor was 7.8 (TOF = 20.68), providing an important enhancement of activity and savings in time.

Therefore, 10Al-MCM-41 in a substrate/catalyst weight ratio of 3 resulted very effective as catalyst.

The decreasing glucose conversion at decreasing S/C ratios with 10Al-MCM-41 was also observed when Al-KIT6-C2 catalyst was used. By doubling the amount of catalyst, fructose and HMF selectivity increased while glucose conversion decreased, indicating external diffusional limits with contributed to slow down the glucose to fructose isomerization rate, which was the limiting step of the reaction (Table 11).

Table 11. Catalytic activity of Al-KIT6-C2 in glucose to HMF conversion at 195 ºC, after 150 min., in water/MIBK, varying S/C weight ratio.

Glucose / Al-KIT6-C2	Glucose conversion (%)	HMF selectivity (%)	fructose selectivity (%)	HMF yield (%)
3	18.5	49.4	0.0	9.2
1.5	16.2	65.5	23.9	10.6
1	8.6	79.0	28.0	6.8

Influence of the aluminum content: 5Al-MCM-41

5Al-MCM-41 possessed larger BET surface area (25%), different porosity and higher acidity (44% referred to surface area), which was

supposed as more suitable for glucose dehydration to HMF. However, the catalytic performance of 5Al-MCM-41, under similar experimental conditions, provided worst results, as shown in Table 12.

Table 12. Catalytic activity of 5Al-MCM-41, after 150 min. at 195 ºC, with a S/C weight ratio of 3, in water/MIBK.

	Glucose conversión (%)	**Fructose selectivity (%)**	**HMF selectivity (%)**	**HMF yield (%)**
5Al-MCM-41	71.8	21.1	31.0	22.6
10Al-MCM-41	86.5	10.1	41.2	35.6

This reduced effectiveness may be due to 5Al-MCM-41 possessed lower Brönsted and Lewis acidity, despite containing more aluminum but mainly in extra-framework positions (Section 6.1.3). The existence of a higher proportion of micropores (Section 6.1.2) could difficult the accessibility of reactants to acid sites, also contributing to the activity worsening [122].

5Al-MCM-41 resulted more selective towards fructose, which required mainly Lewis acidity. Liu *et al.* have studied the catalytic mechanism for the isomerization of glucose into fructose over an aluminium-MCM-41 framework, finding that the catalytic activity of the Al-containing active sites originates from three factors, and not only by the Lewis acidity associated to Al sites (although mainly), but also from a proton donor in the form of an Al–O(H)–Si group and from proton acceptor in the form of an Al–OH group. 5Al-MCM-41

containing lower Lewis acidity should be less selective towards fructose than 10Al-MCM-41. Higher presence of fructose after reaction could point out those contributions, but it can also be suggested that a higher fructose formation did not mean only a higher selectivity to fructose but also lower dehydration of fructose into HMF because of lower Brönsted acidity.

Catalyst reusability

Recovery and reusability of catalysts without complex and/or high expensive operations is an essential aspect in heterogeneous catalysis.

10Al-MCM-41 reusability in subsequent glucose to HMF dehydration runs was studied at the same operation conditions: biphasic NaCl (aq., 20 %wt.)/MIBK medium, 195 ºC, 30 min., S/C weight ratio of 3. Fresh catalyst was white after synthesis but turned brown after first use due to adsorption of undesirable reaction products. Reusability of the catalyst was carried out without any regeneration treatment. Along four runs, glucose conversion decreased, although HMF selectivity kept almost invariable during 3 runs. Fructose was significant from the third run (Figure 60). These results indicated Lewis and Brönsted acid sites kept unmodified. The species adsorbed on the catalyst reduced both the available active area and mesopores allowing the access of reactants. The increasing fructose selectivity constituted another evidence that glucose isomerization to fructose is the limiting step, and from the third run, the catalyst, worked under non optimal conditions. Thus, the catalyst could be reused for three catalytic runs without any treatment after reaction, achieving high HMF yields.

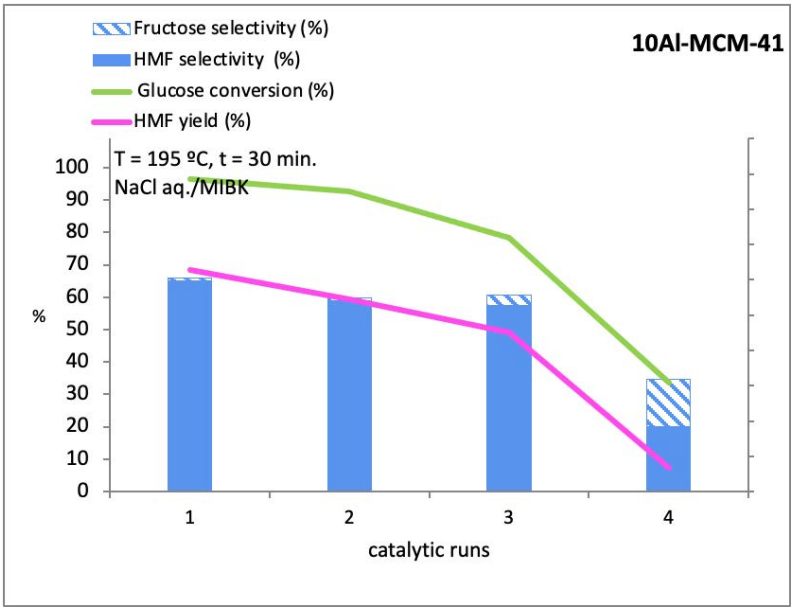

Figure 60. 10Al-MCM-41 catalyst reusability along 4 runs in biphasic system NaCl/MIBK with S/C ratio 3 at 195 °c after 30 minutes.

MCM-41 based catalyst has been used for Knoevenagel condensation reaction along three catalytic cycles with only 4 % yield loss.

In this case, the catalyst was previously regenerated by separation through centrifugation, washed several times with distillated water and dried [137].

On the other hand, the effect of the Fe/MCM-41 catalyst synthesis method was studied and the catalyst was tested in the green synthesis of xanthene derivatives. The catalyst reusability was also evaluated, for which it was filtered and washed with ethyl acetate to remove any unreacted precursor and organic products. The catalyst showed only

minor deactivation after five catalytic runs (from 91 % to 86 % yield) with small loss of iron [138].

Zr-MCM-41, synthesized by Jiménez-Morales *et al.* and studied in the glucose to HMF dehydration reaction, was also reused without any treatment along several runs, showing glucose conversion and HMF yield trends similar to 10Al-MCM-41. Zr-MCM-41 used in four runs was separated by filtration and calcined (500 ºC, 2 hours), showing significant recovery. Nevertheless, Zr-MCM-41 catalyst was also calcined after only one catalytic run, achieving almost fully initial catalytic activity [122].

10Al-MCM-41 reusability was also tested after separation by filtration and calcination (550 ºC, 2 hours), not showing as high catalytic activity as initially, in contrast to the cited Zr-MCM-41. Glucose conversion decreased (from 96.4 to 54.9 %) and HMF yield fell by half, indicating structural and textural changes after a second calcination, probably moving aluminum to extra-framework positions.

6.2.3. Zeolites (ZSM-5, Y, Beta)

H-zeolites (ZSM-5, Beta and Y), with Si/Al molar ratios of 15, 12.5 and 6, respectively were tested as acid heterogeneous catalysts for glucose to HMF dehydration under the optimal reaction conditions previously determined using 10Al-MCM-41: 195 ºC , S/C weight ratio of 3 and 150 min. in biphasic water/MIBK medium. H-Beta-12.5 and H-Y-6 attained glucose conversion higher than the 86 % achieved using 10Al-MCM-41, and fructose selectivities under 10 % produced with the MCM-41 catalyst (Figure 61).

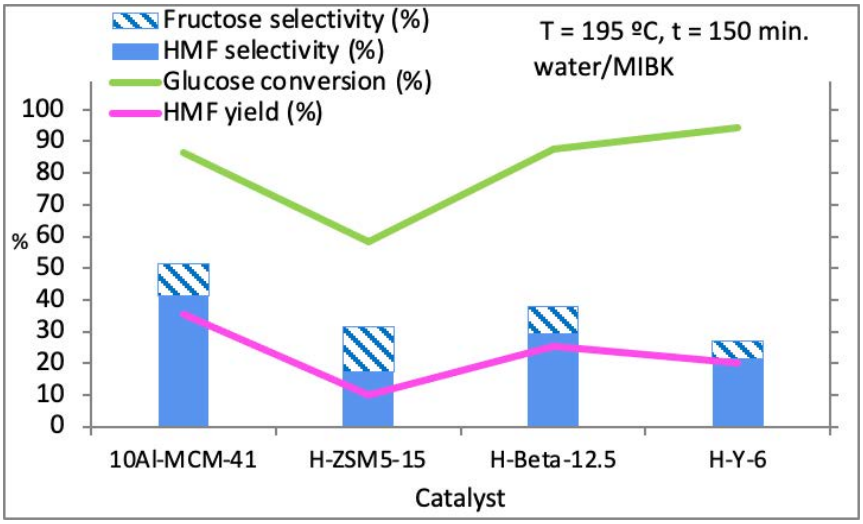

Figure 61. Catalytic activity using H-zeolites and comparison with 10Al-MCM-41 catalyst, in water/MIBK, at 195 ºC after 150 min. with S/C ratio 3.

However, the highest HMF selectivity of H-zeolites was lower than 30%, by using H-Beta-12.5. The H-ZSM5-15 zeolite presented the lowest activity, which can be explained taking into account its lowest Lewis and Brönsted acidities. In addition, H-ZSM5-15 had more micropores and acid sites than the other H-zeolites, locating the acidity mostly in its micropores, which makes difficult for glucose molecules to access. H-Beta-12.5 zeolite achieved similar glucose conversion than 10Al-MCM-41, although a lower HMF selectivity (29.2 *vs* 41.2 %), which can be explained by considering the high concentration of acid sites, specially Lewis ones, of moderate-strong acidity, and overall, the important developed mesoporosity, pointing

out the key role of the textural properties in the catalytic performance of porous acid solids in glucose and fructose dehydration reactions.

The effect of NaCl (20 wt.%) addition to the aqueous phase with 10Al-MCM-41 as catalyst, allowed to attain glucose conversion over 95%, high selectivity towards HMF and barely fructose, and, extremely important, shortening the reaction time from 150 to 30 min. Thus, similar experimental conditions were stablished to test the H-zeolites. Higher glucose conversion values were achieved in all cases, fructose selectivities became lower and HMF resulted higher than 42 % (). Under these conditions, also H-Beta-12.5 produced the best results, quite similar to those with 10Al-MCM-41, mostly due to its mesoporosity.

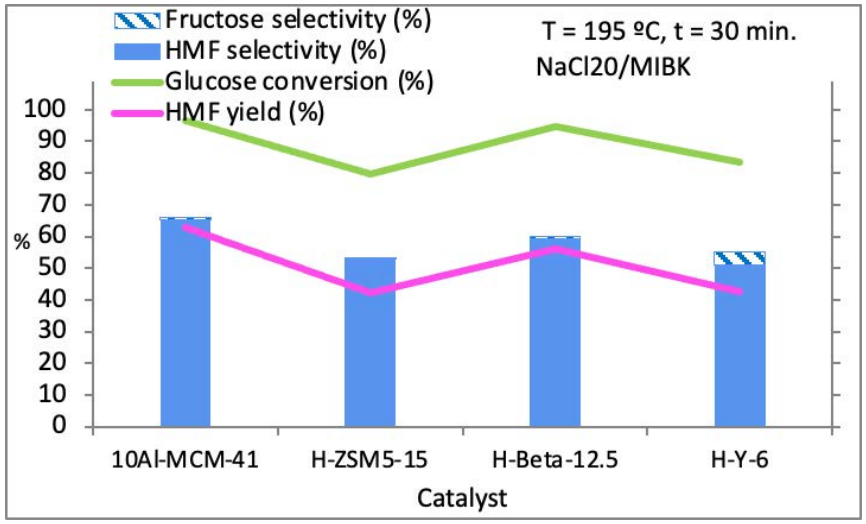

Figure 62. Influence of the NaCl aq. addition in the reaction medium using H-zeolites and comparison with 10Al-MCM-41 at 195 ºC after 30 minutes in water/MIBK system with S/C ratio 3.

By using H-ZSM5-15 and starting from fructose, complete sugar conversion was achieved, although HMF selectivity was slightly lower, which can be explain by the lowest proportion of Brönsted acid sites. Moreau *et al.* studied H-zeolites for fructose conversion to HMF in biphasic water/MIBK systems, at 165°C, finding conversion and HMF selectivity dependent on acid and structural properties of catalysts, achieving the maxima fructose conversion with H-Y faujasite (Si/Al= 15) and H-mordenite (Si/Al= 11) [139]. Thus, H-zeolites possessed low, but enough Brönsted acidity to dehydrate fructose to HMF.

The positive effect of NaCl, as in 10Al-MCM-41, increased the partition coefficient (from 1.1 to 1.9 in H-ZSM5-15), preserving HMF from other transformations. After reaction, all the catalysts turned into brown, due to the formation of undesirable products which diminished the HMF yield. The formation of polymeric species from carbohydrates and HMF condensation takes place on Lewis acid sites [140], and the formation of products from HMF rehydration [117], on Brönsted acid sites. Levulinic acid was not detected.

These results can be compared to other reported in literature, although considering that different experimental conditions are used in this particular case. Nikolla *et al.* [141] used Sn-Beta and Ti-Beta zeolites for glucose dehydration to HMF, achieving a 18% HMF selectivity at 75% glucose conversion, after 90 min. in a biphasic H_2O/1-butanol/NaCl system, at 160 ºC, and obtaining a 55% HMF selectivity after addition of HCl.

Lourvanij *et al.* employed a H-Y zeolite, reaching full glucose conversion after 8 hours, at 160 ºC [142]. Ordomsky *et al.* [102]

employed also a biphasic water/MIBK system with a H-MOR, H-ZSM5 and H-BEA zeolites starting from fructose. With H-ZSM-5, a conversion of 80 % and a HMF selectivity over 60 % were achieved, higher than with H-BEA.

Reaction temperature (H-zeolites)

The influence of the reaction temperature on the H-ZSM5-15 zeolite activity was studied from 175 to 205 ºC (operational limitation), obtaining the results showed in . Glucose conversion increases with the reaction temperature, existing a direct dependence of glucose conversion with the temperature, as expected. A strong rise was produced from 185 to 195 ºC, where conversion increased from 37 to 80 %, and, consequently, the HMF yield from 18 to 42 %.

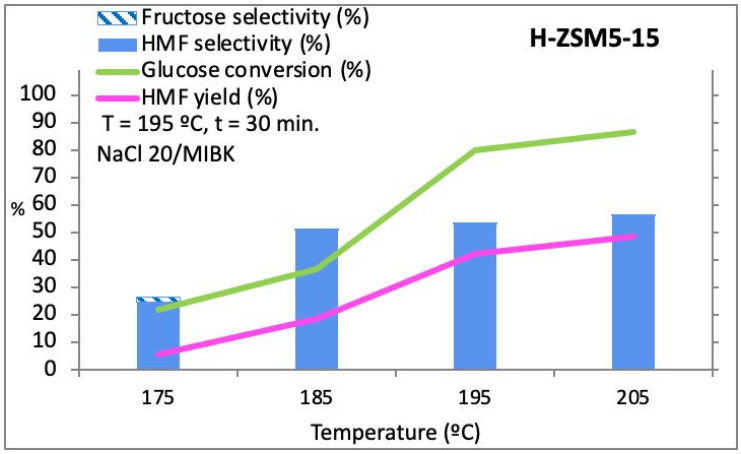

Figure 63. Influence of the temperature on glucose dehydration to HMF in NaCl (aq.)/MIBK, after 30 min., with H-ZSM5-15 with S/C ratio 3.

The influence of the temperature with H-Beta-12.5 as catalyst was also studied from 175 to 195 ºC, showing similar trends to those with H-ZSM5-15, but with high fructose selectivity under 195 ºC, due to its high Lewis acidity, which quickly isomerized glucose, and a low amount of Brönsted acid sites needed for dehydration ().

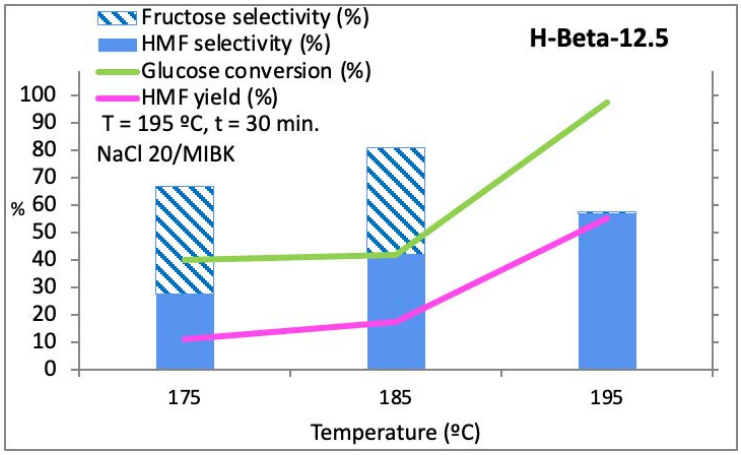

Figure 64. Influence of the temperature on glucose dehydration to HMF, in NaCl (aq.)/MIBK, after 30 min., with H-Beta-12.5 with S/C ratio 3.

Otomo *et al.* [140] studied different Beta zeolites in the glucose to HMF reaction, and with the most active zeolite, Beta-ST600, at 170 ºC after 15 min., fructose was obtained as main product with 71% selectivity, due to the role of Lewis acid sites.

At every temperature, soluble and insoluble byproducts, such as humins were formed, as could be inferred from the change of color of the H-ZSM5-15 catalyst from the first 15 min. of reaction, which diminished the HMF yield.

Reaction time

The kinetic study was carried out with H-ZSM5-15 as catalyst, in a biphasic NaCl (aq., 20 %wt.)/MIBK system, at 195 ºC, according to the previous results. It was revealed that maxima HMF selectivity and yield were attained after only 30 min., although glucose conversion improved at longer reaction times, indicating that, from 30 min., HMF was exposed to secondary reactions generating insoluble polymers which blocked active sites of the catalyst, decreasing the HMF selectivity from 53 to 28% between 30 and 75 min. ().

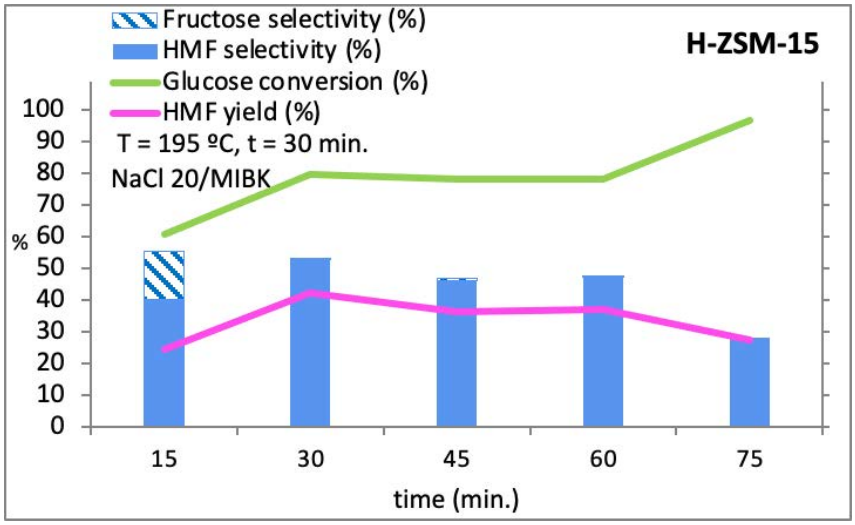

Figure 65. Kinetic study using H-ZSM5-15 in biphasic $NaCl_{aq}$/MIBK medium, at 195 ºC after 30 minutes with S/C ratio 3.

Catalytic activity with H-Beta-12.5 was also compared after 15 and 30 min., showing important differences in this time range than H-ZSM5-15, achieving lower glucose conversion and HMF selectivity (52.6 and

29.9%, respectively) than with H-ZSM5-15 (60.1 and 40.4%) after 15 min., but leading to 97.2 % *vs* 79.7 % glucose conversion and similar HMF selectivities after 30 min., which could be explained by the highest Lewis acidity of Beta zeolite, which could quickly isomerize glucose, but similar Brönsted acidity for both zeolites, which are responsible for dehydration to HMF.

Biphasic systems

Previous catalytic studies were carried out in a biphasic water/organic solvent, with a volume ratio of 0.43, which resulted optimal with other tested catalysts. After determining 195 ºC and 30 min. as standard experimental conditions, the influence of the organic phase volume (MIBK as solvent) in biphasic system with NaCl (aq., 20 wt.%) was evaluated ().

A low aqueous to organic phase (high volume of MIBK) ratio improved not only the HMF selectivity, but also the glucose conversion, resulting in a significant increase in HMF yield, nearly triple. These data confirmed the role of the organic phase for HMF extraction, favoring the equilibrium towards its formation and also preventing from subsequent degradation reactions. The achievement by the use of a biphasic system was supported also by the results obtained in the absence of MIBK, with high glucose conversion but only 3.6 % of HMF yield, due to rehydration of the formed HMF evidenced by the identification of levulinic acid in the aqueous phase after reaction (not quantified).

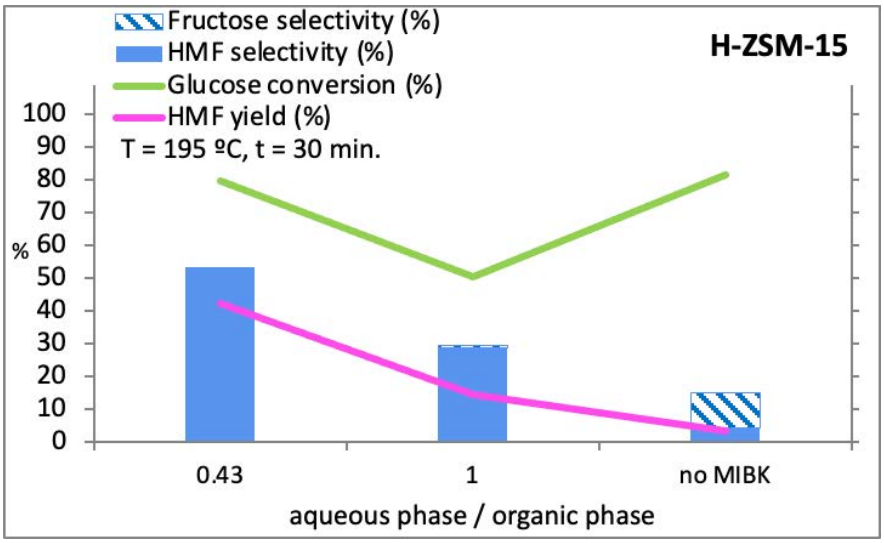

Figure 66. Influence of the organic phase volume, using H-ZSM5-15, with NaCl as aqueous phase, at 195 ºC after 30 min.

The presence of salt ions in the aqueous phase favored a high glucose conversion (81.6 %), but the introduction or the absence of an organic phase modified the HMF yield (42.2 *vs* 3.6 %). The high glucose conversions due to the presence of NaCl sustained the role of the alkaline and alkaline earth salts, not only by increasing the partition coefficient when an organic phase exists, but also taking part in the reaction mechanism [143,144]. This latter became more evident when glucose dehydration was studied at 195 ºC, in the absence of catalyst, in biphasic water/MIBK medium and also with NaCl (aq.) instead of water. After 30 min., HMF yield resulted 6.3% with NaCl and 1.9% with water, due to higher glucose conversion and HMF selectivity in the presence of salts (Figure 67).

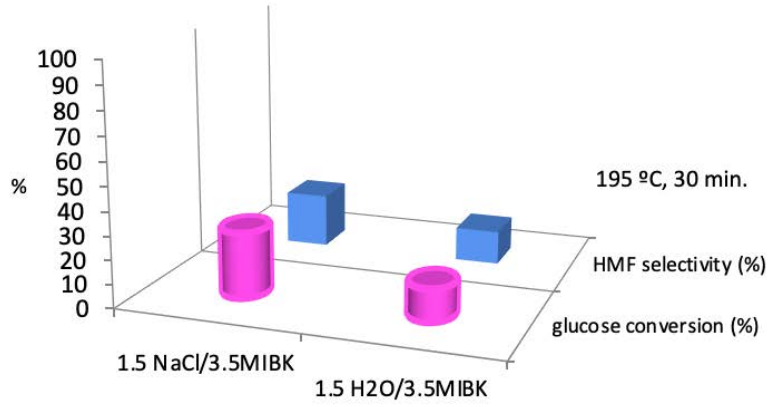

Figure 67. Catalytic activity in the absence of catalyst, in biphasic $NaCl_{aq}$/MIBK and water/MIBK systems.

Yu *et al.* have studied zeolites as catalysts for sugar valorization processes. Regarding glucose/fructose dehydration to HMF, the participation of cations and anions in the reaction has been stated using NaCl and ionic liquid. Thus, by using the ionic liquid BMIMCl, the cation can be exchanged with the Brönsted acid sites of the zeolite, releasing the proton and favoring the diffusion of the Brönsted acid sites. Moreover, the nucleophilicity of chloride anion is favorable for isomerization of glucose to fructose over Lewis acid sites [145].

In order to gain more in-depth knowledge on the role of ions of the inorganic salts into the glucose dehydration to HMF, several salts with different monovalent and divalent ions were evaluated.

Görgényi had previously studied the salting-out effect of inorganic cations and ions, concluding that, with respect to cations, the strongest effect was produced by the smallest hydrated ions, Na^+ and K^+, while,

regarding to anions, the double charged ones, as sulphate, were more effective than the simple charged ions [146].

More studies using a biphasic water/1-butanol medium with different inorganic salts for fructose dehydration to HMF had been reported by Román-Leshkov and Dumesic [123]. They found Na^+ and K^+ from chlorides showed the best combination of extracting power and HMF selectivity. As regards anion effect, changing Cl^- to Br^-, the partition coefficient (R) and the HMF selectivity resulted similar to non-salt systems, but changing to SO_4^{2-}, a high R value was obtained, while a low HMF selectivity was reached.

Glucose reaction was tested in a biphasic aqueous salt solution/MIBK system, with H-ZSM5-15 as catalyst, at 195 ºC for 30 min.. First comparison was in the presence of chloride anions. The glucose conversion followed the trend: $Na^+ > Li^+ > K^+$, whereas the selectivity values were very close, between 40 and 47% (). These results were consistent with those previously reported [132,146]. By maintaining the counterion (Na^+) and varying the nature of the anion, there were no significant differences in glucose conversions or HMF selectivities. The best catalytic performance was achieved with NaCl. These results also corroborated the previous results about the improvement of catalytic activity in glucose dehydration to HMF using alkali and alkaline earth metal chloride [147]. The role of NaCl in MFI type zeolites, as ZSM-5, has been explained by Gardner *et al.* through the enhancement of the hydrolysis of Si–O–Al bridges, releasing Al^{3+} species that catalyze the conversion of glucose under homogeneous conditions [148].

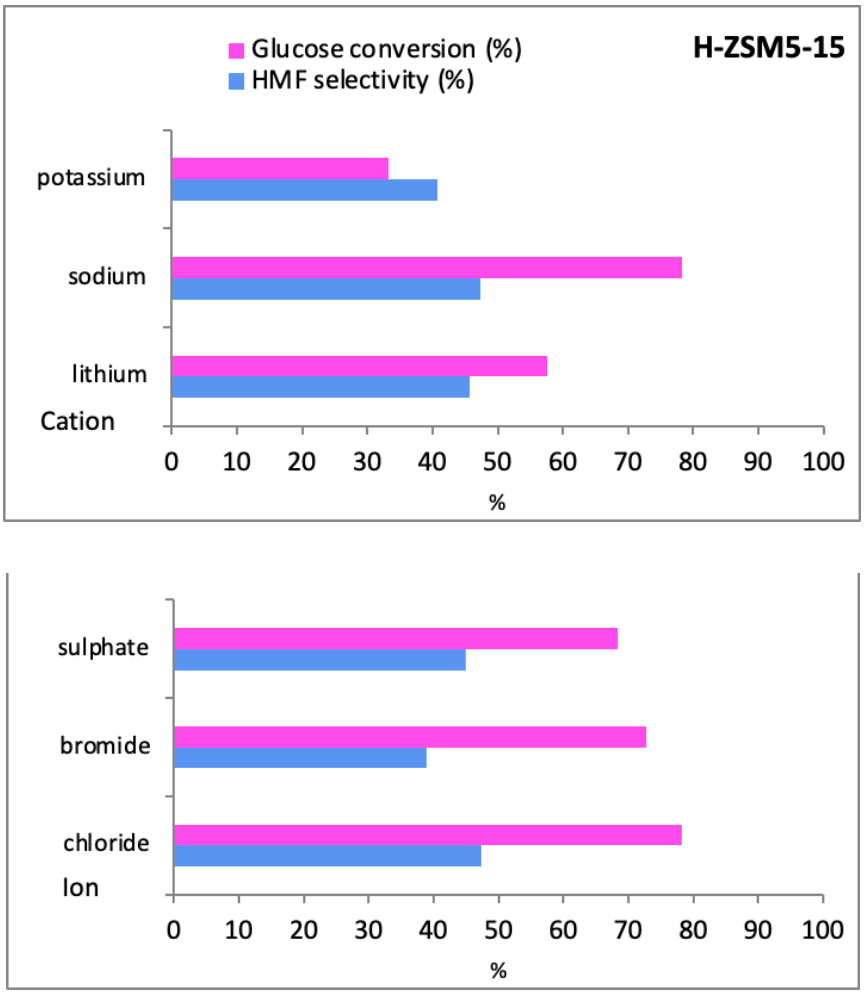

Figure 68. Effect of the cation (above) and the anion (below) in biphasic aqueous/MIBK medium, with H-ZSM5-15 at 195 ºC after 30 minutes with S/C ratio 3.

Thus, heterogeneous catalysis on the ZSM-5 zeolite and homogeneous one by aluminum cations seemed to occur simultaneously. $CaCl_2$ addition to the aqueous phase in the absence of catalyst led to higher HMF selectivity than with 10Al-MCM-41 as catalysts, and

glucose conversion resulted in similar values. By using H-ZSM5-15 as catalyst, better results than without catalyst were achieved, starting from glucose or fructose, but also higher conversion and HMF selectivity were obtained in the absence of catalyst, from both carbohydrates. These results suggested that $CaCl_2$ was involved in both glucose isomerization, occuring very fast, and in sugar dehydration. After the addition of the acid catalyst, more sugar can be converted.

Róman-Leshkov studied different biphasic systems with saturated salt solutions as aqueous phase for fructose dehydration to HMF [132] and using 1-butanol as organic phase, at 180 ºC, similar fructose conversion and HMF selectivity were achieved in the absence of salt and in the presence of calcium chloride, after 35 min.. Nevertheless, the addition of NaCl produced higher fructose conversion and HMF selectivity. In comparison with these reported results, but at different experimental conditions (temperature, time, solvent), the results in aqueous salt solution/MIBK, at 195 ºC, followed a different trend, with higher activity in the presence of salts, and the highest conversion and HMF selectivity with calcium chloride.

Rasrendra *et al.* studied glucose conversion catalyzed by inorganic salts of aluminum, zinc and chromium. At 140 ºC, HMF was also relevant by using zinc salts, and, observing the reactivitty and the chemo-selectivity changes by using salt solutions, they concluded metal ions of the salts played a key role [144].

Torres-Olea *et al.* studied the influence of Lewis acidity and $CaCl_2$ on the glucose dehydration to HMF with Nb-Zr oxides. They analyzed the catalysts after reaction, finding that Ca^{2+} cations interacted with

the catalysts, but specially with the catalyst with high Nb concentration. They suggested cation exchange between Ca^{2+} and protons in the Brönsted acid sites of these catalysts. Except with Nb_2O_5 as catalyst, they did not find fructose, pointing out another pathway for glucose conversion to HMF, not involving glucose to fructose isomerization [149].

The addition to $CaCl_2$ in the aqueous phase with H-ZSM5-15 was as effective as the addition to NaCl in the aqueous phase with 10Al-MCM-41, in terms of glucose conversion and HMF yield. Thus, the main role was suggested to be played by the cations.

It can be concluded that alkaline and alkaline earth salts can promote the glucose/fructose dehydration to HMF, but the cause and the effect of the salt cations and ions is not only related to the type of ions, but also to the interactions with each catalyst and to the specific reaction conditions.

Catalyst loading

The influence of the catalyst loading was previously studied in water/MIBK systems with Ta_2O_5 and 10Al-MCM-41 catalysts and in NaClaq/MIBK systems with 10Al-MCM-41, providing an optimum substrate/catalyst (S/C) weight ratio of 3 in any case. H-ZSM5-15 catalyst was loaded for having S/C weight ratios of 6, 3 and 2 in NaCl/MIBK ,in order to study the influence of the catalyst loading, finding that the glucose conversion increased from 46 to 80% when the glucose/catalyst weight ratio decreased from 6 to 3, but not varying from 3 to 2, that is, by increasing the amount of catalyst.

However, the HMF selectivity did not vary from 6 to 3 and slightly diminished from S/C weight ratio of 3 to 2 (50 % more of catalyst), due to the excess of active sites catalyzed also secondary reactions with HMF (Figure 69).

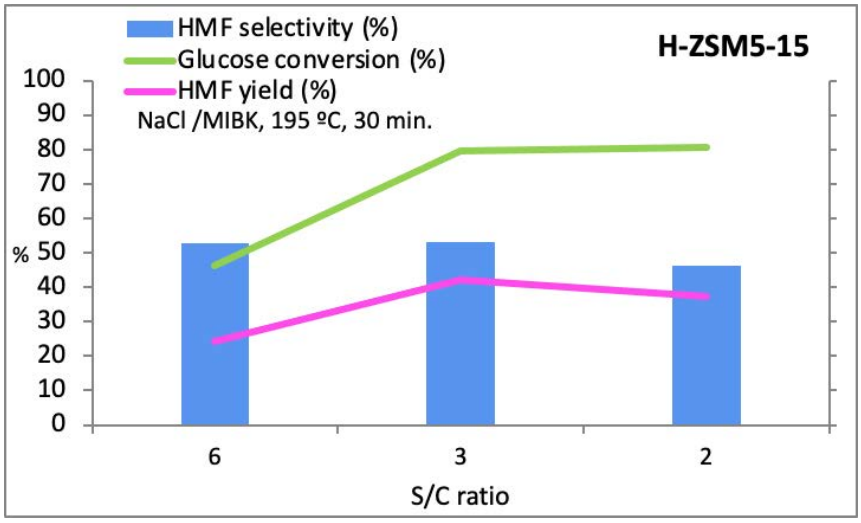

Figure 69. Influence of the catalyst loading at 195 ºC, in biphasic NaClaq/MIBK system, with H-ZSM5-15 at 195 ºC after 30 minutes.

External surface area and pore volume of the previously reported catalysts were very different, ranging between 79 and 587 $m^2\ g^{-1}$ and 0.06 and 1.45 $cm^3 g^{-1}$, respectively, but a S/C weight ratio of 3 resulted optimum for all of them, with 1.5 mL of aqueous phase and 3.5 mL of MIBK, which indicated that external diffusion would be the rate controlling step which limited the glucose adsorption.

Influence of the nature of the acid sites

Purely siliceous zeolites are not acidic, although structural defects in the lattice can origin acid sites. In zeolites with aluminum in isomorphous substitution of silicon, Brönsted acid sites are generated by protons which compensate the negative charge of the lattice. There are different types of hydroxyl groups in zeolites: bridged Si-O(H)-Al associated to Brönsted acidity; silanols (Si-OH), which can act as Brönsted acid sites and interact with penta-coordinated aluminum (Section 5.3.7. Figure 4) and sometimes, extra-framework Al-OH species. The strength of the O-H bonds determines inverse proportionally the strength of Brönsted acid sites, but, in zeolites, the location of the Brönsted acid sites into channels and defects in the crystalline structure are also factors controlling the acidity [149]. Lewis acidity, related to coordinatively unsaturated cations, is originated by extra-framework aluminum, but also by tetrahedral framework aluminum, as in resonant SiOH-->Al [150,151] that can accept electrons. Moreover, interconversion between Brönsted and Lewis acid sites can occur in zeolites [152].

The introduction of heteroato—modifies the nature and strength of the acidity, as a function of the number, coordination and framework position of these atoms. In this sense, it is an effective way for tuning the acidity. Cations(III) in the framework (Fe, B, Ga…) also provide Brönsted acid sites, as Al, and others such as Zr, Nb, Ti, Ta…provide Lewis acid sites. These cations provide more hydrophobicity and, consequently, more hydrothermal stability compared to zeolites with only Al and Si. Moreover, the heteroatoms together with the aluminum atoms are responsible of the overall acidity and can display

cooperative effects. Besides this, the structure of the zeolite determines preferential positions for Al or heteroatoms in the framework, and, in some zeolite crystals, a gradient of Al concentration throughout the crystal has been observed [150].

Concerning Fe-zeolites, iron can be present as isolated iron species (mononuclear or binuclear oxygen-bridged iron species), oligomeric iron oxide clusters and/or iron oxide nanoparticles, located in the framework, pores, extra-framework and also external surface, modifying the properties of the zeolites in different ways. In addition, isolated iron species can exist as isolated entities into the framework or extra-framework bounded to silicon hydroxyl "nests", as iron species coordinated with extra-framework aluminum, and as iron species at cation exchange sites [153]. By using ion-exchange method for iron introduction, this would be mainly deposited at the cation-exchange sites, although small clusters of iron species in the pores, coordinated unsaturated iron species, extra-framework and agglomerates of iron oxides on the surface, could also be formed [154]. The Si/Al ratio also influences on the iron dispersion, as the lower ratio, the more ionic sites and the better dispersion.

Once catalytic conditions for maximum activity were established for the zeolite-based catalysts, the influence of the nature of the acid properties was evaluated, by comparison of H-zeolites with Fe- and Cu-zeolites, with lower acidity, but, particularly, with Lewis acidity (Section 6.1.3). Firstly, ion-xchanged ZSM-5 zeolites (Fe-ZSM5-15 and Cu-ZSM5-15) were tested in biphasic water/MIBK medium at 195 ºC and after 150 min. Both Lewis catalysts led to higher glucose conversions (nearly 100 %), higher HMF selectivity and much lower

fructose selectivity, increasing the HMF yield from 1.6% (H-ZSM-5) to 30% (Fe-ZSM-5) and 26% (Cu-ZSM-5) (). Weak to moderate Lewis acid sites are considered to play the main role in the formation of HMF, as strong acidity promotes the formation of other byproducts [155]. Fe-ZSM5-15 and, specially, Cu-ZSM5-15 possessed more Brönsted and Lewis acid sites than the protonated form. Y and Beta-type zeolites were also tested and compared under similar reaction conditions (). Fe-Y-6 and Fe-Beta-12.5 enhanced the catalytic activity in comparison with the H-forms, although not as much as in the case of ZSM-5 catalysts. Iron in the Y zeolite highly increased the Lewis acidity with respect to H-Y-6, which favored the HMF selectivity. Fe-Beta-12.5 led to similar catalytic activity than H-Beta-12.5, which had resulted more active than the other H-zeolites. Lewis acidity resulted 50 % lower in Fe-Beta than in H-Beta, as well as total acidity, although external surface area and pore volume were larger. Synergistic effect between Brönsted and Lewis acid sites in Fe-Beta zeolites has been reported for glucose conversion to HMF [153,156]. Thus, cooperation between Fe and Al and better textural parameters would be responsible of the activity of Fe-Beta-12.5 despite possessing lower Lewis acidity. Cu-Y-6 and Cu-Beta-12.5 had much more Lewis acidity than the respective H-zeolites and even than the Fe-zeolites, which would reduce the HMF selectivity by the enhancement of secondary reactions with HMF, despite a lower fructose selectivity. Thus, not only Brönsted and Lewis acid sites should be taken into account, but also the possible Lewis-Brönsted acid sites synergy.

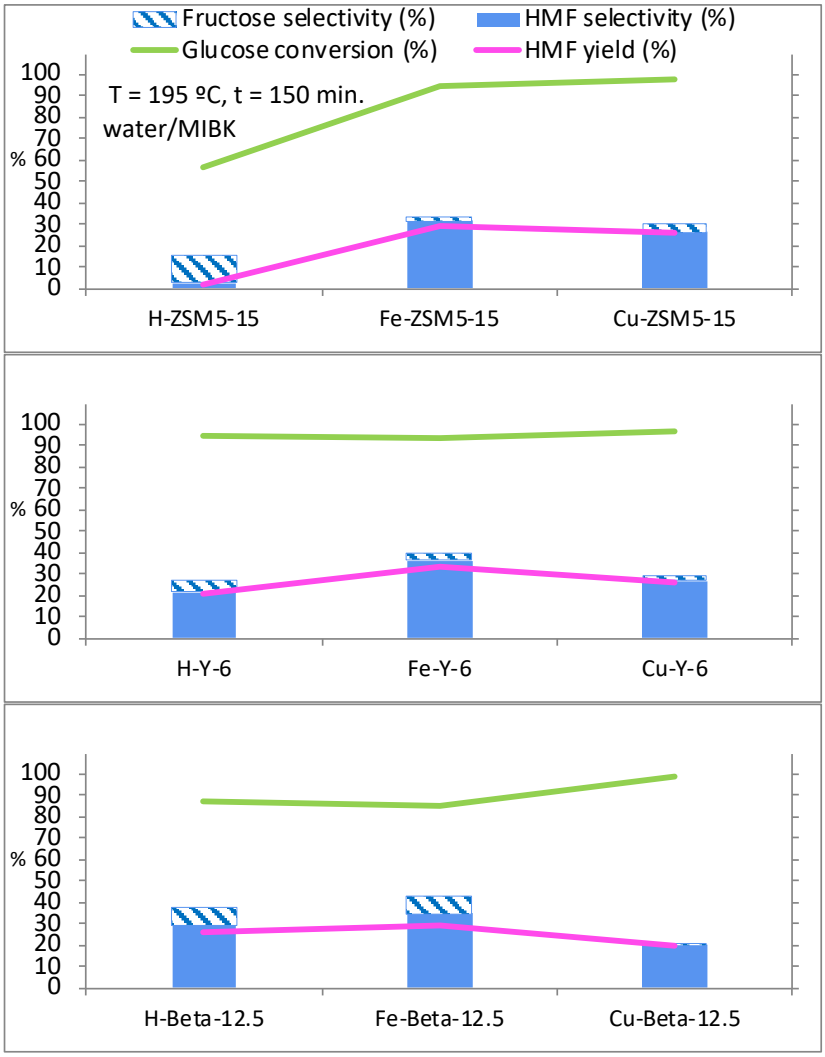

Figure 70. Catalytic activity at 195 ºC after 150 min. of H-, Fe- and Cu- zeolites in a biphasic water/MIBK system with S/C ratio 3.

Direct cooperation between Lewis acid sites and the neighboring proton donors influences on the catalytic properties of Lewis acid zeolites, such as Sn, Ti and Zr-containing aluminosilicates. Sn-Beta zeolites have been reported as very effective catalysts for selective

glucose isomerization to fructose, due not only to the higher Lewis acidity but also to secondary effects produced by neighboring proton-donating [157,158].

Co, Fe and Cu-BEA zeolites were prepared by Sobús *et al.* for the synthesis of acrylic acid from lactic acid [159], showing Co– and Cu–BEA zeolites the best catalytic properties for the direct dehydration of lactic acid to acrylic acid. Dimeric M–O–M species, such as [Cu^{2+}-O^{2-}–Cu^{2+}]. Were essential for this reaction [159].

A significant improvement by the introduction of metal transition cations (Fe(II) and Cu(II)) was only achieved for ZSM-5 zeolites. All the Fe-zeolites resulted more active than the H-form, reaching HMF yields around 30%, and also than Cu-zeolites. Thus, these zeolites were tested at a lower temperature, although the catalytic activity resulted lower than at 195 ºC, as expected. From 185 to 195 ºC, fructose selectivity decreased around 13% for all the Fe-zeolites, but HMF did not improve proportionally, especially in Fe-ZSM5-15 zeolite, with the strongest acidity, which favored secondary HMF reactions ().

Secondly, only the most effective cation-exchanged zeolites in comparison with the H-form (Fe- and Cu-ZSM-5) were tested in NaCl aqueous solution, at 195 ºC, under similar operation conditions at which H-ZSM5-15 catalyst showed a high activity, that is, after 30 min. (glucose conversion and HMF yield were 80 and 42%, respectively). HMF selectivity values resulted very close, and the main differences were found in terms of glucose conversion, which were similar with Cu- and H-ZSM5-15 zeolites and the half with Fe-ZSM5-15 ().

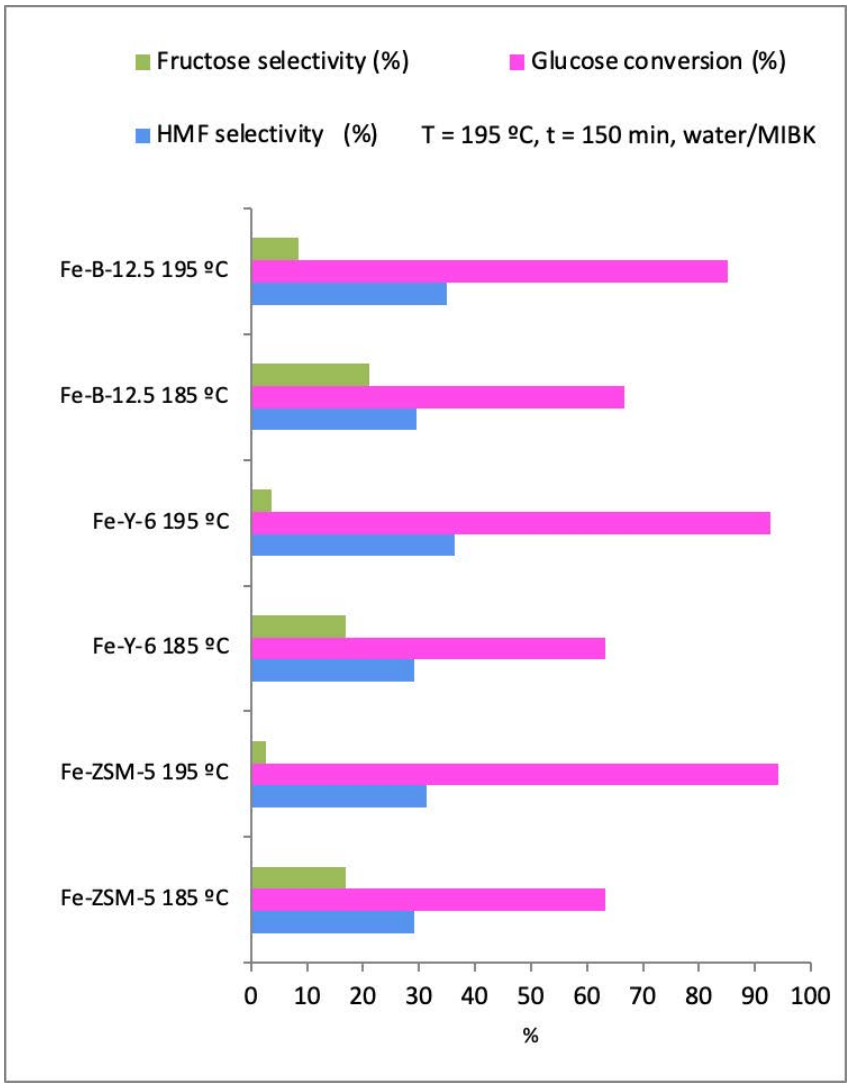

Figure 71. Catalytic activity of Fe-zeolites at different reaction temperatures in a biphasic water/MIBK system, after 150 min. with S/C ratio 3.

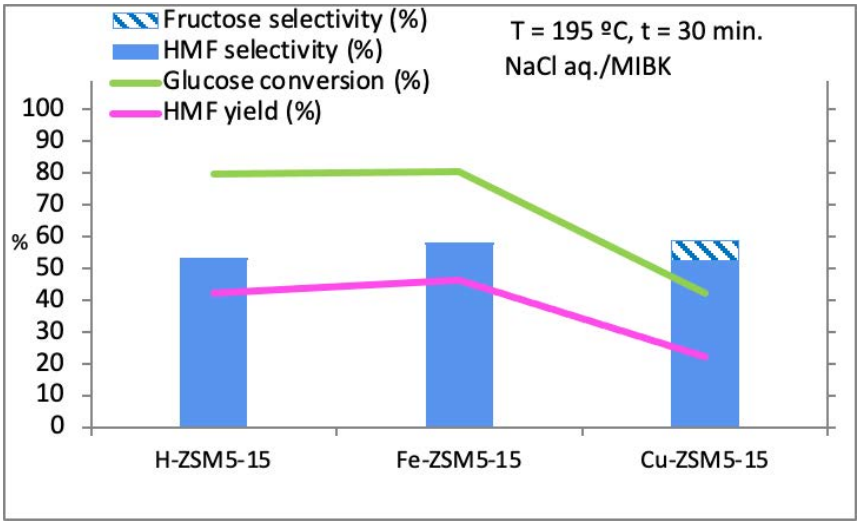

Figure 72. ZSM-5-type catalyst comparison in a biphasic $NaCl_{aq}$/MIBK system, at 195 ºC after 30 min. with S/C ratio 3.

In this sense, it was previously reported the role of NaCl in MFI type zeolites, as ZSM-5, hydrolyzing the Si-O-Al bridges and releasing Al^{3+} species that catalyzed the conversion of glucose through homogeneous catalytic processes [148]. Fe- and Cu-ZSM5-15 possessed very similar textural properties, but very different Lewis acidity, probably due to the aluminum enrichment on the surface of Cu-ZSM5-15, which was about the 25 % of the aluminum. This increase in surface produced an aluminum decrease into the framework, which could hinder the Al^{3+} promotion by Na^{+} cations. Another cause could be a cation exchange occurring between Fe(II,III) or Cu(II) ions with Na cations, reducing the number of Lewis acid sites available for the glucose reaction, since these iron and copper cations would be in solution as anionic chlorocomplexes, due to the high concentration of chloride ions.

In order to get insights into this possible cation-exchange process, the surface of the spent catalysts was analyzed by XPS, resulting in Na/Al atomic ratios of 0.47 (Fe-ZSM5-15) and 0.1 (Cu-ZSM5-15), while chloride ions were not detected. In addition, the surface M/Al atomic ratios were compared in fresh and spent catalysts. Fe/Al decreased from 0.2 to 0.13 and Cu/Al decreased from 0.08 to 0.05, resulting in both catalysts a metal (Fe, Cu) decrease around 35 % after reacting in the presence of NaCl aqueous solution. Thus, these data confirmed an exchange between Na and Fe or Cu cations. Hydrolyzed cations in the channels are weakly electrostatically bonded to the aluminum-silicate structure and have easy mobility and are able to be exchanged with the cations of the salt solution.

NaCl, as well as other inorganic salts, has been demonstrated to improve the zeolite adsorption properties when high concentration of salts are used. In the large cavities and channels of the zeolite structure, the exchangeable cations contact with cations of the salt solution, such as Na^+, producing chemical modifications. These modifications are essential in some processes, as in water treatment ones [160].

Catalyst reusability

Catalyst reusability is important not only for economical as also for environmental reasons. After separation from the reaction mixture, the used catalyst must be useful in a subsequent catalytic cycle, several times. Nevertheless, carbon deposition, thermal degradation, leaching, poisoning, among other factors, would lead to lower activity and,

finally, to deactivation. In glucose dehydration to HMF, humins and insoluble polymers were formed in every reaction test, as was clearly visible.

Oftenly, the loss of activity is reversed by regeneration processes for poison or deposition removal, being the most common the calcination [161]. Mesoporous tantalum oxide reutilization was tested without any treatment, and it was concluded that only one catalytic cycle was possible at reasonable catalytic activity. After washing with water and regenerated by calcination at 550 ºC (2 hours), the activity was well maintained for two additional catalytic cycles. 10Al-MCM-41 catalyst was reused without regeneration for four catalytic cycles, showing high catalytic activity along three cycles.

Spent H-ZSM5-15 was analysed by thermogravimetry in order to elucidate the calcination temperature required to regenerate it by decomposing the organic matter present in the catalyst. The weight loss from room temperature to 500 ºC resulted 11.3%, attributed to organic species removal. Thus, a thermal treatment at 550 °C (2 hours) was fixed in the calcination program to regenerate the used catalyst. After calcination, the acid characterization by Pyr-FTIR was carried out to get information about the catalyst modification. Fresh H-ZSM5-15 possessed 103 μmol g^{-1} of Lewis acid sites, while spent H-ZSM-15 increased until 345 μmol g^{-1}, which suggested the weakening of aluminum bonds in the framework and the generation of extra-framework aluminum. XPS analysis provided a Si/Al atomic ratio for the spent catalyst of 13, showing a surface aluminum enrichment as Si/Al ratio of the fresh catalyst was 18.

After regeneration and analysis, spent H-ZSM5-15 catalyst was tested in biphasic water/MIBK reaction medium at 195 ºC, showing an important glucose conversion increase, from 58.5 (fresh) to 81.9% (spent) while fructose selectivity diminished from 14.6 (fresh) to 10.3% (spent). Thus, glucose conversion was directly related to the Lewis acidity. HMF yield was kept, as HMF selectivity slightly decreased due to the loss of some Brönsted acid sites.

H-Beta-12.5 was also regenerated by calcination and tested in biphasic water/MIBK and in NaCl (aq., 20 wt.%)/MIBK in a second catalytic cycle, respectively. Besides XPS, which did not provide changes in the Si/Al ratio, XRD analysis were carried out of the spent catalysts, not showing important structural changes after reaction and calcination (Figure 73).

In water/MIBK (195 ºC, 150 min.), the results revealed a decrease in HMF yield, from 26 to 18%, mainly associated to the HMF selectivity decrease, as occurred in H-ZSM5-15, as expected for spent catalysts (Figure 74). With respect to the reuse of H-Beta-12.5 with NaCl solution as aqueous phase, the high glucose conversion achieved with the fresh catalyst experimented an important decrease, by about half, and the HMF selectivity was similarly reduced, leading to a lower HMF yield (31% instead of 56%). Pyr FTIR spectroscopy analysis of the spent catalyst showed reduction of both Brönsted and Lewis acidity with respect to the fresh catalyst. The low HMF yield could be due to a partial cation exchange of mobile acidic protons by sodium ions, due to the presence of NaCl in high concentration and weaker bonds in the framework, originating an important reduction of the Brönsted acidity. The performance in a second catalytic cycle of H-

Beta-12.5 was far from the activity of 10Al-MCM-41catalyst under similar experimental conditions, which after thermal regeneration still attained 49 % of HMF yield.

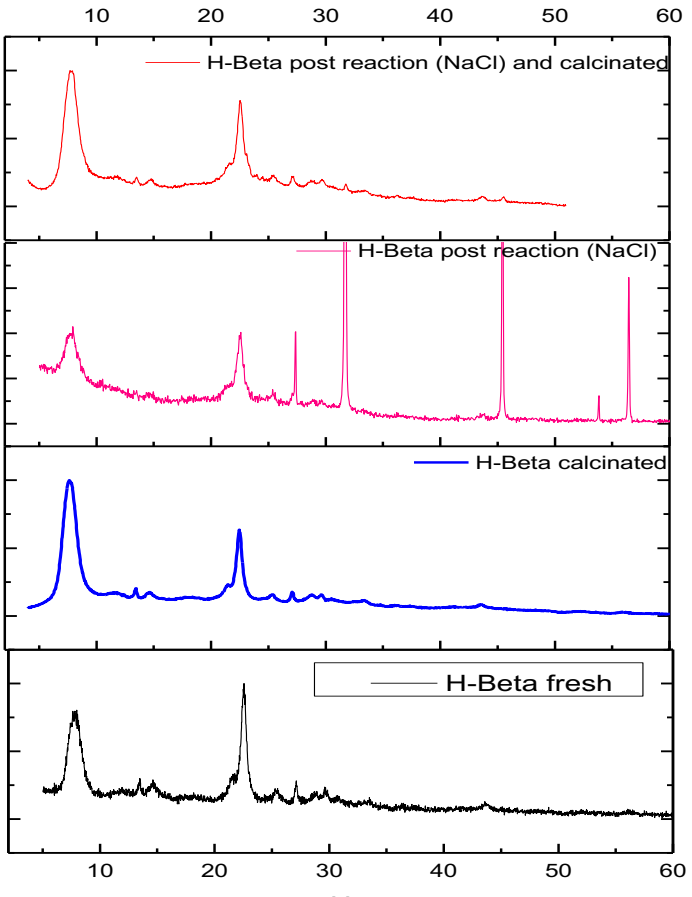

Figure 73. XRD patterns of H-Beta-12.5 catalyst fresh, calcined after reaction, and calcined after reaction in $NaCl_{aq}$/MIBK medium.

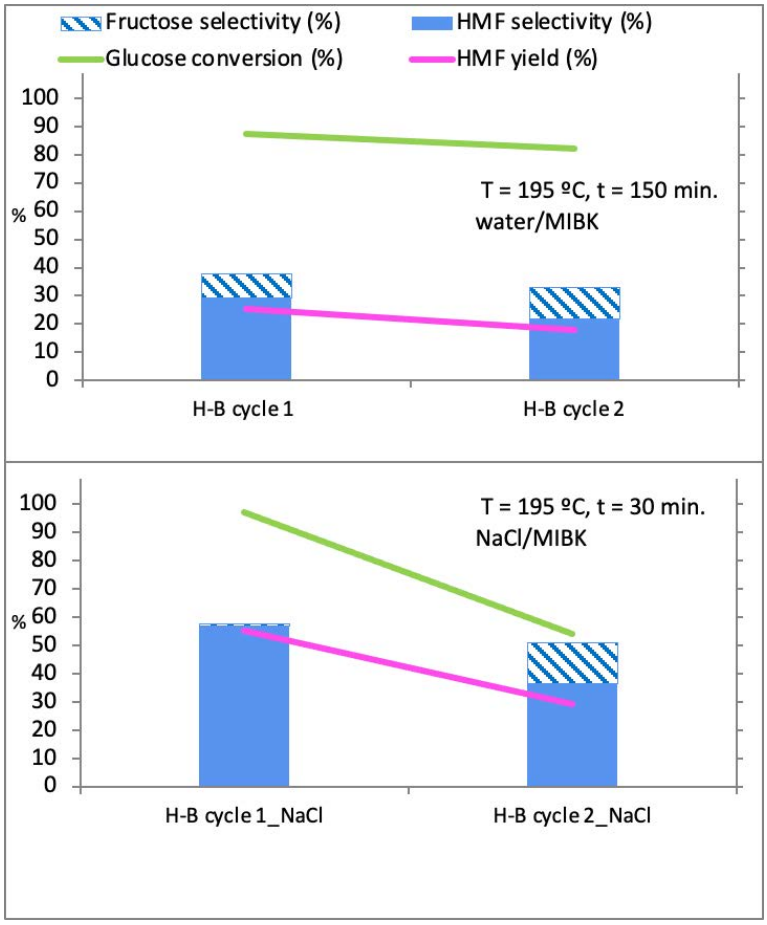

Figure 74. Catalytic activity of fresh (cycle 1) and used (cycle 2) H-Beta-12.5 catalyst at 195 ºC with S/C ratio 3.

Spent Fe-zeolites were also evaluated after calcination at 550 ºC (two hours) in biphasic water/MIBK system, leading to the catalytic results shown in . Fe-ZSM5-15 kept the activity from the first to second catalytic cycle, exhibiting high stability. Nevertheless, Fe-Y-6 and Fe-Beta-12.5 highly worsens glucose conversion, mostly Fe-Beta-12.5, which also decreased HMF selectivity and highly increased fructose selectivity. XPS data of spent Fe-Beta-12.5 barely indicated iron on the

surface. Analysis atomic spectrometry of the after reaction mixture revealed the presence of iron, indicating leaching from the catalyst. This fact would remove the acid sites, being responsible of the loss of activity.

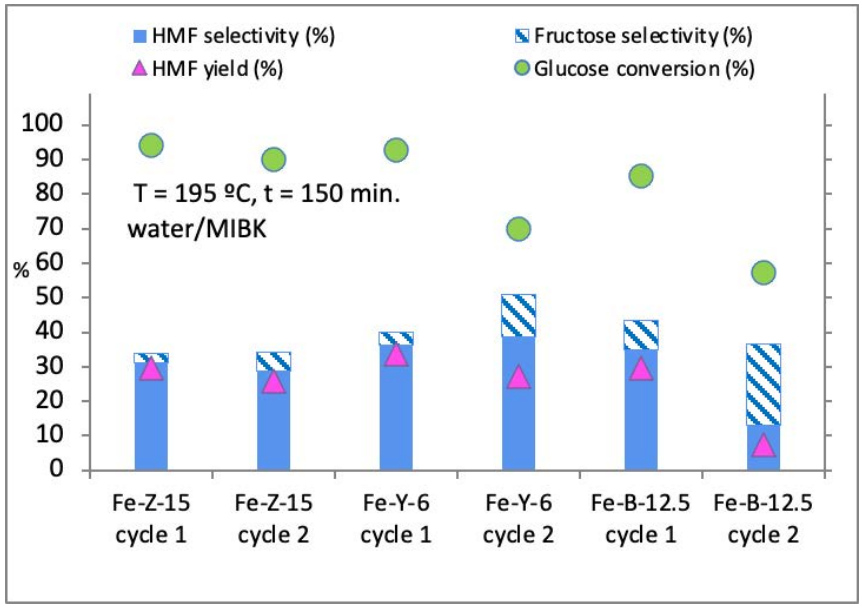

Figure 75. Catalytic activity of iron-containing zeolites as fresh (cycle 1) and used (cycle 2) catalysts at 195 ºC after 150 minutes in biphasic system water/MIBK with S/C ratio 3.

Cu-Beta-12.5 as fresh had previously shown lower activity than H- and Fe-Beta-12.5. The spent catalyst was regenerated by calcination and tested in biphasic water/MIBK system, at 195 ºC (). The results mostly indicated an increase in fructose selectivity, but also HMF selectivity increased. Si/Al atomic ratio determined by XPS increased from 9 (fresh) to 16.3 (spent). This partial dealumination could occur after reaction in hot water and calcination, and would increase the

hydrophobicity, preventing HMF from secondary reactions in the zeolite channels. The substitution of Al by Cu reduces Si-OH-Al groups, more hydrophilic. Also copper was barely found after reaction, which would be responsible of the glucose conversion decrease and the fructose selectivity increase, by the alteration of the acidic properties of the catalyst.

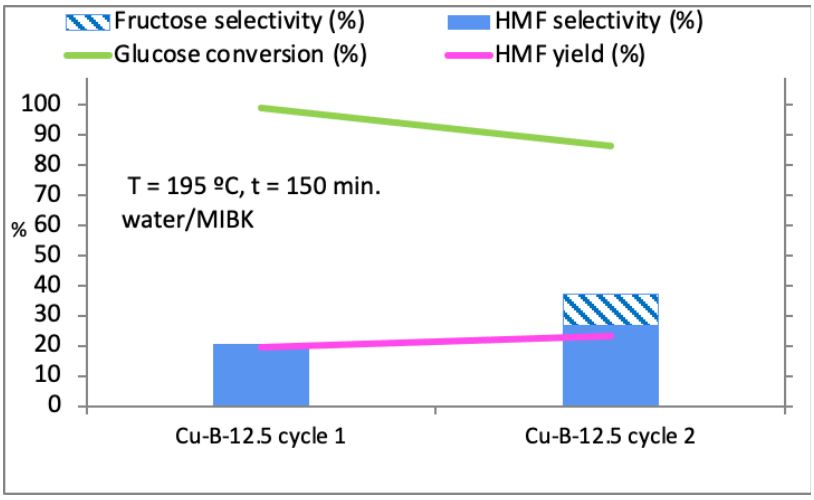

Figure 76. Catalytic activity of Cu-Beta-12.5 catalyst for two catalytic cycles at 195 ºC after 150 minutes in biphasic system water/MIBK with S/C ratio 3.

Thus, in a second catalytic cycle, also Fe-Y-6 resulted the most active.

6.2.4. Acidic carbons

Acidic carbons, chemically activated with phosphoric acid, with totally different structures and properties than the tested mesoporous oxides,

mesoporous aluminosilicates and zeolites, were also tested in the catalytic dehydration of glucose to HMF, under similar experimental conditions and procedures.

Firstly, acidic carbons derived from olive stones (HA series) and from lignin (L series) were evaluated in a biphasic water/MIBK medium, at 195 ºC for 150 min., optimal conditions for 10Al-MCM-41 and zeolites, maintaining a substrate/catalyst weight ratio of 3. The catalytic data reveal the absence of fructose and higher HMF selectivity and glucose conversion values were detected as general trend ().

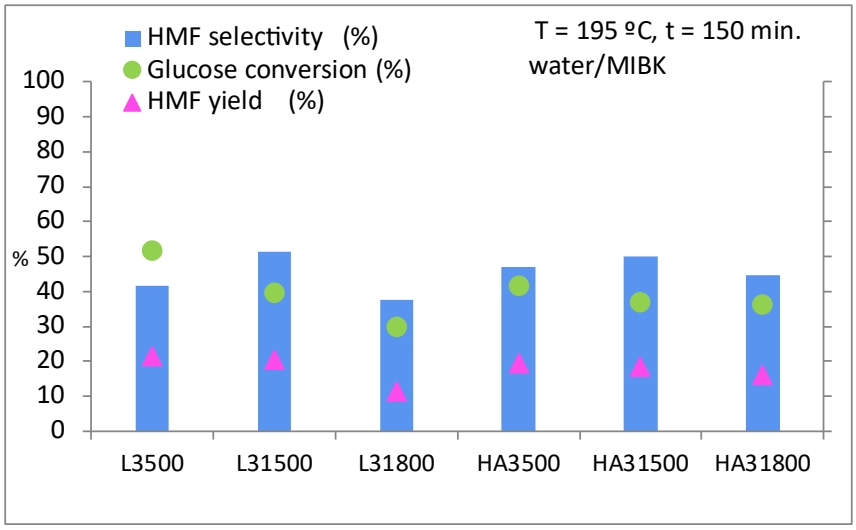

Figure 77. Catalytic activity of acidic carbons in glucose conversion to HMF in a biphasic water/MIBK system, at 195 ºC after 150 min. with S/C ratio 3.

Activated carbons at 800 ºC, with lowest porosity and acidity, converted less glucose than the corresponding carbons activated at 500 ºC, and also provided lower amounts of HMF. HMF selectivity was in the range 42 – 51% in the carbons activated at 500 ºC, being L31500 and HA31500 the most selective. These carbons possessed the largest specific surface area and wider micropores surface, with small micropores which limited the HMF degradation, and high porosity in combination to weak and medium acid sites for glucose conversion. Glucose conversion was maximal by using L3500 and HA3500, which possessed the smallest surface area and micropores, but large mesopores and the strongest acidity, associated to Brönsted acid sites .

Reaction temperature

To ensure maximum activity at the mildest reaction conditions, L3500, with the maximum glucose conversion, was also tested at 180 ºC, but only 38.2 % glucose conversion was achieved and HMF selectivity resulted 15.8 % after 150 min, giving a HMF yield of 6.1 %, lower to the one attained at 195 ºC (21.5 %).

As fructose was not detected in any catalytic reaction, HA31500 was studied under similar experimental conditions, but starting from fructose. At 160 ºC, HMF selectivity was similar than the ones achieved starting from glucose at 195 ºC. When reaction temperature was increased to 195 ºC, almost complete fructose conversion was achieved and HMF yield resulted to be 78%, much higher than starting from glucose (). These results and the absence of fructose in the reaction mixture when starting from glucose suggested a different

mechanism for glucose conversion by using these carbon-based catalysts, which did not isomerize glucose to fructose previously to the dehydration of the sugar to HMF. This hypothesis matches well with the detection (not quantification or identification) of a substance in the analysis (by HPLC) of the aqueous phase, which would be an intermediate of reaction.

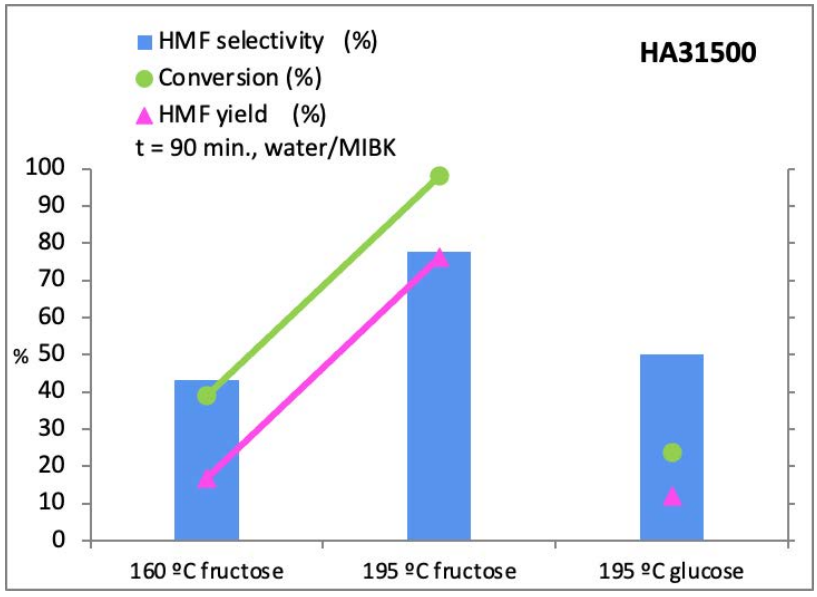

Figure 78. Catalytic activity of HA31500 acidic carbon starting from fructose or glucose, at different reaction temperatures after 90 minutes in biphasic system water/MIBK with S/C ratio 3.

Activated carbon had been reported as efficient adsorbent in the fructose dehydration to HMF, in order to suppress the formation of side-products such as levulinic acid [162].

Kuster and Van Steen, using a biphasic water/MIBK system, obtained similar results under similar experimental conditions than those used with HA31500, over 90% fructose conversion and around 70% fructose selectivity by using phosphoric acid as homogeneous catalyst (0.1 M) [163]. As the acidic carbons used as catalysts had been previously activated with phosphoric acid, it could be possible partial leaching of phosphoric acid groups, acting as Brönsted catalyst in the glucose dehydration to HMF. Thus, different concentrations of phosphoric acid were used as catalyst at 195 ºC for the glucose dehydration in water/MIBK. Catalytic data, shown in Figure 79, were worse than those reached by using acidic carbons, even at high concentration of phosphoric acid, and a possible partial contribution would be very low.

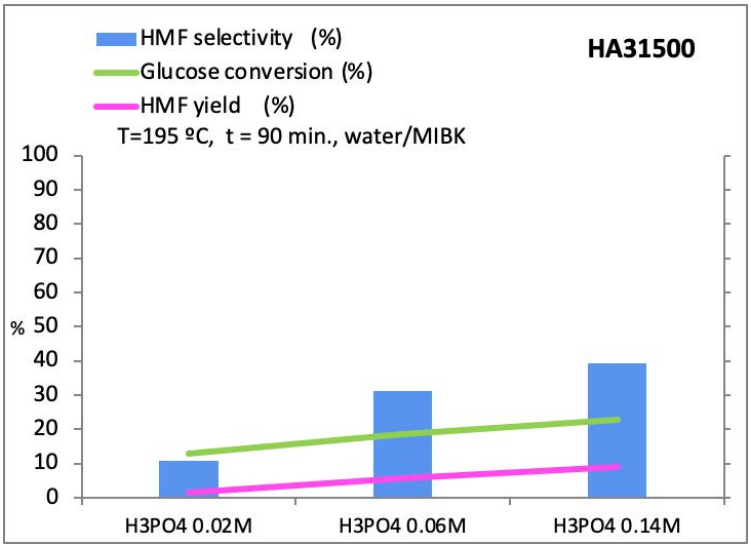

Figure 79. Catalytic activity of phosphoric acid at different concentrations in glucose dehydration to HMF in biphasic water/MIBK system, at 195 ºC after 90 min. with S/C ratio 3.

Reaction time

As L3500 was the most effective in terms of glucose conversion at 150 min., it was also studied at shorter reaction times. Glucose conversion rose with the reaction time, as expected, and HMF selectivity increased to a maximum value at 120 min.. Longer reaction times seemed to favor secondary reactions with the formed HMF, as is shown in .

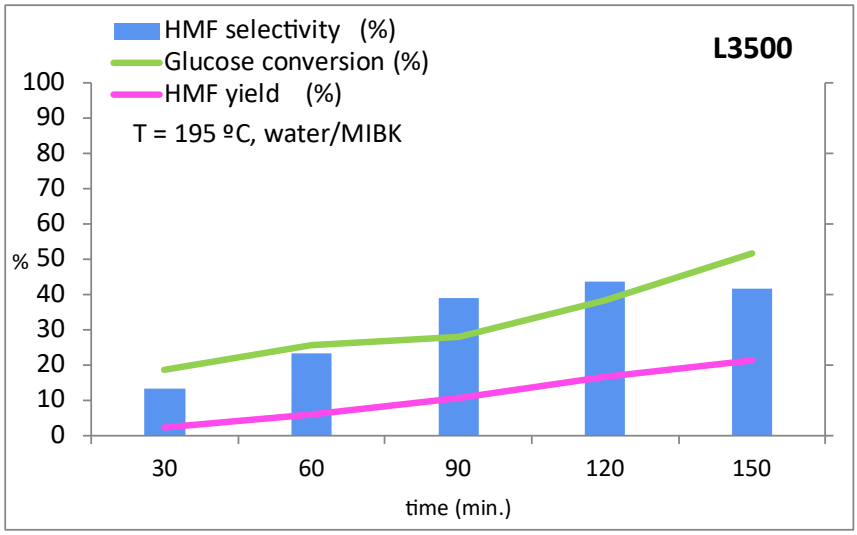

Figure 80. Kinetic of the reaction with L3500 acidic carbon catalyst in a biphasic water/MIBK system, at 195 ºC with S/C ratio 3.

This catalyst, under identical experimental conditions, provided similar glucose conversion than H-ZSM5-15 catalyst (41%) and similar HMF selectivity than 10Al-MCM-41. Therefore, L3500 would combine the advantage of the other two catalysts, but from the economic and

environmental point of view, as it has been obtained from biomass wastes, it would be preferred. These data highlight that the catalytic activity is driven by both textural characteristics and acidic properties.

L31500 and HA31500, which reached the highest HMF selectivity, were tested at shorter reaction time, 90 min., at which mesoporous tantalum oxide resulted more active, also in biphasic water/MIBK system, at 195 ºC. Both activated carbons showed lower glucose conversion at shorter reaction times, as expected, but the same HMF selectivity, around 50 % (Figure 81), due to a longer reaction time favored HMF subsequent reactions, also catalyzed by weak and medium acid sites. Thus, a time of 90 min. could be considered as optimal, recovering back glucose for another reaction cycle.

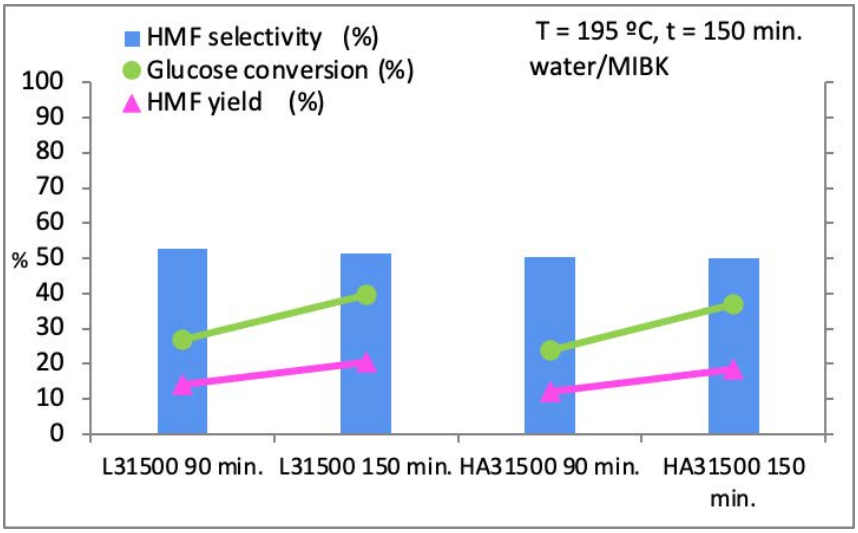

Figure 81. Catalytic activity in a biphasic water/MIBK system, at 195 ºC after 90 and 150 min. with S/C ratio 3.

As fructose conversion resulted lower than 40% at 160 ºC, but fructose is more reactive than glucose and more selective to HMF [164], a kinetic test was carried at this temperature. Catalytic activity increased with the time as expected, but HMF selectivity remained between 120 and 150 min., which indicated secondary reactions at longer reaction times.

Biphasic systems

The influence of the reaction medium was also studied with L31500 and HA31500 as catalysts. Water/MIBK has demonstrated to prevent HMF for further reactions and selectivity in the range 40-52% had been achieved. They were also tested in water, with only the aqueous phase, and selectivity were lower than 13 % (Figure 82).

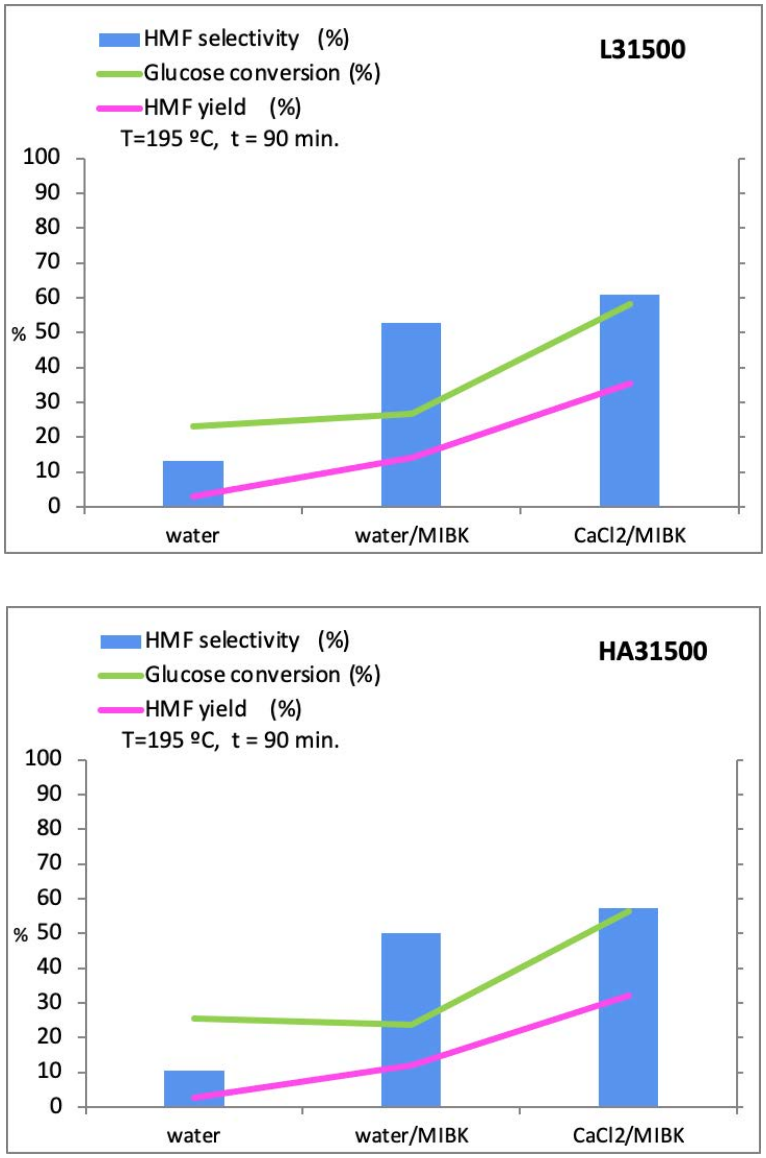

Figure 82. Catalytic activity of L31500 and HA31500 acidic carbons in different reaction medium, at 195 ºC after 90 min. with S/C ratios 3.

The influence of the proportion of MIBK in the reaction medium was studied in order to use as much lower amount as necessary, but maximum HMF yield. Previous catalytic tests were carried out with 1.5 mL water and 3.5 mL MIBK, which represented 70% of organic phase. Experiments with lower organic phase percentages (Figure 83), did not lead to better HMF yield.

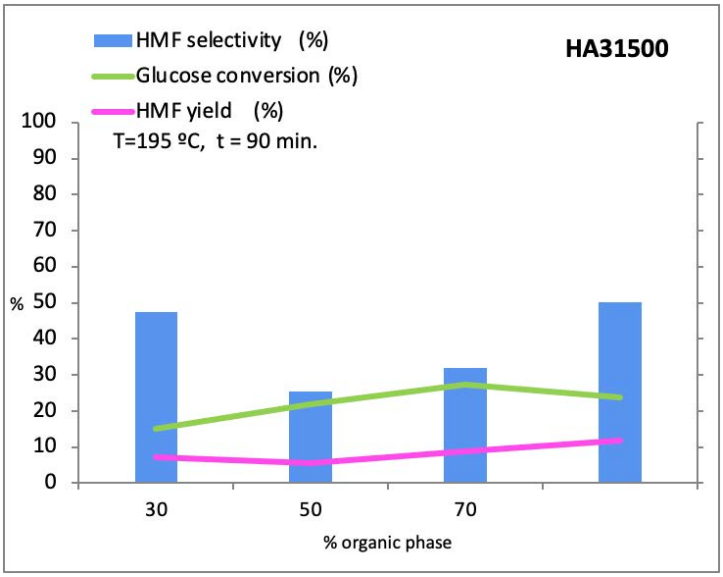

Figure 83. Influence of the organic phase proportion in biphasic water/MIBK systems, at 195 ºC after 90 minutes, using HA31500 with a S/C ratio 3.

With the lowest amount of MIBK, glucose conversion was very low as partition coefficient resulted only 0.15, not shifting towards reaction products. When the proportion of MIBK was increased to 30, 50 and 70%, the partition coefficient improved to 0.45, 1 and 2.1 respectively. At 70 % of organic phase, HMF resulted maximum, although glucose

conversion decreased, due to diffusional limitations in a small volume of aqueous phase.

As a biphasic medium consisting of aqueous $CaCl_2$ solution/MIBK with other studied catalysts (10Al-MCM-41 and H-ZSM5-15) led to high activity values, the acidic carbons were also tested in this biphasic system. The obtained results, in , showed the importance of the organic phase, which retains the major part of the formed HMF, avoiding degradation reactions. In only water, HMF selectivity were around 12% and glucose conversion under 25%. The introduction of MIBK increased HMF selectivity over 50% for both catalysts. When calcium and chlorine ions are introduced, glucose conversion was doubled, although HMF selectivity was slightly increased. These ions participated mainly in the mechanism of glucose conversion. In the reactions with H-ZSM5-15 catalyst, they seemed to favor the glucose isomerization to fructose. Nevertheless, in other reported studies, where fructose was not detected, another pathway from glucose conversion to HMF not involving isomerization to fructose was suggested [149]. With the acidic carbons, isomerization to fructose did not occur. Calcium ions could interact with hydroxyl group of glucose and with phosphate groups of activated carbons, facilitating the glucose conversion, or could only shift the reaction towards the products due to the improvement of the partition coefficient between the organic and the aqueous phase.

Cyclopentylmethyl ether (CPME), an eco-solvent [165] tested in the catalyzed dehydration of glucose using 10Al-MCM-41, was also used with HA31500 acidic carbon, as catalyst, at 195 ºC in a biphasic water/organic solvent medium. After 90 min., glucose conversion was

higher than with MIBK as organic solvent (34% vs 24%), but HMF selectivity was much lower (Figure 84). A similar effect was observed when water/CPME was employed with 10Al-MCM-41, which was due to a very low partition coefficient. R was calculated and resulted 2.1 in water/MIBK and only 0.61 in water/CPME.

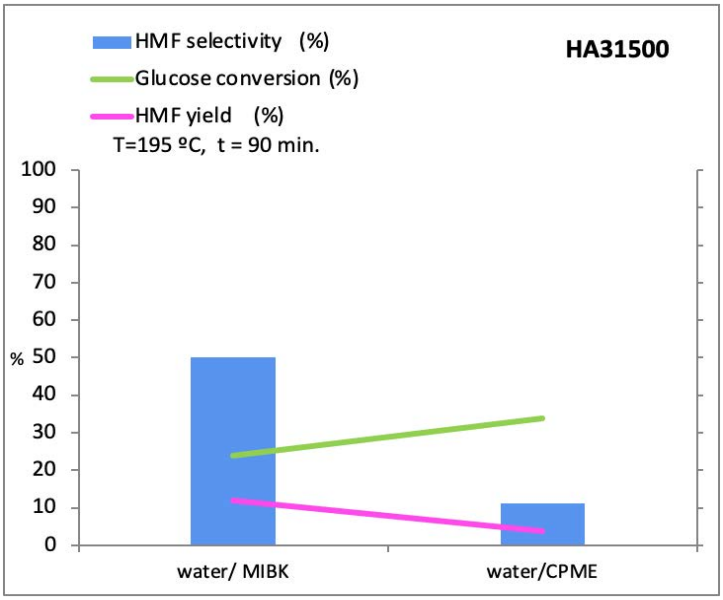

Figure 84. Catalytic activity by using HA31500 acidic carbon in biphasic system, using MIBK or CPME as organic phase at 195 ºC after 90 minutes with S/C ratio 3.

When CPME was used as organic phase with HA31500 catalyst, furfural was detected. Ouwen *et al.* [166] studied the glucose conversion in HMF and furfural in the presence of Brönsted acids (H_2SO_4, HCl, HNO_3 and H_3PO_4) and Lewis acids ($SnSO_4$, $CuSO_4$ and $MnSO_4$), as co-catalysts. Maximum HMF selectivity (47%) was achieved by using the HCl-$SnSO_4$ system, with selectivity towards

furfural of 19%, while maximum furfural selectivity (30%) was achieved with H_2SO_4-$SnSO_4$, with a HMF selectivity of 14%. A weaker Brönsted acid as H_3PO_4 only produced HMF and furfural with a selectivity of 1%.

These results suggested that the presence of strong Brönsted acid sites together with Lewis acid sites, such as in HA31500, favored not only HMF formation but also furfural. A proposed mechanism [167] when fructose is not detected is that glucose dehydrates through 3-deoxy-glucosone as key-intermediate, which can be twice dehydrated to HMF, but also 3-deoxyglucosane could be dehydrated to an unstable intermediate, which would loss carbon as formaldehyde, forming furfural. MIBK, with a high partition coefficient, retains much HMF, displacing the reaction towards its production, but CPME, with a lower partition coefficient, enable both reactions, although favoring HMF *versus* furfural.

Wang *et al.* studied the catalytic conversion of glucose and also directly from corncob residues with mixtures of $AlCl_3$-HCl as catalyst, reaching 54.5% HMF yield at 175 ºC after 20 min., in a biphasic system $NaCl_{aq}$/CPME (ratio 1:3) system, starting from glucose. In biphasic water/CPME system, glucose conversion reached 60%, and HMF yield resulted lower than 10%. The influence of the CPME/water ratio was also studied, finding that ratios higher than 3 decreased glucose conversion values, explained by a possible competition between water and CPME, due to its character dipolar and alkaline character, affecting the acid strength [168].

The biphasic system for highest catalytic activity was $CaCl_2$ (aq.)/MIBK, although in the absence of $CaCl_2$, some HMF selectivity was achieved.

Catalyst loading

The influence of the substrate/catalyst weight ratio of L31500 and HA31500 acidic carbons in a biphasic water/MIBK system was studied, as performed for mesoporous tantalum oxide and 10Al-MCM-41. For zeolites, it was also studied but the aqueous phase consisted of a NaCl aqueous solution instead of pure water. For both catalysts, glucose conversion increased from S/C ratio of 6 to 3, decreasing with a higher proportion of catalyst (Figure 88). This trend was also observed with 10Al-MCM-41, and was explained by external diffusional as controlling step, which limited the glucose adsorption, leading to lower conversion. The larger pores and surface acidity promoted the glucose reaction, increasing notably the HMF yield from S/C of 6 to 3. At higher amount of catalyst, despite lower glucose conversion, HMF selectivity notably increased, due to the presence of many active sites for the reduce adsorbed glucose molecules, especially in L31500, with the better textural-acidic properties tandem for HMF selectivity, as demonstrated in every catalytic test. The trend for these acidic carbons was similar to that of 10Al-MCM-41, which pointed out more physical than chemical causes.

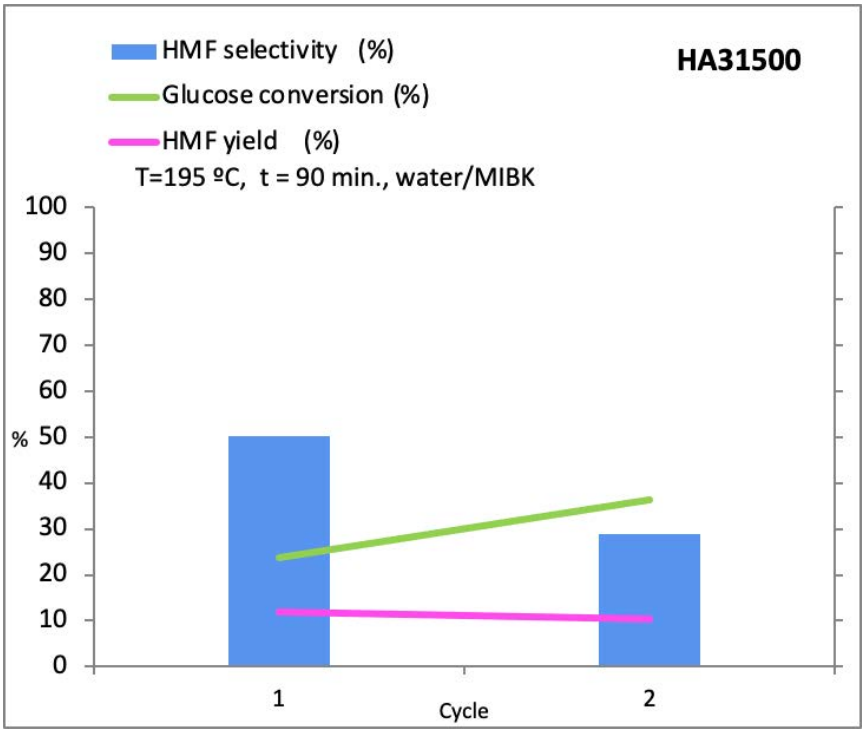

Figure 85. Comparison of catalytic activity of HA31500 of fresh catalyst (cycle 1) and used catalyst (cycle 2) in biphasic system water/MIBK with S/C ratio 3 at 195 ºC after 90 minutes.

Catalysts reusability

The formation of reaction byproducts, such as humins, was also observed in the reaction medium, which in subsequent catalytic cycles deactivate the catalyst. HA31500 was essayed without any treatment in a second catalytic cycle. The achieved HMF yield resulted very similar (Figure 86), but whereas with the fresh catalyst glucose conversion resulted 24% and HMF selectivity over 50%, with the used catalyst in a second cycle, HMF selectivity decreased under 30%, but glucose conversion increased to 36%.

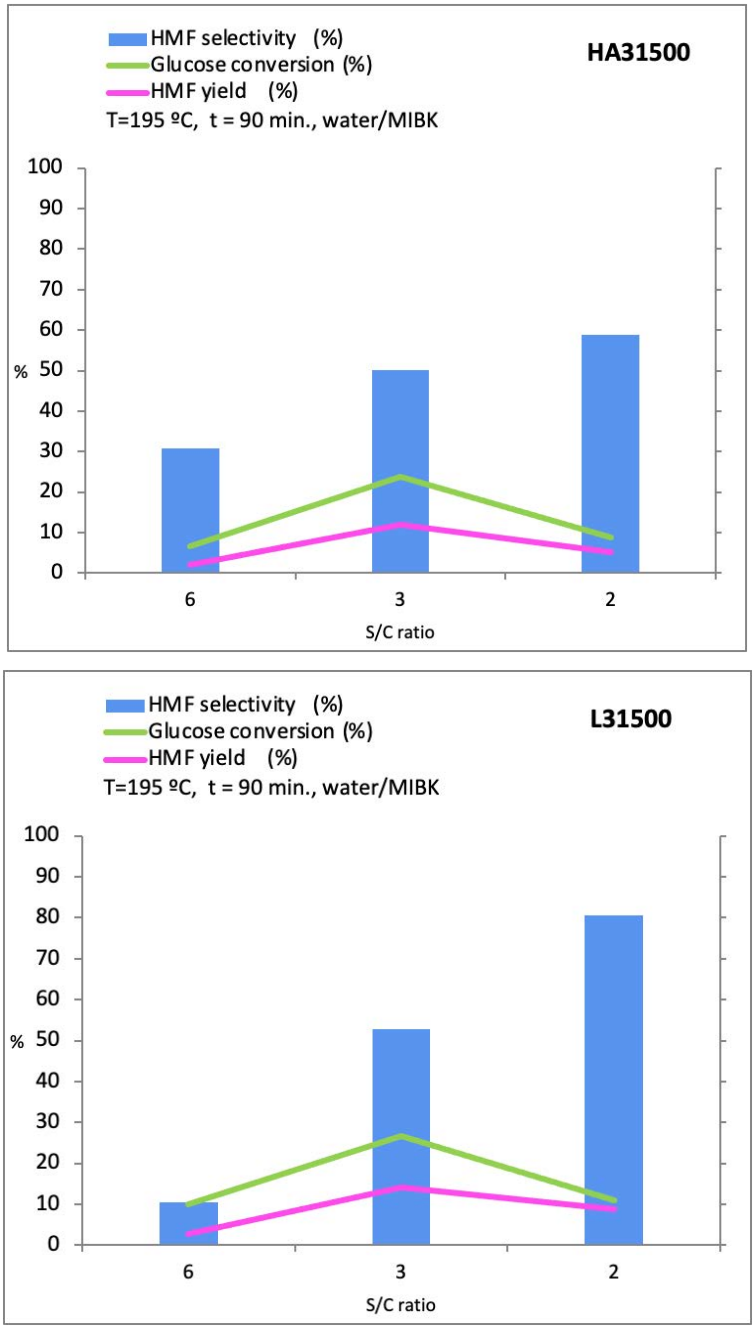

Figure 86. Influence of the substrate/catalyst ratio of HA- and L-31500 catalysts in a biphasic water/MIBK system, at 195 ºC after 90 minutes.

These data, also considering the previous catalytic test with homogeneous phosphorous-based catalyst, suggested that if partial leaching could have occurred, which would have acted as homogenous catalyst not only for glucose conversion, achieving higher values, but also for HMF degradation reactions. But analysis of phosphorous were not carried out. Thus, the decrease in HMF formation was considered as related to the deposition of byproducts, blocking active sites.

Villa *et al.* investigated phosphorylated mesoporous carbons (PMCs) for fructose conversion to HMF [94]. They found that the concentration of P-O groups was directly related with the activity, but inversely with the HMF selectivity and also with the degradation of HMF. Regarding the reusability of the catalyst, they reused it without any treatment and P/N-0.25 catalyst reduced only the activity after the first cycle, but not in the subsequent cycles, but other catalysts P/N-0.50 and P/N-0.75, decreased the activity in every catalytic cycle. P was analyzed but not detected, and the deactivation was related to the coverage of the surface and blocking of the pores by carbonaceous material. The morphology of the catalyst did not change.

Rechia-Goracy *et al.* [169] synthesized acidic carbons by different methods and tested in transesterification of rapeseed oil to biodiesel. Carbons with sulphonic groups resulted appropriate as catalysts. They found the catalytic activity of AW-BDS-20 to drop considerably after the first reaction cycle, being the yield very low in the fourth cycle. The analysis reported only a small number of sulfonic functional groups having leached out from the catalyst surface, but after four cycles, partial removal of -SO_3H groups.

6.3. List of Figures

Figure 62. Influence of the NaCl aq. addition in the reaction medium using H-zeolites and comparison with 10Al-MCM-41 at 195 ºC after 30 minutes in water/MIBK system with S/C ratio 3.

Figure 63. Influence of the temperature on glucose dehydration to HMF in NaCl (aq.)/MIBK, after 30 min., with H-ZSM5-15 with S/C ratio 3.

Figure 64. Influence of the temperature on glucose dehydration to HMF, in NaCl (aq.)/MIBK, after 30 min., with H-Beta-12.5 with S/C ratio 3.

Figure 65. Kinetic study using H-ZSM5-15 in biphasic $NaCl_{aq}$/MIBK medium, at 195 ºC after 30 minutes with S/C ratio 3.

Figure 66. Influence of the organic phase volume, using H-ZSM5-15, with NaCl as aqueous phase, at 195 ºC after 30 min.

Figure 67. Catalytic activity in the absence of catalyst, in biphasic $NaCl_{aq}$/MIBK and water/MIBK systems.

Figure 68. Effect of the cation (above) and the anion (below) in biphasic aqueous/MIBK medium, with H-ZSM5-15 at 195 ºC after 30 minutes with S/C ratio 3.

Figure 69. Influence of the catalyst loading at 195 ºC, in biphasic NaClaq/MIBK system, with H-ZSM5-15 at 195 ºC after 30 minutes.

Figure 70. Catalytic activity at 195 ºC after 150 min. of H-, Fe- and Cu- zeolites in a biphasic water/MIBK system with S/C ratio 3.

Figure 71. Catalytic activity of Fe-zeolites at different reaction temperatures in a biphasic water/MIBK system, after 150 min. with S/C ratio 3.

Figure 82. Catalytic activity of L31500 and HA31500 acidic carbons in different reaction medium, at 195 ºC after 90 min. with S/C ratios 3.

Figure 83. Influence of the organic phase proportion in biphasic water/MIBK systems, at 195 ºC after 90 minutes, using HA31500 with a S/C ratio 3.

Figure 84. Catalytic activity by using HA31500 acidic carbon in biphasic system, using MIBK or CPME as organic phase at 195 ºC after 90 minutes with S/C ratio 3.

Figure 85. Comparison of catalytic activity of HA31500 of fresh catalyst (cycle 1) and used catalyst (cycle 2) in biphasic system water/MIBK with S/C ratio 3 at 195 ºC after 90 minutes.

Figure 86. Influence of the substrate/catalyst ratio of HA- and L-31500 catalysts in a biphasic water/MIBK system, at 195 ºC after 90 minutes.

6.4. List of Tables

6.5. References

[1] D.M. Antonelli, J.Y. Ying, Synthesis and Characterization of Hexagonally Packed Mesoporous Tantalum Oxide Molecular Sieves, Chem. Mater. 8 (1996) 874–881. https://doi.org/10.1021/cm9504697.

[2] F. Yang, Y. Li, Q. Zhang, X. Sun, H. Fan, N. Xu, G. Li, Selective conversion of cotton cellulose to glucose and 5-hydroxymethyl furfural with SO4(2-)/MxOy solid superacid catalyst., Carbohydr. Polym. 131 (2015) 9–14. https://doi.org/10.1016/j.carbpol.2015.05.036.

[3] K. Brezesinski, J. Wang, J. Haetge, C. Reitz, S.O. Steinmueller, S.H. Tolbert, B.M. Smarsly, B. Dunn, T. Brezesinski, Pseudocapacitive Contributions to Charge Storage in Highly Ordered Mesoporous Group V Transition Metal Oxides with Iso-Oriented Layered Nanocrystalline Domains, J. Am. Chem. Soc. 132 (2010) 6982–6990. https://doi.org/10.1021/ja9106385.

[4] L. Xu, J. Guan, W. Shi, L. Liu, Heterostructured mesoporous In2O3/Ta2O5 composite photocatalysts for hydrogen evolution: Impacts of In2O3 content and calcination temperature, J. Colloid Interface Sci. 377 (2012) 160–168. https://doi.org/http://dx.doi.org/10.1016/j.jcis.2012.04.010.

[5] L.A. Aleshina, S. V Loginova, Rietveld analysis of X-ray diffraction pattern from β-Ta2O5 oxide, Crystallogr. Reports. 47 (2002) 415–419. https://doi.org/10.1134/1.1481927.

[6] M. Thommes, Physisorption of gases, with special reference to the evaluation of surface area and pore size distribution (IUPAC Technical Report), 2016. https://doi.org/10.1515/ci-2016-0119.

[7] P.A. Monson, Understanding adsorption/desorption hysteresis for fluids in mesoporous materials using simple molecular models and classical density functional theory, Microporous Mesoporous Mater. 160 (2012) 47–66. https://doi.org/https://doi.org/10.1016/j.micromeso.2012.04.043.

[8] C.G. Sonwane, S.K. Bhatia, Characterization of Pore Size Distributions of Mesoporous Materials from Adsorption Isotherms, J. Phys. Chem. B. 104 (2000) 9099–9110. https://doi.org/10.1021/jp000907j.

[9] S. Brunauer, P.H. Emmett, E. Teller, Adsorption of gases in multimolecular layers, J. Am. Chem. Soc. 60 (1938) 309–319.

[10] L. Xu, J. Guan, W. Shi, L. Liu, Heterostructured mesoporous In2O3/Ta2O5 composite photocatalysts for hydrogen evolution: Impacts of In2O3 content and calcination temperature, J. Colloid Interface Sci. 377 (2012) 160–168. https://doi.org/10.1016/j.jcis.2012.04.010.

[11] P. Yang, D. Zhao, D.I. Margolese, B.F. Chmelka, G.D. Stucky, Block Copolymer Templating Syntheses of Mesoporous Metal Oxides with Large Ordering Lengths and Semicrystalline Framework, Chem. Mater. 11 (1999) 2813–2826. https://doi.org/10.1021/cm990185c.

[12] E.G. Vaschetto, G.A. Monti, E.R. Herrero, S.G. Casuscelli, G.A. Eimer, Influence of the synthesis conditions on the physicochemical properties and acidity of Al-MCM-41 as catalysts for the cyclohexanone oxime rearrangement, Appl. Catal. A Gen. 453 (2013) 391–402. https://doi.org/10.1016/j.apcata.2012.12.016.

[13] R.S. Araújo, D.C.S. Azevedo, E. Rodríguez-Castellón, A. Jiménez-López, C.L. Cavalcante, Al and Ti-containing mesoporous molecular sieves: Synthesis, characterization and redox activity in the anthracene oxidation, J. Mol. Catal. A Chem. 281 (2008) 154–163. https://doi.org/10.1016/j.molcata.2007.09.001.

[14] M. Adjdir, T. Ali-Dahmane, P.G. Weidler, The structural comparison between Al-MCM-41 and B-MCM-41, Comptes Rendus Chim. 12 (2009) 793–800. https://doi.org/10.1016/J.CRCI.2008.09.014.

[15] K. Soni, B.S. Rana, A.K. Sinha, A. Bhaumik, M. Nandi, M. Kumar, G.M. Dhar, 3-D ordered mesoporous KIT-6 support for effective hydrodesulfurization catalysts, Appl. Catal. B Environ. 90 (2009) 55–63. https://doi.org/10.1016/j.apcatb.2009.02.010.

[16] G. Karthikeyan, A. Pandurangan, Post synthesis alumination of KIT-6 materials with Ia3d symmetry and their catalytic efficiency towards multicomponent synthesis of 1H-pyrazolo[1,2-]phthalazine-5,10-dione carbonitriles and carboxylates, J. Mol. Catal. A Chem. 361 (2012) 58–67. https://doi.org/10.1016/j.molcata.2012.05.003.

[17] A. Prabhu, L. Kumaresan, M. Palanichamy, V. Murugesan, Synthesis and characterization of aluminium incorporated mesoporous KIT-6: Efficient catalyst for acylation of phenol, Appl. Catal. A Gen. 360 (2009) 59–65. https://doi.org/10.1016/j.apcata.2009.03.004.

[18] A. Matsumoto, H. Chen, K. Tsutsumi, M. Grün, K. Unger, Novel route in the synthesis of MCM-41 containing framework aluminum and its characterization, Microporous Mesoporous Mater. 32 (1999) 55–62. https://doi.org/10.1016/S1387-1811(99)00089-X.

[19] M.M.L. Ribeiro Carrott, F.L. Conceição, J.M. Lopes, P.J.M. Carrott, C. Bernardes, J. Rocha, F. Ramôa Ribeiro, Comparative study of Al-MCM materials prepared at room temperature with different aluminium sources and by some hydrothermal methods, Microporous Mesoporous Mater. 92 (2006) 270–285. https://doi.org/10.1016/j.micromeso.2006.01.010.

[20] K.S.W. Sing, R.T. Williams, Physisorption Hysteresis Loops and the Characterization of Nanoporous Materials, Adsorpt. Sci. Technol. 22 (2004) 773–782. https://doi.org/10.1260/0263617053499032.

[21] M. Thommes, K.A. Cychosz, Physical adsorption characterization of nanoporous materials: progress and challenges, Adsorption. 20 (2014) 233–250. https://doi.org/10.1007/s10450-014-9606-z.

[22] W. Wang, R. Qi, W. Shan, X. Wang, Q. Jia, J. Zhao, C. Zhang,

H. Ru, Synthesis of KIT-6 type mesoporous silicas with tunable pore sizes, wall thickness and particle sizes via the partitioned cooperative self-assembly process, Microporous Mesoporous Mater. 194 (2014) 167–173. https://doi.org/10.1016/j.micromeso.2013.10.028.

[23] A. Vinu, N. Gokulakrishnan, V.V. Balasubramanian, S. Alam, M.P. Kapoor, K. Ariga, T. Mori, Three-Dimensional Ultralarge-Pore Ia3d Mesoporous Silica with Various Pore Diameters and Their Application in Biomolecule Immobilization, Chem. - A Eur. J. 14 (2008) 11529–11538. https://doi.org/10.1002/chem.200801304.

[24] K. Foger, J. Sanders, D. Seddon, Channel arrangements and activity of some ZSM zeolites, Zeolites. 4 (1984) 337–345.

[25] International Zeolite Association - Structure Commission, Database of Zeolite Structures, (2017). http://www.iza-structure.org/databases/.

[26] PANalytical B., X'Pert HighScore Plus Software, (2012).

[27] M. Rutkowska, I. Pacia, S. Basąg, A. Kowalczyk, Z. Piwowarska, M. Duda, K.A. Tarach, K. Góra-Marek, M. Michalik, U. Díaz, L. Chmielarz, Catalytic performance of commercial Cu-ZSM-5 zeolite modified by desilication in NH3-SCR and NH3-SCO processes, Microporous Mesoporous Mater. 246 (2017) 193–206. https://doi.org/10.1016/j.micromeso.2017.03.017.

[28] S. Yashnik, Z. Ismagilov, Cu-substituted ZSM-5 catalyst: Controlling of DeNOx reactivity via ion-exchange mode with

copper–ammonia solution, Appl. Catal. B Environ. 170 (2015) 241–254. https://doi.org/10.1016/j.apcatb.2015.01.021.

[29] J.M. Newsam, M.M.J. Treacy, W.T. Koetsier, C.B. De Gruyter, Structural Characterization of Zeolite Beta, Proc. R. Soc. London. A. Math. Phys. Sci. 420 (1988) 375–405. http://rspa.royalsocietypublishing.org/content/420/1859/375.abstract.

[30] R.B. Borade, A. Clearfield, Preparation of aluminum-rich Beta zeolite, Microporous Mater. 5 (1996) 289–297. https://doi.org/10.1016/0927-6513(95)00064-X.

[31] P. Boroń, L. Chmielarz, J. Gurgul, K. Łątka, B. Gil, B. Marszałek, S. Dzwigaj, Influence of iron state and acidity of zeolites on the catalytic activity of FeHBEA, FeHZSM-5 and FeHMOR in SCR of NO with NH3 and N2O decomposition, Microporous Mesoporous Mater. 203 (2015) 73–85. https://doi.org/10.1016/j.micromeso.2014.10.023.

[32] R. Baran, F. Averseng, D. Wierzbicki, K. Chalupka, J.-M. Krafft, T. Grzybek, S. Dzwigaj, Effect of postsynthesis preparation procedure on the state of copper in CuBEA zeolites and its catalytic properties in SCR of NO with NH3, Appl. Catal. A Gen. 523 (2016) 332–342. https://doi.org/10.1016/j.apcata.2016.06.008.

[33] L. Zhang, H. Liu, X. Li, S. Xie, Y. Wang, W. Xin, S. Liu, L. Xu, Differences between ZSM-5 and ZSM-11 zeolite catalysts in 1-hexene aromatization and isomerization, Fuel Process. Technol. 91 (2010) 449–455.

https://doi.org/10.1016/j.fuproc.2009.12.003.

[34] M. Mauvezin, G. Delahay, B. Coq, S. Kieger, J.C. Jumas, J. Olivier-Fourcade, Identification of Iron Species in Fe−BEA: Influence of the Exchange Level, J. Phys. Chem. B. 105 (2001) 928–935. https://doi.org/10.1021/jp0021906.

[35] T. V Voskoboinikov, H.-Y. Chen, W.M.. Sachtler, On the nature of active sites in Fe/ZSM-5 catalysts for NOx abatement, Appl. Catal. B Environ. 19 (1998) 279–287. https://doi.org/10.1016/S0926-3373(98)00082-4.

[36] S. Campisi, S. Palliggiano, A. Gervasini, C. Evangelisti, Finely Iron-Dispersed Particles on β Zeolite from Solvated Iron Atoms: Promising Catalysts for NH3-SCO, J. Phys. Chem. C. 123 (2019) 11723–11733. https://doi.org/10.1021/acs.jpcc.9b01474.

[37] J. Bedia, R. Barrionuevo, J. Rodríguez-Mirasol, T. Cordero, Ethanol dehydration to ethylene on acid carbon catalysts, Appl. Catal. B Environ. 103 (2011) 302–310. https://doi.org/10.1016/j.apcatb.2011.01.032.

[38] J.M. Rosas, R. Ruiz-Rosas, J. Rodríguez-Mirasol, T. Cordero, Kinetic study of the oxidation resistance of phosphorus-containing activated carbons, Carbon N. Y. 50 (2012) 1523–1537. https://doi.org/10.1016/j.carbon.2011.11.030.

[39] A. Jimenez-Lopez, P. Maireles-Torres, P. Olivera-Pastor, E. Rodriguez-Castellon, E. Paparazzo, E. Severini, A.A.G. Tomlinson, Surface chemistry of chromia-pillared tin and zirconium phosphate materials: an X-ray photoelectron

spectroscopic study, J. Mater. Chem. 2 (1992) 1175–1178. https://doi.org/10.1039/JM9920201175.

[40] Y. Guan, S. Wang, X. Wang, C. Sun, Y. Wang, L. Hu, Preparation of mesoporous Al-MCM-41 from natural palygorskite and its adsorption performance for hazardous aniline dye-basic fuchsin, Microporous Mesoporous Mater. 265 (2018) 266–274. https://doi.org/10.1016/J.MICROMESO.2016.04.025.

[41] S.W. Gaarenstroom, N. Winograd, Initial and final state effects in the ESCA spectra of cadmium and silver oxides, J. Chem. Phys. 67 (1977) 3500–3506. https://doi.org/10.1063/1.435347.

[42] M.J. Remy, M.J. Genet, G. Poncelet, P.F. Lardinois, P.P. Notte, Investigation of dealuminated mordenites by x-ray photoelectron spectroscopy, J. Phys. Chem. 96 (1992) 2614–2617. https://doi.org/10.1021/j100185a041.

[43] J. van den Brand, P.C. Snijders, W.G. Sloof, H. Terryn, J.H.W. de Wit, Acid−Base Characterization of Aluminum Oxide Surfaces with XPS, J. Phys. Chem. B. 108 (2004) 6017–6024. https://doi.org/10.1021/jp037877f.

[44] G. Engelhardt, H. Koller, P. Sieger, W. Depmeier, A. Samoson, 27Al and 23Na double-rotation NMR of sodalites, Solid State Nucl. Magn. Reson. 1 (1992) 127–135. https://doi.org/10.1016/0926-2040(92)90013-Y.

[45] Z. Luan, Alumination and ion exchange of mesoporous SBA-15 molecular sieves, Chem. Mater. 11 (1999).

[46] M. Richter, M.J.G. Fait, R. Eckelt, E. Schreier, M. Schneider,

M.M. Pohl, R. Fricke, Oxidative gas phase carbonylation of methanol to dimethyl carbonate over chloride-free Cu-impregnated zeolite Y catalysts at elevated pressure, Appl. Catal. B Environ. 73 (2007) 269–281. https://doi.org/http://dx.doi.org/10.1016/j.apcatb.2006.11.015.

[47] D.L. Hoang, T.T.H. Dang, J. Engeldinger, M. Schneider, J. Radnik, M. Richter, A. Martin, TPR investigations on the reducibility of Cu supported on Al2O3, zeolite Y and SAPO-5, J. Solid State Chem. 184 (2011) 1915–1923. https://doi.org/http://dx.doi.org/10.1016/j.jssc.2011.05.042.

[48] M. Müller, G. Harvey, R. Prins, Quantitative multinuclear MAS NMR studies of zeolites, Microporous Mesoporous Mater. 34 (2000) 281–290. https://doi.org/10.1016/S1387-1811(99)00180-8.

[49] J. Pérez-Ramírez, G. Mul, F. Kapteijn, J.A. Moulijn, A.R. Overweg, A. Doménech, A. Ribera, I.W.C.E. Arends, Physicochemical Characterization of Isomorphously Substituted FeZSM-5 during Activation, J. Catal. 207 (2002) 113–126. https://doi.org/https://doi.org/10.1006/jcat.2002.3511.

[50] S.R. Bare, A. Knop-Gericke, D. Teschner, M. Hävacker, R. Blume, T. Rocha, R. Schlögl, A.S.Y. Chan, N. Blackwell, M.E. Charochak, R. ter Veen, H.H. Brongersma, Surface analysis of zeolites: An XPS, variable kinetic energy XPS, and low energy ion scattering study, Surf. Sci. (2015). https://doi.org/10.1016/j.susc.2015.10.048.

[51] B. Xu, S. Bordiga, R. Prins, J.A. van Bokhoven, Effect of framework Si/Al ratio and extra-framework aluminum on the catalytic activity of Y zeolite, Appl. Catal. A Gen. 333 (2007) 245–253. https://doi.org/10.1016/j.apcata.2007.09.018.

[52] H.-Y. Chen, X. Wang, W.M.. Sachtler, Reduction of NOx over various Fe/zeolite catalysts, Appl. Catal. A Gen. 194–195 (2000) 159–168. https://doi.org/10.1016/S0926-860X(99)00364-6.

[53] J. Janas, T. Machej, J. Gurgul, R.P. Socha, M. Che, S. Dzwigaj, Effect of Co content on the catalytic activity of CoSiBEA zeolite in the selective catalytic reduction of NO with ethanol: Nature of the cobalt species, Appl. Catal. B Environ. 75 (2007) 239–248. https://doi.org/10.1016/j.apcatb.2007.07.029.

[54] K. Arishtirova, P. Kovacheva, A. Predoeva, Activity and basicity of BaO modified zeolite and zeolite-type catalysts, Appl. Catal. A Gen. 243 (2003) 191–196. https://doi.org/10.1016/S0926-860X(02)00544-6.

[55] L.P. Oleksenko, Characteristics of active site formation in Co-containing catalysts for CO oxidation on chemically different supports, Theor. Exp. Chem. 40 (2004) 331–336. https://doi.org/10.1023/B:THEC.0000049081.04366.a7.

[56] J. Pérez-Pariente, J. Sanz, V. Fornés, A. Corma, 29Si and 27Al MAS NMR study of zeolite β with different Si/Al Ratios, J. Catal. 124 (1990) 217–223. https://doi.org/https://doi.org/10.1016/0021-9517(90)90116-2.

[57] B. Carriere, J.P. Deville, D. Brion, J. Escard, X-ray photoelectron study of some silicon-oxygen compounds, J. Electron Spectros. Relat. Phenomena. 10 (1977) 85–91. https://doi.org/10.1016/0368-2048(77)85006-8.

[58] T.L. Barr, Recent advances in x-ray photoelectron spectroscopy studies of oxides, J. Vac. Sci. Technol. A. 9 (1991) 1793–1805. https://doi.org/10.1116/1.577464.

[59] T.L. Barr, The nature of the relative bonding chemistry in zeolites: An XPS study, Zeolites. 10 (1990) 760–765. https://doi.org/10.1016/0144-2449(90)90058-Y.

[60] C.D. T., T.H. R., Applications of ESCA to polymer chemistry. XVII. Systematic investigation of the core levels of simple homopolymers, J. Polym. Sci. Polym. Chem. Ed. 16 (2018) 791–820. https://doi.org/10.1002/pol.1978.170160407.

[61] C.D. T., T.H. R., Applications of ESCA to polymer chemistry. X. Core and valence energy levels of a series of polyacrylates, J. Polym. Sci. Polym. Chem. Ed. 14 (2018) 1671–1700. https://doi.org/10.1002/pol.1976.170140710.

[62] P. Kovacheva, K. Arishtirova, A. Predoeva, Basic zeolite and zeolite-type catalysts for the oxidative methylation of toluene with methane, React. Kinet. Catal. Lett. 79 (2003) 149–155. https://doi.org/10.1023/A:1024176121544.

[63] N.S. McIntyre, M.G. Cook, X-Ray photoelectron studies on some oxides and hydroxides of cobalt, nickel and copper, Anal. Chem. 47 (1975) 2208–2213. http://www.scopus.com/inward/record.url?eid=2-s2.0-

0016569995&partnerID=40&md5=a025ab725ca8dc8a0bce6ca45d85fcb2.

[64] T. Yamashita, P. Hayes, Analysis of XPS spectra of Fe2+ and Fe3+ ions in oxide materials, Appl. Surf. Sci. 254 (2008) 2441–2449. https://doi.org/https://doi.org/10.1016/j.apsusc.2007.09.063.

[65] F.J. Pérez-Alonso, C. Adán, S. Rojas, M.A. Peña, J.L.G. Fierro, Ni/Fe electrodes prepared by electrodeposition method over different substrates for oxygen evolution reaction in alkaline medium, Int. J. Hydrogen Energy. 39 (2014) 5204–5212. https://doi.org/10.1016/J.IJHYDENE.2013.12.186.

[66] T.-C. Lin, G. Seshadri, J.A. Kelber, A consistent method for quantitative XPS peak analysis of thin oxide films on clean polycrystalline iron surfaces, Appl. Surf. Sci. 119 (1997) 83–92. https://doi.org/10.1016/S0169-4332(97)00167-0.

[67] P.C.J. Graat, M.A.J. Somers, Simultaneous determination of composition and thickness of thin iron-oxide films from XPS Fe 2p spectra, Appl. Surf. Sci. 100–101 (1996) 36–40. https://doi.org/10.1016/0169-4332(96)00252-8.

[68] J. Pérez-Ramírez, M. Santhosh Kumar, A. Brückner, Reduction of N2O with CO over FeMFI zeolites: influence of the preparation method on the iron species and catalytic behavior, J. Catal. 223 (2004) 13–27. https://doi.org/https://doi.org/10.1016/j.jcat.2004.01.007.

[69] J. V SMITH, Faujasite-Type Structures: Aluminosilicate Framework: Positions of Cations and Molecules:

Nomenclature, in: Mol. Sieve Zeolites-I, American Chemical Society, 1974: pp. 15–171. https://doi.org/doi:10.1021/ba-1971-0101.ch015.

[70] I.J. Drake, Y. Zhang, D. Briggs, B. Lim, T. Chau, A.T. Bell, The Local Environment of Cu+ in Cu−Y Zeolite and Its Relationship to the Synthesis of Dimethyl Carbonate, J. Phys. Chem. B. 110 (2006) 11654–11664. https://doi.org/10.1021/jp058245r.

[71] M. Giuliano, F. Francesco, S. Mauro, Use of Auger parameter and Wagner plot in the characterization of Cu-ZSM-5 catalysts, Surf. Interface Anal. 31 (2001) 249–254. https://doi.org/10.1002/sia.985.

[72] C.D. Wagner, W.M. Riggs, L.E. Davis, J.F. Moulder, Handbook of X-ray photoelectron spectroscopy, Perkin-Elmer Corporation, 1979.

[73] Practical surface analysis: Edited by D Briggs and M P Seah, Second Edition, Volume 1: Auger and X-Ray Photoelectron Spectroscopy. J Wiley & Sons, Chichester, 1990, ISBN 0-471-92081-9, 674 pp., Vacuum. 45 (1994) 1227. https://doi.org/https://doi.org/10.1016/0042-207X(94)90086-8.

[74] B. Wichterlova, J. Dedecek, A. Vondrova, Identification of Cu Sites in ZSM-5 Active in NO Decomposition, J. Phys. Chem. 99 (1995) 1065–1067. https://doi.org/10.1021/j100004a001.

[75] E. Derouane, Concerning the aluminum distribution gradient in ZSM-5 zeolites, J. Catal. 71 (1981) 447–448.

https://doi.org/10.1016/0021-9517(81)90253-0.

[76] H. Kosslick, G. Lischke, B. Parlitz, W. Storek, R. Fricke, Acidity and active sites of Al-MCM-41, Appl. Catal. A Gen. 184 (1999) 49–60. https://doi.org/10.1016/S0926-860X(99)00078-2.

[77] E.F. Iliopoulou, E.V. Antonakou, S.A. Karakoulia, I.A. Vasalos, A.A. Lappas, K.S. Triantafyllidis, Catalytic conversion of biomass pyrolysis products by mesoporous materials: Effect of steam stability and acidity of Al-MCM-41 catalysts, Chem. Eng. J. 134 (2007) 51–57. https://doi.org/10.1016/J.CEJ.2007.03.066.

[78] G. Guiu, P. Grange, Acidic and Catalytic Properties of SiO2-Ta2O5 Mixed Oxides Prepared by the Sol-Gel Method, J. Catal. 156 (1995) 132–138. https://doi.org/10.1006/JCAT.1995.1238.

[79] T. Ushikubo, Recent topics of research and development of catalysis by niobium and tantalum oxides, Catal. Today. 57 (2000) 331–338. https://doi.org/10.1016/S0920-5861(99)00344-2.

[80] M. Baltes, A. Kytökivi, B.M. Weckhuysen, R.A. Schoonheydt, P. Van Der Voort, E.F. Vansant, Supported Tantalum Oxide and Supported Vanadia-tantala Mixed Oxides: Structural Characterization and Surface Properties, J. Phys. Chem. B. 105 (2001) 6211–6220. https://doi.org/10.1021/jp010628b.

[81] A. Jentys, K. Kleestorfer, H. Vinek, Concentration of surface hydroxyl groups on MCM-41, Microporous Mesoporous Mater.

27 (1999) 321–328. https://doi.org/10.1016/S1387-1811(98)00265-0.

[82] V.L. Zholobenko, D. Plant, A.J. Evans, S.M. Holmes, Acid sites in mesoporous materials: A DRIFTS study, Microporous Mesoporous Mater. 44–45 (2001) 793–799. https://doi.org/10.1016/S1387-1811(01)00262-1.

[83] G.P. Heitmann, G. Dahlhoff, W.F. Hölderich, Modified Beta zeolites as catalysts for the Beckmann rearrangement of cyclohexanone oxime, Appl. Catal. A Gen. 185 (1999) 99–108. https://doi.org/10.1016/S0926-860X(99)00126-X.

[84] Y. Izumi, H. Ichihashi, Y. Shimazu, M. Kitamura, H. Sato, Development and industrialization of the vapor-phase beekmann rearrangement process, Bull. Chem. Soc. Jpn. 80 (2007) 1280–1287. https://doi.org/10.1246/bcsj.80.1280.

[85] D. Freude, M. Hunger, H. Pfeifer, W. Schwieger, 1H MAS NMR studies on the acidity of zeolites, Chem. Phys. Lett. 128 (1986) 62–66. https://doi.org/https://doi.org/10.1016/0009-2614(86)80146-4.

[86] A.M. Camiloti, S.L. Jahn, N.D. Velasco, L.F. Moura, D. Cardoso, Acidity of Beta zeolite determined by TPD of ammonia and ethylbenzene disproportionation, Appl. Catal. A Gen. 182 (1999) 107–113. https://doi.org/https://doi.org/10.1016/S0926-860X(98)00418-9.

[87] A. V. Kucherov, J.L. Gerlock, H.-W. Jen, M. Shelef, In situ e.s.r. monitoring of the coordination and oxidation states of

copper in Cu-ZSM-5 up to 500°C in flowing gas mixtures: 1. Interaction with He, O_2, NO, NO_2, and H_2O, Zeolites. 15 (1995) 9–14. https://doi.org/10.1016/0144-2449(94)00007-F.

[88] S.C. Larsen, A. Aylor, A.T. Bell, J.A. Reimer, Electron Paramagnetic Resonance Studies of Copper Ion-Exchanged ZSM-5, J. Phys. Chem. 98 (1994) 11533–11540. https://doi.org/10.1021/j100095a039.

[89] S.A. Yashnik, A. V. Salnikov, N.T. Vasenin, V.F. Anufrienko, Z.R. Ismagilov, Regulation of the copper-oxide cluster structure and DeNOx activity of Cu-ZSM-5 catalysts by variation of OH/Cu2+, Catal. Today. 197 (2012) 214–227. https://doi.org/10.1016/J.CATTOD.2012.08.033.

[90] S.A. Yashnik, Z.R. Ismagilov, V.F. Anufrienko, Catalytic properties and electronic structure of copper ions in Cu-ZSM-5, Catal. Today. 110 (2005) 310–322. https://doi.org/10.1016/J.Cattod.2005.09.029.

[91] Y. Kuroda, A. Kotani, H. Maeda, H. Moriwaki, T. Morimato, M. Nagao, The state of excessively lon-exchanged copper in mordenite: formation of tetragonal hydroxy-bridged copper ion, J. Chem. Soc. Faraday Trans. 88 (1992) 1583–1590. https://doi.org/10.1039/FT9928801583.

[92] R. Beaumont, D. Barthomeuf, X, Y, aluminum-deficient and ultrastable faujasite-type zeolites: I. Acidic and structural properties, J. Catal. 26 (1972) 218–225. https://doi.org/10.1016/0021-9517(72)90052-8.

[93] J. Zhao, C. Zhou, C. He, Y. Dai, X. Jia, Y. Yang, Efficient

dehydration of fructose to 5-hydroxymethylfurfural over sulfonated carbon sphere solid acid catalysts, Catal. Today. (2015). https://doi.org/10.1016/j.cattod.2015.07.005.

[94] A. Villa, M. Schiavoni, P.F. Fulvio, S.M. Mahurin, S. Dai, R.T. Mayes, G.M. Veith, L. Prati, Phosphorylated mesoporous carbon as effective catalyst for the selective fructose dehydration to HMF, J. Energy Chem. 22 (2013) 305–311. https://doi.org/https://doi.org/10.1016/S2095-4956(13)60037-6.

[95] J. Bedia, R. Ruiz-Rosas, J. Rodríguez-Mirasol, T. Cordero, Kinetic study of the decomposition of 2-butanol on carbon-based acid catalyst, AIChE J. 56 (2009) 1557–1568. https://doi.org/10.1002/aic.12056.

[96] J. Bedia, R. Ruiz-Rosas, J. Rodríguez-Mirasol, T. Cordero, A kinetic study of 2-propanol dehydration on carbon acid catalysts, J. Catal. 271 (2010) 33–42. https://doi.org/https://doi.org/10.1016/j.jcat.2010.01.023.

[97] J. Bedia, J.M. Rosas, J. Márquez, J. Rodríguez-Mirasol, T. Cordero, Preparation and characterization of carbon based acid catalysts for the dehydration of 2-propanol, Carbon N. Y. 47 (2009) 286–294. https://doi.org/10.1016/j.carbon.2008.10.008.

[98] J. Bedia, J.M. Rosas, D. Vera, J. Rodríguez-Mirasol, T. Cordero, Isopropanol decomposition on carbon based acid and basic catalysts, Catal. Today. 158 (2010) 89–96. https://doi.org/10.1016/j.cattod.2010.04.043.

[99] I. Jiménez-Morales, J. Santamaría-González, P. Maireles-Torres,

A. Jiménez-López, Methanolysis of sunflower oil catalyzed by acidic Ta2O5 supported on SBA-15, Appl. Catal. A Gen. 405 (2011) 93–100. https://doi.org/10.1016/J. Ap Cata .2011.07.037.

[100] I. Jiménez-Morales, J. Santamaría-González, P. Maireles-Torres, A. Jiménez-López, Mesoporous tantalum phosphate as acidic catalyst for the methanolysis of sunflower oil, Appl. Catal. B Environ. 123–124 (2012) 316–323. https://doi.org/http://dx.doi.org/10.1016/j.apcatb.2012.04.023.

[101] I. Jiménez-Morales, A. Teckchandani-Ortiz, J. Santamaría-González, P. Maireles-Torres, A. Jiménez-López, Selective dehydration of glucose to 5-hydroxymethylfurfural on acidic mesoporous tantalum phosphate, Appl. Catal. B Environ. 144 (2014) 22–28. https://doi.org/10.1016/j.apcatb.2013.07.002.

[102] V.V. Ordomsky, J. van der Schaaf, J.C. Schouten, T.A. Nijhuis, The effect of solvent addition on fructose dehydration to 5-hydroxymethylfurfural in biphasic system over zeolites, J. Catal. 287 (2012) 68–75. https://doi.org/10.1016/j.jcat.2011.12.002.

[103] E. Garrone, R. Chiappetta, G. Spoto, P. Ugliengo, A. Zecchina, F. Fajula, Assessment Of Broensted Acidity In Zeolites By Co Adsorption: An Ir Study, in: R. von Ballmoos, J.B. Higgins, M.M.J.B.T.-P. from the N.I.Z.C. Treacy (Eds.), Butterworth-Heinemann, 1993: pp. 267–273. https://doi.org/https://doi.org/10.1016/B978-1-4832-8383-8.50117-3.

[104] J.N. Kondo, L. Lu, Y. Takahara, K. Maruya, K. Domen, N. Igarashi, T. Tatsumi, IR Characterization of Mesoporous Tantalum Oxide, Ta-TMS-1, Bull. Chem. Soc. Jpn. 73 (2000) 1123–1129. https://doi.org/10.1246/bcsj.73.1123.

[105] V.V. Ordomsky, V.L. Sushkevich, J.C. Schouten, J. van der Schaaf, T.A. Nijhuis, Glucose dehydration to 5-hydroxymethylfurfural over phosphate catalysts, J. Catal. 300 (2013) 37–46. https://doi.org/10.1016/j.jcat.2012.12.028.

[106] K. Nakajima, Y. Baba, R. Noma, M. Kitano, J. N. Kondo, S. Hayashi, M. Hara, Nb2O5·nH2O as a Heterogeneous Catalyst with Water-Tolerant Lewis Acid Sites, J. Am. Chem. Soc. 133 (2011) 4224–4227. https://doi.org/10.1021/ja110482r.

[107] S. Okazaki, A. Kurosaki, Acidic properties and catalytic activities of niobic acid treated with phosphoric acid, Catal. Today. 8 (1990) 113–122. https://doi.org/10.1016/0920-5861(90)87012-R.

[108] G. Portillo Perez, A. Mukherjee, M.-J. Dumont, Insights into HMF catalysis, J. Ind. Eng. Chem. (2018). https://doi.org/10.1016/J.JIEC.2018.10.002.

[109] T. Yoshida, S. Yanachi, Y. Matsumura, Glucose decomposition in water under supercritical pressure at 448-498 K, Nihon Enerugi Gakkaishi/Journal Japan Inst. Energy. 86 (2007) 700–706. https://doi.org/10.3775/jie.86.700.

[110] S.J. Dee, A.T. Bell, A Study of the Acid-Catalyzed Hydrolysis of Cellulose Dissolved in Ionic Liquids and the Factors Influencing the Dehydration of Glucose and the Formation of

Humins, ChemSusChem. 4 (2011) 1166–1173. https://doi.org/10.1002/cssc.201000426.

[111] B.F.M. Kuster, 5-Hydroxymethylfurfural (HMF). A Review Focussing on its Manufacture, Starch - Stärke. 42 (1990) 314.

[112] C. Carlini, P. Patrono, A.M.R. Galletti, G. Sbrana, Heterogeneous catalysts based on vanadyl phosphate for fructose dehydration to 5-hydroxymethyl-2-furaldehyde, Appl. Catal. A Gen. 275 (2004) 111–118. https://doi.org/10.1016/J.APCATA.2004.07.026.

[113] P. Carniti, A. Gervasini, S. Biella, A. Auroux, Niobic acid and niobium phosphate as highly acidic viable catalysts in aqueous medium: Fructose dehydration reaction, Catal. Today. 118 (2006) 373–378. https://doi.org/https://doi.org/10.1016/j.cattod.2006.07.024.

[114] S.K.R. Patil, C.R.F. Lund, Formation and Growth of Humins via Aldol Addition and Condensation during Acid-Catalyzed Conversion of 5-Hydroxymethylfurfural, Energy & Fuels. 25 (2011) 4745–4755. https://doi.org/10.1021/ef2010157.

[115] I. Sádaba, M. López Granados, A. Riisager, E. Taarning, Deactivation of solid catalysts in liquid media: the case of leaching of active sites in biomass conversion reactions, Green Chem. 17 (2015) 4133–4145. https://doi.org/10.1039/C5GC00804B.

[116] M. Guisnet, F.R. Ribeiro, Deactivation and Regeneration of Zeolite Catalysts, Imperial College Press, 2011. https://doi.org/doi:10.1142/p747.

[117] S.K.R. Patil, C.R.F. Lund, Formation and Growth of Humins via Aldol Addition and Condensation during Acid-Catalyzed Conversion of 5-Hydroxymethylfurfural, Energy & Fuels. 25 (2011) 4745–4755. https://doi.org/10.1021/ef2010157.

[118] I. van Zandvoort, Y. Wang, C.B. Rasrendra, E.R.H. van Eck, P.C.A. Bruijnincx, H.J. Heeres, B.M. Weckhuysen, Formation, Molecular Structure, and Morphology of Humins in Biomass Conversion: Influence of Feedstock and Processing Conditions, ChemSusChem. 6 (2013) 1745–1758. https://doi.org/10.1002/cssc.201300332.

[119] G. Tsilomelekis, M.J. Orella, Z. Lin, Z. Cheng, W. Zheng, V. Nikolakis, D.G. Vlachos, Molecular structure, morphology and growth mechanisms and rates of 5-hydroxymethyl furfural (HMF) derived humins, Green Chem. 18 (2016) 1983–1993. https://doi.org/10.1039/C5GC01938A.

[120] J. Kim, B. Shim, G. Lee, J. Han, J.M. Kim, J.-K. Jeon, Synthesis of high-energy-density fuel over mesoporous aluminosilicate catalysts, Catal. Today. 303 (2018) 71–76. https://doi.org/https://doi.org/10.1016/j.cattod.2017.08.024.

[121] A.A. Marianou, C.M. Michailof, A. Pineda, E.F. Iliopoulou, K.S. Triantafyllidis, A.A. Lappas, Effect of Lewis and Brønsted acidity on glucose conversion to 5-HMF and lactic acid in aqueous and organic media, Appl. Catal. A Gen. 555 (2018) 75–87. https://doi.org/10.1016/J.APCATA.2018.01.029.

[122] I. Jiménez-Morales, J. Santamaría-González, A. Jiménez-López, P. Maireles-Torres, Glucose dehydration to 5-

hydroxymethylfurfural on zirconium containing mesoporous MCM-41 silica catalysts, Fuel. 118 (2014) 265–271. https://doi.org/10.1016/j.fuel.2013.10.079.

[123] Y. Román-Leshkov, J.A. Dumesic, Solvent Effects on Fructose Dehydration to 5-Hydroxymethylfurfural in Biphasic Systems Saturated with Inorganic Salts, Top. Catal. 52 (2009) 297–303. https://doi.org/10.1007/s11244-008-9166-0.

[124] Y. Román-Leshkov, J.N. Chheda, J.A. Dumesic, Phase Modifiers Promote Efficient Production of Hydroxymethylfurfural from Fructose, Science (80-.). 312 (2006) 1933–1937. http://science.sciencemag.org/content/312/5782/1933.abstract.

[125] B. Saha, M.M. Abu-Omar, Advances in 5-hydroxymethylfurfural production from biomass in biphasic solvents, Green Chem. 16 (2014) 24–38. https://doi.org/10.1039/C3GC41324A.

[126] S. De, S. Dutta, B. Saha, Microwave assisted conversion of carbohydrates and biopolymers to 5-hydroxymethylfurfural with aluminium chloride catalyst in water, Green Chem. 13 (2011) 2859–2868. https://doi.org/10.1039/C1GC15550D.

[127] A. Dutta, A.K. Patra, S. Dutta, B. Saha, A. Bhaumik, Hierarchically porous titanium phosphate nanoparticles: an efficient solid acid catalyst for microwave assisted conversion of biomass and carbohydrates into 5-hydroxymethylfurfural, J. Mater. Chem. 22 (2012) 14094–14100.

https://doi.org/10.1039/C2JM30623A.

[128] Y.J. Pagán-Torres, T. Wang, J.M.R. Gallo, B.H. Shanks, J.A. Dumesic, Production of 5-Hydroxymethylfurfural from Glucose Using a Combination of Lewis and Brønsted Acid Catalysts in Water in a Biphasic Reactor with an Alkylphenol Solvent, ACS Catal. 2 (2012) 930–934. https://doi.org/10.1021/cs300192z.

[129] M. Ohara, A. Takagaki, S. Nishimura, K. Ebitani, Syntheses of 5-hydroxymethylfurfural and levoglucosan by selective dehydration of glucose using solid acid and base catalysts, Appl. Catal. A Gen. 383 (2010) 149–155. https://doi.org/10.1016/j.apcata.2010.05.040.

[130] G. de Gonzalo, A.R. Alcántara, P. Domínguez de María, Cyclopentyl Methyl Ether (CPME): A Versatile Eco-Friendly Solvent for Applications in Biotechnology and Biorefineries, ChemSusChem. 12 (2019) 2083–2097. https://doi.org/10.1002/cssc.201900079.

[131] Q. Qing, Q. Guo, L. Zhou, Y. Wan, Y. Xu, H. Ji, X. Gao, Y. Zhang, Catalytic conversion of corncob and corncob pretreatment hydrolysate to furfural in a biphasic system with addition of sodium chloride, Bioresour. Technol. 226 (2017) 247–254. https://doi.org/10.1016/J.BIORTECH.2016.11.118.

[132] Y. Roman-Leshkov, J. A. Dumesic, Solvent Effects on Fructose Dehydration to 5-Hydroxymethylfurfural in Biphasic Systems Saturated with Inorganic Salts, 2009. https://doi.org/10.1007/s11244-008-9166-0.

[133] S.K. Tyrlik, D. Szerszen, B. Kurzak, K. Bal, Concentrated Water Solution of Salts as Solvents for Reactions of Carbohydrates. Part 1: Reactions of Glucose Promoted by Concentrated Solutions of Alkaline and Alkaline Earth Metal Salts, Starch - Stärke. 47 (1995) 171–174. https://doi.org/10.1002/star.19950470503.

[134] C. García-Sancho, I. Fúnez-Núñez, R. Moreno-Tost, J. Santamaría-González, E. Pérez-Inestrosa, J.L.G. Fierro, P. Maireles-Torres, Beneficial effects of calcium chloride on glucose dehydration to 5-hydroxymethylfurfural in the presence of alumina as catalyst, Appl. Catal. B Environ. 206 (2017) 617–625. https://doi.org/10.1016/j.apcatb.2017.01.065.

[135] C. Yang, X. Lu, W. Lin, X. Yang, J. Yao, TG-FTIR Study on Corn Straw Pyrolysis-influence of Minerals1 1Supported by the National High Technology Research and Development Program of China(No. 2003AA514023) and the National Basic Research Program of China(No. 2004CB719700)., Chem. Res. Chinese Univ. 22 (2006) 524–532. https://doi.org/https://doi.org/10.1016/S1005-9040(06)60155-4.

[136] I. Jiménez-Morales, J. Santamaría-González, A. Jiménez-López, P. Maireles-Torres, Glucose dehydration to 5-hydroxymethylfurfural on zirconium containing mesoporous MCM-41 silica catalysts, Fuel. 118 (2014) 265–271. https://doi.org/http://dx.doi.org/10.1016/j.fuel.2013.10.079.

[137] K.M. Parida, D. Rath, Amine functionalized MCM-41: An active and reusable catalyst for Knoevenagel condensation

reaction, J. Mol. Catal. A Chem. 310 (2009) 93–100. https://doi.org/https://doi.org/10.1016/j.molcata.2009.06.001.

[138] M. Pirouzmand, A.M. Gharehbaba, Z. Ghasemi, S. Azizi Khaaje, [CTA]Fe/MCM-41: An efficient and reusable catalyst for green synthesis of xanthene derivatives, Arab. J. Chem. 10 (2017) 1070–1076. https://doi.org/https://doi.org/10.1016/j.arabjc.2016.06.017.

[139] C. Moreau, R. Durand, C. Pourcheron, S. Razigade, Preparation of 5-hydroxymethylfurfural from fructose and precursors over H-form zeolites, Ind. Crops Prod. 3 (1994) 85–90. https://doi.org/http://dx.doi.org/10.1016/0926-6690(94)90080-9.

[140] R. Otomo, T. Yokoi, J.N. Kondo, T. Tatsumi, Dealuminated Beta zeolite as effective bifunctional catalyst for direct transformation of glucose to 5-hydroxymethylfurfural, Appl. Catal. A Gen. 470 (2014) 318–326. https://doi.org/https://doi.org/10.1016/j.apcata.2013.11.012.

[141] E. Nikolla, Y. Román-Leshkov, M. Moliner, M.E. Davis, "One-Pot" Synthesis of 5-(Hydroxymethyl) furfural from Carbohydrates using Tin-Beta Zeolite, ACS Catal. 1 (2011) 408–410.

[142] K. Lourvanij, G.L. Rorrer, Reactions of aqueous glucose solutions over solid-acid Y-zeolite catalyst at 110-160 .degree.C, Ind. Eng. Chem. Res. 32 (1993) 11–19. https://doi.org/10.1021/ie00013a002.

[143] G. Marcotullio, W. De Jong, Chloride ions enhance furfural formation from d-xylose in dilute aqueous acidic solutions, Green Chem. 12 (2010) 1739–1746. https://doi.org/10.1039/B927424C.

[144] C.B. Rasrendra, I.G.B.N. Makertihartha, S. Adisasmito, H.J. Heeres, Green Chemicals from d-glucose: Systematic Studies on Catalytic Effects of Inorganic Salts on the Chemo-Selectivity and Yield in Aqueous Solutions, Top. Catal. 53 (2010) 1241–1247. https://doi.org/10.1007/s11244-010-9570-0.

[145] Z. Yu, H. Wu, Y. Li, Y. Xu, H. Li, S. Yang, Chapter 6 - Zeolite-related catalysts for biomass-derived sugar valorization, in: C. Mustansar Hussain, P.B.T.-A.F.S.C. for B.V. Sudarsanam (Eds.), Elsevier, 2020: pp. 141–159. https://doi.org/https://doi.org/10.1016/B978-0-12-820236-4.00006-4.

[146] M. Görgényi, J. Dewulf, H. Van Langenhove, K. Héberger, Aqueous salting-out effect of inorganic cations and anions on non-electrolytes, Chemosphere. 65 (2006) 802–810. https://doi.org/http://dx.doi.org/10.1016/j.chemosphere.2006.03.029.

[147] E. Combs, B. Cinlar, Y. Pagan-Torres, J.A. Dumesic, B.H. Shanks, Influence of alkali and alkaline earth metal salts on glucose conversion to 5-hydroxymethylfurfural in an aqueous system, Catal. Commun. 30 (2013). https://doi.org/10.1016/j.catcom.2012.10.011.

[148] D.W. Gardner, J. Huo, T.C. Hoff, R.L. Johnson, B.H. Shanks,

J.-P. Tessonnier, Insights into the Hydrothermal Stability of ZSM-5 under Relevant Biomass Conversion Reaction Conditions, ACS Catal. 5 (2015) 4418–4422. https://doi.org/10.1021/acscatal.5b00888.

[149] B. Torres-Olea, C. García-Sancho, J.A. Cecilia, M. Oregui-Bengoechea, P.L. Arias, R. Moreno-Tost, P. Maireles-Torres, Influence of Lewis acidity and $CaCl_2$ on the direct transformation of glucose to 5-hydroxymethylfurfural, Mol. Catal. 510 (2021) 111685. https://doi.org/https://doi.org/10.1016/j.mcat.2021.111685.

[150] A. Palčić, V. Valtchev, Analysis and control of acid sites in zeolites, Appl. Catal. A Gen. 606 (2020) 117795. https://doi.org/https://doi.org/10.1016/j.apcata.2020.117795.

[151] M. Boronat, A. Corma, Factors Controlling the Acidity of Zeolites, Catal. Letters. 145 (2015) 162–172. https://doi.org/10.1007/s10562-014-1438-7.

[152] Z. Cui, X. Feng, H. Li, T. Tan, Interconversion of Lewis Acid and Brønsted Acid Catalysts in Biomass-Derived Paraxylene Synthesis, Chem. Eng. Sci. 227 (2020) 115942. https://doi.org/10.1016/j.ces.2020.115942.

[153] H. Xia, H. Hu, S. Xu, K. Xiao, S. Zuo, Catalytic conversion of glucose to 5-hydroxymethyfural over Fe/β zeolites with extra-framework isolated Fe species in a biphasic reaction system, Biomass and Bioenergy. 108 (2018) 426–432. https://doi.org/10.1016/j.biombioe.2017.12.007.

[154] J. Zhang, X. Tang, H. Yi, Q. Yu, Y. Zhang, J. Wei, Y. Yuan,

Synthesis, characterization and application of Fe-zeolite: A review, Appl. Catal. A Gen. 630 (2022) 118467. https://doi.org/https://doi.org/10.1016/j.apcata.2021.118467.

[155] X. Li, Q. Xia, N. Van Chuc, K. Peng, X. Liu, N. Essayem, High yield production of HMF from carbohydrates over silica–alumina composite catalysts, Catal. Sci. Technol. 6 (2016). https://doi.org/10.1039/C6CY01628F.

[156] S. Xu, L. Zhang, K. Xiao, H. Xia, Isomerization of glucose into fructose by environmentally friendly Fe/β zeolite catalysts, Carbohydr. Res. 446–447 (2017) 48–51. https://doi.org/https://doi.org/10.1016/j.carres.2017.05.006.

[157] G. Li, E.A. Pidko, The Nature and Catalytic Function of Cation Sites in Zeolites: a Computational Perspective, ChemCatChem. 11 (2019) 134–156. https://doi.org/https://doi.org/10.1002/cctc.201801493.

[158] M. Moliner, Y. Román-Leshkov, M.E. Davis, Tin-containing zeolites are highly active catalysts for the isomerization of glucose in water, Proc. Natl. Acad. Sci. 107 (2010) 6164–6168. https://doi.org/10.1073/pnas.1002358107.

[159] N. Sobuś, B. Michorczyk, M. Piotrowski, Ł. Kuterasiński, D.K. Chlebda, J. Łojewska, R.J. Jędrzejczyk, P. Jodłowski, P. Kuśtrowski, I. Czekaj, Design of Co, Cu and Fe–BEA Zeolite Catalysts for Selective Conversion of Lactic Acid into Acrylic Acid, Catal. Letters. 149 (2019) 3349–3360. https://doi.org/10.1007/s10562-019-02883-8.

[160] K. Margeta, N. Zabukovec Logar, M. Šiljeg, A. Farkas, Natural

Zeolites in Water Treatment – How Effective is Their Use, in: Water Treat., 2013. https://doi.org/10.5772/50738.

[161] M.D. Argyle, C.H. Bartholomew, Heterogeneous Catalyst Deactivation and Regeneration: A Review, Catal. . 5 (2015) 145–269. https://doi.org/10.3390/catal5010145.

[162] P. Vinke, H. Van Bekkum, The Dehydration of Fructose Towards 5-Hydroxymethylfurfural Using Activated Carbon as Adsorbent, Starch-Starke. 44 (1992) 90–96.

[163] B.F.M. Kuster, H.J.C. Der Van Steen, Preparation of 5-Hydroxymethylfurfural Part I. Dehydration of Fructose in a Continuous Stirred Tank Reactor, Starch - Stärke. 29 (1977) 99–103. https://doi.org/https://doi.org/10.1002/star.19770290306.

[164] B.F.M. Kuster, 5-Hydroxymethylfurfural (HMF). A Review Focussing on its Manufacture, Starch - Stärke. 42 (1990) 314–321. https://doi.org/10.1002/star.19900420808.

[165] G. de Gonzalo, A.R. Alcántara, P. Domínguez de María, Cyclopentyl Methyl Ether (CPME): A Versatile Eco-Friendly Solvent for Applications in Biotechnology and Biorefineries., ChemSusChem. 12 (2019) 2083–2097. https://doi.org/10.1002/cssc.201900079.

[166] H. Ouwen, Y. Zhang, P. Wang, L. Liu, Q. Wang, N. Yang, W. Li, H. Yu, Experimental and Kinetic Study on the Production of Furfural and HMF from Glucose, Catalysts. 11 (2020) 11. https://doi.org/10.3390/catal11010011.

[167] T. Wang, M.W. Nolte, B.H. Shanks, Catalytic dehydration of

C6 carbohydrates for the production of hydroxymethylfurfural (HMF) as a versatile platform chemical, Green Chem. 16 (2014) 548–572. https://doi.org/10.1039/C3GC41365A.

[168] C. Wang, L. Zhang, T. Zhou, J. Chen, F. Xu, Synergy of Lewis and Brønsted acids on catalytic hydrothermal decomposition of carbohydrates and corncob acid hydrolysis residues to 5-hydroxymethylfurfural, Sci. Rep. 7 (2017) 40908. https://doi.org/10.1038/srep40908.

[169] P. Rechnia-Gorący, A. Malaika, M. Kozłowski, Acidic activated carbons as catalysts of biodiesel formation, Diam. Relat. Mater. 87 (2018) 124–133. https://doi.org/10.1016/j.diamond.2018.05.015.

Conclusions

7. Conclusions

Heterogeneous acid catalysts were prepared and/or modified to be active in the glucose dehydration to 5-(hydroxymethil)furfural.

Mesoporous tantalum oxide was active as catalyst or the dehydration of glucose to HMF in a biphasic water/MIBK system, reaching under moderate temperature (175 ºC) a high HMF selectivity of 33 % after only 90 min.. Levulinic and formic acid, degradation products of HMF rehydration, were not detected. The catalytic activity could be correlated with the mesoporous structure (surface area of 79 $m^2\ g^{-1}$) and a suitable acidity (353 μmol $NH_3 g^{-1}$) with the presence of both types of acid sites, Lewis and Brönsted, which were active sites for the reaction.

Mesoporous Al-doped MCM-41 and KIT6 silica catalysts were prepared by a sol–gel method, with Si/Al molar ratios of 5 and 10. They possessed high specific surface areas, moderate acidity with Brönsted and Lewis acid sites. Al-KIT6-C2 was highly selective towards HMF, but 10Al-MCM-41 catalyst resulted the most active, in a biphasic water/MIBK medium at 195 ºC, reaching 87% of glucose conversion and 36% of HMF yield after 150 min of reaction time. The reaction was quite selective towards HMF, since only fructose was detected as by-product. The influence of the reaction medium was studied, as in the organic phase as in the aqueous phase, showing that the use of a NaCl aqueous solution instead of water, in a biphasic system with MIBK, led to an enhancement of the glucose conversion and HMF yield, attaining the high values of 96% and 63%,

respectively, after only 30 min.. The catalytic performance was well maintained after three catalytic cycles.

The positive effect of the addition of inorganic salts on the catalytic performance of acid catalysts based on ZSM-5 was corroborated, being especially effective NaCl, which also enhanced the activity of Y and Beta zeolites. H-Beta can be compared in terms of catalytic activity to 10Al-MCM-41, since the existence of mesopores in its hierarchical meso/microporous system led to an excellent HMF yield of 56% at 195ºC, after only 30 min of reaction. Besides the advantageous biphasic water/MIBK system, salts shifts the equilibrium towards the HMF formation, whereas ionic species in the aqueous phase are involved in glucose conversion reaction mechanism and also ameliorate the HMF migration from the aqueous to the organic phase, by increasing its partition coefficient and then avoiding secondary reactions which produce humins and soluble polymers, leading to higher HMF yields. Moreover, in the absence of inorganic salts, the modification of the acidic properties of the zeolites by introducing Lewis acid sites, increased the HMF yield specially in ZSM-5 from 2 to 29%, with almost a total glucose conversion. The catalytic activity was related to the suitable acid and textural properties.

Phosphorous-containing activated carbons showed high HMF selectivity in biphasic water/MIBK system at 195 ºC, reaching 53% starting from glucose and 78% from fructose, after 90 min. The reaction mechanism did not involve glucose to fructose isomerization. In comparison with acid homogenous H_3PO_4 catalyst, HMF selectivity and glucose conversion were increased. Partial deactivation due to a physical blocking of active sites by deposition of humins decreased the

HMF selectivity in a second catalytic cycle. L3500 acidic carbon catalyst combine the advantage of 10Al-MCM-41 and H-ZSM5-15 catalysts in terms of activity, but from the economic and environmental point of view, as it was obtained from biomass wastes, it would be preferred.

The textural and acid properties of porous materials play a key role in glucose dehydration to HMF. The presence of meso and micropores and Brönsted and Lewis acid active sites, as well as their synergy and interactions with the reaction medium determine the catalytic activity.

Publications

8. Publications

M. Moreno Recio, I. Jiménez Morales, P.L. Arias, J. Santamaría Gonzalez, P. Maireles-Torres, The Key Role of Textural Properties of Aluminosilicates in the Acid-Catalyzed Dehydration of Glucose into 5-Hydroxymethylfurfural, ChemistrySelect. 2 (2017) 2444–2451. https://doi.org/10.1002/slct.201700097.

M. Moreno Recio, J. Santamaría Gonzalez, P. Maireles-Torres, Brönsted and Lewis acid ZSM-5 zeolites for the catalytic dehydration of glucose into 5-hydroxymethylfurfural, Chem. Eng. J. 303 (2016). https://doi.org/10.1016/j.cej.2016.05.120.

I. Jiménez Morales, M. Moreno Recio, J. Santamaría Gonzalez, P. Maireles-Torres, A. Jiménez-López, Production of 5-hydroxymethylfurfural from glucose using aluminum doped MCM-41 silica as acid catalyst, Appl. Catal. B Environ. 164 (2015) 70–76. https://doi.org/10.1016/j.apcatb.2014.09.002.

Solsona, T. García, R. Sanchis, M.D. Soriano, M. Moreno, E. Rodríguez-Castellón, S. Agouram, A. Dejoz, J.M. López Nieto, Total oxidation of VOCs on mesoporous iron oxide catalysts: Soft chemistry route versus hard template method, Chem. Eng. J. 290 (2016) 273–281. https://doi.org/10.106/j.cej.2015.12.109.

I. Jiménez Morales, M. Moreno Recio, J. Santamaría Gonzalez, P. Maireles-Torres, A. Jiménez-López, Mesoporous tantalum oxide as catalyst for dehydration of glucose to 5-hydroxymethylfurfural, Appl. Catal. B Environ. s 154–155 (2014) 190–196. https://doi.org/10.1016/j.apcatb.2014.02.024.